NUREG-1570

Risk Assessment of Severe Accident-Induced Steam Generator Tube Rupture

Manuscript Completed: March 1998
Date Published: March 1998

SGTR Severe Accident Working Group

Division of Systems Safety and Analysis
Office of Nuclear Reactor Regulation
U.S. Nuclear Regulatory Commission
Washington, DC 20555-0001

ABSTRACT

This report describes the basis, results, and related risk implications of an analysis performed by an *ad hoc* working group of the U.S. Nuclear Regulatory Commission (NRC) to assess the containment bypass potential attributable to steam generator tube rupture (SGTR) induced by severe accident conditions. The SGTR Severe Accident Working Group, comprised of staff members from the NRC's Offices of Nuclear Reactor Regulation (NRR) and Nuclear Regulatory Research (RES), undertook the analysis beginning in December 1995 to support a proposed steam generator integrity rule.

The work drew upon previous risk and thermal-hydraulic analyses of core damage sequences, with a focus on the Surry plant as a representative example. This analysis yielded new results, however, derived by predicting thermal-hydraulic conditions of selected severe accident scenarios using the SCDAP/RELAP5 computer code, flawed tube failure modeling, and tube failure probability estimates. These results, in terms of containment bypass probability, form the basis for the findings presented in this report.

The representative calculation using Surry plant data indicates that some existing plants could be vulnerable to containment bypass resulting from tube failure during severe accidents. To specifically identify the population of plants that may pose a significant bypass risk would require more definitive analysis considering uncertainties in some assumptions and plant- and design-specific variables.

CONTENTS

CONTENTS (continued)

CONTENTS (continued)

CONTENTS (continued)

CONTENTS (continued)

LIST OF FIGURES

LIST OF FIGURES (continued)

LIST OF FIGURES (continued)

LIST OF FIGURES (continued)

LIST OF TABLES

LIST OF TABLES (continued)

EXECUTIVE SUMMARY

This report describes the basis, results, and related risk implications of an analysis performed by an *ad hoc* working group of the U.S. Nuclear Regulatory Commission (NRC) to assess the containment bypass potential attributable to steam generator tube rupture (SGTR) induced by severe accident conditions. The SGTR Severe Accident Working Group, comprised of staff members from the NRC's Offices of Nuclear Reactor Regulation (NRR) and Nuclear Regulatory Research (RES), undertook the analysis beginning in December 1995 to give the staff a broader insight into the risk implications of implementing a proposed rule that would change the requirements regarding steam generator tube integrity.

Previous tube integrity assessments have assumed an elevated primary-to-secondary differential pressure challenge resulting from a main steam line break (MSLB). NUREG-0844, "NRC Integrated Program for the Resolution of Unresolved Safety Issues A-3, A-4, and A-5 Regarding Steam Generator Tube Integrity" (1988), estimated the containment bypass potential for a core damage release subsequent to such a pressure-induced tube failure. However, previous assessments gave little consideration to the tube failure potential attributable to severe accident conditions. In such circumstances, elevated tube temperatures could accompany a tube differential pressure challenge.

The analysis described in this report draws upon previous risk and thermal-hydraulic analyses of core damage sequences, with a focus on the Surry plant as a representative example. Section 1 presents related background information and summarizes the staff's analytical approach. Section 2 then assesses the frequencies of severe accident scenarios that would lead to a combination of high steam generator tube temperature and pressure.

For Surry, the dominant sequence was station blackout accompanied by a loss of auxiliary feedwater and a failure to maintain secondary system pressure in at least one steam generator. The staff derived the frequency of this sequence using information regarding plant damage states documented in NUREG-1150, "Severe Accident Risks: An Assessment for Five U.S. Nuclear Power Plants" (1990). In addition, the working group evaluated data obtained by searching the individual plant examination (IPE) database to confirm the information from NUREG-1150 and to identify any major differences in sequences of interest or any significant design biases. The database search confirmed that the sequences contributing to "high/dry" core damage (with high primary system pressure and dry steam generators) are dominated by station blackout events, with an additional contribution from other transient events. Comparison of high/dry core damage frequency across plant designs did not reveal any strong design biases.

Section 2 also describes an accident progression event tree (APET), which was developed to characterize the various primary/secondary system conditions that could challenge the steam generator tubes. In particular, the working group used the APET to evaluate the resulting potential for pressure/temperature challenges and to quantify the probability that the steam generator tubes will maintain their integrity under these challenges.

Section 3 describes new thermal-hydraulic analyses using the SCDAP/RELAP5 computer code to assess the effects of variations in the station blackout sequence for Surry. These analyses yielded pressure and temperature histories of the steam generator tubes, as well as the hot legs and surge line, the two other components considered likely to fail.

A key event tree input developed in this study was the probability of tube failure under severe accident conditions. To derive this probability, the working group used a tube failure model, described in Section 4, which takes into account the high temperature effects of such conditions on the integrity of Alloy 600 tubes with part-through-wall cracks. The basis for this model is the results of high-temperature testing of machine-flawed tubes, carried out to tube failure under various temperature and pressure histories. Section 4 also discusses other weak points in the reactor coolant pressure boundary.

Section 5 describes how the working group used the results of the thermal-hydraulic analyses and the tube failure model to estimate the tube failure probability relative to the failure probabilities for the hot leg and surge line. Notably, the working group estimated tube rupture probability separately for each APET branch. To begin this process, the working group first applied the thermal-hydraulic results to predict the creep failure times for each component. Next, the working group estimated tube failure probability on the basis of the relative times to failure of the hot leg or surge line. After determining the failure probabilities for various size cracks, the working group used a flaw distribution to find the overall tube failure probability for each sequence, and the results were applied to each APET endstate. Finally, the working group computed the containment bypass frequency on the basis of the aggregate of these outcomes.

This analysis revealed a number of areas of uncertainty and variability, which could be addressed through additional plant-specific analysis. Specifically, these areas involved reactor coolant system (RCS) component failure frequencies, thermal-hydraulic analysis, tube failure modes, reactor coolant pressure boundary weak points, and representative flaw distributions. The particulars of these areas are discussed in Section 6.

The primary result of this analysis is an overall estimate of the probabilities of pressure- and temperature-induced failure of steam generator tubes and containment bypass frequency for the severe accident challenges considered. The representative calculation using data from the Surry plant indicates that some existing plants could have a potential for containment bypass resulting from tube failure during severe accidents. To delineate the population of plants that may pose a safety concern requires more definitive analysis to consider the uncertainties and plant- and design- specific variabilities outlined above.

SGTR Severe Accident Working Group and Acknowledgements

The following staff members formed the working group or directed its activities:

	C. Ader	RES/DST/AEB
	T. Collins	NRR/DSSA/SRXB
	J. Donoghue	NRR/DSSA/SRXB
	R. Hermann	NRR/DE/EMCB
	R. Jones	NRR/DSSA/SRXB
	R. Lee	RES/DST/AEB
	S. Long	NRR/DSSA/SPSB
	E. Murphy	NRR/DE/EMCB
	J. Muscara	RES/DET/EMMEB
	R. Palla	NRR/DSSA/SCSB
	T. Reed	NRR/DE/EMCB
	J. Schaperow	RES/DST/AEB
	C. Tinkler	RES/DST/AEB
	H. Vandermolen	RES/DST/PRAB
Other contributors:	Y. Chen	RES/DST/AEB
	C. Hammer	NRR/DE/EMEB
	K. Parczewski I	NRR/DE/EMCB
	J. Ridgely	RES/DST/AEB
	A. Rubin	RES/DST/AEB
	J. Staudenmeier	NRR/DSSA/SASG
ANL:	D. Diercks	
	S. Majumdar	
	W. Shack	
Dominion Engineering:	J. Gorman	
INEL:	C. Dobbe	
	D. Knudsen	
SCIENTECH:	H. Dezfuli	
	D. Meyer	
	J. Meyer	

ABBREVIATIONS

AC	alternating current
ADV	atmospheric dump valve
AFW	auxiliary feed water
ANL	Argonne National Laboratory
ANO	Arkansas Nuclear One
AOV	air-operated valve
APET	accident progression event tree
ASEP	accident sequence evaluation program
ASME	American Society of Mechanical Engineers
ATWS	anticipated trip without scram
B&W	Babcock and Wilcox
BCL	Battelle Columbus Laboratories
BNL	Brookhaven National Laboratory
CDF	core damage frequency
CE	Combustion Engineering
COA	crack opening area
DC	direct current
DCH	direct containment heating
DEI	Dominion Engineering, Inc.
ECCS	emergency core cooling system
EdF	Electricité de France
EDM	electro-discharge machining
EMCB	Materials and Chemical Engineering Branch
EOP	emergency operating procedure
EPRI	Electric Power Research Institute
HL	hot leg
HPI	high-pressure injection
HPSI	high-pressure safety injection
HVAC	heating, ventilation, and air conditioning
IGA	intergranular attack
IGSCC	intergranular stress corrosion cracking
INEL	Idaho National Engineering Laboratory
IPE	individual plant examination
LER	licensee event report
LERF	large early release frequency
LMP	Larson-Miller parameter
LOCA	loss-of-coolant accident
LOOP	loss of offsite power
MSIV	main steam isolation valve
MSLB	main steam line break
MSSV	main steam safety valve
MTC	moderator temperature coefficient
NDE	non-destructive examination
NPP	nuclear power plant
NRC	Nuclear Regulatory Commission
NRR	Office of Nuclear Reactor Regulation
NSSS	nuclear steam supply system
ODSCC	outer diameter stress corrosion cracking

ABBREVIATIONS (continued)

ORNL	Oak Ridge National Laboratory
OTSG	once-through steam generator
PDS	plant damage state
PH	precipitation-hardened
PI-SGTR	pressure-induced steam generator tube rupture
PNL	Pacific Northwest Laboratories
PNNL	Pacific Northwest National Laboratories
POD	probability of detection
PORV	power-operated relief valves
PRA	probabilistic risk assessment
PSV	pressurizer safety valve
PWR	pressurized water reactor
PWSCC	primary water stress corrosion cracking
RC	release category
RCP	reactor coolant pump
RCPB	reactor coolant pressure boundary
RCS	reactor coolant system
RES	Office of Nuclear Regulatory Research
RG	regulatory guide
RMS	root-mean-squared
RPC	rotating pancake coil
RPS	reactor protection system
RPV	reactor pressure vessel
RWST	reactor water storage tank
RY	reactor year
SBO	station blackout
SCC	stress corrosion cracking
SCSS	sequence coding and search system
SG	steam generator
SGTR	steam generator tube rupture
SL	surge line
SORV	stuck-open relief valve
SRV	safety relief valve
SV	safety valve
TI-SGTR	temperature-induced steam generator tube rupture
TS	technical specifications
TMI	Three Mile Island
VEPCO	Virginia Electric and Power Company

1 INTRODUCTION

This report is part of the package intended to be issued for public comment regarding regulatory guidance proposed by the U.S. Nuclear Regulatory Commission (NRC). Specifically, the report discusses analysis conducted by the NRC staff to consider the severe accident risk implications associated with degraded steam generator tubes. Beginning in December 1995, an *ad hoc* working group, comprised of staff members from the NRC's Offices of Nuclear Reactor Regulation (NRR) and Nuclear Regulatory Research (RES), conducted this analysis with the overall objective of estimating the incremental risk impact associated with the rupture of degraded steam generator tubes exposed to severe accident conditions.

The analysis explicitly excluded the risk contribution from spontaneous tube ruptures and those induced by transients and design-basis accidents. Tube rupture risk may be considered to arise from three main contributors:

- spontaneous steam generator tube rupture (SGTR) occurring during normal operation
- pressure transient-induced SGTR (resulting from primary-to-secondary differential pressure conditions caused by a design-basis transient or accident)
- core damage-induced SGTR (resulting from a core damage condition)

The risk from spontaneous and pressure transient-induced SGTRs was previously assessed by the staff in NUREG-0844. More recent assessments have shown that if measures are implemented to maintain tube integrity consistent with current requirements, no significant change is expected in the risk from these contributors (Ellison, 1996).

This report discusses the basis for and methods used in the assessment of containment bypass potential attributable to SGTR induced by severe accident conditions. To assemble the inputs used in this study, the staff used the results of work done in several fields, sponsored by both the NRC and industry. The staff then used the documented results of this study as the basis for judgements regarding the impact that implementation of a revised regulatory approach could have on severe accident risk. The conclusions presented here contribute to an understanding of the overall risk presented by challenges to steam generator tube integrity; however, this report also highlights a number of areas that warrant further inquiry. These may be addressed in plant-specific assessments or more definitive analyses to identify the population of facilities that may pose a safety concern.

1.1 Background

In recent years, the NRC has considered changes to steam generator tube integrity requirements. These changes could affect the leakage and structural integrity of the tubes under pressure and temperature challenges. This is significant because steam generator tubes comprise a substantial portion of the reactor coolant pressure boundary, and also play a role in fission product containment. As a result, the staff sought to determine if tube degradation could seriously undermine severe accident containment assumptions by unduly threatening the containment function of the tubes.

The severe accident integrity of steam generator tubes has been considered in the past. However, the NRC and industry directed little attention toward understanding the incremental risk contribution associated with the potential for severe accident-induced failure of degraded tubes. The following documents indicate the extent to which the NRC and industry

had considered severe accident tube challenges before this study began:

- NUREG-0844, "NRC Integrated Program for the Resolution of Unresolved Safety Issues A-3, A-4, and A-5 Regarding Steam Generator Tube Integrity," September 1988, considered pressure-induced SGTR and the resulting core damage potential, but did not address temperature-induced failure.

- NUREG/CR-4551, Part 1, "Evaluation of Severe Accident Risks: Quantification of Major Input Parameters," Vol. 2, Rev. 1, December 1990, considered temperature-induced SGTR through an expert elicitation process. However, despite efforts to understand the influence of tube degradation on the potential for tube failure, this study was limited by a lack of thermal-hydraulic analyses of predicted tube temperatures for the station blackout event.

- Draft NUREG-1477, "Voltage-Based Interim Plugging Criteria for Steam Generator Tubes," June 1993, discussed the results of thermal-hydraulic studies that showed the vulnerability of hot leg and surge line piping during a station blackout. The staff noted that previous studies may not have sufficiently considered tube degradation (when it was considered at all). However, the staff concluded that the level of tube leakage under interim plugging criteria would be sufficiently low and the structural support offered by tube support plates would be adequate, to ensure the continued validity of existing analyses of tube response to high-pressure severe accidents. Detailed analysis of severe accident response was deemed unnecessary.

These previous SGTR risk assessments addressed the potential for tube failure as a consequence of severe accidents to a lesser extent than the current analysis. For instance, previous severe accident studies related to steam generator tube integrity were conducted without data from high-temperature burst testing of tube specimens. Similarly, previous studies did not entail the current level of thermal-hydraulic analysis to predict the expected conditions of the tubes during these scenarios.

In connection with steam generator rule making considerations, the Electric Power Research Institute (EPRI) has published a number of reports related to severe accident tube performance or its risk implications. Those reports document a significant body of research, and are referenced in this report as appropriate; however, use of information from these sources does not constitute the staff's acceptance of the reports in their entirety.

1.2 Approach

The staff used the frequency of containment bypass as its measure of risk significance, and the results of this study are presented in terms of that parameter. A bypass frequency of 10^{-6} per reactor year or greater was considered a significant value.

Initially, the staff sought to determine if it would be possible or even appropriate to use a generic treatment of the risk associated with tube failure under severe accident conditions. As the work progressed, the staff found that a large number of plant-specific factors significantly influence the potential for induced tube failure. Existing experimental evidence demonstrates that, during a severe accident, flows of superheated gas are not expected to reach steam generator tube bundles in the Babcox & Wilcox once-through steam generator (OTSG) designs. Therefore, consideration of OTSG designs is excluded from this study. In fact, this report only considers plants with u-tube steam generator (SG) designs, using information considered typical of that portion of the pressurized water

reactor (PWR) population.

Further, in order to accommodate the resource and schedule commitments for rule making, the staff largely focused this study on the Surry plant as a single representative example. In this example, the staff considered those severe accident progressions most likely to present a high-pressure thermal challenge to the steam generator tubes. To estimate the containment bypass probability associated with temperature-induced tube rupture following a core damage event, the staff built upon and used information from previous risk assessments, recent thermal-hydraulic calculations, and newly developed high-temperature tube performance evaluations.

1.3 Results and Conclusions

The representative analysis for Surry yielded a containment bypass frequency (associated with severe accident-induced tube failure) of approximately 3.9×10^{-6} per reactor-year (/RY), representing a reduction of approximately 1-in-4 with regard to the initiating frequency for the core damage challenge characterized by high reactor coolant system (RCS) pressure with a dry secondary. Considering the possible range of initiating frequencies among PWRs (see Section 2.1), plant-specific results could range from 10^{-7} to near 10^{-5} per reactor-year.

An important characteristic of the Surry results is that 60 percent of the bypass frequency is attributable to temperature-induced SGTR (2.4×10^{-6}/RY), with pressure-induced SGTR accounting for the balance (1.5×10^{-6}/RY). Also, the major contributor to temperature-induced SGTR (75 percent) is associated with sequences involving failures of reactor coolant pump (RCP) seals resulting in loss-of-coolant accidents (LOCAs). Although such sequences represent only about 18 percent of the initiating event frequency, they account for nearly half of the containment bypass frequency. This disproportionate relationship arises because these sequences have an unusually high probability of temperature-induced SGTR.

The working group drew significant conclusions from the results of sensitivity studies conducted on the basis of the representative Surry analysis (see Section 5.3.2). First, the impact of RCP seal LOCA on tube failure was evident in the results of Sensitivity Case 6. Despite the RCS depressurization benefit that could be assumed from an RCP seal leak, the Surry analysis showed that the associated potential to clear an RCS loop seal greatly contributed to tube failure potential for the sequences studied.

Next, the significance of secondary system pressure integrity appears to be at least as important to tube survivability as is the ability to depressurize the RCS. Although plant-specific differences could yield somewhat different values at other facilities, the large impact of secondary system pressure integrity would probably be evident in the other plant-specific analyses. The sensitivity cases also demonstrated that the assumed flaw distribution can have a major impact on the results. Sections 5 and 6 discuss these insights more thoroughly.

Another insight underlying the representative analysis is that the range of uncertainties encountered and their plant- and design-specific nature limits the generic applicability of the results. While the staff could not demonstrate the associated risk at all facilities through a generic analysis, plant-specific analysis could demonstrate the containment bypass vulnerability at a particular plant. In arriving at an estimate of containment bypass probability, analysts should address uncertainties in a variety of areas, such as those listed below. In addition, analysts should address the effects of a range of plant-specific

factors. For example, plant configurations could affect thermal-hydraulic conditions and event progressions, and tube degradation states could vary among facilities; these could be specified for plant-specific analyses.

Through this analysis, the staff discovered a significant number of areas that could benefit from further study. In particular, the uncertainties surrounding the characterization of flaw distribution make it difficult to draw definitive conclusions from this assessment and to propose practical implementations of these methods. Although the results derived for the Surry plant appear sufficient to permit a scoping assessment for risk, the following plant- and design-specific considerations could significantly change the results, as discussed in Section 6:

- event tree quantification
- thermal-hydraulic analysis
- tube performance modeling, including assumed flaw distribution
- reactor coolant pressure boundary weak points
- implications of tube leakage under high-pressure core damage conditions

An overriding conclusion is that the range of uncertainties involved and the plant- and design-specific nature of the uncertainties encountered in this analysis limit the generic applicability of the Surry results to other facilities. Also, the representative analysis results based on the Surry plant indicate that some PWRs may be subject to a containment bypass risk attributable to tube failure during severe accidents. However, more detailed investigation of plant-specific factors involved in the analysis is needed to determine which plants, if any, may pose a safety concern.

2 SEVERE ACCIDENT CHALLENGES TO STEAM GENERATOR TUBE INTEGRITY

Sections 2.1 and 2.2 discuss challenges to steam generator tubes, with regard to structural integrity and accident-induced leakage, Section 2.3 discusses the staff's use of an accident progression event tree (APET) to assess the frequency of severe accident challenges to the tubes, and summarizes the implications of tube failure on containment bypass frequency. In addition, Section 2.3 quantifies the containment bypass frequency and its implications for Surry, a Westinghouse plant, as an example. Finally, Section 2.4 discusses and evaluates the impact of reactor design differences on accident response, and evaluates the generic applicability of the APET as it relates to those differences.

2.1 Challenges to Structural Integrity

Loss of structural integrity in steam generator tubes can result from excesses in either pressure or temperature. Pressure-induced failures result from increased differential pressures across the steam generator tubes, with the primary and secondary systems near normal operating temperature. Such challenges could result from either secondary side depressurization (e.g., main steam line break (MSLB) or transient with stuck-open atmospheric dump valve), or primary system over pressurization (e.g., certain events involving an anticipated transient without scram (ATWS) that lead to large pressure excursions). The potential for a pressure-induced steam generator tube rupture (SGTR) should be limited through compliance with the criteria for structural integrity and the operational leak rate limit contained in plant Technical Specifications. Section 2.3.4 of this report discusses these events in greater detail.

Temperature-induced failures of flawed steam generator tubes could result from the combination of substantially elevated steam generator tube temperature and differential pressure. Such conditions are predicted to occur during the core damage phase of certain severe accidents. The potential for a temperature-induced tube failure can be characterized relative to other reactor coolant system (RCS) piping in terms of the primary-to-secondary side pressure differential and the tube temperatures resulting from the cladding oxidation phase of the event. In general, the requisite conditions for temperature-induced steam generator tube failure associated with severe accidents include dry steam generator secondary side (no auxiliary feed water available) *and* elevated primary-to-secondary system differential pressure.

Events in which core damage occurs with the primary system at high pressure (i.e., at or near the power-operated or safety relief valve set point) and the secondary side dry and depressurized are generally considered to pose the greatest threat of temperature-induced SGTR. However, analyses performed by the NRC staff indicate that events with the primary system at intermediate pressures (i.e., above normal operating differential pressure) may also pose a substantial threat to tube structural integrity. The following subsections provide additional detail regarding the accident sequences of greatest concern for temperature-induced failure of steam generator tube structural integrity. The expected frequency of these events is discussed in Section 2.3.

2.1.1 High-Pressure Core Melt with Intact or Depressurized Steam Generator(s)

Station blackout (SBO) sequences account for the majority of events in which core damage occurs with the primary system at high pressure and the secondary side dry. SBO sequences can be categorized as short-term or long-term, and may also involve reactor coolant pump

(RCP) seal loss-of-coolant accidents (LOCAs), as summarized below:

- **Short-term SBO** relates to sequences in which turbine-driven auxiliary feedwater (AFW) pump trains fail to operate and AC power is not recovered before the core is damaged. These sequences typically lead to core damage within about 2 hours.

- **Long-term SBO** relates to sequences in which turbine-driven AFW pump trains operate initially, but ultimately fail (normally as a consequence of battery depletion) before recovery of AC power. These sequences typically lead to core damage in more than 2 hours.

- **SBO with RCP seal LOCA** relates to sequences in which RCP seal LOCAs arise because of a loss of cooling to RCP seals with failure to recover AC power before the core is uncovered. These sequences can lead to core damage in either the short-term or long-term, depending on the timing and magnitude of the RCP seal LOCA.

In the typical SBO core melt sequence considered during this analysis, steam generator dryout results in loss of decay heat removal via the steam generators, with eventual loss of RCS inventory and uncovery of the core. (Front-line injection systems are unavailable.) As core damage progresses, the RCS and steam generator tube temperatures increase as substantial amounts of energy are transported from the core region to other parts of the RCS. The rate of accident progression and the primary/secondary system conditions at the time of core damage influence the location and timing of RCS failure. These factors, in turn, depend on plant-specific design features and the details of the sequence. Such details include the impact of stuck-open pressurizer power-operated relief valves (PORVs) or safety valves (SVs), RCP seal LOCAs, operation of steam generator atmospheric dump valves (ADVs) or main steam safety valves (MSSVs), and longer-term depressurization of the secondary side as a consequence of leakage from MSSVs or main steam isolation valves (MSIVs).

In SBO events in which the plant maintains RCS pressure integrity (i.e., pressurizer relief valves reclose and RCP seals remain intact), core damage would occur with the primary system at or near the PORV set point (if PORVs remain available throughout the event) or the SV set point (if PORVs are not available or have failed closed). All Westinghouse plants and the majority of Combustion Engineering (CE) plants are equipped with PORVs. Most PORVs are air-operated with a DC-powered solenoid. However, several plants have either AC- or DC-powered motor-operated PORVs, and several plants operate with some or all PORVs blocked. PORVs would generally be available throughout a short-term SBO (core damage with DC power and instrument air available) and unavailable at the time of core damage in long-term SBO events (core damage following depletion of battery and instrument air), but actual availability is plant- and sequence-dependent.

The secondary side could be depressurized early in an event (before steam generator dryout) as a result of several mechanisms. Such mechanisms may include operator actions to depressurize the steam generator using ADVs or other valve alignments, a stuck-open MSSV, a stuck-open ADV with failure to manually isolate using the block valve, or failure to isolate steam flow to the turbine-driven AFW pump in sequences in which the pump was initially operable. Of these mechanisms, a stuck-open MSSV is generally considered to be the most likely means of depressurization. However, the relative contribution of the various mechanisms will depend on plant-specific design features and operating procedures. For example, ADVs are not available during SBO at certain plants because of dependencies or

limitations on electrical power or instrument air.

Gradual depressurization of the steam generators could also occur in the longer term (during the period between steam generator dryout and core damage) as a consequence of leakage through MSIVs and other secondary side valves. As a result, the steam generators would be depressurized at the time of core damage. Section 2.3.1 provides additional detail concerning the potential for early and gradual depressurization in the context of the accident progression event tree.

2.1.2 Intermediate-Pressure Core Melt With Depressurized Steam Generator(s)

Transient events (such as SBO) generally proceed to core damage with the primary system at or near the PORV or SV set point. However, RCP seal LOCAs or failure of pressurizer valves to reclose/reseat could cause the RCS to be partially depressurized at the time of core damage. The extent of depressurization is sequence- and plant-specific, and depends on such factors as the timing and leak area associated with the valve failure/seal LOCA, and accumulator injection set points.

The staff recognized that a lower RCS pressure at the time of core damage would reduce the challenge to steam generator tube structural integrity. To evaluate the probability of such an RCS pressure reduction, the staff conducted a survey of previous severe accident analyses of scenarios involving stuck or latched open PORVs and various RCP seal LOCAs for Westinghouse and CE plants. That survey considered SCDAP/RELAP5 calculations performed as part of the Severe Accident Management Program, as well as more recent SCDAP/RELAP5 analyses performed in support of the resolution of direct containment heating. In addition, the survey reviewed the results of earlier analyses performed using the MARCH code, as well as available MAAP analyses.

Unfortunately, the staff's survey indicated that a reduction of RCS pressure could be offset by rapid repressurization and heating of steam generator tubes, which may occur during the accumulator injection phase of an accident. For both stuck/latched open PORVs and seal LOCAs, pressure response at the time of core damage tended to be oscillatory in nature and driven by accumulator discharge. Baseline pressures were in the range of the accumulator set point, with periodic pressure increases up to 6.9-9.7 MPa (1000-1400 psia) following accumulator injections. The staff also noted concurrent temperature excursions in the steam generator tubes, with peak temperatures approaching 1200 K (1700°F) for large RCP seal LOCAs, but lower peak tube temperatures for the stuck-open PORV cases.

The staff recognized similar behavior for Westinghouse and CE plants, but the available analyses for CE plants were more limited. A comparison of these observations with the results of available MAAP calculations revealed significant differences in the degree of repressurization following accumulator injection, as predicted by the SCDAP/RELAP5 and MAAP codes. Notably, the predicted pressures at the time of peak steam generator tube challenge ranged from as high as 10 MPa (1450 psig) in early SCDAP/RELAP5 calculations to essentially the accumulator set point (no repressurization) in MAAP calculations.

The reader should note that these observations were reached largely on the basis of analyses of short-term SBOs (i.e., stylized sequences in which AFW failure is assumed to occur as part of the initiating event), and did not consider long-term SBOs (in which AFW typically fails after several hours as a result of battery depletion). However, observations from long-term SBOs involving stuck-open PORVs would not be much different, since the time available between PORV cycling/failure and core damage would not be significantly longer

than in short-term SBOs.

Because of the potential challenge to steam generator tubes from sequences involving RCP seal LOCAs and stuck-open PORVs, the thermal-hydraulic response and the underlying phenomena responsible for primary system repressurization during these sequences were further evaluated as part of this study. Section 3 provides additional detail regarding these analyses.

2.1.3 Contribution of ATWS Sequences to Accident-Induced SGTR

The model for the Surry plant documented in NUREG-1150 (U.S. Nuclear Regulatory Commission, 1990) yielded baseline estimates for the contribution of ATWS to the core damage frequency (CDF) and various plant damage states (PDSs). In this model, the ATWS frequency is 6.7×10^{-5}/RY, which includes the frequency (T) of reactor scram, the probability (K) of the reactor protection system (RPS) failing to trip the reactor, and the probability (R) of the operators failing to trip the reactor manually within 1 minute following RPS failure.

The model divided the scrams by reactor power level, so that the overall ATWS frequency of 6.7×10^{-5}/RY is divided into four main categories:

(1) low power, with a frequency of 6.7×10^{-6}/RY
(2) high power with low moderator temperature coefficient (MTC), at a frequency of 3.0×10^{-5}/RY
(3) high power with intermediate MTC, at a frequency of 2.9×10^{-5}/RY
(4) high power with high MTC at a frequency of 8.4×10^{-7}/RY.

The first category occurs at a power level low enough that turbine trip is not necessary to limit the RCS pressure increase to 22 MPa (3200 psig), and the effects of MTC are not important. The other three groupings are according to MTC, with a probability of 0.5 that the MTC is low enough (less than -20 pcm/°F) that turbine trip and RCS relief valve operation are not necessary to control RCS pressure below 22 MPa (3200 psig). The model uses a probability of 1.4×10^{-2} that the MTC is too high (above -7 pcm/°F) to provide any chance for mitigation of the ATWS transient. The remainder of the model estimates the failure probabilities of turbine trip, primary pressure relief, auxiliary feedwater, relief valve reclosure, and high-pressure injection, with appropriate success criteria applied to each of these five groups.

Only two ATWS sequences contribute to the dominant cutsets in the NUREG-1150 model for Surry. The largest ATWS contributor to CDF is the group with high power and high MTC. This sequence (denoted TKRZ) has a frequency of 8.4×10^{-7}/RY in the NUREG-1150 analysis. The other significant ATWS contributor to CDF is a sequence in the group with high reactor power and intermediate MTC (denoted $TKRD_4$). This sequence involves failure of the high- pressure safety injection (HPSI) system, which prevents boration and causes the core to melt at high pressure when it is uncovered by reactor coolant loss through the pressurizer relief valves. This sequence contributes an additional 5.7×10^{-7}/RY to CDF.

Although the NUREG-1150 process considered the possibility of inducing SGTR by increasing the pressure differential or temperature, this possibility was assigned such a low probability that it was not dominant and, therefore, was discussed only briefly in the documentation. NUREG-1150 also includes a sensitivity study performed to determine the effects of eliminating the probabilities for thermally induced ruptures (hot leg, surge line and tubes, together) on the frequency of various release categories, but the effects were

small. The NUREG-1150 analysis did not include a sensitivity study of the effects of significant increases in tube rupture probability.

The staff found it necessary to consider two potential effects of known tube flaws on the progression of ATWS events. Such flaws are significant because they could be allowed to remain in service under revised Technical Specifications. One potential effect is pressure-induced rupture of one or more of the flaws as a consequence of the increase in RCS pressure that occurs early in an ATWS event. This could lead to core damage by the same mechanisms considered for pressure-induced SGTR caused by secondary-side depressurization events (increasing the core damage frequency and the frequency of containment bypass type releases). The second potential effect is thermally induced SGTR as a result of the high-temperature gases evolved in the core melting phase of ATWS events that are already counted in the core damage frequency. This could increase the estimated frequency for the containment bypass type release without increasing core damage frequency.

Since the completion of NUREG-1150, two significant changes in reactor operations have occurred that directly affect this analysis. The first change is a reduction in the frequency of reactor trips. The NUREG-1150 analysis was conducted when the average scram frequency was about 6.6/year. Since then, a scram reduction program conducted by the industry has reduced that frequency to about 1.4/year for PWR plants (Smith, 1996). This, in turn, reduces the frequency of all ATWS sequences (core damage and successful mitigation) by a factor of 0.21.

The second change since NUREG-1150 was completed involves the fraction of time that MTC is above -7 pcm/°F. The NUREG-1150 analysis assumed that this condition exists during 1.4 percent of the operating cycle (corresponding to a probability of 1.4×10^{-2} as previously stated). The NRC analysis conducted for the ATWS rule making process assumed that Westinghouse reactors would exceed an MTC of -7 pcm/°F approximately 5 percent of the time. Since that analysis, the NRC has approved many plant-specific technical specification changes that could allow the occurrence of this MTC condition for a substantially greater portion of the operating cycle.

For instance, a report of core operating limits for Surry allows an MTC as high as 0.0 pcm/°F when the reactor is above 50 percent rated power. However, informal discussions with Surry plant engineers indicated that the last four Surry fuel cycles actually incurred no operating time with MTC less negative than -7 pcm/°F with the reactor at full power, all rods out, and no xenon. It appears that administrative limits on fuel load fabrication, which account for uncertainties to avoid violation of the technical specifications, can have a significant effect on the actual fraction of the fuel cycle with MTC above -7 pcm/°F. Therefore, for this analysis, the staff chose a value of 5 percent to be consistent with the value most recently used by the agency, with a caution that plant-specific values may differ substantially.

Use of the 5 percent value increases (by a factor of 3.6) the frequency of ATWS core damage sequences resulting from high MTC. Presumably, this increase also has an effect on the fraction of the cycle during which MTC is low enough ($\leq$-20 pcm/°F) that turbine trip and primary pressure relief are not important; however, NUREG-1150 used 50 percent for that fraction. Therefore, the effect on the frequency of the core damage sequences between -7 and -20 pcm/°F is limited to a factor of 2 and is expected to be much smaller than that. The staff did not consider this effect further for the analyses discussed below.

The following discussions first focus on the effects of ATWS-induced SGTR on the analyses

presented in NUREG-1150, and then discuss the effects of the more recent operating parameters.

2.1.3.1 Pressure-Induced SGTR Resulting from ATWS Events

The frequency for ATWS events used in NUREG-1150 is 6.7×10^{-5}/RY. Of those events, a subset associated with high power and high MTC (denoted TKRZ) may result in RCS pressure exceeding 22 MPa (3200 psig) with a frequency of 8.4×10^{-7}/RY. In addition, the RCS pressure can exceed 22 MPa (3200 psig) as a result of non-dominant core damage sequences associated with failure of the operator to promptly trip the turbine, or failure of two pressurizer relief valves, or failures in the AFW system. On the basis of information available in supporting documents for NUREG-1150, the staff estimated that TKRZ events plus these additional non-dominant sequences have a combined frequency of 1.2×10^{-6}/RY. Thus, of all ATWS events, the subset leading to high RCS pressure (approximately 98 percent) would not produce a differential pressure across the steam generator tubes in excess of approximately 15.2 MPa (2200 psid). An alternative considered by the staff would limit the conditional probability of tube rupture to 0.05 per steam generator experiencing a differential pressure of 17.2 MPa (2500 psid). Therefore, the probability of rupturing at least one tube in each steam generator would not exceed 0.05 for 98 percent of the ATWS frequency. The other 2 percent of the ATWS frequency is already reflected in the CDF, as addressed later in this section.

2.1.3.2 Pressure-Induced SGTR Resulting from ATWS Events Not Reflected in CDF

The low-power and low-MTC ATWS events are expected to yield much lower RCS pressures, probably in the range of the RCS relief valve set points. Therefore, the staff excluded these events from further consideration of pressure-induced SGTR resulting from ATWS. This leaves only the ATWS events with high RCS power and intermediate MTC for this part of the analysis. That group has a frequency of 2.9×10^{-5}/RY. These events will subject all steam generators in the plant to elevated differential pressures up to 15.2 MPa (2200 psid). As a bounding analysis for this class of ATWS events, each steam generator is assumed to have a probability of 0.05 for induced rupture of one or more tubes. However, these sequences will create pressure differentials below 15.2 MPa (2200 psid) and the proposed limit applies at a higher differential pressure, near 17.2 MPa (2500 psid).

Assuming that the probabilities of rupture in the affected generators are independent of each other, Table 2.1a presents the frequencies for ATWS pressure-induced SGTR as a function of the number of generators in the plant. The assumption of independence is probably conservative. Thermal-hydraulic calculations by Idaho National Engineering Laboratory (INEL, now Idaho National Engineering and Environmental Laboratory or INEEL) have shown that tube ruptures reduce the peak pressure of ATWS transients. This, in turn, reduces the differential pressure across the tubes, as well as the probability of additional tube ruptures in the same or other steam generators. The issue of common cause failures is included by assigning the highest probability of failure to all of the generators.

Table 2.1a Frequencies for ATWS Pressure-Induced SGTR (NUREG-1150 Probabilities)

No. of SGs in Plant	Frequency of ATWS Pressure-Induced Rupture of			
	1 SG	2 SGs	3 SGs	4 SGs
2	$2.8X10^{-6}$	$7.3X10^{-8}$	-	-
3	$4.1X10^{-6}$	$2.1X10^{-7}$	$3.6x10^{-9}$	-
4	$5.0X10^{-6}$	$3.9X10^{-7}$	$1.4X10^{-8}$	$1.8X10^{-11}$

Table 2.1b Frequencies for ATWS Pressure-Induced SGTR (Updated Probabilities)

No. of SGs in Plant	Frequency of ATWS Pressure-Induced Rupture of			
	1 SG	2 SGs	3 SGs	4 SGs
2	$5.9X10^{-7}$	$1.5X10^{-8}$	-	-
3	$8.6X10^{-7}$	$4.4X10^{-8}$	$7.6X10^{-10}$	-
4	$1.1X10^{-6}$	$8.2X10^{-8}$	$2.9x10^{-9}$	$3.4X10^{-11}$

As shown in Table 2.1b, however, these frequencies are reduced when more recent data on reactor trip frequency are considered. The staff did not consider the effects of the higher probability of unfavorable MTC because the slight decrease caused by a higher probability of exceeding an MTC of -7 pcm/°F may be offset by a slight increase in the probability of exceeding -20 pcm/°F. (Here, the term *exceeding* is used in the sense of an absolute value.)

With regard to the ATWS sequences, the effects of a pressure-induced SGTR would allow for increased boration of the core, except for the 0.95 percent of the time that the HPSI system fails. (This is the $TKRD_4$ sequence that is already expected to result in core damage, as discussed shortly.) For the remaining ATWS sequences, increased boration should help to ensure that the reactor is effectively shut down. The issue therefore becomes the ability to mitigate the SGTR by cooling down and depressurizing the reactor before the refueling water storage tank (RWST) is emptied and the core becomes uncovered.

Thus, these ATWS pressure-induced SGTR sequences should transfer to the trees used for SGTR induced by secondary-side depressurizations. For the majority of the ATWS pressure-induced SGTR frequency, tubes are expected to rupture in only one generator, so the scenario is similar to the effect from secondary depressurization. Because it may still be possible to eventually isolate the secondary side in the ATWS pressure-induced sequences, the event trees originating with secondary side failures should be conservative for ATWS pressure-induced SGTR when they involve tube ruptures in only one steam generator. However, the recovery may be complicated by the actuation of containment spray, which would transfer some of the RWST inventory to the containment sump and require the emergency core cooling system (ECCS) system suction to be transferred to the containment sump during recovery. Because the other initiator frequencies for the secondary depressurization-induced SGTR trees include events in the range of 10^{-3}/RY, these additional ATWS events are not expected to have a significant effect on the estimated frequency of pressure-induced SGTR leading to core damage with bypass type releases.

Ruptures involving only two steam generators in a four-loop plant are not expected to complicate the recovery very much, and can be treated similarly. By contrast, ATWS pressure-induced ruptures involving three steam generators at a four-loop plant or two steam generators at a three-loop plant are somewhat more complicated. This is because the operators may hesitate to use faulted steam generators, which may be required for cooldown. Successful recovery is still possible with tube ruptures in all generators. Sequences affecting most or all of the steam generators are considered to be sufficiently infrequent to be neglected without further detailed analysis. This is because the frequencies are already low, because they are upper bound estimates, and because the mitigation probability is expected to decrease the frequencies by at least another order of magnitude.

2.1.3.3 Pressure-Induced SGTR Resulting from ATWS Core Damage Sequences

Next, it is necessary to consider the potential increase in the frequency of containment bypass type releases as a consequence of pressure-induced SGTR during the ATWS sequences that exceed an RCS pressure of 22.1 MPa (3200 psig). Bounding considerations are not very helpful because the differential pressure across the steam generators may exceed the value used as the basis for tube structural integrity considerations. As a result, the conditional probability of SGTR is not limited to 0.05 in this analysis, and other information would be necessary to show that the frequency of inducing SGTR is less than the frequency with which the RCS exceeds 22.1 MPa (3200 psig).

Use of the more recent scram frequency and MTC probability data would decrease the frequency of all ATWS sequences by a factor of 0.21 and increase the TKRZ sequence frequency by a factor of 3.6. The net effect would be a slight decrease in the bounding estimate (to 7.2×10^{-7}/RY) for the frequency of ATWS pressure-induced bypass releases from the sequences in which the RCS exceeds 22.1 MPa (3200 psig).

An ATWS pressure-induced SGTR would alter the course of the high-power, high- MTC (TKRZ) sequence, and possibly the PDS. Thermal-hydraulic analyses of this sequence conducted using the SCDAP/RELAP5 code (Coryell, 1995) show that the induced SGTRs substantially decrease the maximum pressure in the RCS. However, in at least 95 percent of the events, this should not occur before the differential pressure across the tubes exceeds 17.2 MPa (2500 psid), which is equivalent to the RCS exceeding 24.1 MPa (3500 psig), assuming about 6.9 MPa (1000 psig) secondary side pressure.

RCS pressures above 22.1 MPa (3200 psig) are assumed to cause plastic deformation of the injection valves to the RCS and fail ECCS functions. Consequently, subsequent depressurization of the RCS by induced SGTR would not allow the HPSI system to borate or restore RCS inventory, and the core would melt with the primary-to-secondary boundary breached. In order to more precisely estimate the conditional probability of pressure-induced SGTR for the high-power, high-MTC (TRKZ) sequences, it would be necessary to develop a frequency distribution for the maximum RCS pressures and a probability distribution for SGTR as a function of differential pressure.

It is also important to consider that the risk of ATWS is greatest at the beginning of the fuel cycle, but the steam generator tubes are weakest at the end of the fuel cycle. This temporal anti-correlation will also decrease the "best estimate" from the estimate derived above. However, quantification of that decrease would depend on the plant-specific nature and rate of tube degradation processes, the probability of detecting flaws through routine tube inspections, and the MTC as a function of time for the specific core load. Because this subset of ATWS events can cause pressures to exceed structural integrity values for the

tubes, it is not possible to argue that the tubes are capable of withstanding these events at the beginning of core life.

2.1.3.4 ATWS Thermally Induced SGTR

The remaining consideration is the potential for thermally-induced SGTR during the fuel cladding oxidation phase of the ATWS core damage sequences. The ATWS sequences that appear in the dominant cutsets for core damage frequency are those associated with high reactor power and high or intermediate MTC (TKRZ and $TKRD_4$). For the high-power, high-MTC (TKRZ) sequence, NUREG-1150 assigned a PDS (S_3NYY-YxN) involving the following conditions:

- A very small break has been induced in the RCS pressure boundary.
- ECCS is not operating and not recoverable.
- The RWST inventory has been injected into containment.
- At least one AFW pump is operating.
- The steam generators are still pressurized.

For the high-power, intermediate-MTC sequence ($TKRD_4$), NUREG-1150 assigned a PDS (TLYY-YxY) involving the following conditions:

- The RCS is intact (and at high pressure).
- Only low-pressure ECCS is available.
- The RWST inventory has been injected into containment.
- At least one AFW pump is operating.
- The steam generators are still pressurized.

Thermal-hydraulic calculations performed using SCDAP/RELAP5 indicate that high-pressure core melt events will not result in thermally induced SGTR unless the secondary sides of the steam generators are dry and depressurized. Therefore, neither PDS assigned to the dominant ATWS core damage sequences would be capable of thermally inducing SGTR and altering the nature of the release to increase the frequency of the bypass type of release.

The staff further considered the contribution of non-dominant high-pressure ATWS sequences. The $TKRL_2$ sequence is part of the group of non-dominant ATWS core damage sequences that exceed 22.1 MPa (3200 psig) in the RCS. That group was included (with a frequency of 2.9×10^{-5}/RY) in the estimated frequency of pressure-induced SGTR discussed above, where the conditional probability of SGTR was left at 1.0. Thus, it should not be counted again for thermally induced SGTR. The non-dominant $TKRL_2$ ATWS sequence involving failure of the AFW system had a frequency of 6.8×10^{-8}/RY before recovery and was dropped from further analysis in NUREG-1150. Using NUREG-1150 information considering equipment failures in addition to AFW during ATWS events leading to high RCS pressure, the staff back-calculated a probability of 2.3×10^{-3} for AFW system failure.

Other sequences that involve AFW failure are $TKRPL_2$ (which occurs at low power) and $TKRZ_1L_2$ (which occurs at high power with low MTC). Using 2.3×10^{-3} for the probability of AFW system failure (as explained above), these sequences are estimated to have a combined frequency of 1.2×10^{-7}/RY before recovery. Consideration of the more recent reactor trip frequencies would reduce this estimate to 2.5×10^{-8}/RY. In addition to recovery, this frequency would be reduced by the probability that the steam generators would not actually be dry or depressurized.

Because successful recovery from ATWS requires operation of two motor-driven AFW pumps or

the turbine-driven AFW pump, one motor-driven pump may be operating in many of the cutsets for these two sequences. On that basis, the staff eliminated these sequences from further consideration because they are insignificant with respect to the contributions to the frequency of thermally induced SGTR during SBO sequences, and are only minimally significant with respect to the surrogate safety goal.

Thus, in consideration of the evaluation discussed in this section, the staff does not expect thermally induced SGTR during ATWS core damage sequences to have a significant effect on the frequency of bypass releases.

2.1.3.5 Conclusions

ATWS sequences that would not lead to core damage in the NUREG-1150 analysis are not expected to significantly increase the frequency of core damage with bypass type releases by inducing SGTRs that then lead to core damage. Similarly, ATWS sequences that lead to core damage in the NUREG-1150 analysis by paths that do not involve RCS pressures in excess of 22.1 MPa (3200 psig) are not expected to contribute significantly to the frequency of thermally induced SGTRs during severe accidents because the majority of those sequences have water on the secondary side of the steam generators.

ATWS sequences in the NUREG-1150 analysis that lead to core damage by paths involving RCS pressures in excess of 22.1 MPa (3200 psig) may produce a non-negligible contribution to the bypass release frequency. Assuming that the conditional probability of rupturing one or more tube(s) is equal to 1. bounding calculations result in a frequency estimate in the mid-10^{-7}/RY range. The staff derived this estimate using an assumption that MTC is above -7 pcm/°F for only 5 percent of the fuel cycle. However, the possibility exists that recent fuel loads might exceed this percentage by a significant factor. If so, plant-specific evaluation may be warranted.

2.2 Accident-Induced Challenges to Leakage Integrity

Besides SGTR, severe accident conditions can lead to elevated primary-to-secondary leakage through existing tube flaws. The maximum tube leakage condition is expected under high primary and low secondary system pressures, which present the highest leakage driving force.

Section 2.2.1 discusses the expected magnitude of primary-to-secondary leakage through existing tube flaws under the elevated temperatures associated with severe accidents. Section 2.2.2 then addresses the modeling and impact of tube leakage on thermal-hydraulic response.

2.2.1 Expected Leak Rates Under Severe Accident Conditions

Previous studies conducted by the NRC and industry predicted leak rates associated with flawed tubes under accident conditions near operating temperatures, and usually assumed MSLB differential pressures. For example, NUREG/CR-2336 (Kurtz, 1988) describes a model to predict leak rates from axial and circumferential through-wall cracks in steam generator tubes. That model involved applying fracture mechanics solutions to determine the crack opening area as a function of crack length and internal pressure. The model then used fluid mechanics to predict the flow of primary water through the crack. Primary conditions were saturated or subcooled, and the flow became two-phase through the crack. Further, the tube temperatures were relatively low compared to those expected during severe accident

conditions. Therefore, the model presumed that only differential pressure loads on the tube would affect the crack opening area. Leak rates computed using this model ranged from about 0.04 Lpm (0.01 gpm) for a 0.51-cm (0.2-inch) crack to almost 37.9 Lpm (10 gpm) for a 2.54-cm (1-inch) crack, as shown in Figure 2.1.

EPRI also described a study of leakage rates associated with flawed tubes in their report regarding expansion zone primary water stress corrosion cracking (PWSCC) in roll transitions (EPRI Committee for Alternate Repair Limits, 1993). In that study, EPRI used a model with a similar basis (fracture mechanics and thermal-hydraulics) to estimate leak rates under MSLB conditions through an axial crack initiated on the primary-side tube wall. The model predicted leak rates ranging from less than 0.04 Lpm (0.01 gpm) for a 0.51-cm (0.2-inch) axial crack, to about 22.7 Lpm (6 gpm) for a 1.3-cm (0.5-inch) crack.

The drawback in applying either of these approaches to the severe accident case is that the earlier MSLB models use fluid and tube temperatures that are much lower than those expected in severe accident scenarios. These lower temperatures mean that the models consider the flow of liquid rather than steam, and the crack opening area model does not include thermal effects at extreme temperatures.

The most recent and directly relevant study, conducted by EPRI (FUller, January 1996), employed a structural evaluation method to furnish a best-estimate leak rate for high-pressure and temperature primary side conditions. In addition, this study used a crack opening area model to estimate the effect of elevated temperatures on the crack size. Table 3-4 of the EPRI report summarized the estimated leakage of water for all of the tubes in the steam generator ranging from 0 Lpm (0 gpm) at a peak tube temperature of 935 K (1223°F) to 757 Lpm (200 gpm) at 960 K (1268°F). The report did not offer the thermal-hydraulic basis for this prediction, although it did provide an equivalence of 1 kg/s (2.2 lbm/s) steam flow through a crack opening that would allow water leakage of 379 Lpm (100 gpm).

The plausibility of these leakage rates may be explored, starting with the equation for leakage from an axial crack in a tube with internal pressure (provided as equation 5-1 in EPRI report NP-6864-L). Assuming RCS conditions during an MSLB of 589 K (600°F) and 16.5 MPa (2400 psig), the crack area obtained for the 379-Lpm (100-gpm) value is approximately 0.65 cm^2 (0.1 in^2). This value is consistent with the crack opening area presented for normal operating temperatures in EPRI NP-6864-L and EPRI TR-106194. Applying the same leakage equation and using a crack opening area of 0.97 cm^2 (0.15 in^2) (as in EPRI TR-106194 and Figure 2.2) for fifty 1.02-cm (0.4-inch) long cracks at 589 K (600°F) and a tube differential pressure of 16.5 MPa (2400 psig), yields a leak rate of 852 Lpm (225 gpm). This predicted leak rate is on the order of the liquid leak rates discussed in EPRI TR-106194.

To check the equivalent high-temperature steam flow rates through similarly sized cracks, the same number of 1.02-cm (0.4-inch) long flaws that opened under elevated differential pressure should be expected to open to a greater extent under the additional condition of extreme temperature. The crack opening area model in EPRI TR-106194 shows this, giving a crack opening area of 4.0 cm^2 (0.62 in^2) for fifty 1.02-cm (0.4-inch) long cracks at 987 K (1316°F) (Figure 2.2), the average hot tube temperature calculated for Case 3R (see Section 3). However, the relation for leaking fluid used above is not applicable under these high-temperature conditions where superheated steam is expected to exist on the primary side of the tube wall. In this case, the superheated steam may be taken to behave nearly as an ideal gas.

Assuming that the crack acts as an orifice, fluid equations are available from the literature to estimate a steam flow rate. *Mark's Standard Handbook for Mechanical Engineers* (Avallone, 1987) was used in this example. With the average fluid temperature calculated for the base case 987 K (1316°F) and a primary pressure of 17.2 MPa (2500 psig) (the safety valve set point), the equations used yield a steam leak rate of 4.5 kg/s (9.9 lbm/s). A smaller steam flow (3.0 kg/s, 6.6 lbm/s) is predicted for a steam generator with one thousand 0.51-cm (0.2-inch) long cracks. These flow rates are somewhat higher than the EPRI estimate of 1 kg/s (2.2 lbm/s).

An important assumption implicit in these considerations is the nature of the flaw distribution that will be exposed to the severe accident temperatures and pressures. Further, uncertainties exist in the prediction of crack opening area, and the coefficient of discharge for crack flow. However, the estimates documented in EPRI report TR-106194 appear reasonable, although the leakage rates calculated above are somewhat higher. In light of these uncertainties and assumptions, and to ensure that an adequate range of leakage rates is considered for further study, values consistent with the EPRI high-temperature crack opening area model should be used on the basis of the hot steam temperatures calculated in Section 3 of this report. Assuming that the flawed tube populations in Figure 2.2 are reasonable, this yields steam leak rates under severe accident conditions of 3 to 7 kg/s (6.6 to 15.4 lbm/s).

2.2.2 Impact of Tube Leakage

In this analysis, the staff performed SCDAP/RELAP5 calculations (denoted Case 7N in this report) to evaluate the effects on secondary system conditions upstream of the ADV of 379-Lpm (100-gpm) tube leakage escalating to larger leaks of steam under the effects of severe accident temperatures. In these evaluations, the ADV was assumed to be operational, and the crack size associated with the initial leakage of 379 Lpm (100 gpm) was assumed to open, allowing steam leakage, in one case, of 3 kg/s (6.6 lbm/s), and then 7 kg/s (15.4 lbm/s) once steam generator temperatures reached 978 K (1300°F).

The results showed that RCS pressure rapidly decreases to the secondary side relief set point pressure following crack opening. The only difference was the rate of depressurization. Temperature response on the secondary side was similar in the cases, as well. The 379-Lpm (100-gpm) leak produced steam line temperatures of about 790 K (962°F) just before the crack opened. Following crack opening, peak steam line temperatures reached about 915 K (1187°F). Temperatures of important secondary side components downstream from this point (such as ADVs) would probably experience a much smaller temperature increase because of the large heat sink provided by the steam line piping. However, a more detailed evaluation should be conducted to determine the extent of the potential thermal challenge to secondary system components.

2.3 Accident Progression Event Tree

The accident progression event tree (APET) provides a structure for assessing accident progression through the following analyses:

- estimating the frequency of the various primary/secondary system conditions that could challenge the steam generator tubes
- characterizing the core degradation process and resulting pressure/temperature challenges to the RCS and steam generator tubes for each condition or APET branch

- establishing the overall probability that steam generator tube integrity will be maintained over the range of tube challenges

This assessment yields an overall estimate of the frequency of pressure- and temperature-induced failures of steam generator tubes and containment bypass attributable to severe accidents.

Figure 2.3 presents a representative APET addressing pressure- and temperature-induced challenges to steam generator tubes. This APET consists of 1 entry condition and 12 top events. The entry condition (identified by top event heading A on Figure 2.3) is the frequency of core damage events in which core uncovery occurs with the primary system at relatively high pressure and the secondary side dry. This subset of the total core damage frequency is derived from a decomposition of Level 1 probabilistic risk assessment (PRA) results. The first four top events (events B through E) are sorting events that partition the entry condition frequency into nine states reflecting different combinations of primary side conditions (intact, stuck-open pressurizer relief valve, or RCP seal LOCA) and secondary side conditions (intact, one steam generator depressurized, or all steam generators depressurized) that could exist at the time of core uncovery. These states are shown as endstates A1 through C3 on Figure 2.3, and transfer to a continuation of the event tree on Figures 2.3a through 2.3d.

The next four top events (events F through I) reflect changes to the conditions on the primary and secondary side during the accident progression, specifically, primary system depressurization attributable to either failure or manual operation of pressurizer relief valves following core uncovery (event F), and gradual depressurization of one, two, or three steam generators via leakage through MSIVs or valve bonnets (events G, H, and I). At this point in the APET, an icon is provided on each branch summarize the associated primary and secondary system (indicated in the boxes below the "p" and "s" on the icon, respectively). Conditions early and late in the event are separately shown, to the left and right of the fine vertical lines within the icon. Secondary system conditions are separately displayed for each of the three SG loops.

The next three top events (events J through L) address the likelihood of pressure- and temperature-induced tube failures. Top event J addresses the potential for a tube rupture to occur as a result of pressure effects only, before steam generator tube heatup, for the distribution of flaws assumed to be present in the steam generator tubes. Given that the tubes survive the pressure challenge, the next two top events (events K and L) address the likelihood of temperature-induced tube failures under the representative thermal-hydraulic conditions for each branch. Event K represents the probability that loop seal clearing occurs in the same loop in which a steam generator is depressurized. Concurrent loop seal clearing and steam generator depressurization was found to result in enhanced tube heating and high probabilities of failing even pristine tubes in the reference plant analysis. It was therefore treated as a separate event in the APET. Event L addresses the probability of temperature-induced failure of steam generator tubes prior to any other breach of the RCS pressure boundary, given the temperature and pressure histories throughout the RCS for each APET branch, and the distribution of flaws assumed to be present in the steam generator tubes.

The final top event (event M) addresses whether the resulting primary and secondary system conditions are expected to result in significant fission product holdup and retention. Such holdup is expected in sequences in which the primary system is partially depressurized (e.g., as a result of an open pressurizer PORV) and the secondary system is intact but

leaking.

Section 2.3.1 discusses the frequency of challenges to the steam generator tubes. Sections 2.3.2 through 2.3.9 then describe the APET top events. Next, Section 2.4 introduces the process by which the staff determined the probability of thermally induced SGTR. (Section 5 discusses this process in greater detail.) In addition, Section 2.4 discuses the impact of design differences on severe accident challenges, and considers the generic applicability of the event tree to other reactor designs.

2.3.1 Frequency of Events with High RCS Pressure and Dry Steam Generators (APET Entry Frequency)

The initiating event frequency for the APET (event A on Figure 2.3) represents the frequency of events in which core damage occurs with the primary system at relatively high pressure and the secondary side dry. This includes events with the RCS at either full system pressure or partially depressurized, and with the secondary side either intact (at high pressure) or depressurized. Events with a partially depressurized RCS or an intact secondary may appear to represent a less severe challenge to steam generator tubes than events involving full RCS pressure or a depressurized SG, respectively. Nonetheless, the staff retained these constituent events because preliminary thermal-hydraulic and structural analyses suggested that these conditions may also pose some threat to flawed steam generator tubes.

Implicit in the initiating event frequency are the impacts associated with failures of valves to reclose, unavailability of valves caused by a loss of support systems, and operator actions that impact RCS depressurization (e.g., operator actions to depressurize using ADVs or to isolate stuck-open SVs using block valves) to the degree that such actions were modeled in the PRA. The reader should note that operator actions modeled in the NUREG-1150 study were generally limited to actions included within the plant-specific emergency operating procedures (EOPs) as they existed at the time of the study. As such, the frequency estimates do not reflect the impact of more recent guidance and procedures, such as the severe accident management guidelines currently being implemented by licensees as part of the nuclear industry initiative on accident management.

The system failures required to produce the requisite conditions for tube challenge are generally consistent with those associated with SBO sequences. Thus, the frequency of tube challenge could be estimated from the total frequency of SBO events as a first approximation. However, not all SBO events would produce these conditions. For example, SBO events with continued operation of AFW (wet secondary side) and core melt caused by a loss of primary inventory through a stuck-open pressurizer PORV/SV or a failed RCP seal would not contribute to temperature-induced SGTR and should be eliminated from consideration. By contrast, several other transient events (such as those involving a total loss of feedwater and failure of feed-and-bleed) *could* produce the requisite conditions and *should* be considered. Accordingly, the staff performed a more detailed assessment of the primary and secondary system conditions at the time of core damage on the basis of NUREG-1150 analyses for two PWR plants (Surry and Sequoyah). In addition, the staff addressed the applicability of the resulting frequency estimate to the broader population of Westinghouse and CE plants by developing and comparing corresponding frequency estimates for a number of additional plants on the basis of information contained in the IPE database.

2.3.1.1 High/Dry Frequency on the Basis of NUREG-1150

Accident sequences that proceed to core damage in a similar fashion in the accident frequency analysis (Level 1 PRA) are grouped together into PDSs for further evaluation in the accident progression analysis (Level 2 PRA). The characteristics that define these PDSs are determined by the accident progression analysts on the basis of information needed in the APET. The process of assigning accident sequences to PDSs forms the interface between the accident frequency analysis and the accident progression analysis.

The NUREG-1150 analyses for PWRs used a seven-character PDS indicator to denote characteristics of the plant condition when the water level falls below the top of the active fuel. The status of the primary and secondary systems at the onset of core damage are indicated by the first and sixth characters of the PDS indicator, respectively.

The first PDS character denotes the pressure of the RCS and its integrity at the onset of core damage. Events with relatively high RCS pressure at core damage correspond with three different status categories indicated by this PDS character:

- transients (T)
- very small LOCAs with a break diameter less than 1.3 cm (0.5 inch) (S_3)
- small LOCAs with a break diameter between 1.3 and 5.1 cm (0.5 and 2 inches) (S_2)

In general, the RCS pressure at core damage depends on the size of the LOCA and the specific accident, but would generally range from the PORV/SV set point to the accumulator set point. (Transients would result in RCS pressures at or near the pressurizer PORV/SV set point, whereas very small and small LOCAs would result in a partially depressurized RCS at core damage.)

The sixth PDS character denotes the status of the AFW system and its ability to provide steam generator heat removal. Events with a dry secondary side involve loss of main and auxiliary feedwater, and correspond with four different status categories indicated by this PDS character:

- AFW is operated until battery depletion with the steam generators at pressure at the time of core damage (C).
- AFW is operated until battery depletion with the steam generators depressurized at the time of core damage (D).
- and AFW is failed at the outset of the event (S and N).

However, as discussed below, SBO sequences with an RCP seal LOCA represent a special case in which a significant fraction of the events involve a wet secondary side at the time of tube challenge. This is because core uncovery occurs early relative to the time of battery depletion and steam generator dryout.

On the basis of point estimates tabulated for Surry sequences and PDSs (Wheeler, 1989), the frequency of events involving both core uncovery with the RCS at relatively high pressure (events T, S_2, and S_3) and loss of main and auxiliary feedwater (PDS characters C, D, S, or N) is 2.2×10^{-5}/RY. The initiating events for the screened sequences are mostly single- and double- unit losses of offsite power (92 percent), with the balance dominated by transients with loss of main feedwater or loss of a DC bus. A similar assessment for Sequoyah indicates a point estimate of 1.4×10^{-5}/RY for the frequency of high primary pressure and loss of feedwater. For Sequoyah, the initiating events for the screened sequences are mostly

losses of offsite power (80 percent), with the balance dominated by transients with loss of main feedwater or loss of a DC bus.

About 29 percent of the events identified through the screening process involve an RCP seal LOCA (6.4×10^{-6}/RY). A closer examination reveals that all of these RCP seal LOCA events involve successful AFW operation. In such sequences, the steam generators could be wet or dry, depending on the size and timing of the seal LOCA. The staff further evaluated the underlying sequences in terms of the conditions on the secondary side, as discussed below.

The NUREG-1150 analysis identified three individual RCP seal LOCA sequences from the SBO event trees, which were in the NUREG-1150 analysis and captured in the high/dry screening process. Each involved successful operation of turbine-driven AFW, with core damage resulting from a seal LOCA with failure to restore AC power in time to reestablish HPSI flow before core uncovery. The two largest contributors involve successful depressurization of the RCS and were classified as having AFW until battery depletion with the steam generators depressurized at the time of core damage (PDS parameter "D"). The smallest contributor involves operator failure to depressurize the RCS and was classified as having AFW until battery depletion with the steam generators at pressure at the time of core damage (PDS parameter "C"). In the current study, the staff reviewed the NUREG-1150 RCP seal LOCA model to determine the fraction of these SBO sequences that would involve a wet secondary at the time of RCS pressure boundary failure.

The progression of events in a long-term SBO with an intact primary would generally involve a loss of AFW upon depletion of station batteries at 4.0 hours, steam generator dryout at 5.5 hours, core uncovery at 6.5 hours, and first failure of the RCS pressure boundary at approximately 8.0 hours. SCDAP/RELAP5 analyses for Surry indicate that introducing a 946-Lpm/pump (250-gpm/pump) seal LOCA at the time of RCS saturation would actually increase the time interval between core uncovery and first RCS pressure boundary failure from 1.5 hour to approximately 2 hours, for reasons described in Section 4. Thus, SBOs with RCP seal LOCAs sufficient to result in core uncovery in 3.5 hours (the difference between the SG dryout time and the interval between core uncovery and RCPB failure) or less would have a wet secondary side at the time of RCS pressure boundary failure.

Review of the corrected seal LOCA model developed by Brookhaven National Laboratory (BNL) (Ruger, 1995) indicates that approximately 67 percent of seal LOCA events would produce core uncovery in 3.5 hours or less. Furthermore, this corrected seal LOCA model suggests that about 95 percent of the seal LOCA events that result in core damage involve core uncovery in about 3.5 hours or less. Thus, essentially all of the SBO seal LOCA events captured through the screening process would have a wet secondary side at the time of cladding oxidation and RCS heatup. As such, steam generator tubes would not be challenged by high temperatures in these events, and RCS failure would be expected to occur in an alternative location, such as the pressurizer surge line or a hot leg.

For purposes of the present analysis, the staff determined the fraction of high primary system pressure/dry secondary side events that involve early failure of the pressurizer PORV/SVs or RCP seal LOCAs on the basis of the PDS information for Surry (contained in NUREG-1150), with corrections for proper treatment of SBO events with RCP seal LOCAs. The staff eliminated from further consideration the entire frequency of SBO seal LOCA events with successful AFW (6.4×10^{-6}/RY, or 29 percent of the high/dry frequency) because of the presence of a wet secondary side through the time of first RCS pressure boundary failure. This screening yields a more representative value for frequency of core damage with the primary system at relatively high pressure and the secondary side dry. The resulting

frequency is approximately 1.6×10^{-5}/RY for Surry. A similar correction for Sequoyah yields a core damage frequency (with high primary pressure and dry secondary side) of approximately 1.1×10^{-5}/RY for that plant.

2.3.1.2 High/Dry Frequency on the Basis of the IPE Database

The staff searched the IPE database (as of May 1996) to determine whether the information from the NUREG-1150 analyses regarding the frequency of challenge was reasonably consistent with available information from the IPEs. In particular, the staff focused this search on core damage events with the primary system at high pressure and the secondary system dry. However, the staff could not conduct a direct, automated search for the sequences of interest. This is because the database allows automatic queries for high-pressure core damage events, but secondary system water level is not an explicit field in the database records. As a result, the staff searched the database for sequences involving high primary pressure and loss of all feedwater.

The database search of 42 PWR IPEs yielded a set of 1351 sequences. (Some of these IPEs represent two plants. For example, North Anna, Surry, and Zion each have a single IPE that applies to both units.) To make the analysis of this large number of sequences more tractable, the results of the database search were written out in a format compatible with a spreadsheet program, and the staff performed the remainder of the analysis with the aid of this spreadsheet.

All 42 IPEs had some sequences with the primary system at high pressure and the secondary system dry at the time of core damage. The sum of the frequencies of these sequences for each plant ranged from a low of 4.9×10^{-7}/RY (McGuire 1&2) to a high of 7.9×10^{-5}/RY (Indian Point 2). Figure 2.4 presents a plot of these CDFs. Direct inspection revealed that most plants fall in the range of 2×10^{-6}/RY to 4×10^{-5}/RY.

The staff then further evaluated the results of the IPE database search to identify any major differences among the sequences contributing to core damage with high primary pressure and dry steam generators, or any significant design biases. For this evaluation, the staff used two distinct approaches. First, the staff examined all high/dry sequences from the three IPEs with the greatest frequency of core damage, as well as the top five high/dry sequences in each of the remaining IPEs. Specifically, the plants with the highest frequency of core damage with high primary pressure and dry steam generators were Indian Point 2 (7.9×10^{-5}/RY), North Anna 1&2 (5.4×10^{-5}/RY), and Surry 1&2 (3.9×10^{-5}/RY). The reader should note, however, that the frequency of core damage with high primary system pressure and dry steam generators from the Surry IPE, as recorded in the IPE database, is higher than the corresponding value from the NUREG-1150 study (2.2×10^{-5}/RY). This higher value results from the inclusion of several internal flood-related sequences in the IPE database that were not included in the NUREG-1150 study.

Second, the staff broke out and compared (by reactor design) the frequency of core damage with high primary pressure/dry steam generators. However, the staff did not pursue more in-depth correlations on the basis of the relatively small variation observed in event frequency. Station blackout and battery depletion appear most frequently in the high pressure/dry steam generator sequences; however, these contributors are not dominant in many of the IPEs surveyed. The specific initiators include loss of offsite power, reactor scram, turbine trip, loss of main feedwater, loss of DC power, loss of emergency service water, and ATWS. These initiators are to be expected, since they can all lead to secondary dryout, and all initiators need not involve station blackout. In addition, some principal contributor

sequences were initiated by internal flooding or loss of heating, ventilation, and air conditioning (HVAC).

Essentially all of the above initiators (including the HVAC initiator) also appear among the top five sequences of all of the remaining PWR IPEs. In addition, the list includes loss of component cooling water, loss of instrument air, loss of onsite AC power (some plants have onsite sources in addition to the diesels), steam line break inside containment, and loss of the ultimate heat sink, with some of these initiators having frequencies as high as 10^{-6}. However, the relative contribution from the constituent sequences to the frequency of high pressure/dry steam generator varies considerably from plant to plant. For example, SBO sequences account for a majority of the high/dry frequency at some plants, but very little of the high/dry frequency at other plants. Thus, the characterization of primary and secondary system status in subsequent APET branches in the present analysis for Surry *should not be generalized to other plants*.

Table 2.2 summarizes the frequency of core damage with high primary pressure and dry steam generators, sorted by reactor design (i.e., Westinghouse plants with two, three, and four loops, and CE plants with and without PORVs). The reader should note, however, that these results are not weighted to reflect multiple units at certain sites; thus, the number of plants reflected in the table is less than 42.

As shown in Table 2.2, the mean frequency derived from the IPE database ranges from a low of 6×10^{-6}/RY for CE plants with PORVs to a high of 3×10^{-5}/RY for two-loop Westinghouse plants – a factor of five variation. Within Westinghouse designs, the frequency decreases from two-loop to three-loop to four-loop, but the mean frequencies for two-loop and four-loop plants still vary by less than a factor of 2. CE plants without PORVs have about the same mean frequency as the Westinghouse four-loop plants, but CE plants with PORVs have about half the frequency of Westinghouse four-loop plants or CE plants without PORVs.

By contrast, NUREG-1150 reported that the high/dry frequency is 2.2×10^{-5}/RY for Surry (three-loop) and 1.4×10^{-5}/RY for Sequoyah (four-loop). These values are very close to the mean high/dry frequencies derived from the IPE database for three-loop and four-loop Westinghouse plants, and they fit well within the range of IPE data. Furthermore, the NUREG-1150 value for Surry envelops the CDFs derived from the IPE database for the majority (all but 10) of the plants considered, and it is within a factor of 4 of the highest IPE high/dry frequency.

The reader should note that, for Westinghouse plants, the frequencies reported in IPEs include the contribution of SBO events with RCP seal LOCA. Most IPE submittals for Westinghouse plants qualitatively indicated that short-term SBO sequences were not significant contributors to the SBO CDF because additional failures are needed for the short-term case (e.g., turbine-driven auxiliary feedwater must fail). In addition, most of these submittals indicated that, on average, the SBO CDF was dominated by long-term SBOs with RCP seal LOCAs. In contrast, the IPE submittals for CE plants considered RCP seal LOCAs to be an unimportant contributor to CDF because these plants exhibit a low susceptibility to RCP seal LOCAs as a result of the Byron-Jackson four-stage seal design.

Table 2.2 Frequency of High/Dry Events from IPEs (Sorted by Reactor Design)

Design	Number of Plants in Sample	High/Dry Frequencies (per RY)			
		Low	High	Mean	Median
W 2-loop	3	$2X10^{-5}$	$4X10^{-5}$	$3X10^{-5}$	$3X10^{-5}$
W 3-loop	7	$1X10^{-5}$	$5X10^{-5}$	$2X10^{-5}$	$2X10^{-5}$
W 4-loop	19	$5X10^{-7}$	$8X10^{-5}$	$2X10^{-5}$	$2X10^{-5}$
All W	29	$5X10^{-7}$	$8X10^{-5}$	$2X10^{-5}$	$2X10^{-5}$
CE w/PORVs	5	$5X10^{-7}$	$1X10^{-5}$	$6X10^{-6}$	$6X10^{-6}$
CE w/o PORVs	3	$9X10^{-6}$	$3X10^{-5}$	$2X10^{-5}$	$2X10^{-5}$
All CE	8	$5X10^{-7}$	$3X10^{-5}$	$1X10^{-5}$	$1X10^{-5}$

The staff did not attempt to further assess the IPE submittals to determine the status of the steam generator secondary side at the time of core damage. Such an assessment would need to consider plant-specific features. These features might include the relative contribution of short- and long-term SBO, the time of battery depletion and steam generator dryout relative to the time of core uncovery for the spectrum of possible RCP seal and O-ring failure combinations and times, and the plant-specific probability distribution for non-recovery of AC-power before core uncovery. The frequency of high/dry events derived through this plant-specific assessment would be reduced (relative to the staff's findings) by eliminating those RCP seal LOCA events that would have a wet secondary side up to the time of the initial RCS failure. This reduction could be significant if SBO seal LOCA events are dominant contributors to the events captured in the screening process, and would tend to reduce the observed differences in high/dry frequency between Westinghouse and CE plants.

In conclusion, the staff's database search confirms that the sequences contributing to core damage with high primary system pressure and dry steam generators in the IPEs surveyed are similar to the contributing sequences for Surry and Sequoyah, as reported in NUREG-1150. Furthermore, comparison of high/dry core damage frequency across nuclear steam supply system (NSSS) designs does not reveal any strong design biases. The staff concludes that the frequency of core damage with high primary system pressure and dry steam generators derived from the Surry analysis reported in NUREG-1150 (1.6×10^{-5}/RY) is reasonably representative of the frequency of steam generator tube challenges for the population of Westinghouse and CE plants. The staff, therefore, based its risk assessment on this value.

The staff recognizes the potential for significantly different challenge frequencies at different plants, and has addressed this issue as a sensitivity study. Moreover, because of the large plant-to-plant variation in the relative contribution from constituent sequences, the characterization of primary and secondary system status in subsequent APET branches in the present analysis are not necessarily representative and should not be generalized to other plants.

2.3.2 RCS Status at Time of Core Uncovery

The first two top events in the APET (events B and C) address the potential for either a stuck-open pressurizer PORV or SV, or an RCP seal LOCA before core damage, respectively. As previously discussed, these failures would cause the RCS to be partially depressurized at

the time of core damage, with the degree of depressurization dependent on the size and timing of the RCS failure.

In NUREG-1150, two time regimes were used to evaluate the failure of a pressurizer PORV to successfully reclose after lifting in an SBO. Specifically, these regimes encompassed the RCS boildown phase before core damage (as part of the accident frequency analysis/Level 1 PRA), and after the core degradation process has proceeded for some time and the valves are operating at temperatures well in excess of their design value (as part of the accident progression analysis/Level 2 PRA).

The staff employed a similar approach in the present study. Specifically, the probability that a pressurizer PORV or SV fails to reclose during RCS boildown was considered in the first top event in the APET, as discussed below. The probability that the valve fails to reclose later in the event during the core degradation process was addressed as the sixth top event in the APET.

On the basis of point estimate values for sequences and plant damage states tabulated for Surry in NUREG/CR-4550, the RCS is intact in approximately 68 percent of the screened events. Another 14 percent of the screened events involve a stuck-open pressurizer PORV or SV, and the remaining 18 percent involve an RCP seal LOCA. As modeled, no events involve *both* a stuck-open pressurizer valve *and* an RCP seal LOCA; however, these failures are not mutually exclusive and can occur together. Table 2.3 summarizes the split fractions derived from the PDS information for Surry, along with corresponding results for Sequoyah for purposes of comparison. The underlying assumptions for the NUREG-1150 values are discussed below.

Table 2.3 Fraction of High/Dry Events with Stuck-Open Pressurizer PORV/SV or RCP Seal LOCA

RCS Status at Time of Core Uncovery	Surry NUREG-1150[1]	Sequoyah NUREG-1150[2]
Intact	0.68	0.49
Stuck Open PORV/SV	0.14	0.03
RCP Seal LOCA	0.18	0.48
Total	1.0	1.0

1 - based on a high/dry frequency for Surry of $1.6X10^{-5}$/RY
2 - based on a high/dry frequency for Sequoyah of $1.1X10^{-5}$/RY

2.3.2.1 Early Failure of Pressurizer Relief/Safety Valves (APET Event B)

The probability that a pressurizer PORV or SV will fail to reclose early in an event was addressed as an uncertainty issue in the Level 1 portion of the NUREG-1150 analysis. In the stand-alone version of the accident frequency analysis, the probability of this event was sampled from a distribution. As a result of this sampling, the uncertainty in the probability was not found to be a significant contributor to the uncertainty in core damage frequency, and the probability that the valve will fail to reclose was set to the mean value of the distribution (0.027) in the integrated analysis (NUREG-1150, Appendix B).

On the basis of NUREG-1150 findings, it appears that the treatment of a stuck-open PORV/SV

during an SBO was limited to consideration of long-term SBOs in which AFW is initially available. It also appears that the probability of a stuck-open PORV was assessed for only a single valve cycle occurring early in the transient following reactor scram. (The 0.027 value is the product of a PORV demand rate of 1.0, a 0.9 probability that at least one PORV is unblocked, and a probability of 0.03/demand that the PORV will fail to reclose).

The discussion of relief valve demand provided in NUREG/CR-4550 indicates that the probability of 0.03/demand used in NUREG-1150 originated from the generic value used in the original accident sequence evaluation program (ASEP). However, the PORV failure rate data reported in Table 8.2-5 of NUREG/CR-4550 indicates a substantially lower mean value of 2×10^{-3}/demand as the probability that the PORV will fail to reclose. This lower value was derived from the NRC's licensee event report (LER) data summary for air-operated valves (AOVs). This value is consistent with current estimates of failure rates for PORVs, but was not used in NUREG-1150. Use of the higher failure rate in conjunction with a single demand in NUREG-1150 would be comparable to use of a lower failure rate given that the valve cycles approximately 15 times before core damage occurs. However, an even greater number of pressurizer PORV/SV cycles is expected before core uncovery, as discussed below.

The number of challenges to the pressurizer PORVs or SVs is a function of plant characteristics, including the volume of the RCS, set point staging of multiple valves, flow capacities of the relief valves, and valve operating characteristics. The number of valve demands before core uncovery can vary markedly from plant to plant, as illustrated by results of SCDAP/RELAP5 and EPRI-sponsored MAAP calculations for an SBO sequence with an intact primary system. As shown in Table 2.4, SCDAP/RELAP5 calculations for Surry predict 30 steam cycles followed by 59 liquid cycles before core uncovery for the case with one steam generator depressurized (Case 3R), and 20 steam cycles followed by 56 liquid cycles for the case with all steam generators depressurized (Case 7R). MAAP results indicate substantially fewer valve cycles, but this difference is largely attributable to different valve operating characteristics (dead bands) assumed in the two codes. For similar valve dead bands, MAAP and SCDAP/RELAP5 results appear comparable.

Sequences involving an RCP seal LOCA can result in a comparable challenge to pressurizer valves if either the magnitude of seal leakage remains small or the onset of significant leakage is delayed. For example, a SCDAP/RELAP5 calculation for ANO-2 (in which a 220-gpm/pump seal LOCA was introduced upon reaching saturated conditions at the RCPs) resulted in 13 steam cycles and 47 liquid cycles before reaching saturation, and an additional 6 steam cycles before core uncovery.

Collectively, these calculations indicate that the PORV/SVs could cycle between 10 and 100 times (approximately) before core uncovery occurs during an SBO, with half or more of these cycles involving flow of liquid or two-phase fluid. The calculations also show that the majority of demands on the pressurizer PORV or SV occur before the RCS coolant temperature reaches saturation at the RCP seals. Valve operating characteristics (particularly the valve opening and closing set points) govern the quantity of fluid passed during each cycle and account for a large portion of this variation.

Table 2.4 Number of Pressurizer PORV/SV Cycles Before Core Uncovery

Flow Through PORV/SV	Number of PORV/SV Cycles Prior to Core Uncovery		
	SCDAP/RELAP5		MAAP
	Surry Intact RCS [1]	ANO-2 Seal LOCA [2]	W 4-Loop Intact RCS [3]
2-Phase/Liquid	59	47	8 - 24
Steam	30	19	5 - 21
Total	89	66	13 - 45

1 - Each cycle represents operation of 2 pressurizer PORVs with the same set points and a dead band of 3 percent (Surry Case 3R).
2 - Each cycle represents operation of 2 pressurizer SVs with the same set points and a dead band of 4 percent (ANO-2 Case 3).
3 - Range represents results assuming a pressurizer SV dead band of 15 percent and 5 percent, respectively.

For a given plant, the number of valve demands is inversely proportional to the quantity of fluid lost during each valve cycle. The quantity of fluid lost per cycle can be characterized in terms of the valve dead band, which is defined as the difference between the design set point (opening) pressure and the actual reseating (closing) pressure, expressed as a percentage of the design set point pressure. The lower the pressure at valve closing (and thus the greater the dead band), the more fluid is lost per cycle and fewer cycles are required to depressurize the RCS. The design dead band for pressurizer PORVs and SVs is typically about 5 percent, but actual values observed in valve testing vary substantially from the design value, as discussed below.

In the early 1980s, EPRI sponsored a test program to evaluate the performance and reliability of primary system safety and relief valves under fluid conditions expected at the valve inlets during their operation in design-basis accidents, including licensing transients, extended operation of HPSI, and cold overpressurization (Bahr, 1982; Meliksetian, 1982; Singh, 1985; and EPRI Valve Test Program Staff, 1982). Under that program, EPRI tested 17 safety Collectively, these calculations indicate that the PORV/SVs could cycle between 10 to 100 times (approximately) before core uncovery occurs during an SBO, with half or more of these cycles involving flow of liquid or two-phase fluid. The calculations and relief valves representative of those used or planned for use in domestic PWRs. These tests, conducted over a range of conditions, included safety valves manufactured by Dresser, Crosby, and Target Rock, and relief valves produced by nine different manufacturers. (Together, Dresser and Crosby valves account for the majority of pressurizer and steam generator code safety valves in use at operating PWRs.)

On the basis of EPRI's findings, the dead band for the two Crosby safety valve designs tested averaged 7 percent (ranging from 0.3 to 18 percent) for valves with an "R" orifice, and 15 percent (ranging from 9 to 23 percent) for valves with a "Q" orifice. The average dead band for the Dresser valves was in the range of 6 to 7 percent.

The SCDAP/RELAP5 calculations cited in Table 2.4 assume valve dead bands of 3 percent for Surry and 4 percent for ANO-2, with simultaneous operation of two valves during each cycle. If the performance of the valves is similar to that observed in the EPRI-sponsored tests,

the total number of valve demands would be approximately the same as reported in the table. However, if the valves perform as modeled, the total number of demands could be as much as twice the number of cycles reported in the table, and the probability of an early failure would increase accordingly.

In the current study, the staff considered the impact of increased pressurizer PORV/SV demands on the likelihood of early RCS depressurization. Using the mean ASEP value of 2×10^{-3} per demand (NUREG/CR-4550), the probability that the PORV will fail to reclose would be about 0.02 to 0.2 for an SBO event, given that the results of the SCDAP/RELAP5 and MAAP calculations suggest that the number of PORV/SV cycles could range from 10 to 100. In contrast, the NUREG-1150 PDS information suggests that events involving a stuck-open PORV at Surry and Sequoyah comprise about 14 percent and 3 percent of frequency of high RCS pressure/dry steam generator sequences, respectively.

This observation leads to the conclusion that use of a constant per-demand failure rate to address the likelihood of failure for multiple valve cycles (failure rate per demand x number of demands) would overestimate valve failure probabilities. This is because generic failure rate data tend to reflect valve availability and the influences of standby-related problems (such as maintenance errors) rather than valve reliability and the ability to function for multiple cycles. A more rigorous and technically correct treatment would separately consider the probability that the valve completes its initial cycle, and the probabilities that the valve operates for successive cycles during which the valve discharges vapor or liquid.

EPRI has recently proposed such a failure model for use in assessing the reliability of pressurizer safety valves (PSVs) and MSSVs for repeated cycling (Fuller, July 1996). To derive this model, EPRI reviewed failure rate data used in IPEs, as well as results from a series of EPRI-sponsored tests conducted on seven PSVs in the early 1980s, and the limited operating experience reported in NRC information notices and LERs. On that basis, EPRI assessed the PSV failure rates per demand to be 2.7×10^{-2} for steam cycles and 1.1×10^{-1} for liquid cycles. In the aggregate, the EPRI model indicates that the PSV will fail to reclose during the boildown phase with a probability of 0.69 to 0.98 (for PSVs with dead bands of 15 and 5 percent, respectively). This value is substantially higher than estimated in the NUREG-1150 Level 1 analysis, and is largely attributable to the consideration of mechanical loads placed on the valve when it passes two-phase/liquid flow.

The staff notes that the failure rates derived by EPRI reflect an assumption that the limited valve damage observed in the EPRI-sponsored tests (2 observations in 75 steam tests, and 3 observations in 25 liquid tests) led to the valves' failure to reclose. However, there is insufficient evidence to conclude that the instances of valve damage observed in the tests constitute a failure to reclose. Specifically, the test documentation does not indicate that the valves failed to reclose in any of the tests, or that the observed damage would prevent continued operation of the valves. Furthermore, in one of the few operating events in which repeated PORV cycling occurred, the PORV cycled approximately 200 times without failure, despite the fact that the valve sustained considerable damage. Thus, the staff concludes that the fraction of sequences involving early PORV/SV failure (about 14 percent, according to the PDS information for Surry) provides a reasonable basis for this scoping assessment. The staff therefore based the split fraction for APET event B on this value.

The staff also noted that the fraction of high primary pressure/dry steam generator events with a stuck-open PORV for Surry is higher than the corresponding value for Sequoyah.

Nonetheless, that fraction generally agrees with results of a separate assessment using the number of valve demands from recent SCDAP/RELAP5 and MAAP analyses in conjunction with valve failure rates from ASEP. A low frequency of events with a stuck-open PORV is also consistent with IPE review insights for Westinghouse and CE plants. Such insights reveal that SBO sequences with stuck-open PORVs were listed in only a few IPE submittals and, even then, they were minor contributors to core damage frequency, as documented in NUREG-1560 (U.S. Nuclear Regulatory Commission, 1996).

The staff acknowledges that it may be appropriate to consider a higher per-demand valve failure rate during the boildown phase (as predicted by the EPRI cumulative damage model) and a higher fraction of sequences with a stuck-open PORV. However, for this study, the staff assigned a relatively high value (0.5) to the probability that the PORV will not reclose later in the event during core degradation (the sixth top event in the APET).

The staff further noted that accident progression would differ for early versus late failure of PORVs. However, previous studies of intentional depressurization as an accident management strategy compared the approach of latching open PORVs early (at the time of steam generator dryout) and late (at the time core exit temperature exceeds 922 K (1200°F)) and found that the RCS pressure response is similar for the two cases (Hanson, 1990). (Early actuation of PORVs led to earlier depressurization of the RCS, but also tended to accelerate the occurrence of core damage. As a result, the RCS pressure at the time of core damage did not differ substantially between the two cases.) Thus, the staff believes that the later APET branch (event F) adequately captures the uncertainty in the probability of early failure of the PORV/SV, and additional justification would be needed to support the use of a substantially higher probability for early failure of the PORV/SV.

2.3.2.2 RCP Seal LOCAs (APET Event C)

As reported in NUREG-1150, a panel of experts considered the probability of RCP seal LOCAs of various sizes as a systems analysis issue. This expert elicitation yielded estimated probabilities of various leak paths and corresponding leak rates as a function of time following a loss of seal cooling. For each scenario represented in the seal LOCA model/event tree, the expert elicitation subsequently determined the conditional probability of core damage on the basis of the estimated time of core uncovery and the probability of AC power recovery before core uncovery.

The seal LOCA model used in NUREG-1150 addresses a combination of time-dependent and time-independent failure modes, including shaft binding or "popping open" failures which can occur shortly following a loss of seal cooling, as well as degradation of pump seals and O-rings in the longer term. The model assumes a nominal 79 Lpm/pump (21-gpm/pump) leak-off immediately following all loss of seal cooling events; this leak-off is attributable to a change in seal geometry and fluid properties. In addition, the model predicts a probability of approximately 15 percent that the "popping open" mode of seal failure will occur about 10 minutes after the loss of seal cooling. This would lead to a seal LOCA of approximately 662 Lpm/pump (175 gpm/pump) beginning essentially at time zero, with an additional but much smaller (0.5 percent) probability of a 1817-Lpm/pump (480-gpm/pump) seal LOCA. At 1.5 hours following the loss of seal cooling, the model recognizes a 70-percent chance of significant seal leakage. The predominant leak path, which has a 53-percent chance of occurrence, results in a leak rate of 946 Lpm/pump (250 gpm/pump). The seals continue to degrade up to 5.5 hours from the loss of seal cooling, when the total probability of significant leakage is 73 percent.

The reader should note that following the completion of NUREG-1150, the staff identified and assessed the impact of errors in the implementation of the seal LOCA model (Ruger, 1995). The most important error was that the model did not reflect the probability of seal failure shortly (about 10 minutes) following the loss of seal cooling. This probability was reflected in the expert elicitation on RCP seal LOCA, but was neglected in implementing the RCP seal LOCA model within the Level 1 analysis. Table 2.5 summarizes the probability and estimated time of core uncovery for each postulated seal failure scenario considered in the NUREG-1150 model for Sequoyah.

The staff subsequently evaluated the effect of correctly incorporating the time-zero seal failures for Sequoyah and found that it increased the frequency of seal LOCA core damage sequences by about 20 percent. Similar results would be expected for Surry. The staff therefore used the corrected RCP seal LOCA model in the present study to assess the fraction of seal LOCA sequences involving a wet or dry secondary. No attempt was made to requantify the NUREG-1150 results for Surry or Sequoyah, since the effect of the correction is comparable to uncertainties associated with other aspects of the present analysis.

As discussed in Section 2.3.1, the staff's examination of the events captured through the high primary/dry secondary screening process reveals that all of the captured SBO seal LOCA events involve successful AFW operation, and essentially all would be expected to have a wet secondary side at the time of cladding oxidation and RCS heatup. As a result, the staff eliminated from further consideration all SBO seal LOCA events involving successful AFW operation.

The NUREG-1150 analysis for Surry includes four major SBO sequences that involve early loss of AFW. The dominant sequences are the SBO involving early loss of AFW without further failures and the sequence with a loss of steam generator integrity (e.g., the steam generator safety valve fails open). The other two sequences involve failure to reclose the pressurizer PORV and are insignificant contributors to core damage frequency. The dominant sequences together contribute a large fraction of the total core damage frequency associated with short-term SBOs (total CDF of 4.3×10^{-6}/RY), after consideration of AC power recovery.

Further review of the Level 1 event tree model reveals that NUREG-1150 also neglected to address the potential for seal LOCAs during short-term SBOs (with AFW unavailable). The occurrence of a seal LOCA during a short-term SBO would not significantly impact the total core damage frequency or the high/dry frequency because the times to core damage are already short for these sequences. Nonetheless, a seal LOCA could subject the steam generator tubes to significant pressure and temperature challenges (relative to the intact RCS case) if the seal LOCA clears the loop seal. Accordingly, the staff further evaluated the impact of RCP seal LOCAs in conjunction with short-term SBOs. Such RCP seal LOCAs should be retained in estimating the frequency of challenges to steam generator tubes since a high primary system pressure and dry secondary side pressure would be expected in these events, if they were to occur.

Occurrence of a seal LOCA would not substantially increase the frequency of core damage for the following reasons:

- The probability is small that a large seal LOCA would occur shortly (within the first few minutes) following a loss of seal cooling.

- Significant increases in seal LOCA size are not expected to occur until at least 1.5 hours following a loss of seal cooling.

According to the corrected interpretation of expert opinion, the probability that initial seal leakage would exceed 79 Lpm/pump (21 gpm/pump) is about 19 percent. Moreover, 94 percent of this frequency would be attributed to seal LOCAs of 662 Lpm/pump (175 gpm/pump) or less, and 6 percent would be attributed to seal LOCAs of 946 Lpm/pump (250 gpm/pump) or more. The probability that RCP seal LOCAs of 946 Lpm/pump (250 gpm/pump) or greater are introduced at 90 minutes is about 53 percent, with LOCAs of 1136 Lpm/pump (300 gpm/pump) or more accounting for less than 1 percent of this value.

Although the RCP seal LOCAs would not substantially increase core damage frequency, they could pose a greater challenge to steam generator tubes because of the potential for RCP loop seal clearing. The corrected RCP seal LOCA model yields a 69-percent chance that a seal LOCA of 946 Lpm (250 gpm) or greater would occur before the first RCS pressure boundary failure (4 hours) in a short-term SBO where AFW is unavailable from the outset. Thus, the frequency of short-term SBO core damage events that would involve an RCP seal LOCA of 946 Lpm/pump (250 gpm/pump) or greater at Surry is approximately 3.0×10^{-6}/RY ($0.69 \times 4.3\times10^{-6}$/RY). This constitutes approximately 18 percent of the total frequency of events with core damage at high RCS pressure and a dry steam generator secondary side.

To represent RCP seal LOCA sequences, the staff used a SCDAP/RELAP5 analysis in which seals were assumed to leak at 79.5 Lpm/pump (21 gpm/pump) until RCS coolant reaches saturation (approximately 2 hours), at which time the seal LOCA increases to 946 Lpm/pump (250 gpm/pump). This seal failure scenario is comparable to the single most likely seal failure scenario postulated in the NUREG-1150 model (see Table 2.5). Nevertheless, other scenarios depict significantly different leakage and timing characteristics.

For the present analysis, the staff used the NUREG-1150 PDS information for Surry as the basis for determining the fraction of high primary system pressure/dry secondary side events that involve RCP seal LOCAs (APET event C). However, the staff has also corrected that information to account for proper treatment of SBO events with RCP seal LOCAs. Specifically, the frequency of long-term SBO seal LOCA events with successful AFW (6.4×10^{-6}/RY) were eliminated from further consideration because of the presence of a wet secondary side through the first pressure boundary failure. Further, the fraction of short-term SBOs that would involve a coincident RCP seal LOCA (3.0×10^{-6}/RY, or 18 percent of the high/dry frequency) was transferred from the "intact" state to the "RCP seal LOCA" state to allow for a more appropriate thermal-hydraulic characterization of these events. Table 2.3 summarizes the final split fractions are provided in for Surry and Sequoyah.

The fraction of events with an RCP seal LOCA and dry secondary for Surry (18 percent) is substantially less than the corresponding value for Sequoyah (48 percent). However, the actual frequency of challenges is comparable for the two plants, since the split fractions for Surry are based on an initiating event frequency of 1.6×10^{-5}/RY rather than 1.1×10^{-5}/RY for Sequoyah. These differences can be attributed to a combination of factors, including plant-to-plant differences that influence the composition of the high primary pressure/dry steam generator sequences. These differences are not considered significant in view of the scoping nature of the risk assessment.

Table 2.5 Probability and Core Uncovery Times for RCP Seal Failure Scenarios Considered in NUREG-1150 Analysis for Sequoyah

4 Pumps - Old O-Ring Material - Non-Depressurized [1]								
Scenario Number	Total Leak Rate (gpm)						Scenario Probability	Estimated Time of Core Uncovery (h)
	Initial	After Time of Transfer						
	0h	1.5h	2.5h	3.5h	4.5h	5.5h		
1	84						$2.47X10^{-1}$	19.2
2	244						$1.33X10^{-2}$	8.20
3	700[2]						$2.83X10^{-4}$	2.26
4	1000						$4.80X10^{-3}$	1.44
5	1920[2]						$5.03X10^{-3}$	0.72
6	84	244	1000				$1.25X10^{-1}$	3.55
7	84	244			1000		$4.37X10^{-3}$	5.06
8	84		244			1000	$5.61X10^{-3}$	5.97
9	84			244			$1.43X10^{-3}$	10.5
10	84	433					$2.69X10^{-3}$	5.44
11	84		433			1000	$3.58X10^{-3}$	6.00
12	84			433	1000		$1.20X10^{-3}$	5.48
13	84	1000[3]					$3.70X10^{-1}$	2.80
14	84		1000				$6.70X10^{-3}$	3.91
15	84			1000			$1.33X10^{-2}$	4.62
16	84				1000		$1.59X10^{-2}$	5.54
17	84					1000	$1.59X10^{-2}$	6.45
18	313	433	1000				$5.12X10^{-3}$	3.01
19	304/313	1000[3]					$9.29X10^{-3}$	2.45
20	543	663	1230				$1.28X10^{-3}$	2.40
21	543	1230					$1.28X10^{-3}$	1.99
22	700[2]	1000[3]					$1.44X10^{-1}$	1.87
23	700[2]		1000				$1.83X10^{-5}$	2.26
24	700[2]			1000			$1.83X10^{-5}$	2.26
25	700[2]				1000		$1.83X10^{-5}$	2.26
26	700[2]					1000	$1.83X10^{-5}$	2.26
27	796	1000[3]					$2.56X10^{-3}$	1.72
28	1000	1230					$6.40X10^{-4}$	1.44

1 - Ref: Letter from C. Ruger, BNL, to S. Shaukat, NRC, dated October 5, 1995
2 - Popping-open mode of seal failure (total scenario probability approx. 15%)
3 - Predominant leak path (total scenario probability approx. 53%)

2.3.3 Secondary Side Status at Time of Core Uncovery (APET Events D and E)

The third and fourth top events in the APET (events D and E) address the potential for depressurization of the steam generator secondary side before steam generator dryout. The following mechanisms can lead to depressurization of one or more steam generators, as discussed below:

- operator actions to depressurize using ADVs or other pressure relief paths
- failure to manually reclose or block a stuck-open ADV
- failure to isolate steam flow to the turbine-driven AFW pump in sequences in which it was initially operable
- failure of an MSSV to reclose

The ADVs in most plants are air-operated with a DC-powered solenoid, but the ADVs in other plants rely on AC power. In either case, use of the ADVs is not generally expected to result in the steam generators being depressurized at the time of core damage. This is because the valves would be unavailable in many SBO events, or would reclose upon eventual loss of DC power in other SBO events. Specifically, in short-term SBOs with loss of DC power, ADVs would not be available from the outset, and the accident would progress with the steam generators at the MSSV set point. In short-term SBOs with DC power available (and turbine-driven AFW unavailable for other reasons), operators could depressurize the steam generators using the ADVs to initiate feed flow using a low-pressure system. Subsequent loss of the low-pressure system could result in the steam generators being depressurized at the time of core damage. However, the likelihood of this occurring is considered small because operator actions could be carried out to close the ADVs or manually isolate any stuck-open valves, even if DC power is lost. Finally, in long-term SBOs, ADVs would be available before battery depletion, but would fail closed upon battery depletion. This would result in steaming of residual water in the SGs, with repressurization of the secondary side to the MSSV set point (provided that the secondary system pressure boundary remains leak-tight). In the event that an ADV sticks open, the valve can be isolated manually, even if DC power is lost.

In sequences in which the turbine-driven AFW pump is lost during the sequence, it is possible that the continued flow of steam to the turbine could also cause depressurization. However, if the turbine-driven pump is the only source of feed water available at that time, it is considered more likely that the plant staff will ensure that the steam supply to the pump is isolated so that repairs can be attempted.

Given the general unavailability of ADVs in the sequences of interest, steam relief is expected to occur via the MSSVs. Calculations performed using the SCDAP/RELAP5 and MAAP computer code indicate that the ADVs (or MSSVs, if ADVs are unavailable) will lift on the order of 50 times as the secondary side boils dry, and several additional times as the remaining vapor in the system continues to be heated. Thus, the potential for failure of the valves on one or more steam generators is significant. For these reasons, a stuck-open MSSV is considered to represent the most likely mechanism by which one or more steam generators could be depressurized in an SBO event.

To develop initial estimates of the probability that one or more steam generators would be depressurized at the time of core damage, the staff used available information from the NUREG-1150 analyses for Surry and Sequoyah. This included an assessment of the estimated frequency of events in which one or more steam generators was depressurized, as surmised from the plant damage state information. In addition, the staff considered the assumptions underlying the NUREG-1150 analyses concerning the number of demands on the valves in conjunction with estimated valve failure rates per demand. The staff then performed a

separate assessment on the basis of more recent thermal-hydraulic analyses and the EPRI cumulative damage failure model for MSSVs.

On the basis of point estimate values tabulated in NUREG/CR-4550 for sequences and plant damage states for Surry, and elimination of RCP seal LOCAs with wet secondary side, the staff classified a total of 74 percent of the high RCS pressure/dry steam generator events as having depressurized steam generators (primarily those events with PDS category D). Approximately 38 percent of the high RCS pressure/dry steam generator events included failure of a secondary safety relief valve to reclose as an explicit element in the cutsets. The remainder (36 percent of the high primary pressure/dry steam generator events) did not include a stuck-open MSSV as an explicit element in the cutsets, but were nevertheless classified as being depressurized.

For the present analyses, events that did not include a stuck-open MSSV as an explicit element in the cutsets, but nevertheless were classified as being depressurized (36 percent of the high primary pressure/dry steam generator events), were assumed to involve depressurization of two or more SGs. These events are reflected in the third top event in the APET (event D). The remaining events that included a stuck-open MSSV (38 percent of the high RCS pressure/dry steam generator events) were assumed to involve depressurization of only one SG, with the other two steam generators remaining at the secondary side pressure. These events are reflected in the fourth top event in the APET (event E). Table 2.6 summarizes the results for Surry, along with corresponding Sequoyah results, which are provided for purposes of comparison.

Table 2.6 Status of Steam Generators at Time of Core Uncovery

SG Condition	Fraction of High/Dry Sequences with SG Condition		
	Surry-1150	Sequoyah-1150	Staff Model [1]
All SGs Intact	0.26	0.95	0.22
1 SG Depressurized	0.38	0.03	0.43
All SGs Depressurized	0.36	0.02	0.35

1 - assumes a 40 percent probability of a stuck-open MSSV in each of 3 steam generators. "All SGs Depressurized" in this case includes 2 and 3 SGs

The differences between the Surry and Sequoyah results are significant, but are largely explained by a plant-specific EOP that would be followed at Surry during a long-term SBO, as discussed below.

The underlying analysis in NUREG-1150 considered the number of times an MSSV may be expected to open during a long-term SBO at Surry, and the rate at which the valves are expected to fail to reclose. The study estimated the number of demands on the MSSVs on the basis of a plant-specific EOP that would be implemented at Surry following a loss of AC power, with DC power available. The Surry procedure involves actions to manually line up valves in the steam system in order to depressurize the steam generators by venting through the condenser. Such an approach is used at Surry since ADVs are not available at the plant because the ADVs depend on AC power. The analysis assumed that during the SBO, one steam generator valve cycle would occur for each steam generator every 20 minutes over a 1-hour period while the procedure was being implemented (a total of nine valve demands). The probability that the valve would fail to reclose was taken to be 0.03 per demand, yielding a mean probability of 0.27 that a valve would fail to reclose during an SBO.

Unlike Surry, the ADVs at most plants are DC- rather than AC-dependent and, in a long-term SBO, the plant procedures would instruct the operators to depressurize the RCS using the ADVs. Once the batteries have been depleted, the ADVs would fail closed and the steam generators would repressurize to the MSSV set point. In this regard, the number of MSSV cycles considered in the Surry NUREG-1150 analysis is considerably less than expected at other plants.

In the current study, the staff has developed a scoping estimate for the likelihood of various secondary side conditions. As the basis for this estimate, the staff used the number of MSSV cycles predicted in more recent SCDAP/RELAP5 and MAAP calculations, combined with a per-demand valve failure rate developed from industry experience. Table 2.7 summarizes the resulting number of MSSV cycles expected in an SBO sequence with an intact RCS for Westinghouse and CE plants.

For a valve dead band of 5 percent, the number of MSSV challenges predicted by SCDAP/RELAP5 and MAAP for the two Westinghouse plants analyzed is on the order of 60 to 80 cycles. As indicated by the MAAP results, a higher actual dead band (such as observed during the tests conducted under the EPRI PWR Safety/Relief Valve Test Program), would result in a proportionately smaller number of valve cycles, and a lower probability of valve failure.

Table 2.7 Total Number of ADV/MSSV Cycles Before Core Uncovery

Total Number of ADV/MSSV Cycles Per Intact Loop		
SCDAP/RELAP5		MAAP
Surry [1]	ANO-2 [2]	W 4-Loop [3]
63	20	27 - 82

1 - value based on operation of 1 ADV with a dead band of 5 percent (Surry Case 3R)
2 - value based on operation of 1 MSSV with a dead band of 5 percent (ANO-2 Case 1)
3 - range based on operation of 1 MSSV with a dead band of 15 percent and 5 percent, respectively

The NUREG-1150 analysis for Surry assumed a probability of 3×10^{-2}/demand that the MSSVs would fail to reclose. As described in NUREG/CR-4550, this value was in the range suggested by a survey of LERs performed in 1980, and was selected as the original generic value for the ASEP. Since that time, the staff has accumulated additional information concerning safety valve performance, including insights developed through the EPRI PWR Safety/Relief Valve Test Program (Singh, 1985), and a limited number of operational events. On the basis of more complete industry data, EPRI reports an MSSV valve failure rate of 7.45×10^{-3}/demand (EPRI SGDSM/PSA Working Group, 1996). In addition, a recent EPRI survey indicates that this value has been widely used in licensee IPEs to represent the probability that an MSSV will fail to close, and a further assessment by EPRI suggests that the failure rate would be even lower (Fuller, July 1996).

EPRI reviewed operational data, as reported in LERs and NRC Information Notices, and proposed a value of 1.4×10^{-2} as the probability that an MSSV will fail to reseat following the initial lift. For a four-loop plant, the probability that one or more valves would fail to reclose would be 5.6×10^{-2}. This value reflects the consequences of failure modes associated with maintenance errors, embrittlement, and corrosion, but does not reflect potential failure modes associated with repeated cycling of the valves during an SBO. EPRI contends that data from the valve test programs indicate that once past the first lift and reclosure, MSSVs would successfully respond to the multiple challenges expected during an SBO event. Thus, only the probability of failure to reclose after the first lift is

relevant to MSSVs.

As a scoping assessment, the staff considered a case in which no operator actions are taken to depressurize the RCS, and steam generator depressurization occurs only as a result of the failure of MSSVs to reclose. The related SCDAP/RELAP5 and MAAP analyses led to the assumption that the MSSVs in each steam generator loop would cycle 70 times. This value is consistent with the analyses for Westinghouse plants and conservatively bounds the results for the CE plant analyzed. The staff also assumed a constant failure rate of 7.5×10^{-3}/demand, resulting in a probability of approximately 0.4 that an MSSV would stick open in each steam generator loop. Given that the failures of the MSSVs in each loop are independent of one another, the staff estimated the probability that no steam generators (0.22), one steam generator (0.43), and two or more steam generators (0.35) would be depressurized as a result of a stuck-open MSSV. Table 2.6 summarizes these values for comparison with the PDS-based results for Surry and Sequoyah.

The results from the scoping assessment are not substantially different than the PDS-based results for Surry. This suggests that comparable results would be obtained for Surry with and without operator actions to depressurize the SGs, given the assumed valve failure rate of 7.5×10^{-3}/demand. However, the failure rate of 1.4×10^{-2}/event proposed by EPRI for each SG would yield depressurization probabilities that are very similar to those obtained from the PDS information for Sequoyah.

For the present analysis, the staff characterized the status of the steam generators at the onset of core damage on the basis of the NUREG-1150 PDS information for Surry. Notably, the MSSV failure rate per demand assumed in the underlying analysis for NUREG-1150 is significantly higher than that indicated by more recent valve experience. Nonetheless, this effect appears to be offset by a substantially smaller number of valve demands assumed in the NUREG-1150 analysis. As a result, the NUREG-1150 results for Surry closely agree with the results from the staff's scoping assessment conducted on the basis of more recent thermal-hydraulic analyses and valve failure probabilities. In addition, the NUREG-1150 results for Surry conservatively bound the corresponding results for Sequoyah. Nonetheless, the staff recognizes the potential for a significantly lower probability of MSSV failure and steam generator depressurization, as claimed by EPRI and reflected in the NUREG-1150 results for Sequoyah. The staff has addressed this issue as a sensitivity case.

2.3.4 RCS Pressure Maintained to Time of Maximum Tube Temperature (APET Event F)

Failure of a PORV to reclose during the early part of a transient (before core uncovery) is addressed in the "front-end" analysis and reflected in the first top event in the APET. After the onset of core damage, the RCS conditions under which the PORVs or SVs will cycle are expected to be more severe than those for which the valves were designed, and for which valve performance has been tested.

The fifth top event in the APET (event F) addresses the potential for failure of the pressurizer PORV or safety valve during the core degradation process. For events involving either an RCP seal LOCA or failed or leaky PORV/SV, considerably less or no valve cycling is expected following core uncovery (although the amount of cycling depends on the size of the leak). Accordingly, the probability of late failure of the PORVs was not considered for these APET branches in the present study (i.e., Figures 2.3c and 2.3d).

In addition to the potential for valve failure, this top event reflects a means to investigate the impact of potential accident management measures to manually depressurize the RCS using PORVs, as described in Section 5.3. However, in order to fully assess the impact of such actions, the staff would need to modify the APET branches for RCP seal LOCA

to consider this top event, and would need to perform additional thermal-hydraulic analyses to characterize the combined effect of an open PORV in conjunction with an RCP seal LOCA.

The NUREG-1150 analyses for PWRs estimated that the pressurizer PORV cycles between 10 and 50 times during core degradation and before vessel breach. The NUREG-1150 analyses also extrapolated the distributions for the frequency of PORV failure-to-close from the front-end elicitation to these demands. This extrapolation yielded an estimated probability that the PORV will fail to reclose after core damage as a uniform distribution from zero to 1.0, and a mean value of 0.5.

Recently, NRC-sponsored SCDAP/RELAP5 calculations performed using Westinghouse and CE plant models (as summarized in Table 2.8) confirm that in an SBO event with an intact primary side, the pressurizer PORVs (or SVs if PORVs are unavailable) would cycle about 40 times between the time of core uncovery and the first predicted failure of the RCS pressure boundary.

Table 2.8 Number of Pressurizer PORV/SV Cycles Following Core Uncovery and Before First Failure of RCS Pressure Boundary

Flow Through PORV/SV	Number of Pressurizer PORV/SV Cycles		
	SCDAP/RELAP5		MAAP
	Surry [1]	ANO-2 [2]	W 4-loop [3]
Single phase/steam	43	38	4 - 14

1 - Each cycle represents operation of 2 pressurizer PORVs with the same set points and a dead band of 3 percent. Similar results were predicted for SBO cases with all steam generators intact, 1 steam generator depressurized, and all steam generators depressurized.
2 - Each cycle represents operation of 2 pressurizer SVs with the same set points and a dead band of 4 percent (ANO-2 Case 1).
3 - Range represents results assuming a pressurizer safety valve dead band of 15 percent and 5 percent, respectively.

All cycles would involve steam rather than liquid flow. Approximately 20 cycles would occur between the time of core uncovery and the onset of cladding oxidation, and an additional 20 cycles would occur before the first RCS failure. In calculations reported by EPRI, the number of pressurizer SV cycles predicted by MAAP for a four-loop Westinghouse plant ranged from 4 to 14 for valves with dead bands of 15 percent and 5 percent, respectively. As such, the SCDAP/RELAP5 and MAAP results are generally consistent with the number of valve cycles considered in the NUREG-1150 study.

The SCDAP/RELAP5 calculations also provide additional information regarding the timing and severity of the temperature challenge to the PORVs during core degradation. Specifically, in the Surry base case (Case 3R), the pressurizer top head steam temperature, which represents an upper bound on the PORV temperature, increases from about 600 K (620°F) at 200 minutes (shortly following onset of cladding oxidation) to a maximum of 900 K (1160°F) at about 240 minutes (roughly the time of first RCS pressure boundary failure). About 20 valve cycles are predicted to occur during this period of increasing steam temperatures, confirming the concerns raised in NUREG-1150 regarding PORV performance at elevated temperatures. The reader should note that elevated steam temperatures occur sufficiently late that over-temperature failure of the PORV in the time frame of maximum steam temperatures may not significantly reduce the primary system pressure at the time of steam generator tube challenge. If significant credit is taken for temperature-related valve failures, additional calculations would be needed to address valve failure modes and the degree of RCS depressurization associated with temperature-related failure of the PORVs.

Consistent with the NUREG-1150 analysis, the staff adopted a 0.5 probability of late failure of pressurizer PORV/SVs in the present study. As previously discussed in the context of early failure of the pressurizer PORV/SVs (Section 2.3.2), the 0.5 value reflects failure of the pressurizer PORV/SV as a result of repeated cycling at elevated temperatures during the core degradation process. It also compensates for a potential underestimate in the probability of early failure of the pressurizer PORV/SVs associated with the large number of valve lifts expected early in the transient (many of which involve the flow of liquid). As described in Section 5.3, the staff also conducted sensitivity studies to explore the impact of higher or lower probabilities for this APET branch on the likelihood of induced rupture of steam generator tubes.

2.3.5 Secondary Side Pressure Maintained to Time of Maximum Tube Temperature (APET Events G, H, I)

The sixth, seventh, and eighth top events in the APET (events G, H, and I) address the potential for the secondary side of one, two, or three steam generators to gradually depressurize following steam generator dryout. Previous analyses of SBO events have generally assumed that if the steam generator secondary side is isolated, the secondary pressure will remain at or near full pressure following steam generator dryout. The staff did not consider the potential for gradual depressurization of the steam generator as a result of leakage through MSIVs and other valves in the secondary side pressure boundary.

Valve leakage is distinct from safety valve actuation or other depressurization mechanisms, which are assumed to occur early in the event. This is a significant point, since valve leakage would alter past assumptions regarding the frequency of high primary-to-secondary differential pressure coincident with high tube temperatures.

Technical specifications for PWRs do not define a maximum leak rate for MSIVs or other steam generator isolation valves. Furthermore, operational data are not readily available with regard to steam generator depressurization times during hot standby conditions. For this study, the staff attempted to use LERs to identify any recorded occurrences of isolated steam generators depressurizing as a result of excessive valve leakage.

In particular, the staff searched the Sequence Coding and Search System (SCSS) database maintained at Oak Ridge National Laboratory (ORNL) to identify LERs reporting problems that could potentially lead to depressurization. The database search covered information from 1980 through early January 1996. The searches identified 498 LERs reporting dry steam generators, steam generator low level or low pressure, leaking or out-of-position MSIVs or other major secondary valves, and loss of feedwater events. Evaluation of the 498 LERs yielded only a single event indicating that secondary isolation may not prevent steam generator depressurization. In this event, which occurred at Arkansas Nuclear One, Unit 1 (ANO-1) in November 1989 (LER 313/89-037), steam generator pressure was reported to be decreasing as a consequence of "various steam system leakage paths." Another report, related to the Davis-Besse event in 1984 (LER 346/84-003), described steam generator depletion occurring when the MSIVs were closed and AFW was isolated. However, the steam generator inventory was depleted through safety valve actuation, not isolation valve leakage. Similarly, the ANO report indicated the potential for steam generator depressurization even if steam isolation valves are closed and feed is unavailable. These conditions could exist during an SBO scenario.

The recently published NUREG/CR-6246, "Effects of Aging and Service Wear on Main Steam Isolation Valves and Valve Operators," (Clark, 1996) discusses failures of PWR MSIVs. However, the leakage paths discussed are not significant and would not lead to

depressurization in the time scale of concern (3 to 4 hours).

In addition to anecdotal information related to the leakage integrity of MSIVs, the staff reviewed an NRC inspection report (Report No. 50-247/88-03). That report described an event involving steam generator dryout and offered detailed information regarding MSIV leakage characteristics for a particular plant. The staff has not assumed that these same conditions exist at all PWRs; however, it is considered reasonable to expect that some MSIV leakage could be assumed in this analysis.

The LER search results do not constitute an adequate basis for precisely estimating the probability of gradual steam generator depressurization. Nonetheless, the search demonstrates the real potential for depressurization of an isolated steam generator. Without further information, the staff assumed equal probabilities for each outcome. That is, the staff assigned a 0.5 probability that one or more steam generators would be depressurized by leakage by the time of first RCS pressure boundary failure. This approach ensured that the analysis considered steam generator isolation valve leakage integrity.

Treatment of steam generator leakage in the APET also provides a means for assessing the impact of higher or lower leakage probabilities on the likelihood of induced rupture of steam generator tubes via sensitivity studies, as described in Section 5.3. In the longer term, the 50/50 split used in the APET can be adjusted to reflect new information justifying a different quantification for this APET branch if it is developed.

Assuming steam generator leakage to be a random rather than common mode failure mechanism, a 0.5 probability of depressurizing one or more of three steam generators is equivalent to a 0.2063 probability of depressurization for each generator. For this study, the staff explicitly determined that it is possible to estimate the probability that an MSIV leak will not depressurize any of the steam generators, or that such a leak will result in depressurization of up to three steam generators. Specifically, the estimate is based on using the failure rate and a binomial distribution.

For APET branches with all three steam generators intact at the time of dryout (e.g., branch C1 on Figure 2.3d), this results in probabilities of 0.5, 0.39, 0.10, and 0.01 that MSIV leakage will result in depressurization of zero, one, two, or three steam generators, respectively. For APET branches with one steam generator depressurized and the remaining two steam generators intact at the time of dryout (e.g., branch C2 on Figure 2.3d), this results in probabilities of 0.63, 0.33, and 0.04 that MSIV leakage will result in depressurization of zero, one, or two, of the two remaining steam generators, respectively.

The likelihood of depressurizing multiple steam generators would be higher if steam generator leakage is considered a common mode failure mechanism. However, because of the paucity of MSIV leakage/failure data, the staff decided to assess the impacts of secondary side depressurization via sensitivity analyses rather than through further refinement of the probability models. These sensitivity analyses are presented in Section 5.3.

The staff also conservatively assumed that the rate of secondary side depressurization would be greater than the rate of primary system depressurization in sequences involving an RCP seal LOCA or a stuck-open pressurizer PORV. This means that the steam generator tubes would be challenged at full differential pressure before experiencing significant primary system depressurization.

2.3.6 Steam Generator Tubes Remain Intact with High Differential Pressure (APET Event J)

The ninth top event in the APET (event J) addresses the potential for core damage events

(identified in the Level 1 PRA analysis) that result in a pressure-induced rupture of flawed steam generator tubes, before tube heatup. The APET includes this top event because the NUREG-1150 analysis did not explicitly address the potential for pressure-induced SGTR (particularly given flawed tubes).

The ninth top event also addresses the probability of pressure-induced SGTR for each APET branch in which the primary system is intact and one or more steam generators depressurize at the same time (early or late, as depicted in the icon on Figures 2.3b through 2.3d). The APET also addresses this issue for sequences involving open pressurizer PORVs or RCP seal LOCAs (in conjunction with a depressurized steam generator). This is because the secondary side depressurization is assumed to precede these events and results in a pressure challenge to the steam generator tubes before the stuck-open PORV or seal LOCA can effectively reduce the primary system pressure.

The degree of pressure challenge in sequences with late primary system depressurization (event FO in the icon on Figures 2.3b and 2.3c) in conjunction with late secondary depressurization resulting from MSIV leakage (event LK in the icon on Figures 2.3b and 2.3c) actually depends on the relative rates of primary and secondary system depressurization in these sequences. Considerably higher primary system depressurization rates or lower secondary system depressurization rates could result in peak differential pressures across the tubes that are substantially less than the full differential pressure assumed in this study as a basis for estimating the probability of pressure-induced SGTR for these sequences.

The present analysis did not reflect the contribution to pressure-induced SGTR resulting from core damage sequences with high primary system pressure and wet secondary because of the low frequency and scrubbed releases for these events. However, a more rigorous assessment would consider the contribution from such events.

The likelihood of pressure-induced SGTR should be limited through compliance with deterministic or probabilistic criteria for structural integrity, as well as operational leak rate limits permitted by Technical Specifications. Plants with steam generators in poor condition and operating near specified tube integrity limits are expected to have a probability of pressure-induced SGTR of no more than 0.05 per steam generator, given an event that leads to complete depressurization of the secondary side (e.g., an MSLB). Plants with steam generators in good condition (i.e., having a relatively small number of flawed tubes) are expected to have a much lower probability of pressure-induced SGTR.

In the present study, the staff quantified the probability of a pressure-induced SGTR on the basis of the probabilistic, limit-load calculation methodology and associated secondary system input parameters described in Section 5.2, in conjunction with assumed steam generator flaw distributions described in Section 4.2. As discussed in Section 4.2, the staff used two different approaches to develop a total of six different flaw distributions representing steam generators in good, average, and poor condition.

The base case analysis in the present study reflected the RES-developed flaw distribution for steam generators with "moderate" degradation. Using that distribution, the staff estimated the probability of a pressure-induced SGTR to be 0.0549, 0.107, and 0.156 for events/APET branches involving depressurization of one, two, or three steam generators. The staff also conducted sensitivity studies, as described in Section 5.3, to explore the impact of different flaw distributions on the probability of pressure-induced tube rupture.

2.3.7 Cold Leg Loop Seals Maintained (APET Event K)

The tenth top event in the APET (event K) represents the probability that loop seal clearing will occur in the same loop in which a steam generator is depressurized. The staff found that concurrent loop seal clearing and steam generator depressurization enhances steam generator tube heating in RCP seal LOCA sequences to the degree that failure of even pristine tubes was expected in the reference plant analyses described in Section 5.2. In the APET, the staff treated concurrent loop seal clearing and steam generator depressurization as separate events. This permitted the staff to isolate the frequency of tube failure from this challenge from other steam generator failure modes.

As discussed in Section 3, one loop seal was predicted to clear in the reference plant thermal-hydraulic analysis for the RCP seal LOCA sequence. (Loop seal clearing did not occur in other sequences analyzed for the reference plant.) For this particular calculation, the loop seal cleared in a different loop than the depressurized steam generator (and therefore did not result in a prediction of steam generator tube creep rupture). Nonetheless, the staff expects some randomness in the clearing of a specific loop, as further described in Section 3.4.

The staff considered the probability of loop seal clearing for all APET branches involving RCP seal LOCAs. For purposes of quantification, the staff assumed that all RCP seal LOCA events will involve clearing of one RCS loop seal, with the location of the cleared loop randomly distributed. Accordingly, the probability of concurrent loop seal clearing and steam generator depressurization is 0.333, 0.667, and 1.0 for RCP seal LOCA branches with one, two, or three steam generators depressurized (see Figure 2.3d).

2.3.8 Thermally Induced SGTR Before Hot Leg or Surge Line Failure (APET Event L)

The eleventh top event in the APET (event L) addresses the probability that thermally induced failure of steam generator tubes occurs before any other breach of the RCS pressure boundary. The staff assessed this probability by considering the following factors:

- the temperature and pressure histories throughout the RCS for each APET branch, which collectively represent the thermal and structural loads for the RCS components and steam generator tubes for the spectrum of severe accidents
- characterization of the distribution of flaws that could be present in the steam generators tubes
- a structural failure model for predicting whether various flaws will fail under the given thermal and structural loads.

Explicit consideration of flaws within the steam generator tubes and assessment of flaw behavior under severe accident conditions are key contributors to accurate assessment of this top event, and distinguish this work from previous analyses.

The process used in the present study to quantify the probability of a temperature-induced SGTR comprised the following steps:

(1) Determine the RCS and steam generator pressure-temperature histories for each APET branch, on the basis of a SCDAP/RELAP5 analysis for a sequence that most closely or conservatively represents the family of sequences addressed by each branch.

(2) Define the steam generator flaw distribution for the plant condition of interest (e.g., moderately degraded steam generator tubes).

(3) For each representative sequence, estimate the probability of a temperature-induced SGTR for each RCS loop, on the basis of the calculated RCS and steam generator pressure-temperature histories and specific steam generator flaw distribution.

(4) Adjust the calculated probabilities of temperature-induced SGTR to account for the number of intact/depressurized steam generators on each APET branch (and loop seal clearing in RCP seal LOCA events) and import the adjusted values into the APET.

Section 5.2. discusses these steps, and the resulting probability values, in greater detail.

2.3.9 Fission Product Holdup (APET Event M)

The twelfth and final top event in the APET (event M) addresses the potential for enhanced fission product holdup in the RCS and the secondary side as a subset of the pressure- or temperature-induced SGTR events. Bypass events would reduce fission product releases if they involve primary system depressurization (caused by a seal LOCA or open pressurizer PORV) with the ADV/MSSV intact but leaking. Factors contributing to the reduction of releases include fission product holdup and deposition within the RCS and steam generators between ADV/MSSV cycles, and the eventual reduction in primary system pressure to a level below the valve opening set point. Events with successful holdup were assigned to a separate release class, termed RC-2.

For those APET branches involving depressurization resulting from leakage in one or more steam generators (LK in the APET icon), the staff addressed this top event in conjunction with a stuck-open ADV/MSSV in another steam generator (SO in the APET icon). An induced rupture in the leaked-down steam generator would offer enhanced fission product holdup; a rupture in the steam generator involving a stuck-open ADV/MSSV would not. The staff therefore determined the probability of successful holdup on the basis of the assumption that a pressure- or temperature-induced rupture of a depressurized steam generator is equally likely regardless of whether the steam generator is depressurized as a result of a stuck-open ADV/MSSV or a leaky MSIV. For those APET branches on which all steam generator depressurization events result from the same cause (e.g., leakage, LK, on branch B1 on Figure 2.3d), the staff assigned all of the frequency to the appropriate release class as part of the endstate classification, and top event M need not be addressed.

2.3.10 APET Endstate Characterization

Releases for a temperature-induced SGTR event could vary significantly depending on the characteristics of tube failure. For example, primary system depressurization (through the failed tubes) would be gradual enough that subsequent creep-rupture of the RCS piping would be expected before significant release of fission products to the environment if each of the following conditions exists:

- Steam generator tube failure results in a primary-to-secondary leak area less than that corresponding to complete rupture of one tube.
- The integrity of adjacent tubes is not compromised.

By contrast, a failure equivalent to the rupture of more than two tubes would lead to more rapid RCS depressurization and would preclude subsequent, beneficial creep-rupture of RCS piping.

Separate analyses performed by the staff (as described in Section 4) indicate that rupture of a single steam generator tube could result in significant heating and possible failure of adjacent tubes. Because of the inability to ensure the integrity of adjacent tubes, the

staff did not intend to delineate between single- and multiple-tube ruptures in characterizing the APET endstates for the present analysis. Further assessment of the impact of SGTR or leakage on adjacent tubes is ongoing and could provide a basis for more thoroughly evaluating the releases associated with the various APET endstates.

To characterize potential releases to the environment, the staff grouped the APET endstates into three release categories (RCs):

- RC-1 - The containment is bypassed and fission products are released directly to the environment via either a failed/latched-open or cycling ADV/MSSV.

- RC-2 - The containment is bypassed but releases are reduced by a partially depressurized RCS and intact but leaky MSIV(s), which increase fission product holdup time.

- RC-3 - Containment integrity is maintained, and releases to the environment are limited to the normal containment leak rate.

Within RC-1, the source terms for sequences with cycling ADV/MSSVs would be smaller than for sequences with failed/latched-open valves because of additional fission product holdup and deposition in the RCS and steam generators between valve cycles. These release modes could be treated separately in more rigorous analyses, but were grouped together in the present study because of the scoping nature of the study and the expectation that both modes would result in relatively large releases.

In contrast, sequences assigned to RC-2 would not involve sustained ADV/MSSV cycling because of the eventual reduction in primary system pressure to a level below the valve opening set point. Such sequences would also have significantly reduced source terms because of fission product holdup and deposition within the RCS, as well as the condenser and turbine building.

The frequency of high primary pressure/dry secondary side events leading to RC-1 or RC-2 was determined separately from the APET. However, given the focus of the present study on bypass frequency rather than offsite consequences, the staff summed these frequencies for purposes of comparison with the surrogate safety goal for large release.

The staff recognizes that a more complete assessment, extending to treatment of offsite consequences, would be needed to determine the risk associated with induced SGTR and to provide meaningful comparisons with current estimates of overall risk for nuclear power plants. A state-of-the-art analysis of fission product release and deposition on primary and secondary side piping structures for each release class would more appropriately be part of that expanded study. Judging by the source-term analyses reported in EPRI TR-106194 and the latest analyses using the VICTORIA code, fission product releases and associated offsite consequences for induced SGTR sequences may be significantly overstated in previous studies such as NUREG-1150.

2.4 Design-Specific Influences

The Surry-based event tree discussed in Section 2.3 of this report assumes several key events in the progression of the SBO sequence. The first is that the natural circulation flow path involving the vessel, hot legs, and steam generators is established and maintained. This requires the existence of specific thermal-hydraulic conditions, especially the cold leg loop seal. Further, the plant is assumed to be in the high RCS pressure and dry secondary situation during an SBO. Key points in the event tree which

determine if the plant is in that state include the status of RCS and steam generator pressures at the time of core damage, when tube temperatures are maximized.

Examination of steam generator severe accident tube challenges has prompted consideration of design differences that might alter sequence progression and the potential for tube failure among the three PWR vendors in the United States. This section emphasizes the significance of differences among the three vendor designs, leaving for further study the detailed assessment of plant-specific differences within a design group.

For the purposes of this study, PWRs may be divided into two groups, encompassing those with U-tube steam generators (Westinghouse and CE plants), and those with once-through steam generators (Babcock and Wilcox (B&W) plants). On the basis of expected loop flow patterns observed in scaled facility studies, severe accident thermal challenges to steam generator tubes are not a concern for the B&W design since the natural circulation of superheated steam is confined to the hot leg and never reaches the steam generator. The "candy-cane" configuration prevents the involvement of the tube bundle in convective flow processes that could exist in the hot leg (Stewart, 1989).

Section 3.4 highlights key differences between Surry, other Westinghouse designs, and CE designs that could introduce significant differences in the accident sequence progression, event tree structure, and quantification. This section also briefly considers the potential differences in the following aspects of the sequence:

- severe accident progression, thermal-hydraulic response, and RCS/steam generator creep failure behavior for unflawed tubes (Section 2.4.1)
- maintenance of the loop seal (Section 2.4.2)
- plant capabilities and operator actions to depressurize (Section 2.4.3)
- pressurizer PORV/SV failure probabilities (Section 2.4.4)
- steam generator ADV/SV failure probabilities (Section 2.4.5)
- probability and magnitude of seal LOCAs (Section 2.4.6)
- steam generator degradation mechanisms, locations, and associated flaw distributions (Section 2.4.7)

Section 2.4.8 presents recommendations regarding the applicability of the generic event tree to other plant designs.

2.4.1 Accident Progression and Thermal-Hydraulic Response

Timing of RCS piping creep failure (relative to steam generator tube failure) is the main factor when estimating the potential for tube failure under severe accident conditions. Component creep failure is a function of RCS pressure and the component temperature history. The RCS pressure during the event will be affected by mechanisms that lead to plant depressurization, such as component failures of the reactor coolant pressure boundary (RCPB).

In particular, survivability of the surge line, hot legs, and steam generator tubes, as well as the RCP seals and relief valves, is examined in previous work. Section 4.1 of this report discusses a broader examination of possible RCPB failure sites. In addition, Section

3.4 compares the timing of events, including failure times, in the SBO thermal-hydraulic analyses for Surry and ANO-2.

Previous studies such as NUREG/CR-5949 (Knudsen, 1993), have addressed the potential for RCS piping failure. This study built upon the earlier work with a detailed examination of the potential for ex-vessel failure of RCS piping (specifically the surge line and hot leg) for Surry. It yielded the general conclusion that a hot leg or surge line failure is likely relative to vessel breach, but CE designs were not considered.

NUREG/CR-6285 (Bayless, 1995) included an assessment of the potential for RCS failures that could lead to rapid depressurization, thereby removing high differential pressure loads on tubes. That report attempted to categorize PWRs on the basis of their potential means of unintentional depressurization as a result of thermally induced failures. However, the conclusion reached in NUREG/CR-6285 was that it is not possible to identify a simple set of parameters that would characterize PWRs in this manner. Differences in hardware, a lack of applicable component failure data, and variations in accident progression present sufficient uncertainties that Surry results cannot be used to determine when RCS failures would occur during severe accidents in other plants. Therefore, the results of past studies could not be relied upon to reach a conclusion regarding the relative potential for RCPB failure between the PWR designs.

2.4.2 Maintenance of the Loop Seal

Maintenance of the cold leg loop seal is a function of the piping configuration that causes it to form and the flow pattern that exists once superheated steam is generated from the vessel. The cold leg piping elevation is somewhat shallower for some CE plants than in the Westinghouse design. This could allow a smaller pressure perturbation from accumulator injection, or some other mechanism, to blow out the seal. INEL (Ellison, 1996) therefore performed thermal-hydraulic analyses of Surry assuming that the loop seal was lost, and resulting in full-loop circulation of superheated steam at a greater rate than in the hot leg counter-current flow situation and higher tube temperatures. The loop seal could also be lost as a result of a large RCP seal leak, allowing the cold leg fluid to be displaced from the RCS by the hot steam.

The two designs also differ in the hot leg diameters 107 cm (42 inches) for CE, and 74 cm (29 inches) for Westinghouse. Other more subtle differences in RCS configuration could also have an impact on natural circulation flow patterns, but studies to date have not determined the effect that these differences present, if any.

2.4.3 Plant Capabilities and Operator Actions to Depressurize

The Westinghouse emergency operating guidelines include a step early in the procedure to direct operators to depressurize intact steam generators to remove heat from the RCS. The procedure also warns operators to maintain steam generator levels and pressures above minimum requirements. Depressurization is accomplished by opening ADVs on the intact steam generators to establish a maximum steaming rate consistent with plant-specific constraints. The step assumes that the ADVs can be operated from the control room, and that accumulators and electrical power are available. However, some plants may not have the capability to open the ADVs from the control room.

AFW flow is necessary to carry out the steam generator depressurization while also maintaining the minimum steam generator levels and pressures. Pressure must be reduced in a controlled manner to preclude lowering RCS pressure to the point of accumulator injection. Also, minimum cold leg temperature requirements must not be violated during

depressurization.

2.4.4 Pressurizer PORV/SV Failure Probabilities

Failure of relief valves may occur under the thermal conditions expected in a high-pressure severe accident. The potential for a failure depends on the design and temperature qualifications of the valves. However, there is no information on relief valve failure modes under the extreme temperatures expected in the cases considered in this study. Therefore, although failures may be expected, the failure mode (open, shut, or some intermediate state) cannot be predicted, and the failure potential cannot be reliably quantified.

The peculiarity most often mentioned for CE plants is that some do not have primary PORVs installed. Specifically, these plants are ANO-2, the Palo Verde Units, San Onofre 2&3, and Waterford. These plants rely upon SVs to limit system pressure. In other plants, PORVs are used to help prevent SV actuations. Typically, the set point difference between SVs and PORVs is about 0.7 MPa (100 psi), with the SV set point higher and always about 17.2 MPa (2500 psig). In high-pressure severe accident analyses for non-PORV plants, the initial pressure relief will not begin until the reactor reaches a higher pressure. Another difference is that SV relief capacity is up to four times greater than PORV flow capacity. This may tend to accelerate surge line heatup for the non-PORV plants (relative to those with PORVs) since the greater flow rate through the surge line during SV lifts would allow the surge line piping to heat up more quickly.

2.4.5 Steam Generator ADV/SV Failure Probabilities

The potential for steam generator SV or ADV failure during an SBO, and the resultant depressurization of the secondary system, depends upon the particular valve configuration and conditions to which the steam generator will be exposed during an event. Steam system SVs are of generally standard design throughout the various PWR designs, so a failure potential related to design differences is not expected. However, there is no information available with regard to the potential for unfavorable conditions developing at the valve location in the secondary system as a consequence of possible primary-to-secondary leakage. Variables such as length and orientation of piping to the valves would affect the temperatures and the potential for thermal failure. Detailed plant-specific information is required to permit a determination of secondary valve failure potential. For this generalized study, the potential for thermal failure of secondary components is considered to be the same for CE and Westinghouse designs.

2.4.6 Probability and Magnitude of Seal LOCAs

The likelihood of RCP seal failure under extreme temperature and pressure conditions may be greater for Westinghouse plants than for CE plants (Bayless, 1995). This is because the Westinghouse pump seals rely on continuous seal cooling, while the CE plants use a different pump design. However, Westinghouse plants have begun replacing seals using a design expected to have improved survivability under high temperatures. It is unclear how many of superheated steam and the potential for ex-Westinghouse-designed plants have upgraded their seals. Although further data are needed to conclusively demonstrate differences in reliability among different seal designs, the staff assumed that a Westinghouse design would generally have a greater chance of failing an RCP seal under severe accident conditions. This has an impact on the ability to maintain the cold leg loop seal, as discussed above.

2.4.7 Steam Generator Degradation Mechanisms and Associated Flaw Distributions

Although steam generator degradation is evident to some extent in all PWR designs, the nature and progression vary among designs. Design-specific features influence the nature of degradation. For example, the drilled-hole tube support plates in some Westinghouse-designed steam generators have been found to be a major factor in the propensity for these plants to experience stress corrosion cracking at the tube support plate elevations. Further, plant-specific differences (such as the steam generator manufacturing process and steam generator chemistry program) influence degradation characteristics.

Section 4 of this report presents the staff's estimates of a generalized tube failure distribution. This distribution incorporates information from across the three PWR designs, but it does not necessarily accurately represent the relative contributions of all degradation types and it does not weight the contributions by plant design. The difficulties encountered in attempting to define a generalized distribution highlighted this factor as a sensitive plant-specific consideration that would require more extensive data to permit application to a plant-specific analysis. This is discussed further later in the report.

2.4.8 Recommendations

The aggregate impact of the factors considered above is that an event tree founded on a Westinghouse plant design could represent the expected course of the same severe accident in a CE design. However, some cautions must be observed, since a potential impact on the event tree quantification arises from differences between the CE design and the Westinghouse plant analyzed. The examination of major design differences shows that the general event progression may be assumed to be similar. However, there are sufficient uncertainties and a lack of information for certain component performance under severe accident conditions that further study is needed to accurately quantify an event tree for either design.

The staff is currently conducting analyses to explore factors that might introduce differences between the designs in predicted thermal-hydraulic response, including those contributing to the ability to maintain the cold leg loop seal. Other uncertainties (such as the nature of the natural circulation essel component failures) have not been sufficiently analyzed to allow the staff to draw firm conclusions.

A comparison of similar severe accident analyses for the two designs (Section 3.4) did not highlight any significant difference in event progression that could be attributed to differences between the designs. Therefore, until further information becomes available for more complete event tree quantification, the Westinghouse event tree presented in this study is adequate for general consideration of the CE design.

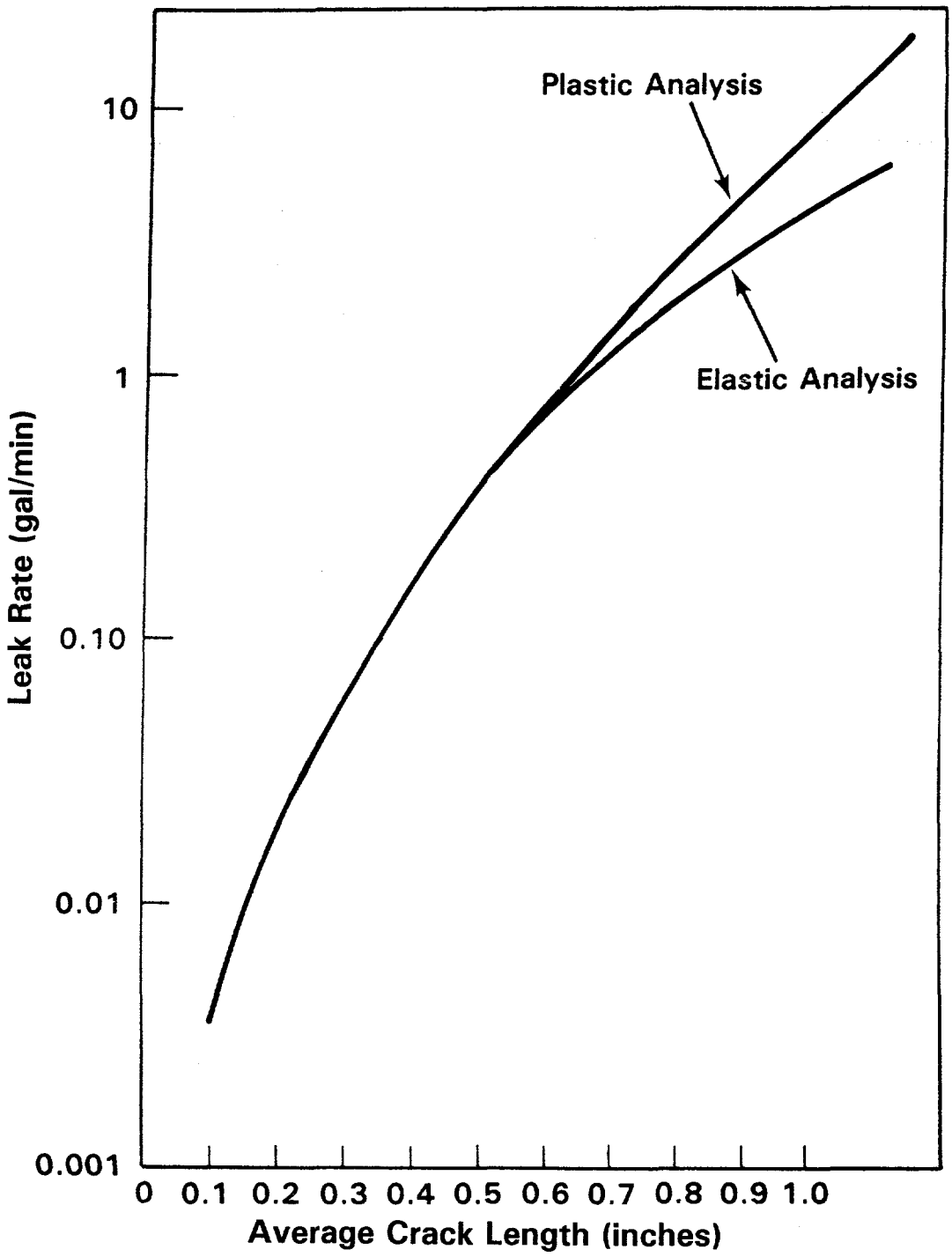

Figure 2.1 **Leak Rate Model Predictions, Normal Operating Conditions**

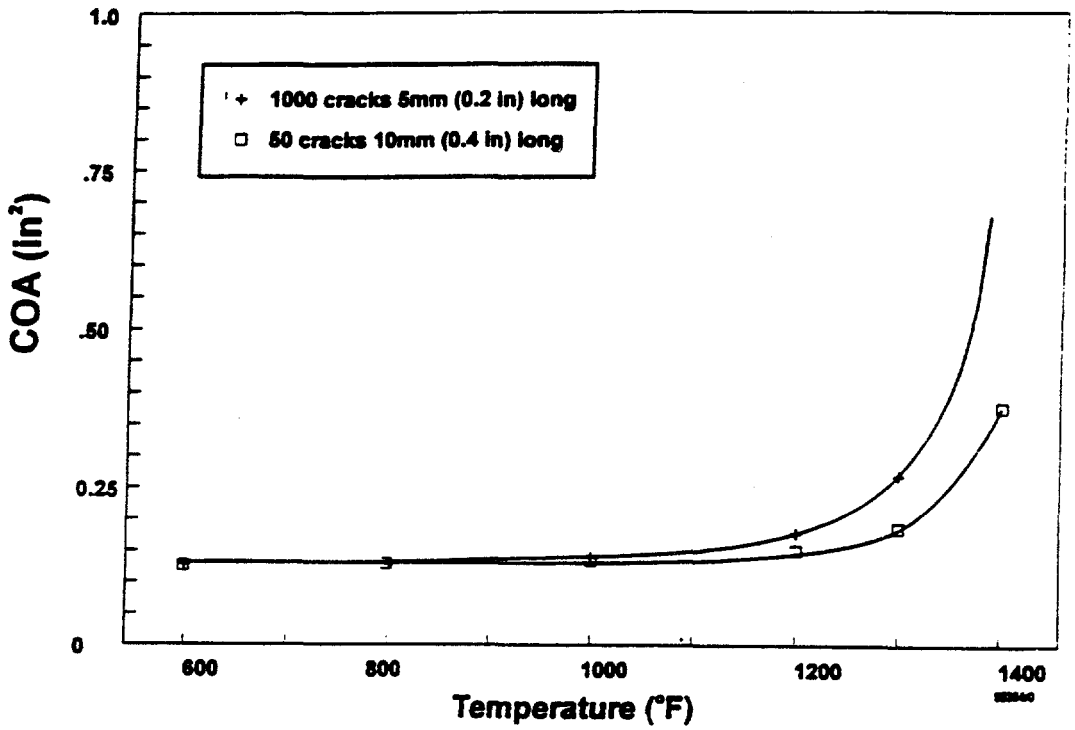

Figure 2.2 **Increase in Crack Opening Area (COA) with Temperature**

(from EPRI TR-106194)

BASE CASE: Reference Plants

EVENT TREE: Induced Steam Generator Tube Rupture

High Primary/Dry Secondary

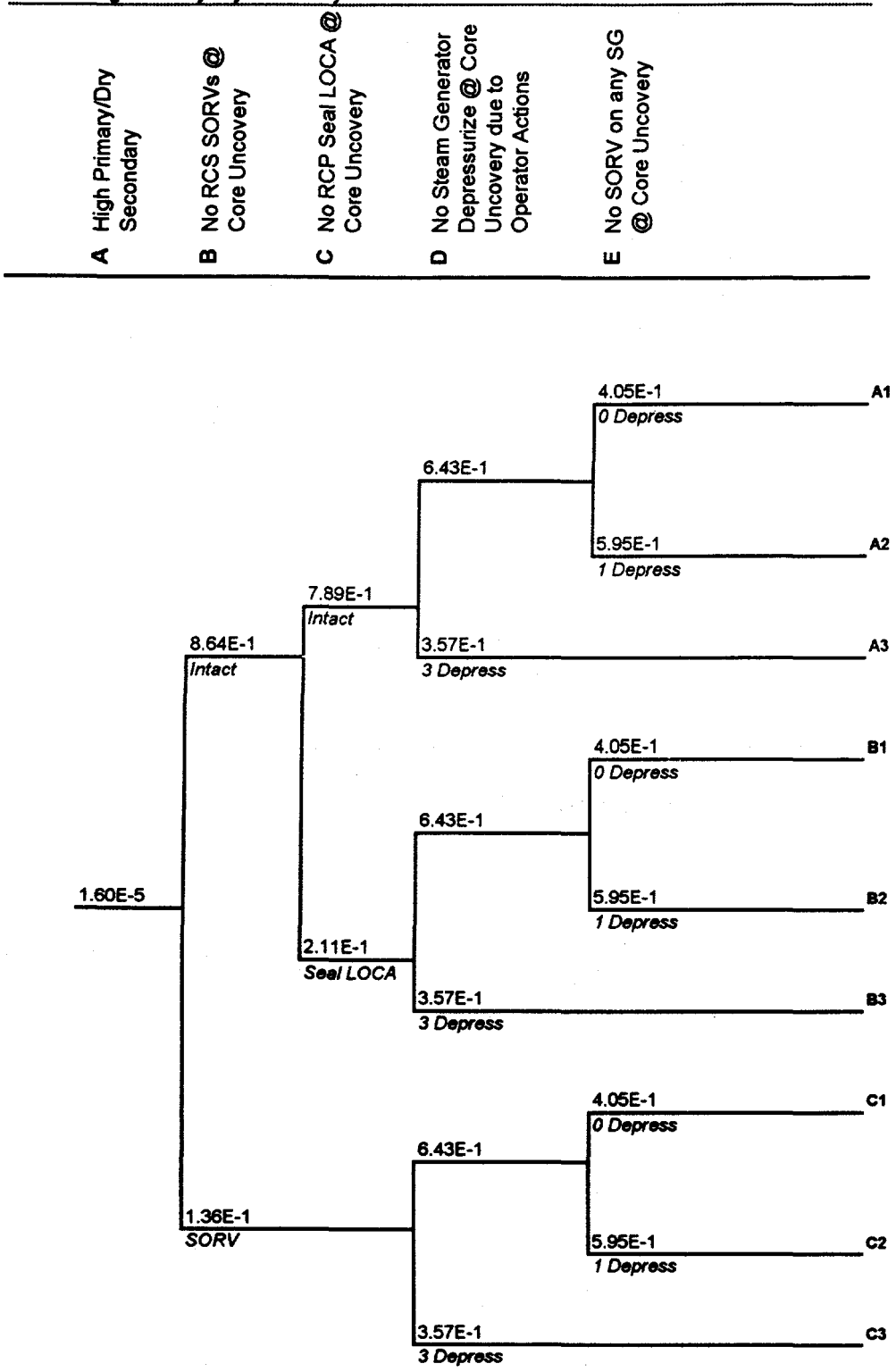

Figure 2.3 Accident Progression Event Tree

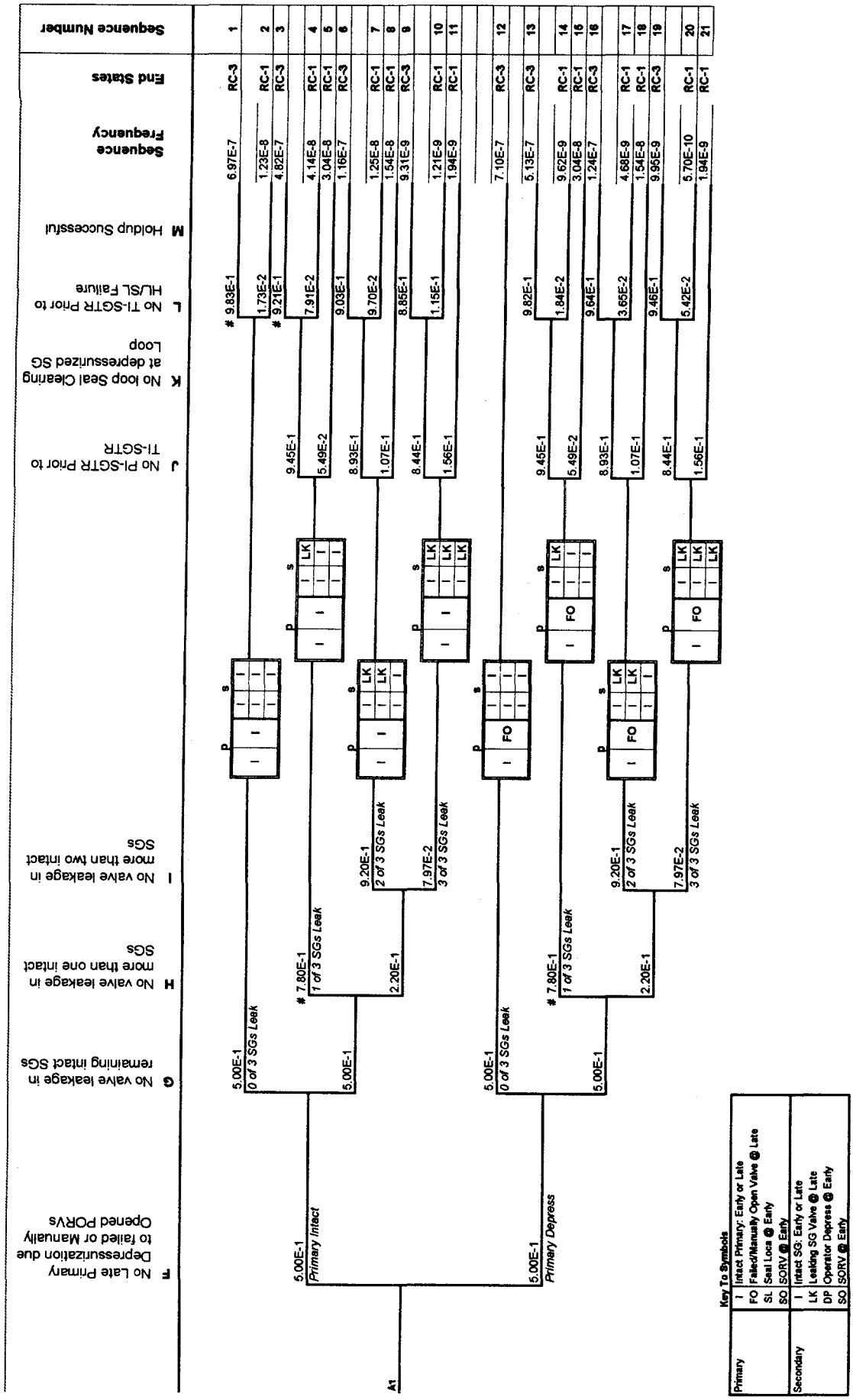

Figure 2.3a Continuation Event Tree, Branch A1

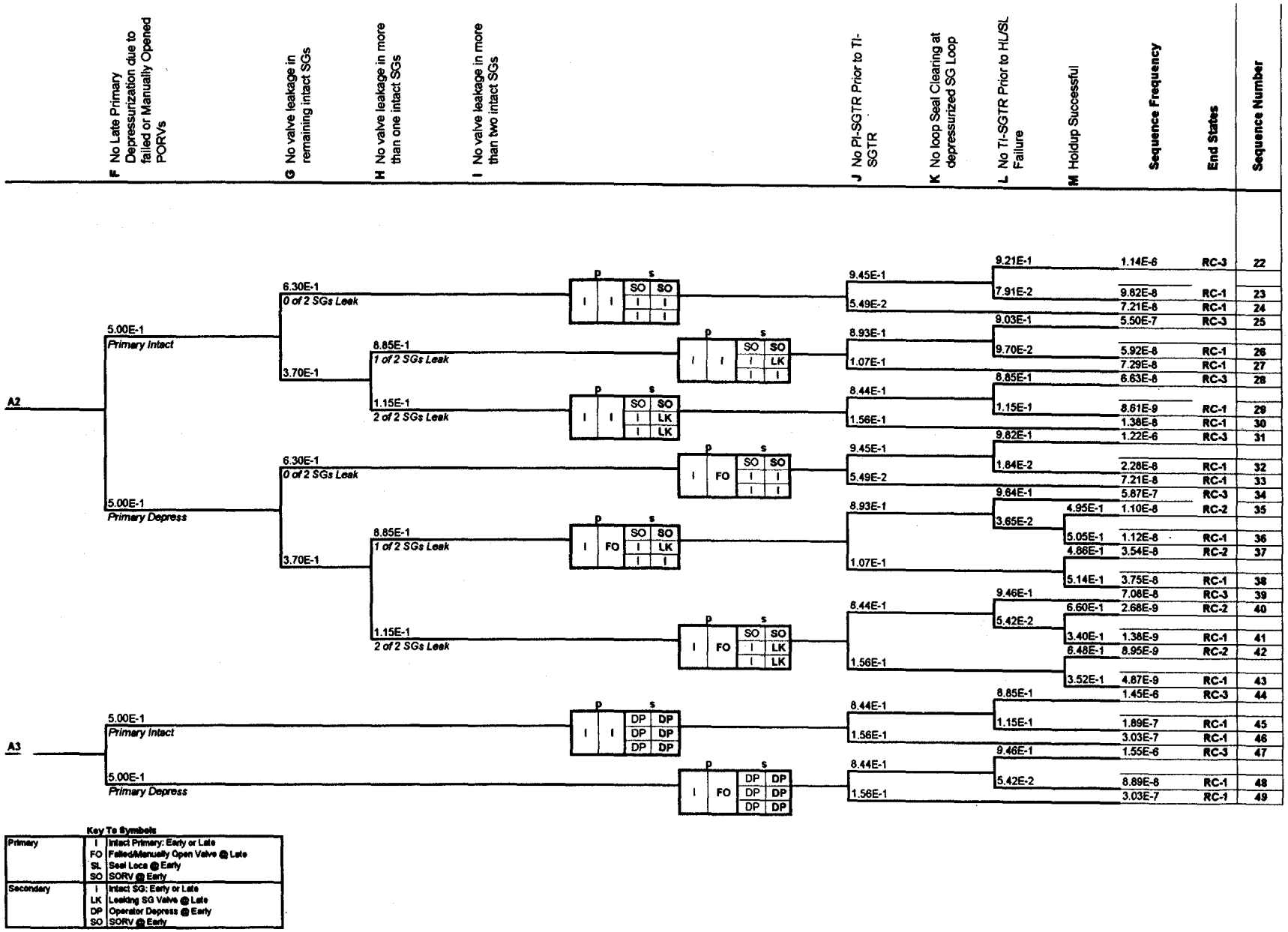

Figure 2.3b Continuation Event Tree, Branches A2 and A3

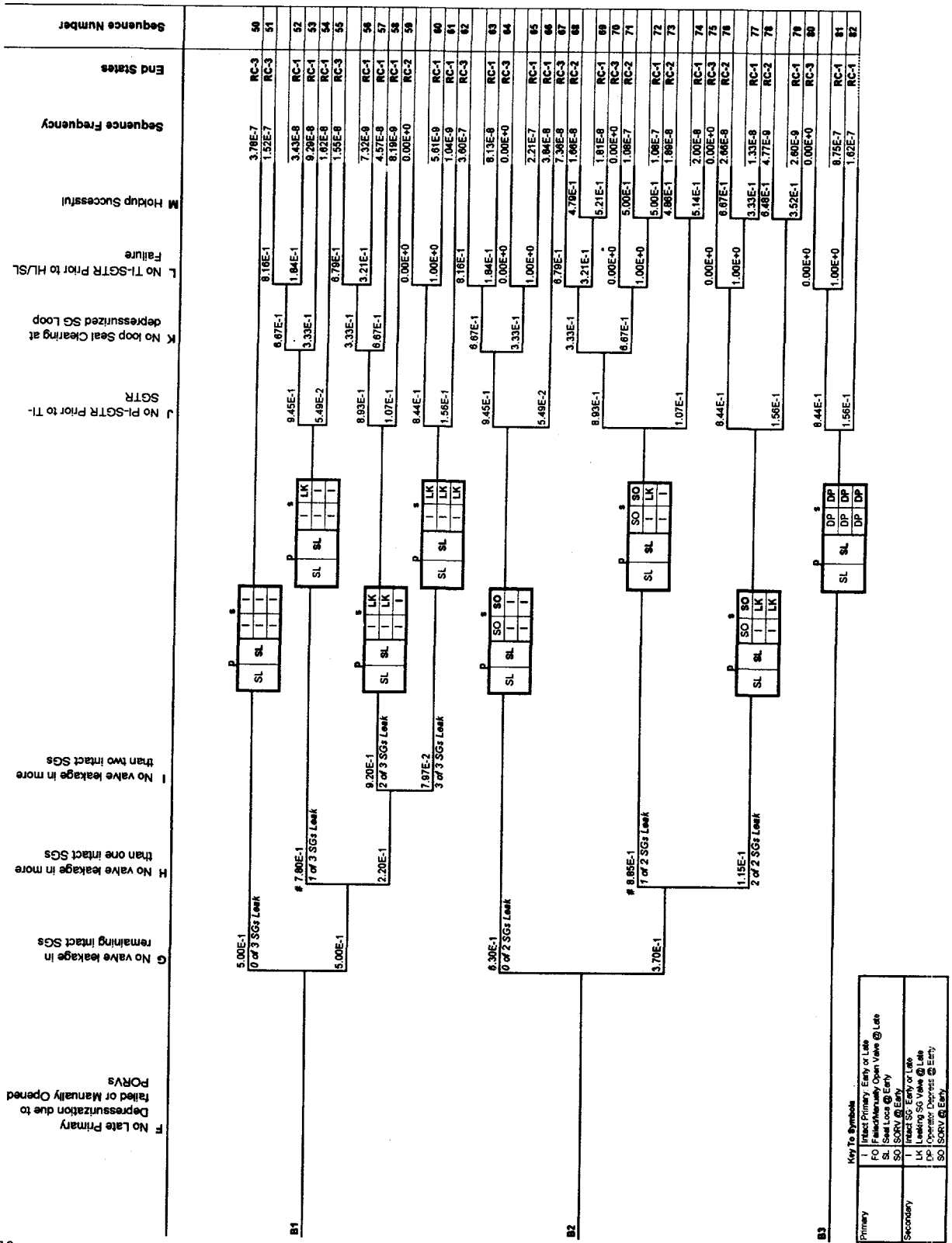

Figure 2.3c Continuation Event Tree, Branches B1, B2, and B3

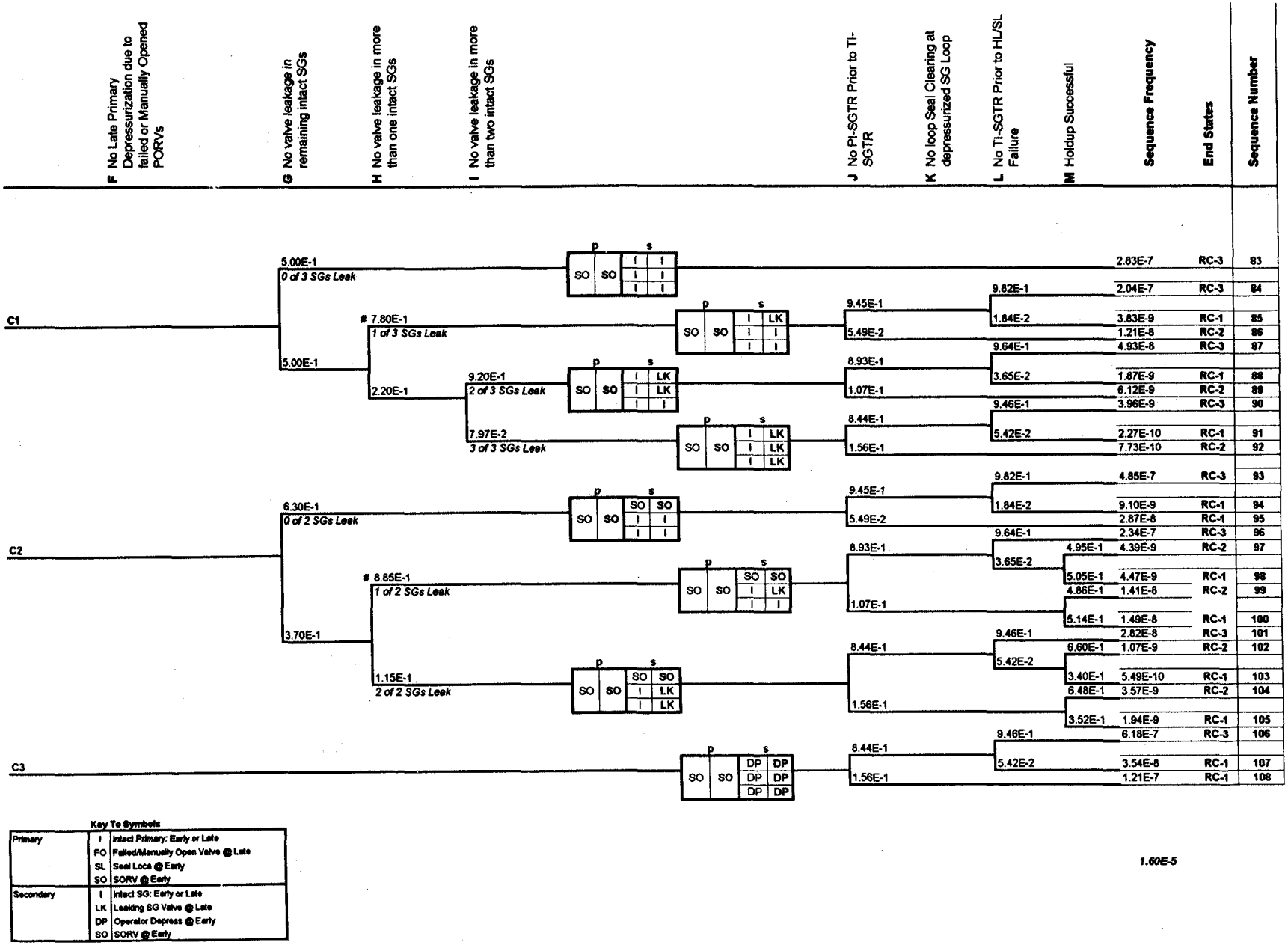

Figure 2.3d Continuation Event Tree, Branches C1, C2, and C3

Figure 2.4 IPE Sequence CDFs (High RCS Pressure/Dry SG)

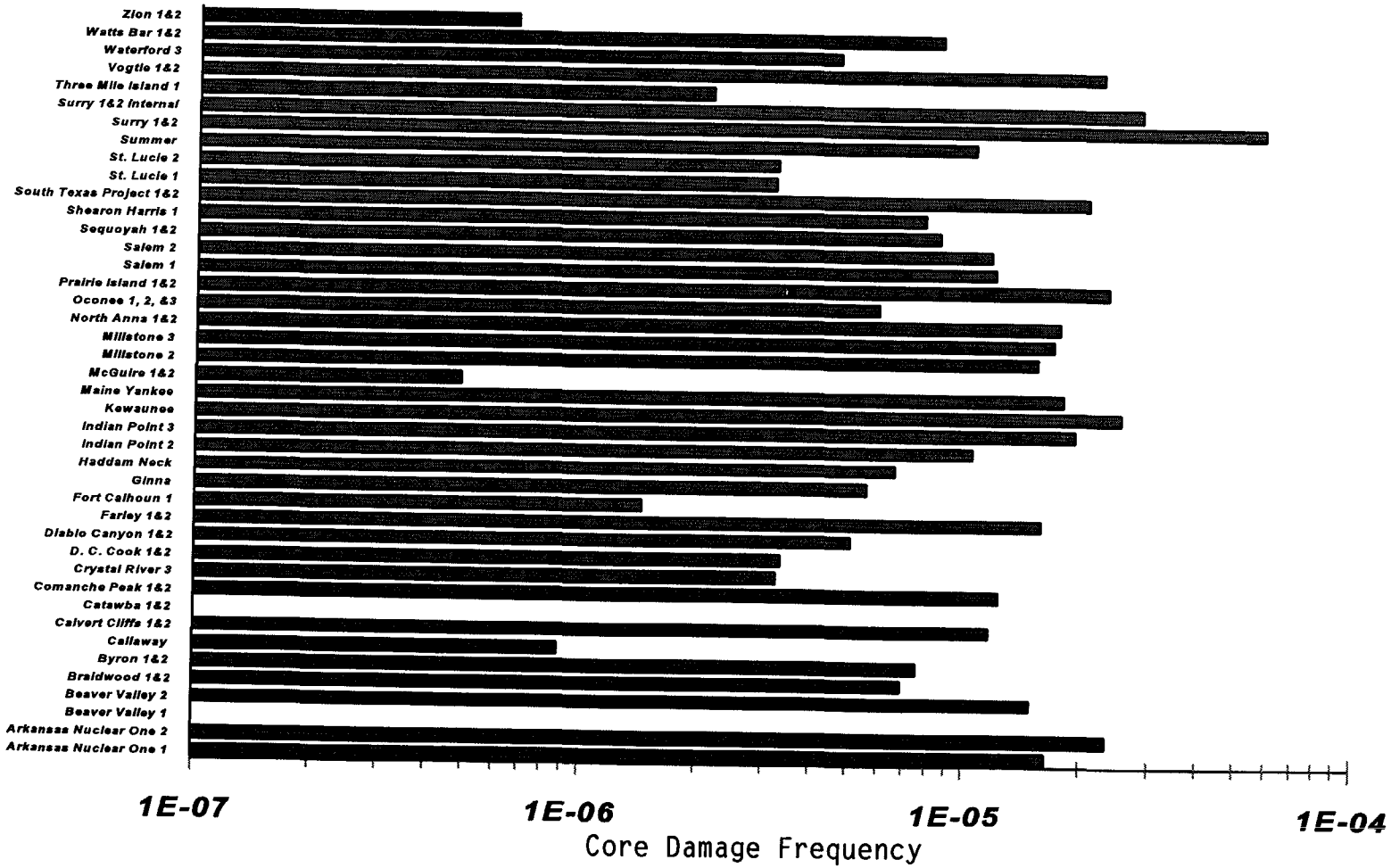

3 BEST-ESTIMATE THERMAL-HYDRAULIC CONDITIONS

3.1 Scope and Objectives of Thermal-Hydraulic Analyses

Induced SGTR during certain severe accidents is a safety consideration since high-temperature steam flow, created by overheating of the core, can circulate through the reactor coolant system, including the steam generator tubes. Components can be heated to much higher temperatures – in the range of 900-1000 K (1160-1340 °F) – than normally considered within the design-basis envelope. Component heating can occur to the extent that the structural capacity of the components is reduced and rupture may be induced as a result of the combined effects of pressure and temperature. The conditions for steam generator tubes can be further aggravated by the depressurization of the secondary system, which increases the pressure differential across the tubes.

In evaluating the risk impacts associated with such a challenge to steam generator tube integrity, detailed analyses have been performed at the Idaho National Engineering Laboratory (INEL) using the SCDAP/RELAP5 code (Coryell, 1995). The overall objective of the analyses was to determine the appropriate thermal-hydraulic boundary conditions (pressure and temperature) affecting steam generator tubes during severe accidents. The analyses were conducted for variations of a station blackout accident sequence, since it is considered a likely sequence to produce high temperature and pressure conditions at the tubes. The boundary conditions established by such analyses have then been used, through further analysis (described in Sections 4 and 5), to assess the likelihood of an induced failure of tubes during severe accidents.

The general philosophy of the severe accident thermal-hydraulic analysis was to use a best-estimate approach within the limitations of available methods and with appropriate consideration of uncertainties. SCDAP/RELAP5, a detailed mechanistic severe accident computer code, was used for these calculations. This code has been applied to this type of calculation (i.e., high-pressure natural circulation sequences in a PWR) in numerous other studies, and considerable experience has been gained in its use. More recently, the code was used extensively as part of the resolution of the direct containment heating (DCH) severe accident issue to analyze the probability of reactor system depressurization before reactor vessel failure for almost the same scenarios of interest for steam generator tube integrity. The principal difference was that the SCDAP/RELAP5 analysis of unintentional depressurization of the primary system (as a result of hot leg, surge line, or steam generator tube failure) performed for resolution of the DCH issue did not consider depressurization of the secondary system, because of assumed failure (in the open position) of the secondary side relief valves. The additional failure of the secondary side relief valves has the significant and obvious effect of increasing the differential pressure across the steam generator tubes (thus, increasing the challenge to tube integrity). Also, blowdown of the steam generator reduces the heat removal capacity of the steam generator, thereby contributing to an increase in the tube temperatures.

As part of the SCDAP/RELAP5 analysis performed in the DCH study, creep rupture failure of the hot leg, surge line, and steam generator tubes was modeled using a Larson-Miller creep rupture model. As described later in Section 4.3, the Larson-Miller model was extended in its application to predict failure of cracked tubes. Previous applications of the SCDAP/RELAP5 Larson-Miller failure predictions considered only unflawed components.

To provide a range of predicted thermal-hydraulic conditions to accommodate the accident progression event tree, and to provide insights regarding the impact of PWR design differences, several analyses were performed for both the Surry and Arkansas Nuclear One Unit-2 (ANO-2) designs. Scenarios analyzed for this study include those listed in Table 3.1. The table also shows the original designations, provided in the contractor reports, along with the designations used in this report. In addition, Table 3.1 indicates those cases used to characterize the APET endstates. Descriptions of the cases used in later portions of the report are provided in Section 3.2. Further details appear in contractor reports sponsored by the NRC (Ellison, 1996; Knudsen, June and December 1996 and 1997).

Within the overall objectives stated above, the SCDAP/RELAP5 analyses were also performed to address a number of subsidiary issues, including variation in tube thermal boundary conditions as a result of the effects of phenomenological and modeling uncertainty (Section 3.3), plant design differences, and sequence variations (Section 3.4). Within the variations caused by plant and sequence differences, the potential for loop seal clearing was examined since loop seal clearing and restoration of full loop circulation would accelerate tube heating because of increased flow through the steam generator. Further analyses were undertaken to explore the sensitivities of major uncertainties in the thermal-hydraulic analysis bearing on the steam generator tube heatup. These analyses are covered in Section 3.3.

3.2 Steam Generator Tube Pressure and Temperature Predictions

Thermal-hydraulic analyses conducted for the Surry and ANO-2 plant designs are discussed in this section. Section 3.2.1 outlines the overall strategy used and some of the modeling details. Specific results for each plant are discussed in Section 3.2.2

3.2.1 Analytical Approach

SCDAP/RELAP5 analyses were carried out for the Surry and ANO-2 plants to calculate the thermal-hydraulic conditions associated with an SBO sequence. For each plant analyzed, variations of the sequence (e.g., assumption of failure or non-failure of the SG secondary side atmospheric dump valves) were considered. Additionally, sensitivity calculations were performed using a single-loop model for the Surry plant to investigate the effects of thermal-hydraulic phenomenological uncertainty related to the SG inlet plenum mixing assumptions on the predicted SG tube temperatures. These calculations are discussed in Section 3.3. Additional sensitivity studies assess issues not addressed in the initial set of analyses. These additional studies are summarized in Tables 3.2 and 3.3, and are also discussed in Section 3.3.

For the Surry and ANO-2 plant analyses, an SBO sequence was assumed to be the accident initiator in all of the calculations. The specific sequence considered includes an immediate loss of AC power and the loss of all feedwater. Additional assumptions made were that the sequence progressed without recovery and without operator actions, and all RCS components that served as pressure boundaries (e.g., hot leg, pressurizer surge line, SG tubes) were assumed to be free of defects. Table 3.4 summarizes the assumed conditions for the analyses.

Table 3.1 Summary of SCDAP/RELAP5 Studies Performed

Original Designation	Revised Designation	Plant	Sequence Description (variations on TMLB')	Remarks
INEL Studies Performed Under NRR Contract				
5	5N	Surry	Nodalization study	Finer nodalization of lower tube bundle
6	6N*	Surry	Stuck-open PORV	PORV failure at 1200°F core outlet temp
7	7N	Surry	>100 gpm SG tube leak	Leak increases with tube temperature
INEL Studies Performed Under RES Contract				
1	1R*	Surry	Base case, no SG nor RCS depressurization	–
2	2R	Surry	RCS depressurization, No SG depressurization	–
3	3R*	Surry	One SG depressurized, no RCS depressurization	SG depressurized by stuck-open ADV
3	3RU	Surry	Same as 3R	Used updated code
4	4R	Surry	Depressurization of one SG and RCS	–
5	5R	Surry	Case 1 variation	Used more even tube bundle flow split
6	6R	Surry	Case 3 variation	Used more even tube bundle flow split
6	6RU	Surry	Same as 6R	Used updated code
7	7R*	Surry	All SGs depressurized	–
8	8R	Surry	RCP seal leak	–
9	9R*	Surry	RCP seal leak	–
1	ANO1	ANO-2	SG depressurized, RCS not depressurized	No RCP seal leak
2	ANO2	ANO-2	SG and RCS depressurized	No RCP seal leak
3	ANO3	ANO-2	SG depressurized, RCS not depressurized	220 gpm RCP seal leak
4	ANO4	ANO-2	SG depressurized, RCS not depressurized	220 gpm RCP seal leak, No quenching of molten material in vessel

* Case used to characterize APET endstate.

Table 3.2 SG Inlet Plenum Mixing Sensitivity Studies*

Case	Percent SG Tubes Fwd Flow	Mixing Fraction	Recirculation Ratio
M1	29	0.87	1.9
M2	53	0.87	1.9
M3	61	0.87	1.9
M4	35	0.76	1.9
M5	35	0.89	1.9
M6	35	0.87	1.69
M7	35	0.87	2.25

* Based on Case 1R using a single-loop model

Table 3.3 Additional Sensitivity Studies

Case	Description	Remarks
6RU.	53%/47% hot/cold tube split	0.87 mixing fraction, 1.9 recirculation ratio
6RU.A	Heat transfer coefficients increased by 20%	Upper plenum, hot legs, surge line, SG tube surfaces
6RU.B	Heat transfer coefficients decreased by 20%	Same locations as 6R.A
6RU.C	Heat transfer coefficients increased by 30%	Hot leg, surge line, SG tube entrance volumes
6RU.D	Heat transfer coefficients increased by 30%	SG tube entrance volumes
6RU.E	Enhanced hot leg heat transfer	Fluid-to-fluid heat transfer and circumferential wall conduction
6RU.F	Based on 5% confidence values of mixing model parameters from transient experiment data	43%/57% hot/cold SG tube split, 0.73 mixing fraction, 1.8 recirculation ratio

The SCDAP/RELAP5 nodalizations of the Surry and ANO-2 plants included both full-loop and in-vessel natural circulation flow models for simulating conditions that would potentially develop during the event. (See Figures 3.1 and 3.2 for schematic representations of expected flows.) Provisions were made to change the SCDAP/RELAP5 nodalization of the hot leg to model countercurrent natural circulation after the hot legs are voided. The hot leg countercurrent flow model was benchmarked against the Westinghouse 1/7-scale experimental data on natural circulation (Stewart, 1993) before any calculations were performed. The cases used in this study were selected to depict the effect on tube conditions of variations in a number of parameters. Specifically, these parameters included depressurization of SG secondaries, treatment of RCS depressurization following predicted pressure boundary failure, and nodalization of the SG tubes (tube bundle flow split).

Table 3.4 Summary of Assumed Conditions for Surry Calculations

Assumed Severe Accident Conditions	Cases											
	1R	2R	3R 3RU	4R	5R	6R 6RU	7R	8R	9R	5N	6N	7N
RCS maintains pressure after predicted RCS boundary failure	x		x		x	x	x	x	x	x		
RCS depressurizes after predicted RCS boundary failure		x		x							x	x
Failed relief valve depressurizes pressurizer loop SG			x	x		x		x	x	x	x	
35% hot tubes/65% cold tubes	x	x	x	x			x	x	x	x	x	x
53% hot tubes/47% cold tubes					x	x						
All SGs depressurized because of failed relief valves							x					
RCP seal leak (250 gpm per pump)								x	x			
Pressurizer PORV fails open											x	
Cold leg loop seal drained												
No quenching of relocated upper plenum steel in vessel									x			

In evaluating the potential sources of uncertainty in the thermal-hydraulic analysis, the variation in the natural circulation test data was examined. It was apparent that the test data indicated a difference in the number of tubes carrying hot flow depending on whether the tests were run in a steady state or transient mode. There were also differences in the reported mixing fraction and the recirculation ratio. The mixing fraction reflects the fraction of the hot inlet flow entering the SG inlet plenum that mixes with the cooler flow returning from the SG tubes, while the recirculation ratio refers to the relative mass flow ratio between the SG natural circulation flow to the hot leg natural circulation flow. Figure 3.2 depicts these different flows. To investigate the effects of thermal-hydraulic phenomenological uncertainty (number of SG tubes participating in forward flow, mixing fraction, and recirculation ratio) related to the SG inlet plenum mixing, seven sensitivity calculations were performed using a single-loop model for the Surry plant as summarized in Table 3.2.

One result of the extended sensitivity studies was the conclusion that the base case analysis should use the results of Case 6R rather than Case 3R, since the former assumes a fairly even tube bundle flow split which is more representative of the transient scaled experiment conditions. As discussed later in this report, this conclusion was reached relatively late in the risk analysis and the staff judged that, although somewhat conservative, the Case 3R results were still a reasonable basis to characterize the APET endstates.

3.2.2 Summary of Analyses and Results

The analyses and key results of cases discussed in this report are covered, including the more recent Surry and ANO-2 studies, and the sensitivity studies based on the Surry model. Table 3.5 summarizes the results.

3.2.2.1 Surry

At initiation of the transient, the reactor is scrammed and the reactor coolant pumps are tripped because of a loss of all AC power. Initially, the RCS depressurizes because heat removal on the secondary side is sufficient to remove core decay heat. For Cases 1R and 2R, all SG ADVs are assumed to operate normally by cycling on secondary pressure. However, the secondary side heat sink is not sustained in the absence of feedwater and, as a result, the RCS pressure increases to the PORV set point near the time of SG dryout. A gradual RCS heatup and boiloff follows with RCS pressure fluctuating between 15.7 MPa (2277 psi) and 16.2 MPa (2350 psi) through PORV cycling. During a brief period of time, the RCS pressure rises above the PORV set point to the safety relief valve (SRV) set point of 17.8 MPa (2582 psi) because the pressurizer begins venting liquid and the PORV does not have the capacity to remove decay heat by venting liquid (Figures. 3.3 and 3.4).

Part of the core decay heat is transported to the SGs by full-loop natural circulation of liquid. When a sufficient amount of vapor generated in the core collects in the top of the SG U-tubes, full-loop natural circulation of liquid ceases. Core uncovery begins as a result of continued boiloff of water and venting through the PORV. When the SG and hot leg void, hot leg countercurrent natural circulation of vapor begins. Because of the degraded heat transfer associated with the hot leg countercurrent natural circulation flow, ex-vessel piping temperatures begin to increase. For Cases 1R and 2R, creep rupture of the pressurizer surge line is predicted at 234 minutes (14,050s) (Figures 3.5 and 3.6).

After surge line failure, in Case 1R, the calculation was continued, suppressing the surge line failure, to determine the timing associated with other potential pressure boundary failures. When continuing the calculation, creep failures of the hot leg nozzles in the pressurizer and non-pressurizer loops are predicted at 252 minutes (15,110s) and 261 minutes (15,670s), respectively. The calculation for Case 1R was terminated at 315 minutes (18,900s) because the surge line and all of the hot legs had failed. It was determined that the SG tubes would not fail for some time, and a margin of time to failure of at least one hour had already been established.

As mentioned earlier, in Case 2R, the surge line was allowed to fail, and the RCS depressurized as shown in Figure 3.4. When the RCS pressure sufficiently decreases to reach the accumulator injection pressure of 4.24 MPa (615 psi), the accumulator injects as illustrated in Figure 3.7, arrests the heatup of the core, and cools the ex-vessel piping as shown in Figure 3.6. Although, core reheating occurs after the accumulator water has boiled off, the energy associated with core reheating is primarily removed via the surge line break, which prevents any significant reheating of ex-vessel piping. Hence, the calculation was terminated at 347 minutes (20,800s). Thus, SG tube rupture is not expected if surge line failure occurs as predicted in Cases 1R and 2R.

Table 3.5 Summary of SG Tube Results for Surry Calculations

Case	Time of First Failure (mins)	Location of First Failure	At First Failure		At Peak Temp.	
			Temp (K)	ΔP (MPa)	Temp (K)	ΔP (MPa)
1R	234	Surge Line	847	9.3	1094	9.11
2R	234	Surge Line	847	9.3	847	9.27
3R	241	Surge Line	987	15.8	1147	16.2
3RU	227	Surge Line	973	15.9	1164[a]	15.9[a]
4R	241	Surge Line	987	15.8	987	15.8
5R	234	Surge Line	825	9.1	825	9.1
6R	229	Surge Line	933	16.0	933	16.0
6RU	229	Surge Line	957	15.9	1161[a]	15.8[a]
7R	218	Surge Line	943	16.0	1041	16.1
8R	275	Hot Leg	1078/1255[b]	8.5/1.5[b]	1090/1286[b]	6.9/0.1[b]
9R	269	Hot Leg	1010/1153[b]	4.0/-3.0[b]	1179/1309[b]	7.7/0.8[b]
5N	246	Surge Line	1036	15.9	1094	15.9
6N	191	Open PORV	709	16.0	1055	4.4
7N	353/390[c]	Surge Line	1043/1086[c]	4.7/10.1[c]	1097/1021[c]	0/0

a. Condition at time of predicted tube failure
b. Pressurizer loop/non-pressurizer loop conditions
c. 3 kg/sec and 7 kg/sec leakage cases

Cases 3R and 4R are similar to Cases 1R and 2R, except for the assumption that the ADV on the pressurizer loop SG fails open when initially challenged. For both cases, the surge line is predicted to fail at 241 minutes (14,460s), which is a slight delay in failure time compared to Cases 1R and 2R (t=14,050s). This delay is caused by an enhanced heat removal during the SG blowdown because of temperature reductions resulting from the open SG ADV. For Case 3R, which was performed without allowing the surge line to fail as in Case 1R, creep ruptures of the pressurizer loop hot leg nozzle and the pressurizer loop SG tubes are predicted at 256 minutes (15,380s) and 259 minutes (15,560s), respectively (Figure 3.8). The calculation was terminated at 259 minutes because all of the potentially vulnerable structures in the pressurizer loop had failed.

Case 4R (like Case 2R) was performed allowing the calculation to proceed with a surge line failure. The depressurization following surge line failure leads to accumulator injection, which prevents any significant reheating of the ex-vessel piping (Figure 3.9). As in Case 2R, the calculation was terminated at 347 minutes (20,800s). Therefore, in Case 3R, surge line and pressurizer loop hot leg are predicted to fail before the prediction of an SG tube rupture, and no tube rupture is predicted for Case 4R.

In the analyses described to this point, at the beginning of the hot leg countercurrent natural circulation, the number of SG tubes participating in forward flow in the SG inlet

plenum is assumed to be 35 percent (i.e., tube split of 35 percent hot tubes to 65 percent cold tubes). In Cases 5R (counterpart to Case 1R or 2R) and 6R (counterpart to Case 3R or 4R), a tube split of 53 percent hot tubes to 47 percent cold tubes was assumed on the basis of the Westinghouse transient natural circulation experiments. Figure 3.10 compares the nearly identical heatup rates of the pressurizer loop SG tubes for the two cases, indicating that in the instance of a pressurized steam generator, the calculations are insensitive to modifications of the SG tube split. Surge line failure is predicted at the same time (234 minutes (14,050s) for both cases). As shown in Figure 3.11, the heatup of the pressurizer surge line is more rapid than the heatup of the hot leg nozzle and the pressurizer loop SG tubes. The calculation was terminated after the surge line failure.

When comparing Case 6R to Case 3R, Figure 3.12 shows that there is a discernible difference in the heatup rate of the surge line as a result of the secondary depressurization which reduces the heat transfer to the pressurizer loop SG secondary. This reduction in heat transfer results in more retention of decay heat in the core region which accelerates oxidation (Figure 3.13). Since the energy produced through oxidation is relieved mostly through the pressurizer PORV, the heatup of the surge line is increased in Case 6R. Therefore, the pressurizer surge line was predicted to fail earlier at 229 minutes (13,720s) (versus 234 minutes for Case 3R). The calculation was terminated after surge line failure.

Case 7R is similar to Case 3R, except an assumption was made in Case 7R that the ADVs failed open in all SGs after they were first challenged. As in Case 3R, the pressurizer surge line is predicted to fail at 219 minutes (13,110s), and creep ruptures of the pressurizer loop hot leg nozzle and the non-pressurizer loop SG tubes are predicted at 229 minutes (13,740s) and 234 minutes (14,030s) (Figure 3.14). Creep rupture of the ex-vessel piping is accelerated in this case since the heat transfer to the secondary side is reduced as a result of depressurization of all steam generators.

Cases 8R and 9R were conducted to evaluate the conditions of the tubes during an SBO sequence involving RCP seal leaks. The difference between the two cases is in the treatment of heat transfer as the upper plenum stainless steel melts and relocates. Specifically, molten stainless steel was assumed to quench in Case 8R as it relocates into the water remaining in the lower vessel head. To model the effect of the steel resolidifying at relatively cooler regions in the core before it could reach the lower head, steel quenching was not simulated for Case 9R. This is considered the more realistic progression of the two. The results of Cases 8R and 9R are identical until the time of stainless steel relocation. The following is a discussion of the progression of events for Case 9R.

RCP seal leaks of 946 Lpm (250 gpm) per pump were assumed once the seals failed. Also, the ADV for the pressurizer loop SG was assumed to fail open following the first challenge. RCP seal leaks of 79 Lpm (21 gpm) per pump were introduced at event initiation to simulate leakage associated with the loss of seal cooling that would accompany a loss of AC power. Saturated conditions in the RCS, specifically at the RCPs, were reached at 125 minutes (7491s), and seal leaks then increased to 946 Lpm (250 gpm) per pump to simulate failures that could develop as a result of two-phase flow across the seals. That flow rate is considered the most probable for Westinghouse RCP seal failures (Wheeler, 1989). Increased flow through the RCP seals and pressurizer PORVs led to core uncovery at 145 minutes (8710 s) as seen in Figure 3.15. Steam venting through RCP seals and heat transfer because of the countercurrent natural circulation reduces RCS pressure. Pressure reduction continues until accumulator injection, beginning at 234 minutes (14,020s) (Figure 3.16). Pressure increases during the accumulator injections, because of vaporization of water reaching the core, which in turn causes temperature perturbations at

the hot legs and SG tubes (Figure 3.17). The increased temperatures (Figure 3.18) cause a non-pressurizer loop hot leg to fail as a result of creep damage at 269 minutes The failing hot leg heats at a faster rate than the other primary coolant loops since its loop seal clears by 220 minutes The calculation was terminated at the point of hot leg failure.

Case 6N was performed to evaluate the effect on SG tube conditions of a stuck- open pressurizer PORV in the early stages of core uncovery. The PORV was assumed to stick open at 190 minutes, when core exit temperatures reach 922 K (1200 °F). RCS pressure decreases until accumulator injection starts at 218 minutes SG tube temperature spikes, resulting from the accumulator injections, are seen in Figures 3.19 and 3.20. The predicted temperatures in this case are somewhat higher than expected because of the modeling of the natural circulation flow path. To maintain the flow directions of circulation through the two portions of the tube bundle (forward and return flow paths), reverse loss coefficients approximately 100 times larger than the forward loss coefficients were specified. Therefore, when superheated steam from the vessel reached the SG inlet plenum, it proceeded through only 35 percent of the tubes. Actually, the flow should proceed through the entire tube bundle in the forward direction whenever the hot leg pressure exceeds the pressure at the pump suction. If full-bundle flow was modeled, the heat transfer surface would be greater, resulting in lower tube temperatures.

In these analyses using the Larson-Miller model for creep rupture, unflawed tubes are calculated to survive the transient heatup past the point where other non-defected RCS components are predicted to fail. A key phenomenon leading to accelerated tube heatup identified in the analyses is loop seal clearing, although for these calculations loop seal clearing did not occur in the depressurized loop. However, uncertainties exist in the prediction of which loop seal clears. (Once one loop seal clears, flow is preferentially drawn to that loop.) Therefore, an equal likelihood of clearing among the loops was assumed.

For cases in which the secondary side is not depressurized, the peak average tube temperature is fairly uniform and centered around 850 K (1070 °F). For cases with the additional assumption of secondary side depressurization, the average peak temperature shows greater variation. For cases with a single depressurized steam generator, the average peak tube temperature in the faulted loop varied between 933 K (1219 °F) and 987 K (1317 °F) depending on the inlet plenum assumption. The case assuming a split of 53 percent hot tubes, and 47 percent cold tubes, which produced an average peak tube temperature of 933 K (1219 °F), could be considered a "best estimate" case since it is based on test data more representative of the sequence of interest. This flow split is similar to that assumed in the EPRI analysis. For these single-faulted SG cases, the average peak tube temperatures in the non-faulted loops was roughly 100 K (180 °F) cooler, varying approximately between 830 to 860 K (1034 to 1088 °F).

In Case 7R, where all SGs are assumed to depressurize, the average peak tube temperature of 950 K (1250 °F) is approximately 40 K (72 °F) cooler than when the single SG was blown down. This is because the greater core heatup and discharge through the PORV leads to earlier surge line failure.

3.2.2.2 ANO-2

The ANO-2 reactor was selected for analysis to examine the potential effects that plant design differences may pose for SG tube integrity. ANO-2 has a higher core power density than Surry (97 MW/m^3 for ANO-2 versus 92 MW/m^3 for Surry). It is one of the CE plants

without a PORV, and its design features a more shallow loop seal (1.24 m (4.1 ft) for ANO-2 versus 1.7 m (5.6 ft) for Surry). These differences will, to varying degrees, affect the natural circulation during the transient. Higher power density may accelerate core damage progression and corresponding heatup. Without PORVs, pressure is controlled by pressurizer SRVs which operate at higher set points of 16.7 to 17.2 MPa (2422 to 2495 psi); therefore, the SG tubes may be subject to a larger differential pressure. With a more shallow loop seal, there may be a greater potential for loop seal clearing and establishing full-loop natural circulation, which would affect the core damage progression and heat transfer between the primary system and the SGs.

As previously indicated, accident initiation in all calculations was based on a station blackout sequence without recovery and without operator actions. In addition, an ADV on the pressurizer loop SG was assumed to fail open on its first challenge in each calculation. This increases the differential pressure across the SG tubes, as well as the potential for SG tube rupture in the pressurizer loop SG. Cases ANO1 and ANO2 are counterparts to Surry Cases 3R and 4R, respectively.

At initiation of the SBO transient, the reactor is scrammed and the reactor coolant pumps are tripped because of a loss of all AC power. Initially, the reactor coolant system depressurizes because heat transfer to the secondary side is sufficient to remove core decay heat and reduce the temperature of the primary coolant. However, the secondary side heat sink is not sustained in the absence of feedwater and, as a result, the RCS pressure rises to the pressurizer SRV set point near the time of SG dryout. A gradual RCS heatup and boiloff follows with RCS pressure fluctuating between 16.7 and 17.2 MPa (2422 and 2495 psi) through pressurizer SRV cycling.

When a sufficient amount of vapor generated in the core collects in the top of the SG U-tubes, full-loop natural circulation of liquid ceases. For Cases ANO1 and ANO2, full-loop natural circulation ceases earlier (82 minutes (4895s) versus 128 minutes (7690s) for Surry Cases 3R and 4R). Core uncovery begins as a result of continued boiloff of water and venting through the SRV. Compared to Surry, ANO-2 calculations indicate that core uncovery begins earlier (102 minutes (6125s) for ANO-2 versus 151 minutes (9030s) for Surry), and is completed in a shorter duration (21 minutes for ANO-2 versus 27 minutes for Surry). Hot leg countercurrent natural circulation of vapor begins earlier (at 106 minutes (6332s) for ANO-2 versus at 152 minutes (9091s) for Surry) as well.

Because of the degraded heat transfer associated with the hot leg countercurrent natural flow, ex-vessel piping temperatures begin to increase. For Cases ANO1 and ANO2, creep rupture of the pressurizer surge line (Figures 3.21 and 3.22) is predicted at 189 minutes (11,330s) which is earlier than in Surry Cases 3R and 4R (234 minutes (14,050s)). After surge line failure in Case ANO1, the calculation was continued, ignoring the prediction of surge line failure, to determine the timing associated with other potential pressure boundary failures. Creep rupture failures of the hot leg nozzle in the pressurizer loop, the non-pressurizer loop hot leg nozzle, and the pressurizer loop SG tubes are predicted at 203 minutes (12,150s), 209 minutes (12,510s), and 229 minutes (13,750s), respectively. The calculation for Case ANO1 was terminated at 229 minutes (13,750s) because all vulnerable structures analyzed (other than the non-pressurizer loop SG tubes) had failed.

In Case ANO2, the surge line was allowed to fail, and the RCS depressurized as shown in Figure 3.23. When the RCS pressure sufficiently decreases to the accumulator injection pressure of 4.3 MPa (624 psi), the accumulator injects as indicated in Figure 3.23, which arrests the heatup of the core and cools the ex-vessel piping as shown in Figure 3.22.

Although, core reheating occurs after the accumulator water has boiled off, the energy associated with core reheating is primarily removed via the surge line break, preventing any significant reheating of ex-vessel piping. Therefore, the calculation was terminated at 359 minutes (21,550s). SG tube rupture is not expected if surge line failure occurs as predicted in Cases AN01 and AN02.

The analysis of Case AN03 is similar to that in Case AN01, except that additional assumptions were made in Case AN03 that the transient began with a nominal pump seal leak of 5.7 Lpm (1.5 gpm) per reactor coolant pump, and the seal leak increased to 833 Lpm (220 gpm) per reactor coolant pump when saturated conditions were reached (to simulate a common-cause failure of the pump seals). Because of increased flows through reactor coolant pump seal leaks and the pressurizer SRV discharge, core uncovery begins earlier in Case AN03. Pressurizer SRV cycling stops only after the pump seal leaks cease their two-phase discharge and begin to vent steam. At that time, RCS pressure begins to drop as indicated in Figure 3.24 because the energy associated with venting steam through the pump seals exceeds core decay power.

As the RCS pressure approaches the accumulator injection pressure of 4.31 MPa (625 psi), some upper plenum steel melting is predicted. However, because of modeling in the SCDAP/RELAP5 code, upper plenum molten steel cannot relocate to the core region, and no molten pool was calculated to form in the core region at that time. The upper plenum molten steel is arbitrarily relocated into the lower head and allowed to quench. As a result, the generated vapor is sufficient to increase the RCS pressure to 8 MPa (1160 psi). This excess pressure is then relieved through the pump seal leaks, with the overall effect of the steel quenching delaying the first accumulator injection.

Several small accumulator injections follow, with essentially no impact on RCS pressure as seen in Figure 3.24. However, these injections are followed by upper plenum stainless steel melting and relocation to the lower head, which has a significant impact on the SG tube temperatures as indicated in Figure 3.25. The temperature and pressure perturbations (Figure 3.26) associated with the steel relocation and quenching in the lower head contribute to the creep failure of the pressurizer loop SG tubes at 307 minutes (18,400s). Although the non-pressurizer loop hot leg nozzle is predicted to fail by creep rupture at 306 minutes (18,330s), or 70 seconds earlier than the predicted failure of SG tubes, the timing difference between the hot leg and the tubes is not significant. Therefore, in Case AN03, there is a potential of induced SG tube rupture before any other RCS pressure boundary failure for the conditions analyzed.

Case AN04 was then run to specifically address the impact on SG tube temperatures and pressures because of unrealistic relocating and quenching of the upper plenum molten steel in the lower head. This "no-quench" case was performed in a manner similar to Case 9R for Surry. The impact of the "no-quench" assumption can be readily seen by comparing the RCS pressures shown in Figures 3.24 and 3.27. Specifically, pressure perturbations associated with stainless steel quenching (Figure 3.24) are not observed in this calculation. Although maximum SG tube temperatures are comparable with or without quenching (Figures 3.25 and 3.28), those temperatures in the absence of pressure perturbations (Figure 3.29) are not high enough to cause SG tube rupture because of the reduced pressure differential across the tubes. Nonetheless, the temperature of the non-pressurizer loop hot leg climbed well ahead of the pressurizer loop hot leg because of early loop seal clearing. The non-pressurizer loop hot leg failed at 350 minutes (21,000s) as indicated in Figure 3.30. The calculation was stopped at 483 minutes (29,000s) because the creep damage terms calculated for the other vulnerable structures were small. Therefore, tube rupture is not a concern in the absence

of pressure perturbations associated with the quenching for the conditions as analyzed. The hot leg failure was also predicted to be delayed by 50 minutes (3000s) (compared to 306 minutes (18,330s) in Case AN03).

3.3 Modeling and Analytical Uncertainties

Consideration of accident analysis uncertainties involved with thermal-hydraulic calculations focused on two main areas. The first area focused on variations that may result from severe accident progression phenomenology, and the second focused on the more problem-specific issues associated with the natural circulation mixing calculation.

Generally, the calculation of thermal-hydraulic boundary conditions in a severe accident can reasonably be said to involve phenomenological uncertainties. However, the bulk of the phenomenological uncertainty relevant to in-vessel accident progression behavior has been attributable to what is referred to as late-phase melt progression. This involves events and behavior that occur after melting and relocation of fuel rods in the core. Early- phase melt progression, including boiloff, fuel heatup, initial zircaloy-steam reaction, hydrogen release, and control rod material relocation, has been recognized as an area better understood and modeled. Rather, it is the late phase of the accident, involving fuel melting and relocation, formation of molten pools with blockages or drainage, and interactions in the lower plenum, which is still uncertain and is the focus of international severe accident research programs.

Fortunately, the severe accident analysis to assess SG tube integrity comprises, as its period of interest, those events up to and including early- phase melt progression but excluding late-phase behavior. This is demonstrated by the analyses which uniformly predict failure of some portion of the RCS pressure boundary before the formation of an in-core molten pool. In the Surry analysis described previously (Case 3R as an example), the first formation of an in-core molten pool did not occur for roughly 70 minutes after the prediction of surge line failure. This is generally consistent with earlier DCH-related calculations, performed at high pressure, which indicated the onset of the significant fuel melting after the heatup and failure of loop piping. It can also be argued that if substantial core relocation were to occur earlier in the transient, the disruption of the optimal flow configuration (i.e., intact fuel geometry) would most likely impede redistribution of energy from the core region, thereby mitigating tube heatup relative to other components.

The major uncertainty addressed by these analyses has been the modeling approach used in the SCDAP/RELAP5 treatment of natural circulation and the resulting redistribution of energy from the core to the reactor vessel upper plenum and from there to the steam generators. The major uncertainty identified within the natural circulation flow path calculation has been the treatment of mixing of flow within the SG inlet plenum. The results of sensitivity analyses to examine the impact of the recirculation ratio, mixing fraction, and number of outflow tubes carrying hotter flow indicate that those parameters characterizing the flow calculations have only a modest effect on peak average tube temperatures, approximately ±20 K (36 °F). However, as noted in the discussion of Surry calculations, one of the analyses (Case 6R) was performed assuming that roughly half of the tubes carried hotter outflow, on the basis of an average value observed in the 1/7-scale transient tests. In addition to that assumption, the full-plant analyses, unlike the single sensitivity calculations, was performed without fixing the other mixing parameters, allowing the code to calculate a mixing fraction and recirculation ratio. The result of allowing the calculation

to "float" was that it predicted a minimal increase in the mixing fraction (from 0.87 to 0.89) and a slight increase in the recirculation ratio (from 1.9 to 2.3). The net effect of the combined changes was to decrease peak average tube temperatures by roughly 50 K (90 °F). From this, the staff concluded that further refinements to the model were not likely to substantially alter the calculation of tube temperatures.

3.3.1 SG Inlet Plenum Mixing Parameters Sensitivity Study

When SCDAP/RELAP5 was used to simulate an SBO accident, the code was benchmarked against average experimental values for hot leg countercurrent natural circulation flow behavior derived from a series of 1/7-scale experiments (Stewart, 1993). In the current study, SCDAP/RELAP5 was used to evaluate the potential impact on the Surry SG tube temperatures if natural circulation parameters were allowed to vary over the range of values observed in the Westinghouse experiments.

There are three SG inlet plenum mixing model parameters including the mixing fraction, the hot leg to tube bundle flow ratio, and the fraction of forward flow or hot tubes. The basis for the mixing model is given in the EPRI report detailing the Westinghouse scaled experiment results (Stewart, 1993). The mixing fraction indicates the degree of mixing that occurs between the flow from the hot leg into the inlet plenum, and the flow from the tube bundle into the inlet plenum. An increased mixing fraction indicates a greater degree of mixing between the streams. The flow ratio is simply a comparison of the flow rate from the hot leg to SG to the flow in the tube bundle, and represents the dilution of the hot leg flow by the colder SG flow.

For these analyses, an SBO sequence for Surry was analyzed for the case with no reactor coolant pump seal leaks; the SG ADVs were assumed not to fail. The calculation using the full-system model of the reactor vessel and three coolant loops was performed up to the predicted time of surge line creep rupture failure, the first RCS pressure boundary failure prediction. The calculated results were then used to provide boundary conditions to a model of the pressurizer loop between the reactor vessel and the reactor coolant pump suction line. This approach was used to simplify the adjustment of the hot leg countercurrent flow mixing parameters by limiting it to a single loop. The justification for this simplification is that it allowed varying the mixing parameters one at a time to ascertain their individual effect on SG tube temperature response. The single-loop model was benchmarked against the full-plant system model to ensure that the specification of time-dependent conditions was sufficient to produce the same transient results for the pressurizer loop hot leg in both cases.

The "base case" SG inlet mixing parameter values (35 percent of tubes carrying forward flow, mixing fraction of 0.87, and recirculation ratio of 1.9), representing the average for the four steady-state, high-pressure SF_6 experiments, are shown in Table 3.2. Note that case 6R, using a more even flow split representative of the transient high-pressure SF_6 experiments was eventually recommended for use as the base case. As discussed earlier, using Case 3R results as the base case introduces some conservatism, but does not significantly alter tube failure probability estimates that would result from using Case 6R.

The first two sensitivity calculations, Cases M1, and M3, represented the minimum and maximum percentage of hot tubes participating in the forward flow in the SG. Likewise, Cases M4 and M5 bracketed the minimum and maximum values for the mixing fraction, and Cases M6 and M7 explored the minimum and maximum values for the recirculation ratio.

For the tube split sensitivity calculations (Cases M1 to M3), as shown in Figure 3.31, the volume-averaged tube temperatures in the first volume of the forward flow portion of the SG tube bundle showed a higher temperature for Case 1 with 29 percent of the tubes carrying hot flow, and a lower temperature for Case M3 with 61 percent of the tubes carrying hot flow, when compared with the base case. However, this variation in temperature is relatively small; at 250 minutes (15,000s) the greatest increase in temperature is 10 K (18 °F) (Case M1) and the greatest decrease is 25 K (45 °F) (Case M3). The reason is that the surface area for heat transfer from the primary side to the secondary side is increased with an increasing number of tubes participating as hot tubes, but the velocity is decreased given a fixed mass flux from the SG inlet plenum. The lower flow velocity reduced the heat transfer coefficient from the vapor to the tube. Given the reduction in heat transfer, one would expect that the tube temperature would decrease with an increasing number of tubes. The opposite is true when the number of hot tubes is reduced.

The mixing fraction sensitivity calculations, Cases M4 and M5, varied the fraction of hot leg mass flow entering the SG inlet plenum that was mixed with flow returning to the inlet plenum from the return flow tubes. Increasing the mixing fraction reduces the temperature of the steam entering the SG tube sheet for the forward flow (hot) tubes. As observed in Figure 3.32, the range of temperature variation at 250 minutes (15,000s) was only 20 K (36°F) over the range of mixing fraction values investigated.

The recirculation ratio sensitivity calculations, Cases M6 and M7, varied the ratio of the flow through the SG tubes to the hot leg mass flow entering the SG inlet plenum. In this case, increasing the recirculation flow ratio reduces the temperature of the steam entering the tube sheet for the forward flow (hot) tubes since the mass flow of steam from the mixing volume to the tube sheet increases with increased recirculation ratio. As shown in Figure 3.33, the difference in the predicted tube temperature in the first volume of the forward flow portion of the tube bundle was less than 10 K (18 °F) over the range of recirculation ratios investigated, with a maximum value of 5 K (9 °F) over the base case.

In summary, the sensitivity studies done by individually varying the SG inlet mixing parameter values within the range of values observed in the Westinghouse experiments showed that the impact is ± 20 K (36 °F) on the predicted tube temperatures. This is compared to results predicted when the average values were used for these mixing parameters. Thus, the uncertainty is modest with respect to the tube temperature predictions in the Surry and ANO-2 analyses of SGTR.

3.3.2 Hot Tube Nodalization Sensitivity Study

Case 5N was performed to evaluate the effect on tube temperatures of a variation in nodalization at the tube bundle inlet. The nodalization change was introduced into the calculation at the time counter-current natural circulation commenced. This study used a more detailed nodalization of the tube inlet volumes and the associated heat structures. The first inlet volume was subdivided into five volumes so that a series of volumes in series represented the tube section previously represented by a single volume. The base case nodalization yielded a temperature representative of 0.79 m (2.6 ft) above the tube sheet (the midpoint of the volume). The temperature of the volume immediately above the tube sheet gave a tube temperature at the time of predicted surge line failure only about 5 K (9 °F) above the base case value. At the time of surge line failure, Figure 3.34 shows that tube temperatures along the subdivided nodes remain within a range of 15 K (27 °F). Thus, the initial nodalization seems sufficient for these calculations.

3.3.3 Extended Sensitivity Study

Additional SCDAP/RELAP5 calculations were conducted to supplement the mixing model sensitivity studies. These extended studies included heat transfer modeling effects and possible synergistic effects of the SG inlet plenum mixing model parameters. The sensitivity studies used an updated version of the SCDAP/RELAP5 code to more appropriately treat the combined effects of forced and free convection heat transfer in vertical pipes. The use of an updated code version complicates direct comparison with previous analyses; however, the results are quite similar and trends are consistent.

Cases 3R and 6R were repeated with the updated code to offer a comparison of results with the previously run cases. These cases are designated 3RU and 6RU, and were limited to the period extending from the onset of hot leg countercurrent natural circulation at 151 minutes. The earlier portion of the sequences did not need to be considered since no threat to RCPB components is expected, and the heat transfer updates should only introduce minor changes in timing of the sequence leading up to the onset of countercurrent flow. The results from the updated runs are considered refinements of the previous versions of those cases since the mixed convection updates should improve the simulation. However, tube failure probability calculations founded on previous results, using the cases indicated in Table 3.1, were already evaluated when the refined calculations became available. Therefore, these most recent calculations were only used to ascertain the sensitivity of results.

The additional sensitivity calculations, designated 6RU.A through 6RU.F, are listed in Table 3.3 and are used to show the influence on the following:

- uncertainties in heat transfer coefficients
- absence of fluid-to-fluid heat transfer and circumferential pipe wall conduction in the split hot leg model
- synergistic effects associated with simultaneous variations on natural circulation SG inlet plenum mixing model parameters

Case 6R was chosen as the basis for these studies since the tube split for this case represents the average of values observed in the Westinghouse high- pressure transient tests (Stewart, 1993), which more closely resemble the condition of interest. As noted earlier, this is a shift from the originally selected base case conditions represented by Case 3R. The shift of the base case results in slightly lower tube temperatures and a corresponding change in tube failure probability. Using the Case 6RU results, estimated tube failure probabilities are not significantly changed (about 5 percent for the plant with an average flaw distribution, and about 15 percent assuming a severe plant flaw distribution; different flaw distributions are discussed in Section 4).

The tube bundle flow split used in all of these studies (53 percent forward flow) represents results of the transient scaled experiments, versus 35 percent seen in the steady-state tests and modeled in Case 3R. Cases 6RU.A and 6RU.B used heat transfer coefficients altered by ±20 percent in the upper plenum, hot legs, surge line, and on the inner and outer surfaces of the SG tubes. Cases 6RU.C and 6RU.D used heat transfer coefficients increased by 30 percent in the hot leg, surge line, and SG tube entrance volumes to examine uncertainties associated with entrance effects. Case 6RU.D represents an extreme case of increasing the heat transfer coefficients only in the tube entrance volumes. Case 6RU.E addressed the absence of fluid-to-fluid heat transfer and circumferential pipe wall conduction in the split hot leg model. Case 6RU.F used 5 percent confidence values for the

natural circulation inlet plenum mixing parameters, assuming a normal distribution of the Westinghouse high-pressure transient data and independence among the parameters. The values selected from the distribution are below the ranges (i.e., more severe) than the parameters actually observed in the experiments.

When heat transfer coefficients were uniformly increased (Cases 6RU.A, and 6RU.C), vapor temperatures entering the tubes decreased since more energy was transferred from the vapor to structures. This resulted in slightly lower tube temperatures for two of the cases, as seen in Table 3.6, with Case 6RU.A yielding the largest temperature drop (19 K (34 °F)). The results of the first four sensitivity cases (6RU.A through D) indicate that the time of tube failure could be altered by about ±1 minute over the range of heat transfer uncertainty considered. Tube temperatures at the time of surge line failure could vary from 938 to 964 K (1228 to 1275 °F), centered around the base case (6RU) value of 957 K (1263 °F).

When fluid-to-fluid heat transfer and circumferential pipe wall conduction were modeled in Case 6RU.E, the temperature difference between the hot vapor in the upper portion of the hot leg and the cooler fluid below it was reduced relative to Case 6RU. The lower temperature differential led to a reduction in countercurrent flow and an associated reduction in the heat transferred to loop structures. With less energy being transferred to loop structures, more energy was rejected from the primary through PORV cycling. Consequently, predicted creep failure of the pressurizer surge line was about 3 minutes earlier than in Case 6RU. Also, vapor temperature entering the tubes was reduced in Case 6RU.E as a result of heat transferred from the hot vapor to cooler vapor in the hot leg. This lowered tube temperatures and delayed tube failure relative to Case 6RU by about 5 minutes, as seen in Table 3.6.

The mixing parameters used in Case 6RU.F represent 5-percent confidence values, assuming a normal distribution for the Westinghouse transient test data. The parameters for Cases 3RU, 6RU, and 6RU.F can be compared in Table 3.3. Results for these calculations, as seen in Table 3.6, included higher tube temperatures at surge line failure than in the other calculations.

In general, when heat transfer coefficients outside the core region were increased (cases 6RU.A and 6RU.C), the heat transfer outside of the core also increased while the corresponding vapor and structure temperatures decreased. Consequently, SG tube temperatures at the time of surge line failure also decreased. Further, the period of time between tube failure and surge line failure increased. The opposite was true when heat transfer coefficients outside of the core were decreased Case 6RU.B versus Case 6RU.

Comparison of Case 6RU.D with Case 6RU shows that arbitrarily increasing the heat transfer coefficient in the tube entrance region does not have a significant impact. When radiative heat exchange between the hot and cold streams in the hot leg and circumferential wall heat conduction in the hot leg were accounted for (Case 6RU.E) the buoyancy-driven flow between the hot leg and SG was decreased, thereby increasing the time between tube failure and surge line failure. Case 6RU.F represents a combined sensitivity/uncertainty analysis, which incorporated the lower 5-percent confidence limits on the mixing fraction, recirculation ratio, and tube flow split applied simultaneously. As expected, this case showed a greater effect on peak tube temperature, on the order of 50 K (90 °F). The result is considered unduly conservative since this case did not consider compensating factors that could be expected to mitigate the effects of a change in any single parameter.

Table 3.6 Results of Additional Sensitivity Studies

Case	Time of surge line failure (mins)	Tube temp.at surge line failure (K)	ΔP (MPa)	Time of predicted tube failure (mins)	Tube temp at time of tube failure (K)	ΔP (MPa)	Surge line and tube failure time difference (mins)
6RU	229	957	15.9	249	1161	15.8	21
6RU.A	227	938	15.9	248	1154	15.7	22
6RU.B	227	964	15.8	247	1162	15.8	20
6RU.C	228	944	15.9	249	1160	16.1	21
6RU.D	228	957	16.0	249	1159	15.7	20
6RU.E	226	937	15.8	252	1155	16.1	25
6RU.F	230	1007	16.0	243	1161	15.7	13
3RU	227	973	15.9	244	1164	15.9	17

The overall conclusion from the final set of studies is that the uncertainties and sensitivities in the thermal-hydraulic results are within the ranges identified in previous analyses. Using Case 6RU as the base case, the SG tube temperature at the time of surge line failure is approximately 960 K ±20 K (1268 ±36 °F), indicating that the other cases used in this report are slightly conservative.

3.3.4 Fission Product Deposition

As part of the assessment of the thermal-hydraulic boundary conditions experienced by the tubes, the staff also evaluated the collateral impact of fission product deposition in the reactor coolant system, including the SG tubes. Fission product deposition was evaluated to determine both the incremental heating of the tubes as a result of local deposition, as well as the influence of fission product deposition on the natural circulation flow behavior in the RCS and particularly flow in the tube bundle. Stand-alone analysis, described in further detail in Appendix D, concluded that fission product deposition had negligible effects on the tube boundary conditions.

3.4 Relevance of Design-Specific Factors

The nature of predicted severe accident conditions, specifically counter-current natural circulation, suggests that design factors serve key roles in the potential for tube thermal challenge and the severity of the challenge if it occurs. The first clear evidence for this is the experimental information which demonstrates that countercurrent hot leg natural circulation flows of superheated gas are not expected to reach SG tube bundles in the B&W designs, as is expected to occur in the U-tube SG designs. When considering the Westinghouse and CE designs, or even the differences between plant designs in a single design class, a number of possible factors could affect the prediction of SG tube temperatures.

Much of the early analysis performed to specifically assess SG tube performance focused on Westinghouse plants (e.g., NRC analyses addressed Surry and industry analysis (Wong, 1993, Fuller, January 1996) were calculated on the basis of a generic Zion-like four-loop plant). Consideration of predicted RCS thermal-hydraulic conditions undertaken during the DCH study (i.e., natural circulation within the RPV and countercurrent natural circulation in the hot-leg and steam generator) suggested the need to examine the difference between reactor designs with a downcomer bypass or core bypass. However, in that study, analysis of Zion and Surry, which have different bypass configurations, did not reveal significant differences in fundamental behavior.

Differences in loop seal depth were considered possible factors determining the potential for tube failure, since any clearing of the loop seal (formed at the reactor coolant pump) would increase circulation of unmixed flow through the SGs and contribute to greater heating of the tubes. Further, the staff sought an assessment of resulting tube conditions for CE plant designs without pressurizer PORVs. ANO-2 possesses a number of the characteristics of interest and, thus, made a suitable candidate for additional analysis. ANO-2 represents those CE reactors without a PORV and which, therefore, rely on primary pressure relief through safety valves at a higher set point of ~17 MPa (2466 psi). Further, ANO-2 includes a rather shallow loop seal depth 1.2 m (3.9 ft) versus 1.7 m (5.6 ft) for Surry, which would allow for examination of loop seal clearing effects. Table 3.1 lists the ANO-2 calculations performed, and Table 3.7 summarizes the results. The small number of calculations available for comparison to the Surry results precludes an assessment of the effects of the entire range of design differences. However, some basic assessments can be made when comparing the results. Table 3.8 gives a comparison of the timing of key events in the accident progression for the base case and the RCP seal leak cases for Surry and ANO-2.

The most obvious difference is the speed of event progression in the ANO-2 analyses. For both cases, beginning with SG dryout, key events occur in advance of the Surry progression. Two factors may contribute to this difference. First, the core power for ANO-2 is higher than Surry (2815 MWt for ANO-2 versus 2441 MWt for Surry). Second, the SG secondary side water inventory for CE designs is somewhat smaller than Westinghouse Series 51 SGs, such as those in Surry (122 kg versus 132 kg). The combination of high core power and smaller secondary water inventory available for boiloff leads to a shorter time to dryout in ANO-2.

The time differences between Surry and ANO-2 sequences after dryout becomes larger and deserves further examination. A first step is to compare the ratio of core power to RCS inventory for the designs. A greater core power relative to RCS inventory means that energy will be transferred more quickly out of the core to the SGs or out through lifting relief valves. A smaller RCS inventory will not be able to absorb as much energy during the initial phase of the event. The core power-to-RCS inventory ratio for ANO-2 is higher than for Surry (by approximately 15 percent). From the time of dryout, the progression of most key events during the ANO-2 accident analyses happen earlier than for Surry relative to the difference in SG dryout times. Also, the sequence of events is consistent with the Westinghouse design. Thus, design differences do not appear to contribute to any fundamental alteration of sequence progression between the designs, only the rate at which they occur. However, closer examination of the timing for key events raises interesting points.

Table 3.7 Summary of SG Tube Results for ANO-2 Calculations

Case	Time of First Failure (mins)	Location of First Failure	At First Failure		At Peak Temp.	
			Temp (K)	ΔP (MPa)	Temp (K)	ΔP (MPa)
ANO1	189	Surge Line	1063	17.0	1137	17.4
ANO2	189	Surge Line	1063	17.0	1063	17.0
ANO3[a]	306	Hot Leg[b]	1301	7.3	1359	10.8
ANO4[a]	357	Hot Leg	1278	2.2	1466	3.0

a. Loop seals predicted to clear in these cases
b. SG tube failure predicted nearly 1 minute later

Table 3.8 Comparison of Event Timing for Surry and ANO-2

Event	Times (mins)					
	Base Case[a]			RCP Seal Leak[b]		
	Surry	ANO-2	Δ Time[c]	Surry	ANO-2	Δ Time[c]
SG dryout (pressurizer/non-pressurizer loops)	34/88	25/54	9/34	34/85	25/54	9/31
RCP saturation; RCP seal leaks increase to 250 gpm for Surry, 220 gpm for ANO-2	NA	NA	NA	125	80	45
Vessel level below top of fuel	149	102	47	145	99	46
Core exit superheat; hot leg counter-current circulation begins	152	106	46	146	102	44
Pressurizer PORV or SRV final cycle	NA	NA	NA	149	107	42
Vessel level below bottom of fuel	175	123	52	185	119	66
Onset of fuel oxidation	188	137	51	185	139	46
At least one loop seal clears	NA	NA	NA	220	144	55
First accumulator injection	NA	NA	NA	234	197	37
Surge line creep failure	241	189	52	NC	NC	NA
Hot leg creep failure	256	203	53	269	357	-88

a. Represented by Surry Case 3R, ANO-2 Case ANO1
b. Represented by Surry Case 9R, ANO-2 Case ANO4
c. Δ time is ANO-2 time subtracted from Surry time

Following SG dryout, events for the ANO-2 progression occur about 40 minutes to 1 hour ahead of the same events for Surry, for both the base case and RCP seal-leak case. Also, the potential for loop seal clearing for ANO-2 is not restricted to the RCP seal-leak case as it is for Surry. The lack of pressurizer PORVs in ANO-2 did not appear to introduce

differences in event progression, except for maintaining a peak RCS pressure in the ANO-2 analyses about 0.7 MPa (100 psi) above those for Surry. The greater flow capacity for the ANO-2 SRVs relative to the Surry PORVs could play an indirect role in some of the results (timing of depressurization), but these results do not clearly demonstrate such a distinction.

3.4.1 Loop Seal Clearing

Maintenance of the cold leg loop seal could be expected to depend on the piping configuration that causes it to form and the flow pattern that exists once superheated steam is generated from the vessel. The cold leg piping elevation is somewhat shallower in the ANO-2 design than in the Surry design. This could allow a smaller pressure perturbation from accumulator injection, or some other mechanism, to clear the seal. A large enough RCP seal leak could also allow the cold leg fluid to be displaced from the RCS by the hot steam. Loop seals may be lost in RCP seal-leak progressions, as both Cases ANO3 and ANO4 resulted in lost loop seals. Surry Case 9R also resulted in a cleared loop seal, but in a non-pressurizer loop. These analysis results demonstrate that loop seal clearing may be expected in Westinghouse and CE analyses involving RCP seal leaks.

The potential for loop seal clearing is a function of plant geometry and hydrodynamic conditions. Some of the more important geometrical factors include the depth of the seal, the total volume of the seal, the horizontal length of the seal, the elevation of the bottom of the downcomer skirt relative to the elevation of the seal, and the downcomer/core bypass configuration. Hydrodynamic conditions that can affect the loop seal include pressurization events (which could result from accumulator injection or quenching of core debris), the presence and size of RCP seal leaks, and the depressurization rate of the RCS.

SCDAP/RELAP5 will account for interaction of all of those factors during transient calculations and, if appropriate, loop seal clearing will be predicted. SCDAP/RELAP5 models are typically developed from design drawings, which generally indicate that all primary coolant loops are geometrically identical, and may not reflect as-built conditions that may affect the potential for loop seal clearing in one loop compared to the potential in other loops of the same plant. In the absence of geometrical modeling differences, loop seal clearing could also be predicted when numerical differences develop (because of roundoff, truncation, or convergence) into (small) hydrodynamic differences that favor clearing in one loop. Consequently, calculations can predict clearing in any loop, while one may expect some randomness in the clearing of a specific loop of a specific plant.

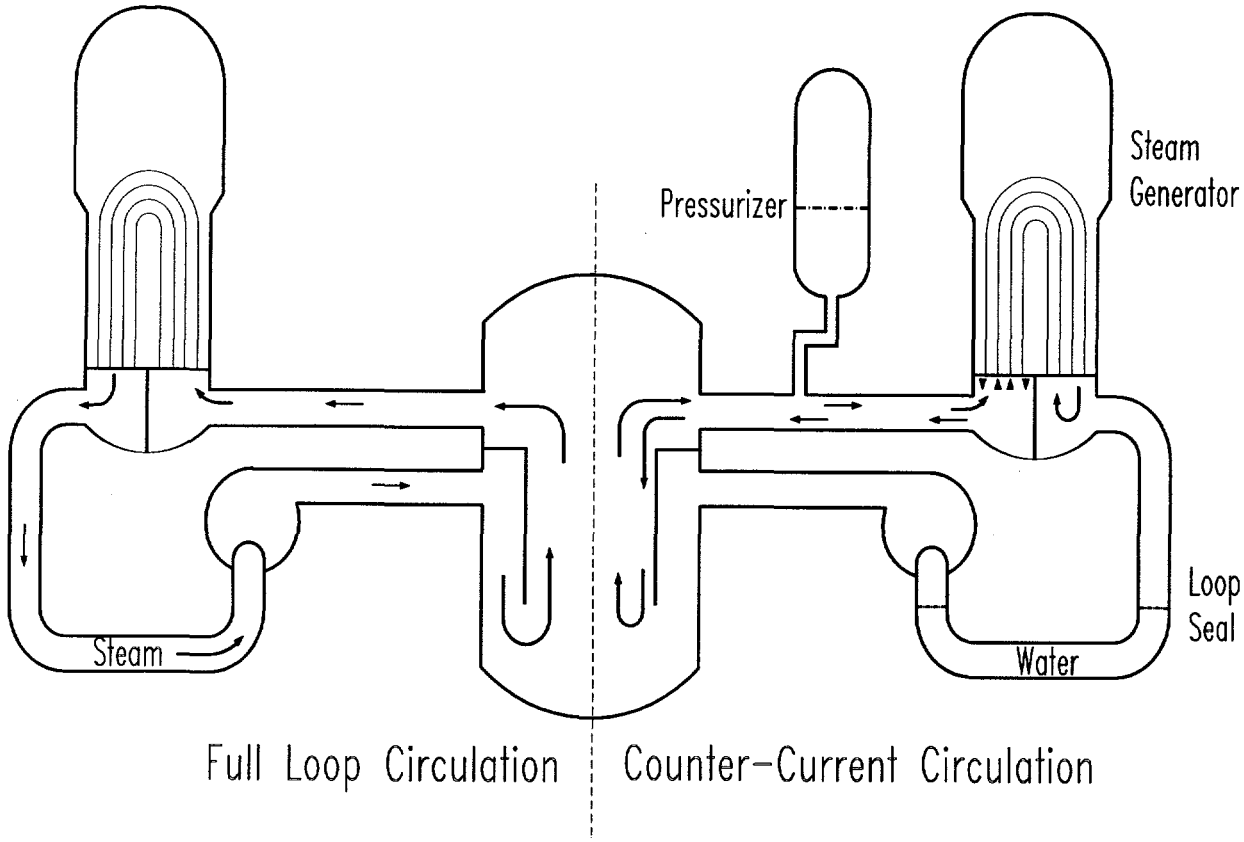

Figure 3.1 Severe Accident Natural Circulation Flows

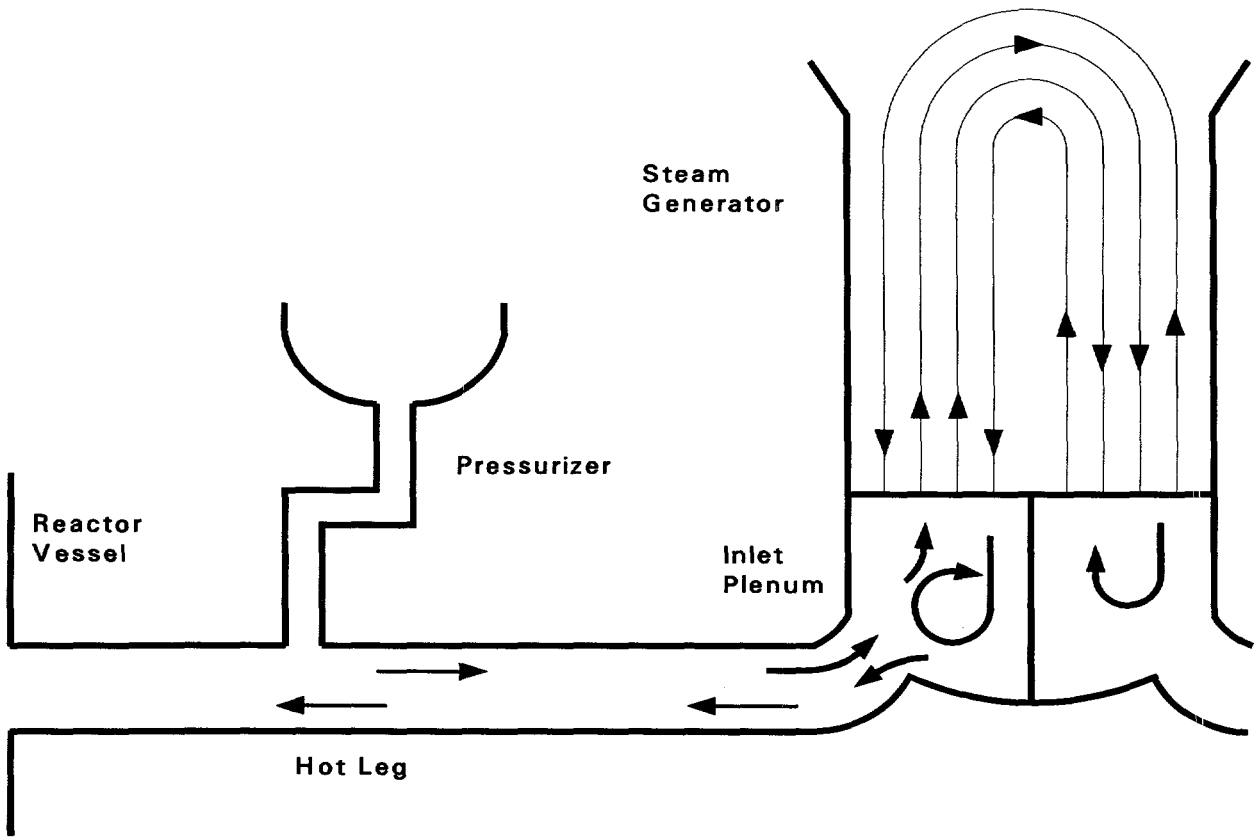

Figure 3.2 Counter Current Natural Circulation Flow

(Note: Inlet plenum flow patterns depicted should be considered representative only.)

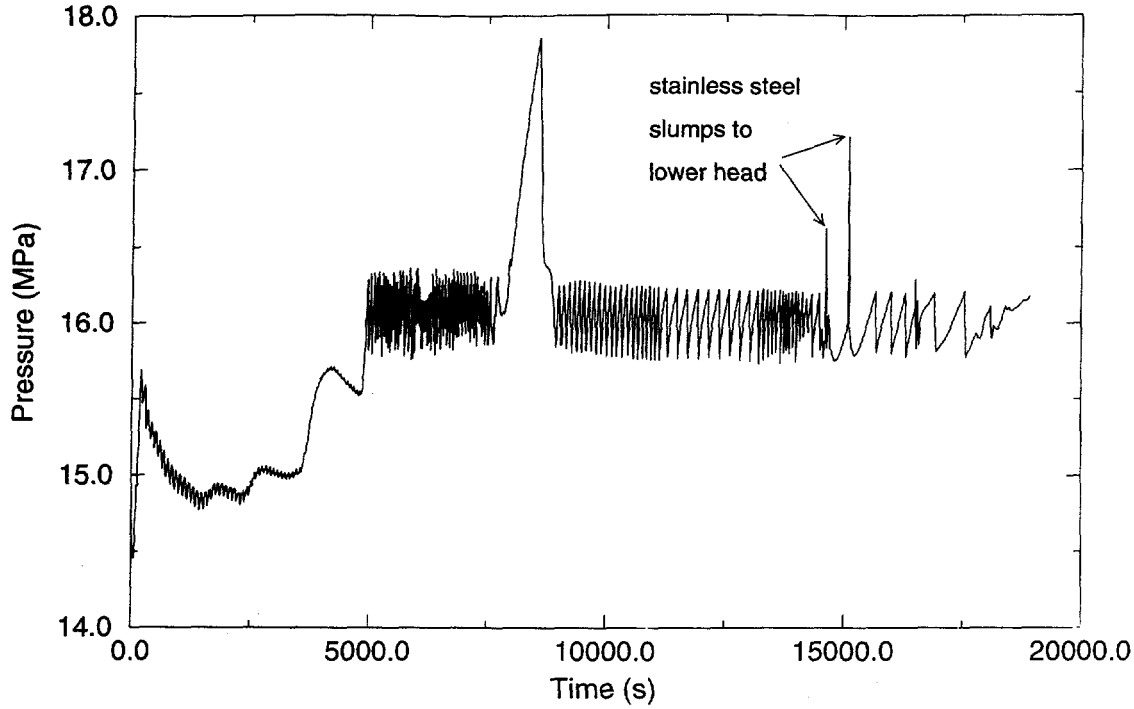

Figure 3.3. Pressure in the reactor vessel lower head: Case 1R.

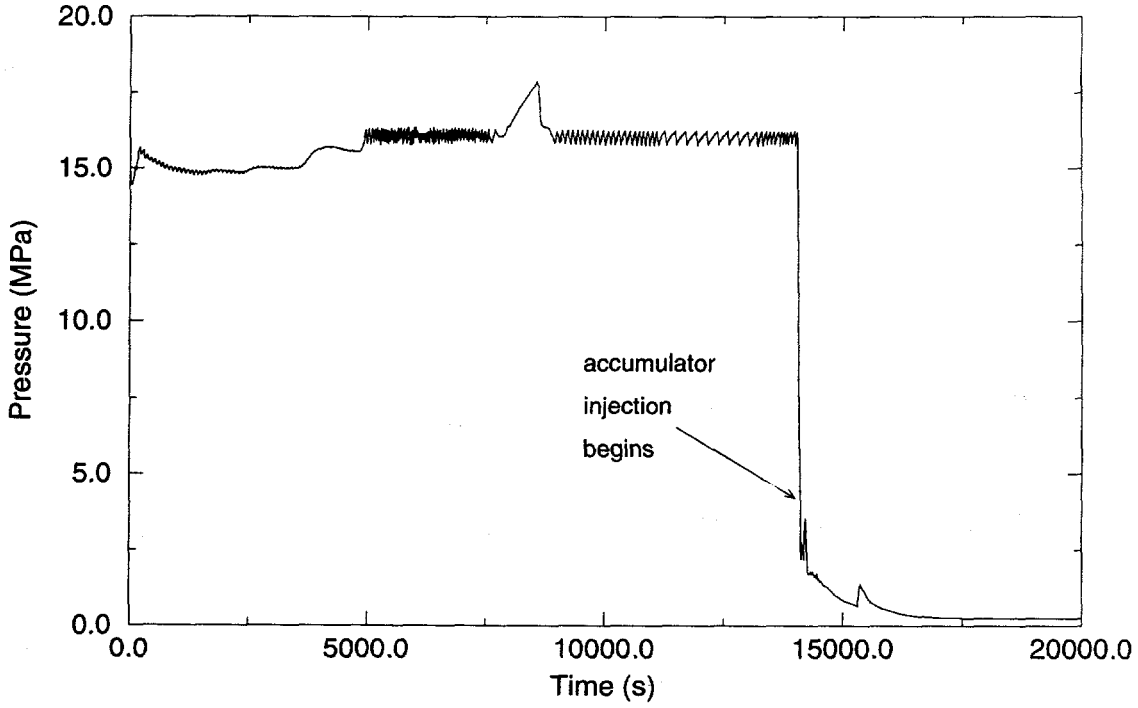

Figure 3.4. Pressure in the reactor vessel lower head: Case 2R.

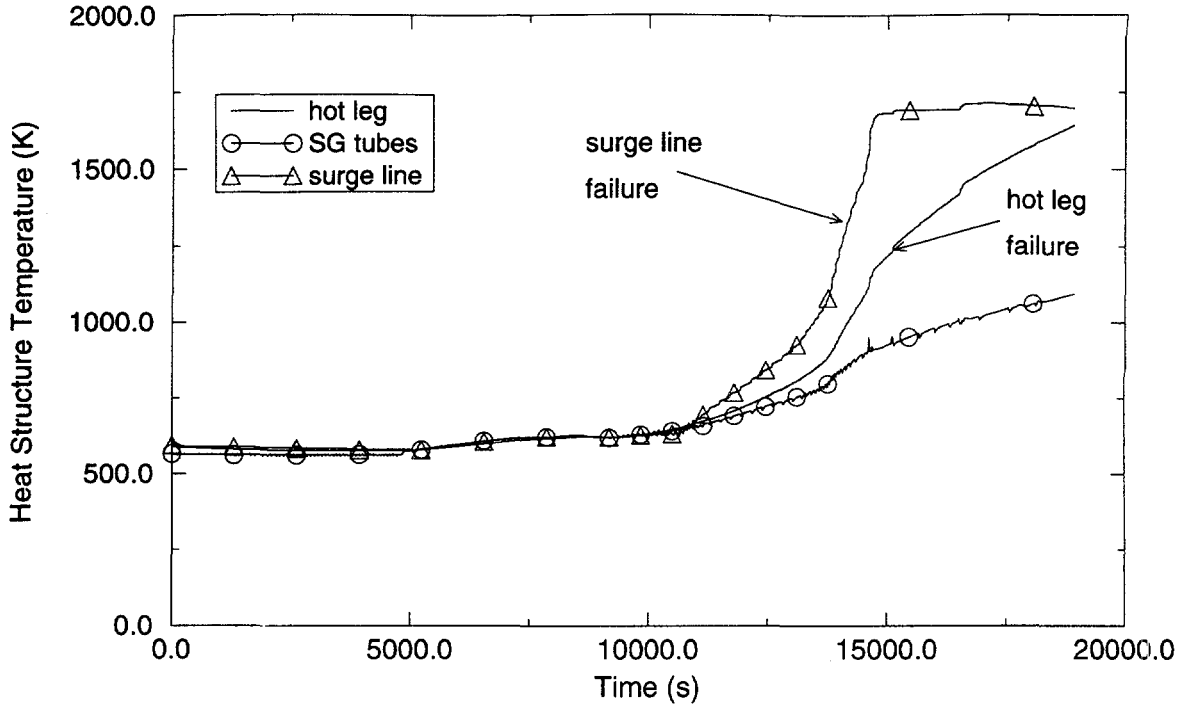

Figure 3.5. Volume-averaged temperatures of pressurizer loop piping: Case 1R.

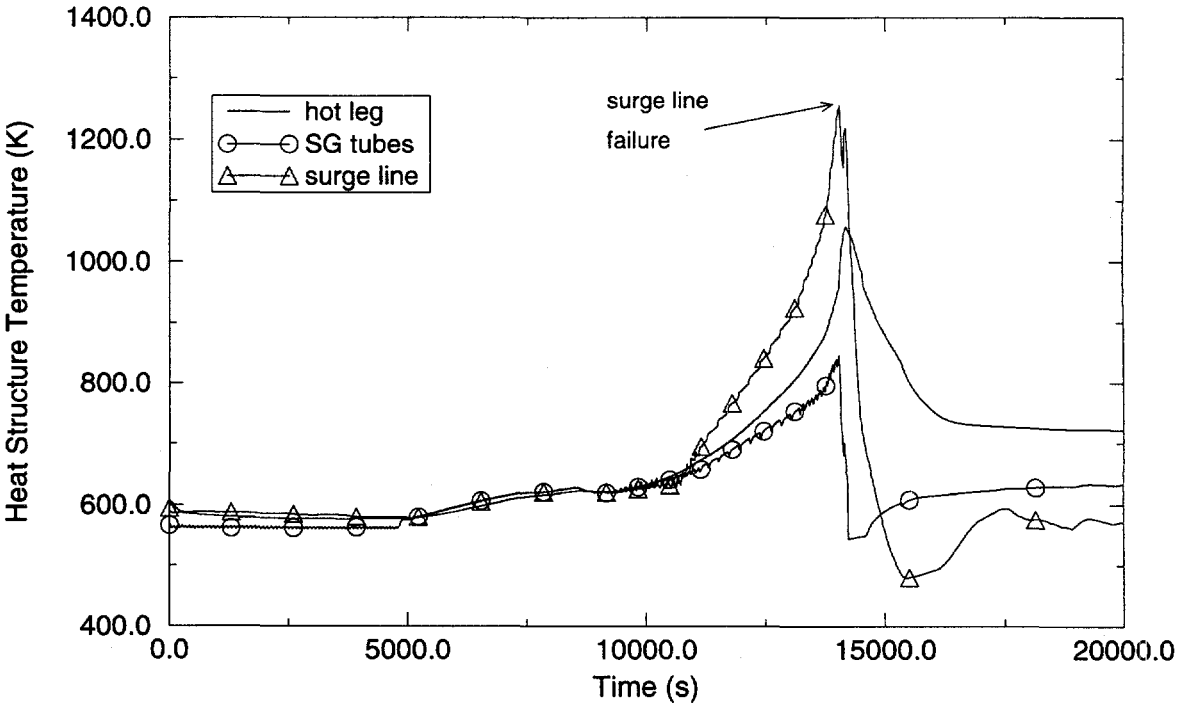

Figure 3.6. Volume-averaged temperatures of pressurizer loop piping: Case 2R.

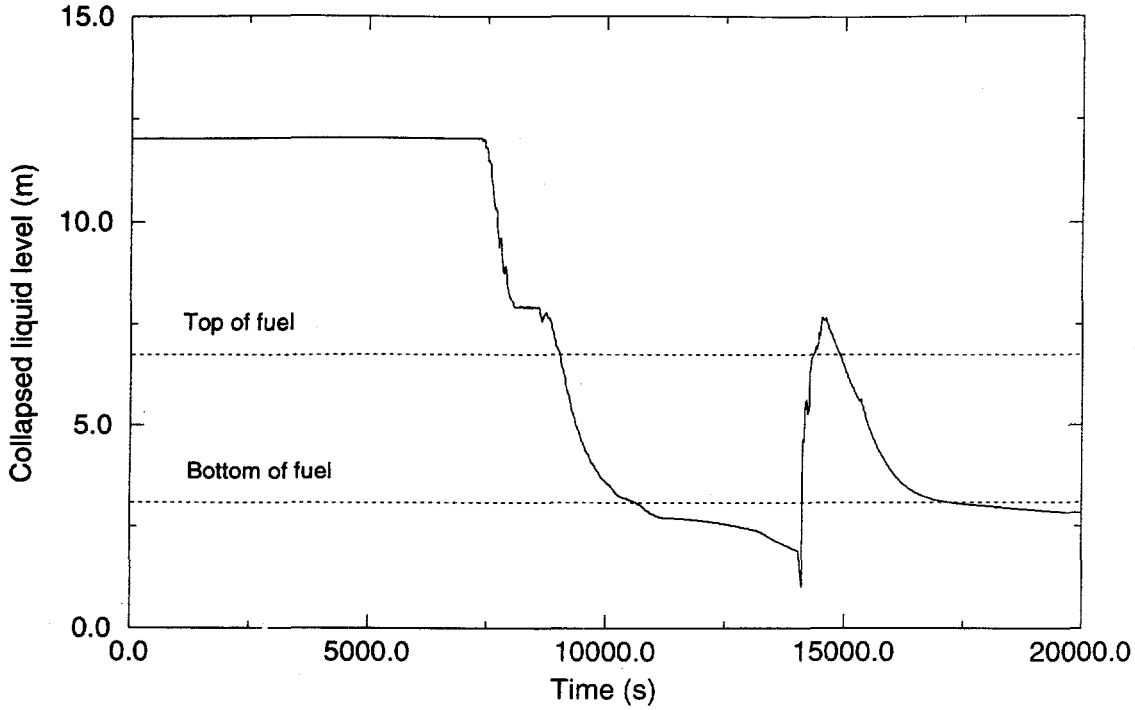

Figure 3.7. Collapsed liquid level in the reactor vessel: Case 2R.

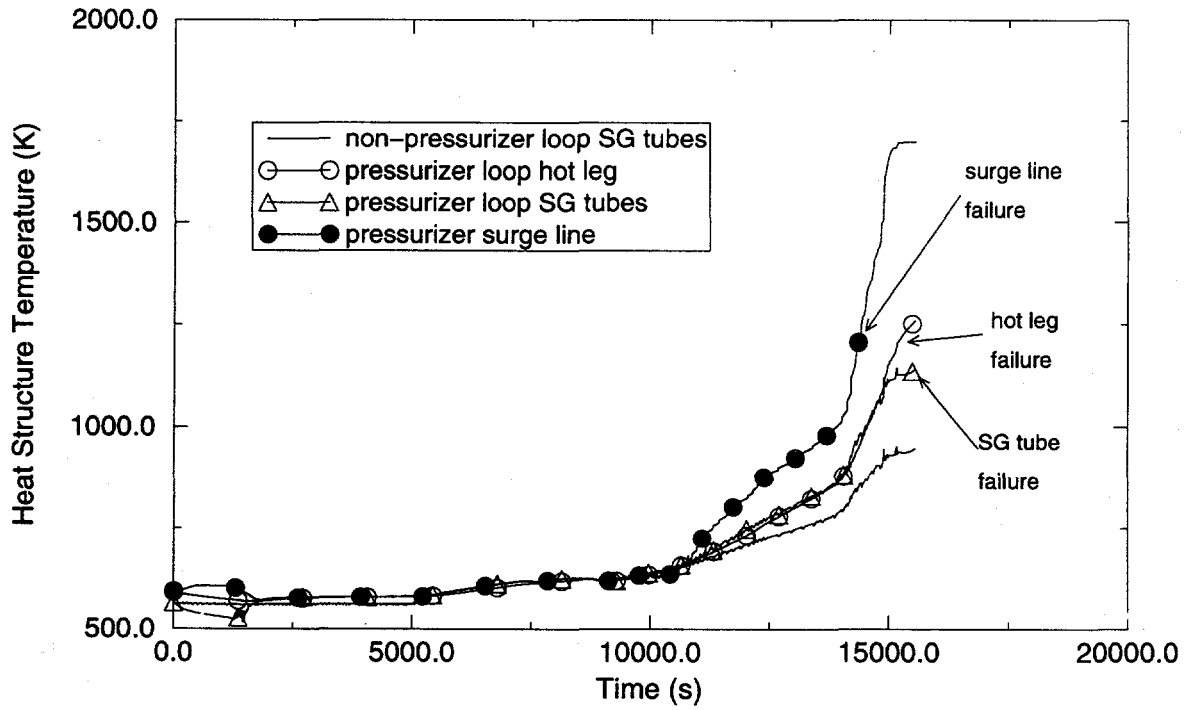

Figure 3.8. Volume-averaged temperatures of ex-vessel structures: Case 3R.

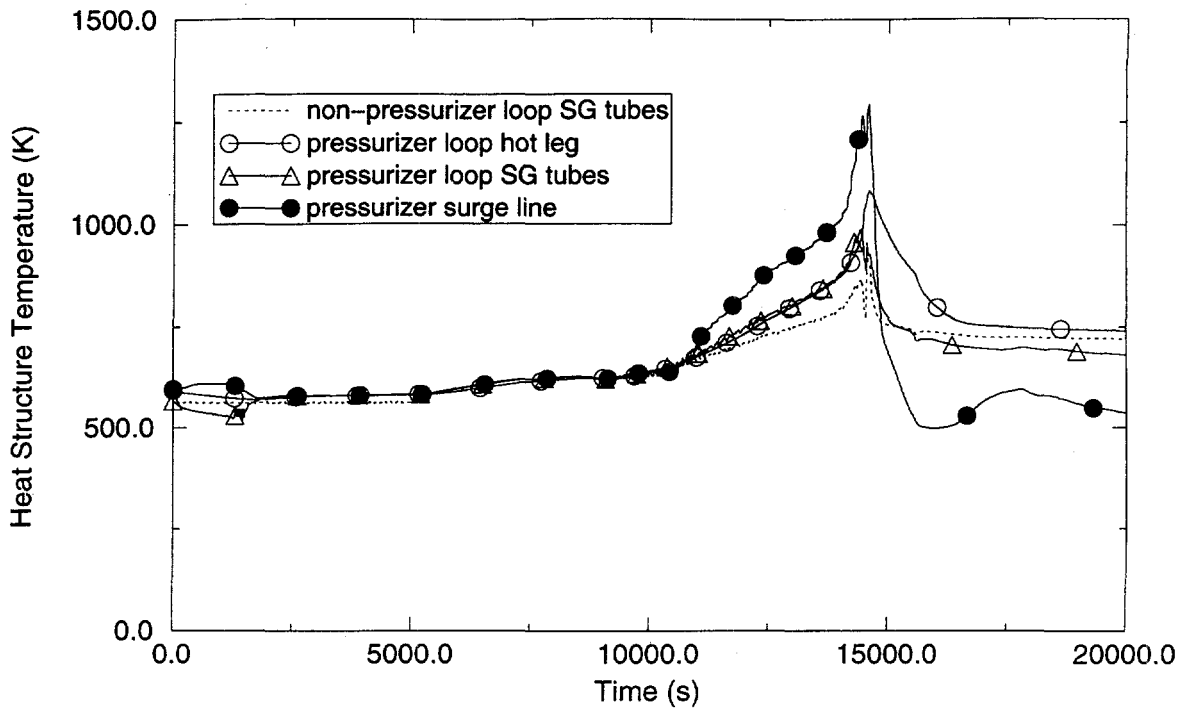

Figure 3.9. Volume-averaged temperatures of ex-vessel structures: Case 4R.

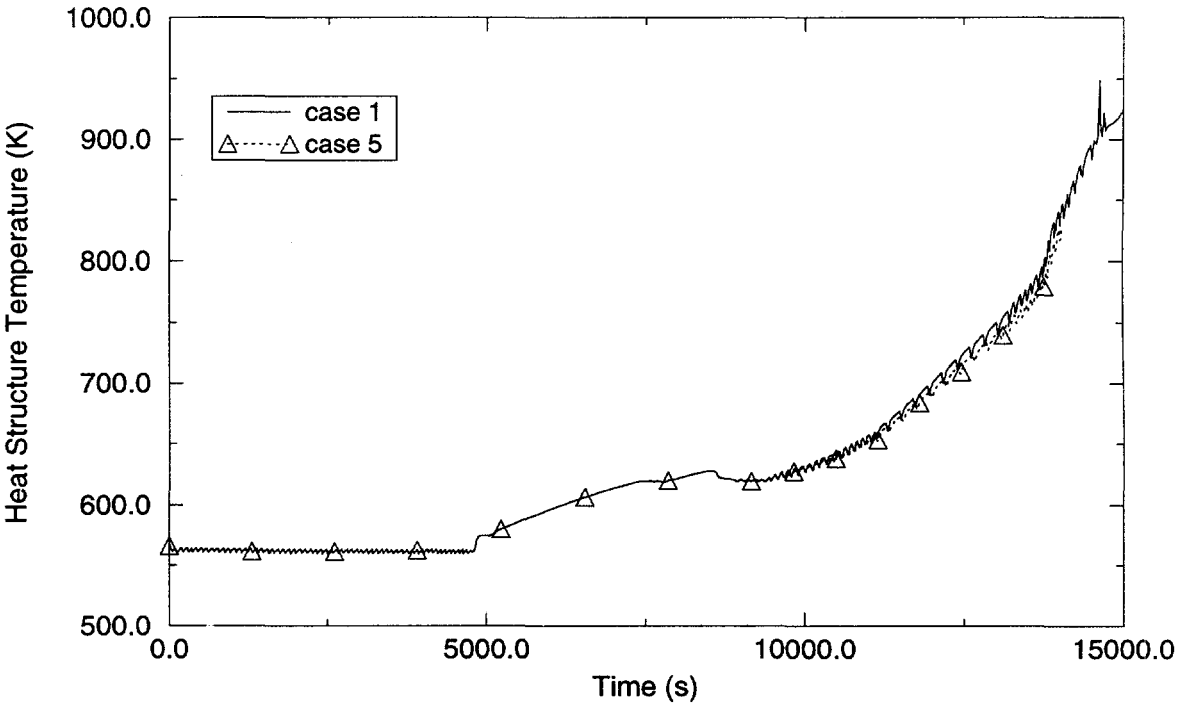

Figure 3.10. Volume-averaged temperature comparison for pressurizer loop SG tubes: Cases 1R and 5R.

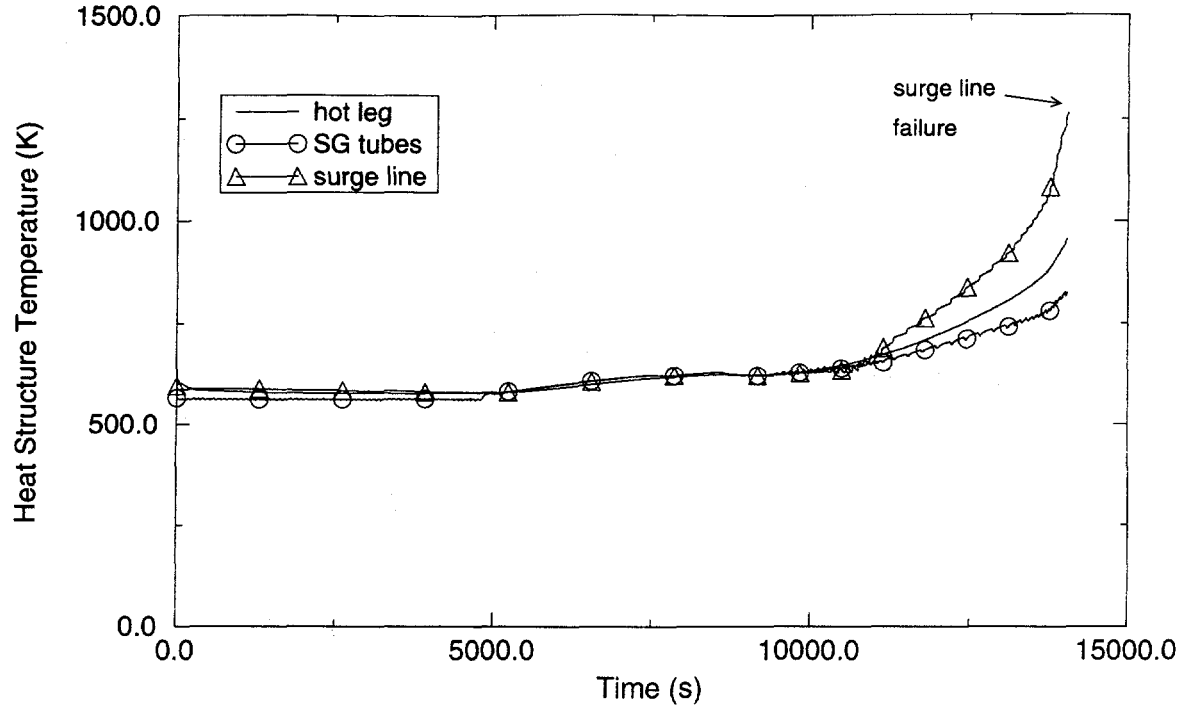

Figure 3.11. Volume-averaged temperatures of pressurizer loop piping: Case 5R.

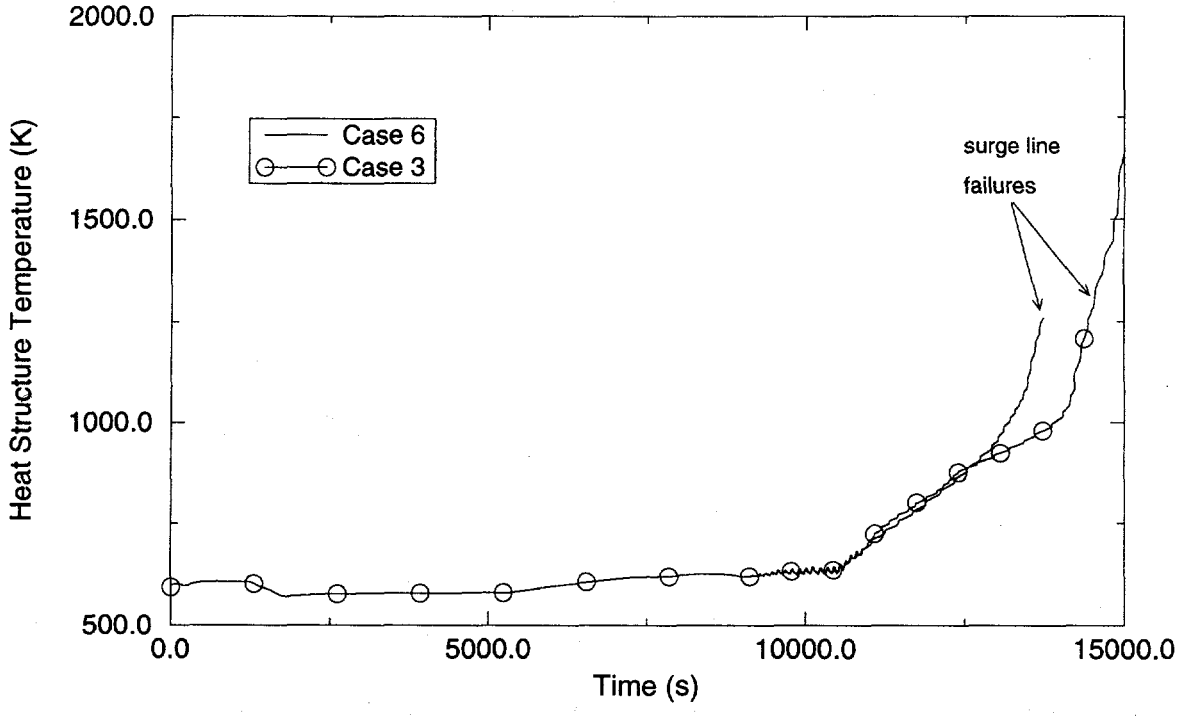

Figure 3.12. Volume-averaged temperature comparison for pressurizer surge lines: Cases 3R and 6R.

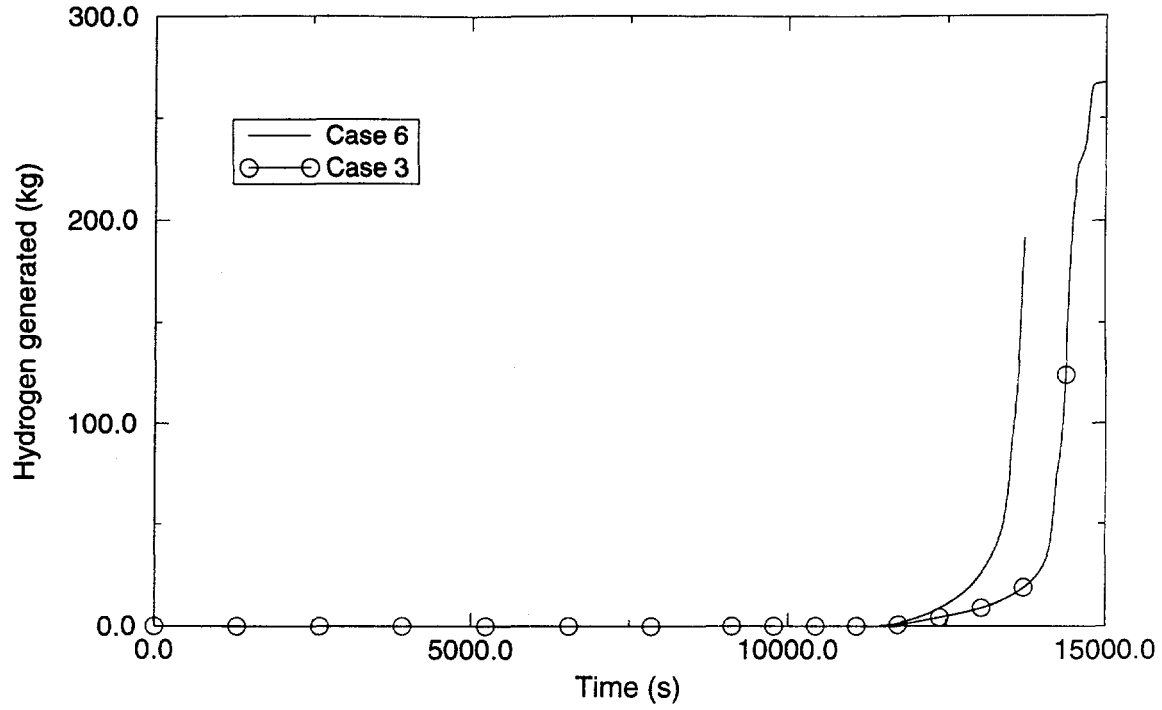

Figure 3.13. Hydrogen generation comparison: Cases 3R and 6R.

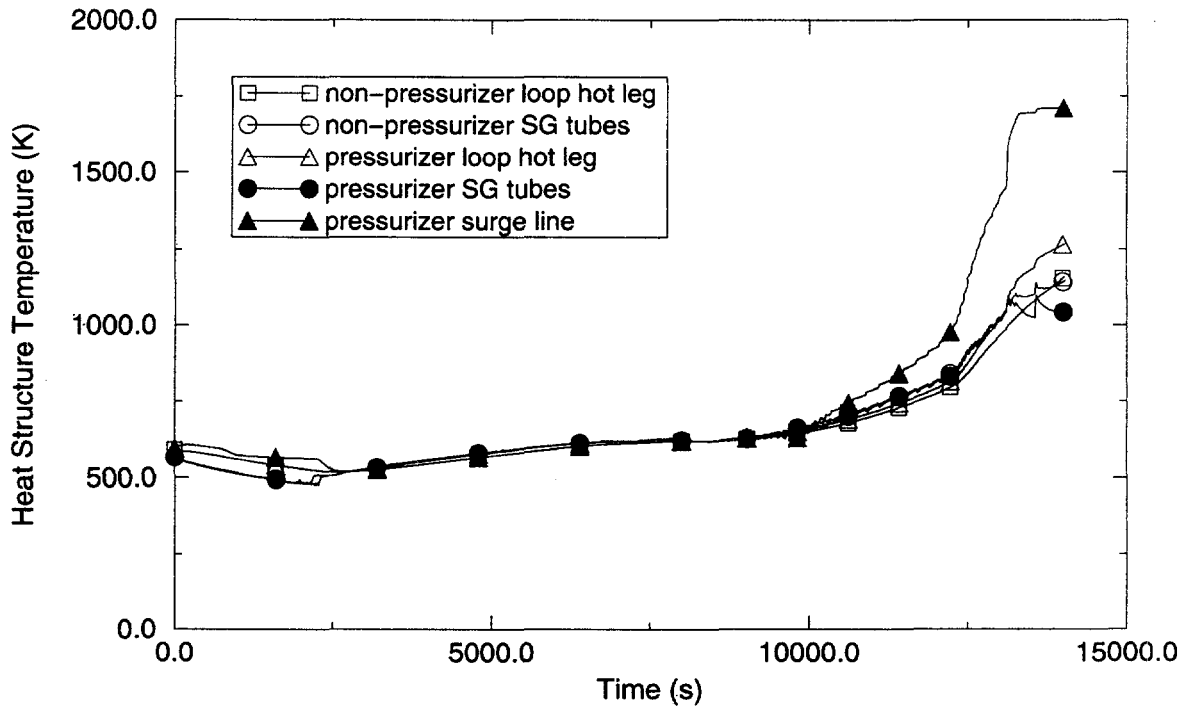

Figure 3.14. Volume-averaged temperatures of ex-vessel structures: Case 7R.

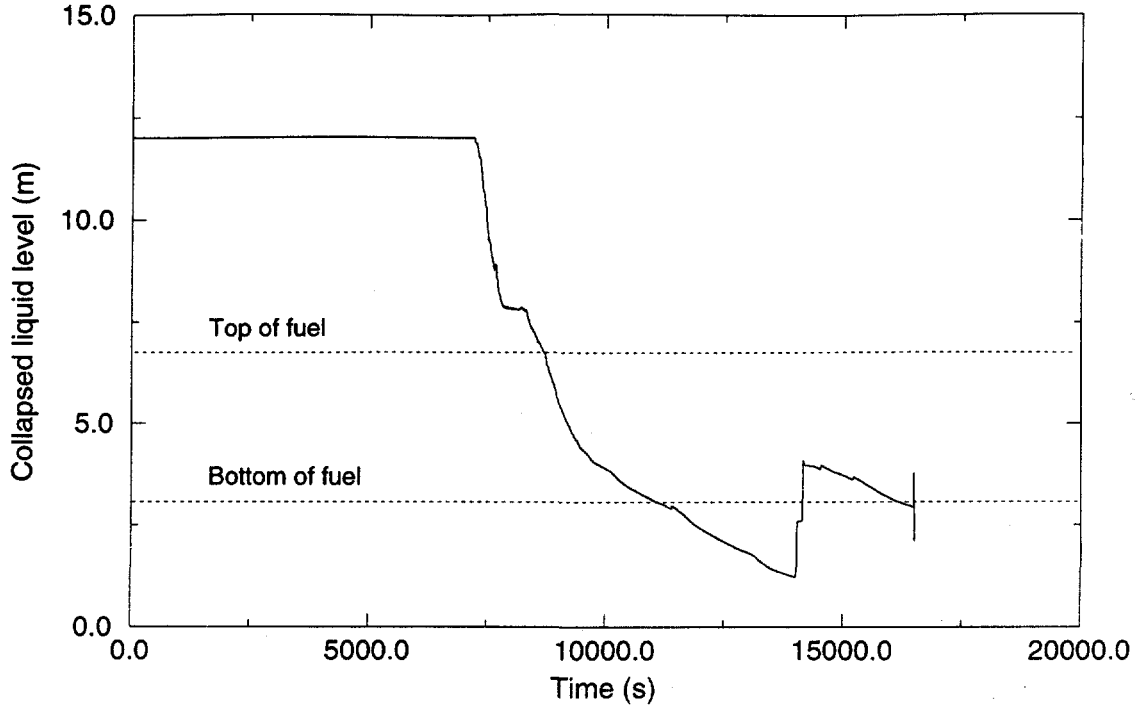

Figure 3.15. Collapsed liquid level in the reactor vessel: Case 8R.

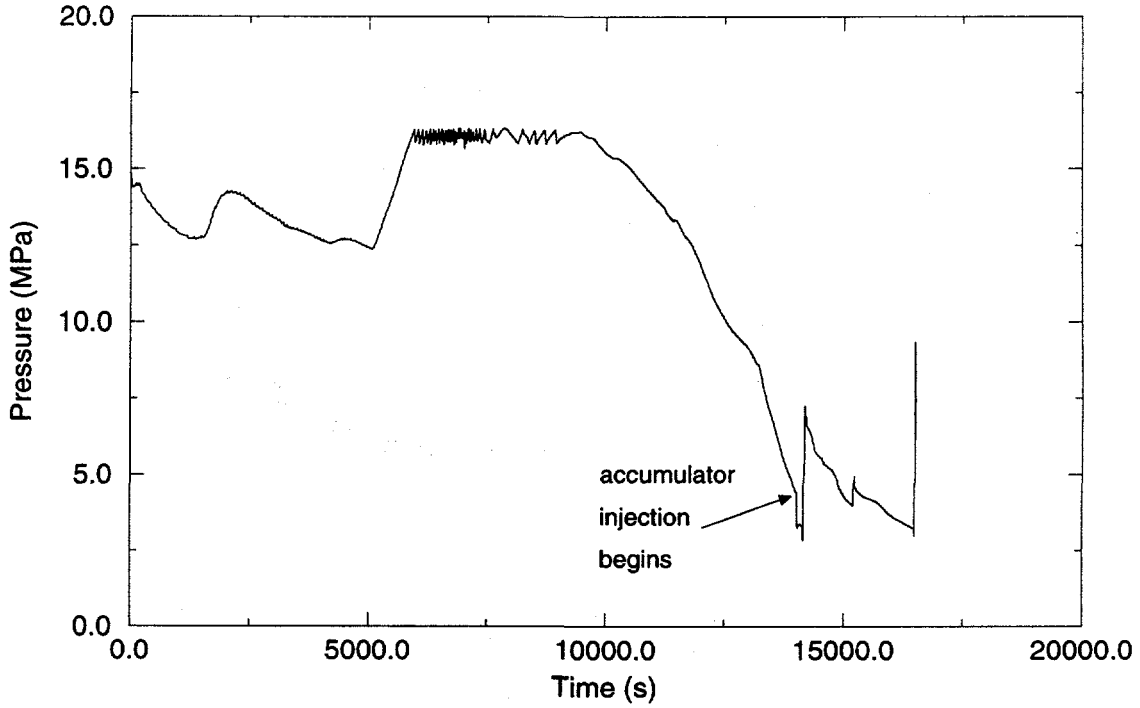

Figure 3.16. Pressure in the reactor vessel lower head: Case 8R.

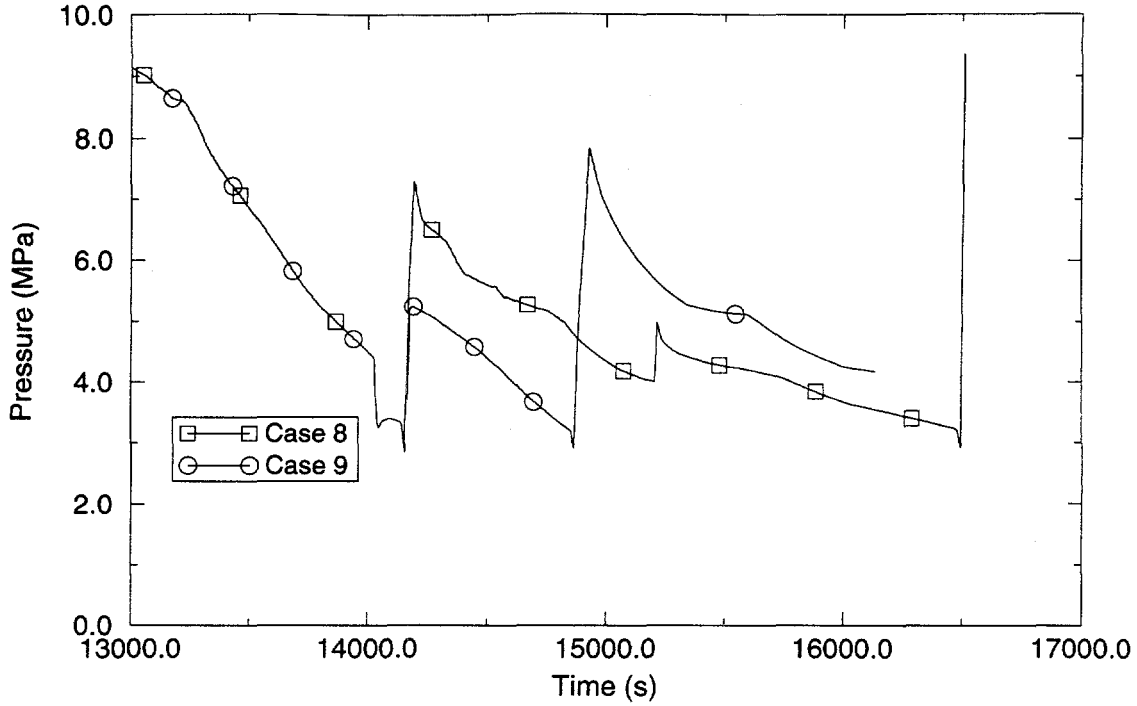

Figure 3.17. RCS pressure comparison: Cases 8R and 9R.

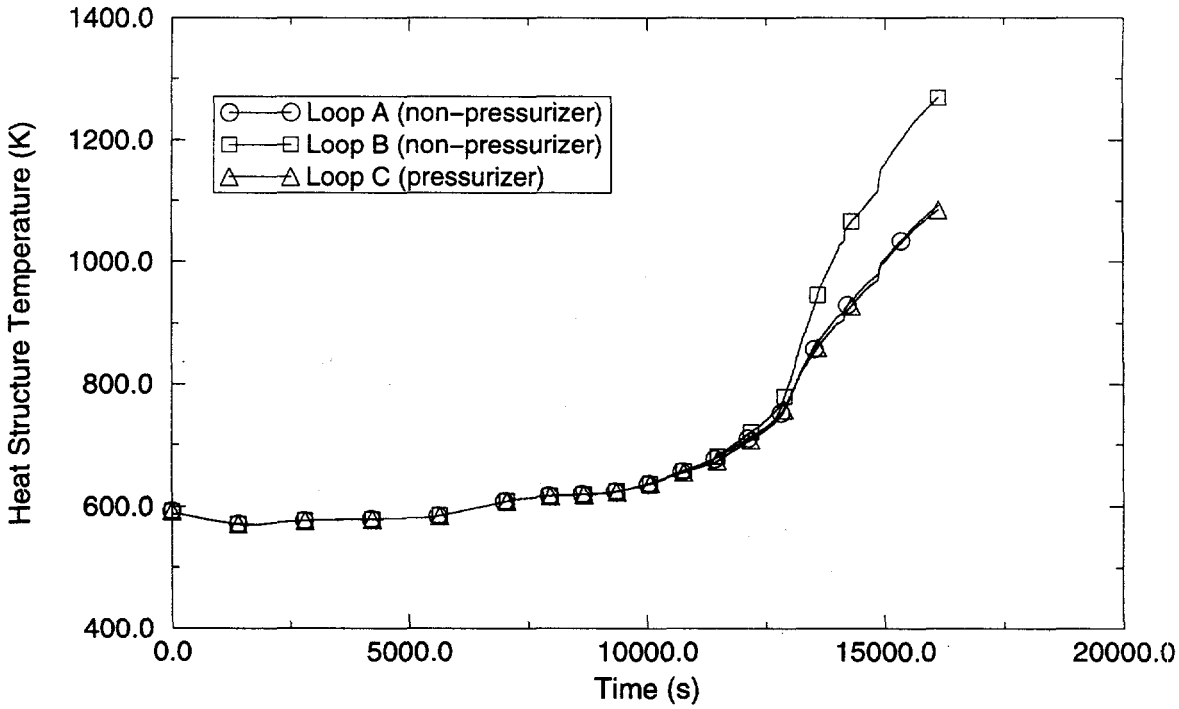

Figure 3.18. Volume-averaged temperatures of hot leg piping: Case 9R.

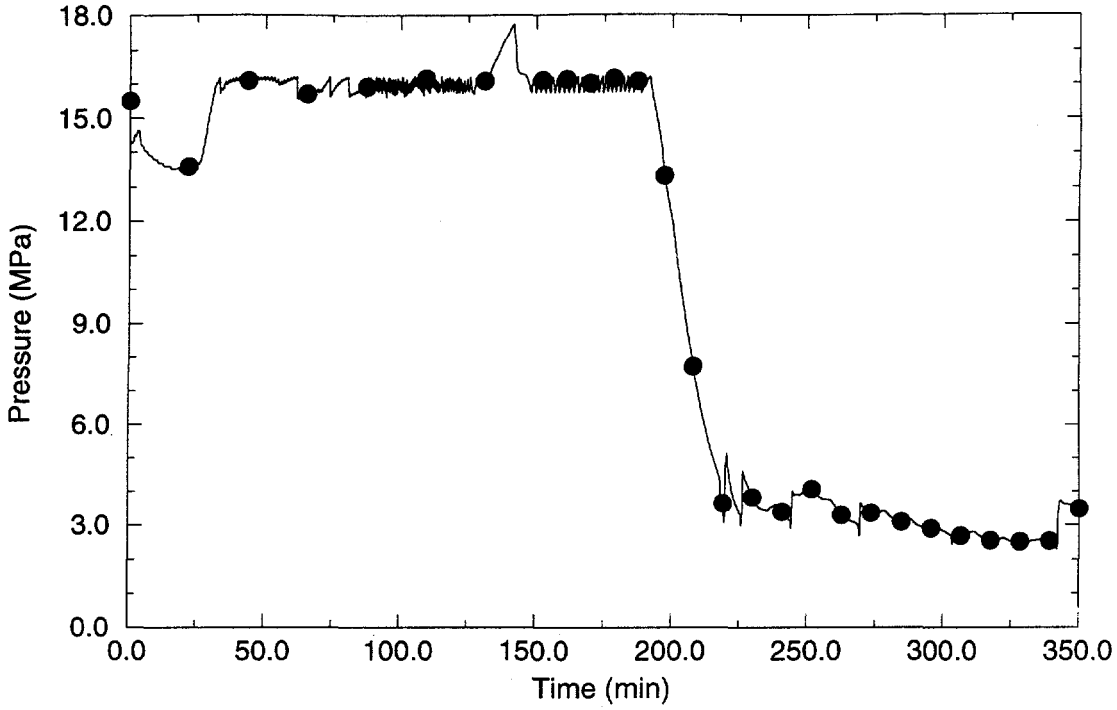

Figure 3.19. Pressurizer pressure: Case 6N.

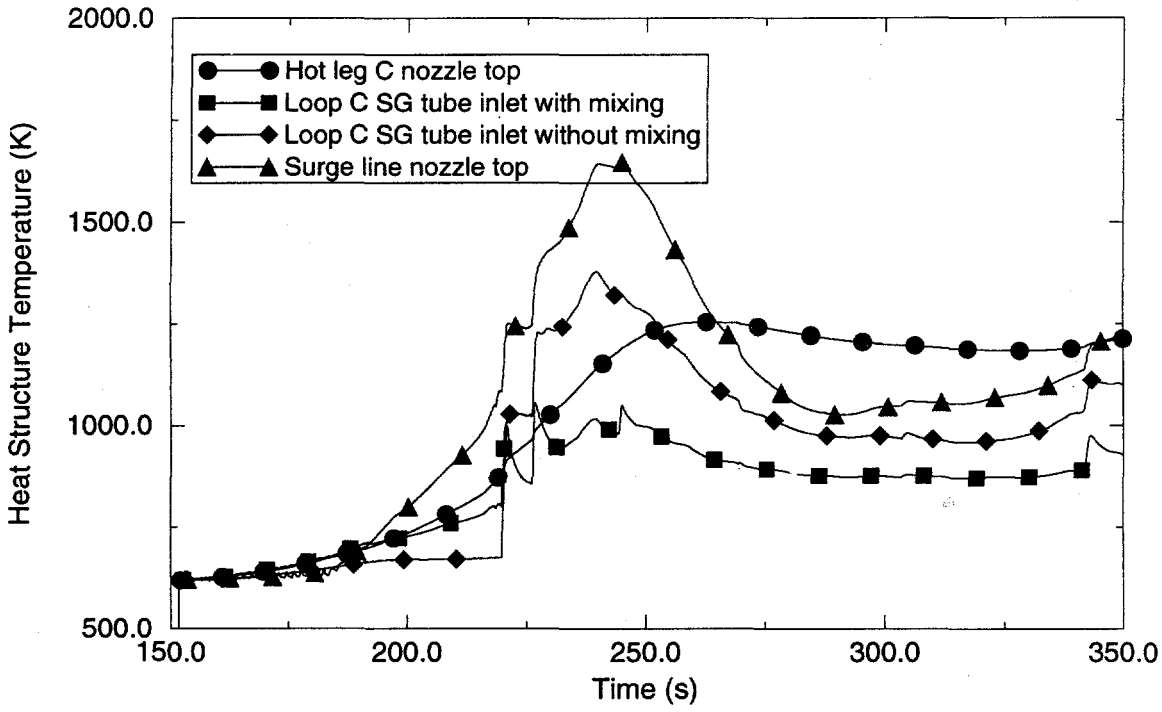

Figure 3.20. Volume-averaged temperatures of ex-vessel structures: Case 6N.

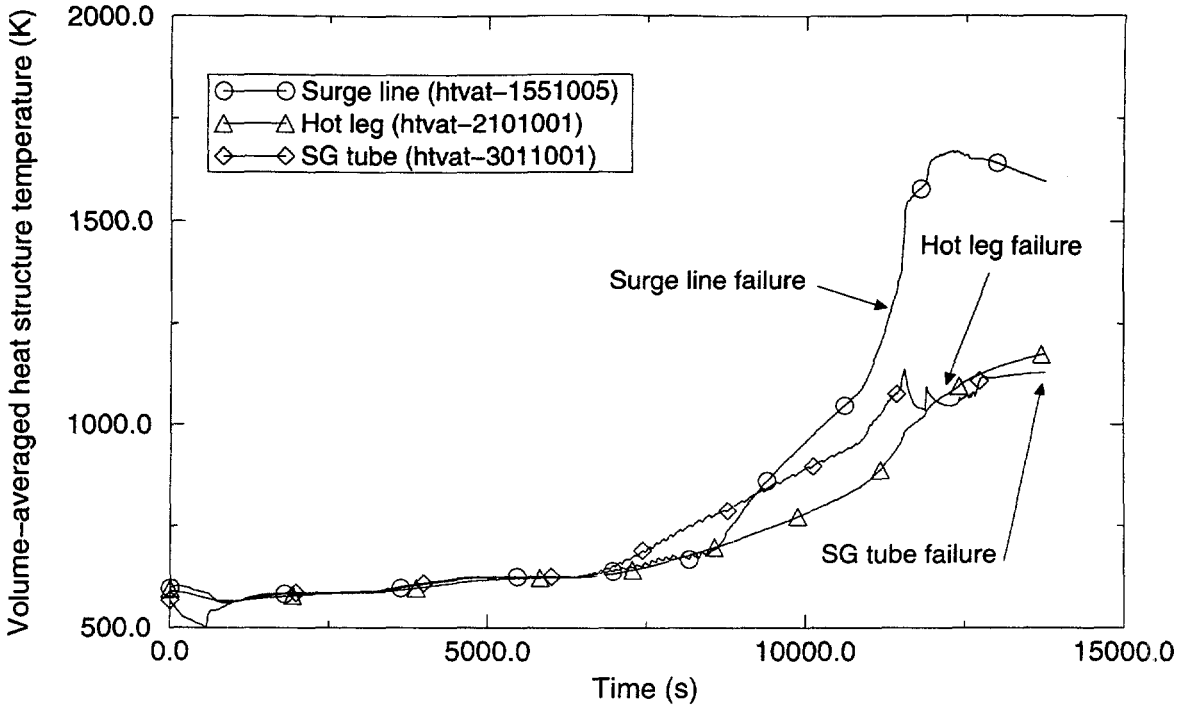

Figure 3.21. Structure temperatures in pressurizer loop: Case ANO1.

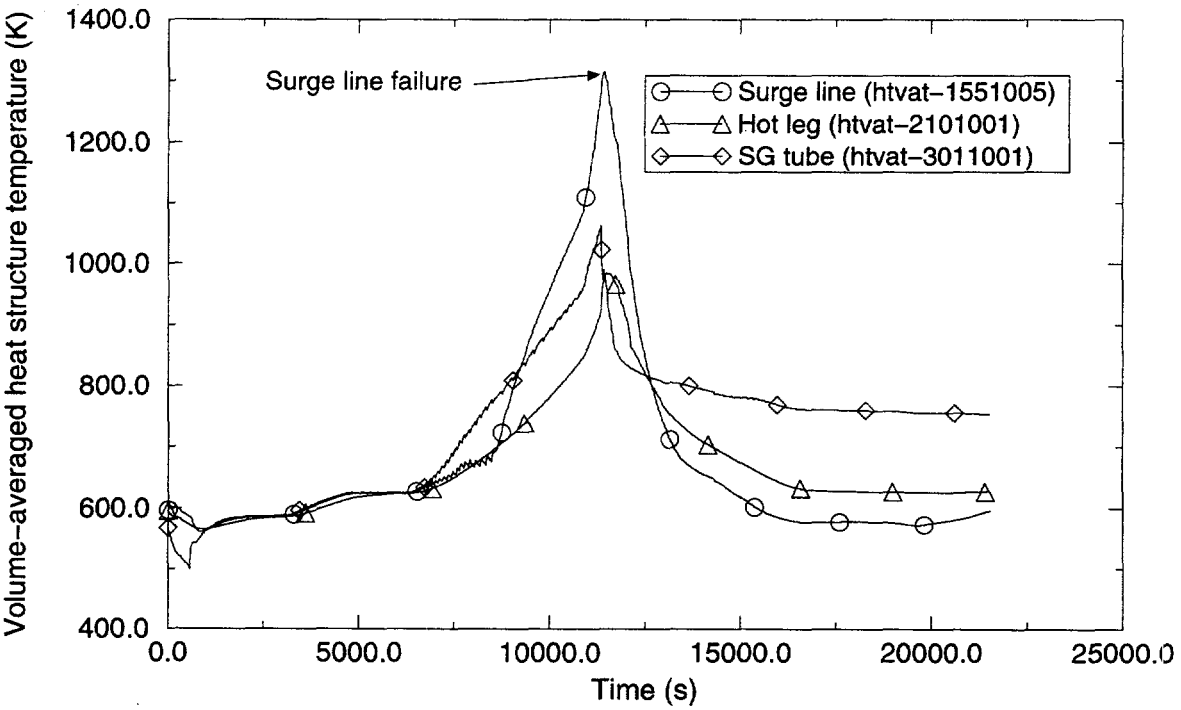

Figure 3.22. Structure temperatures in pressurizer loop: Case ANO2.

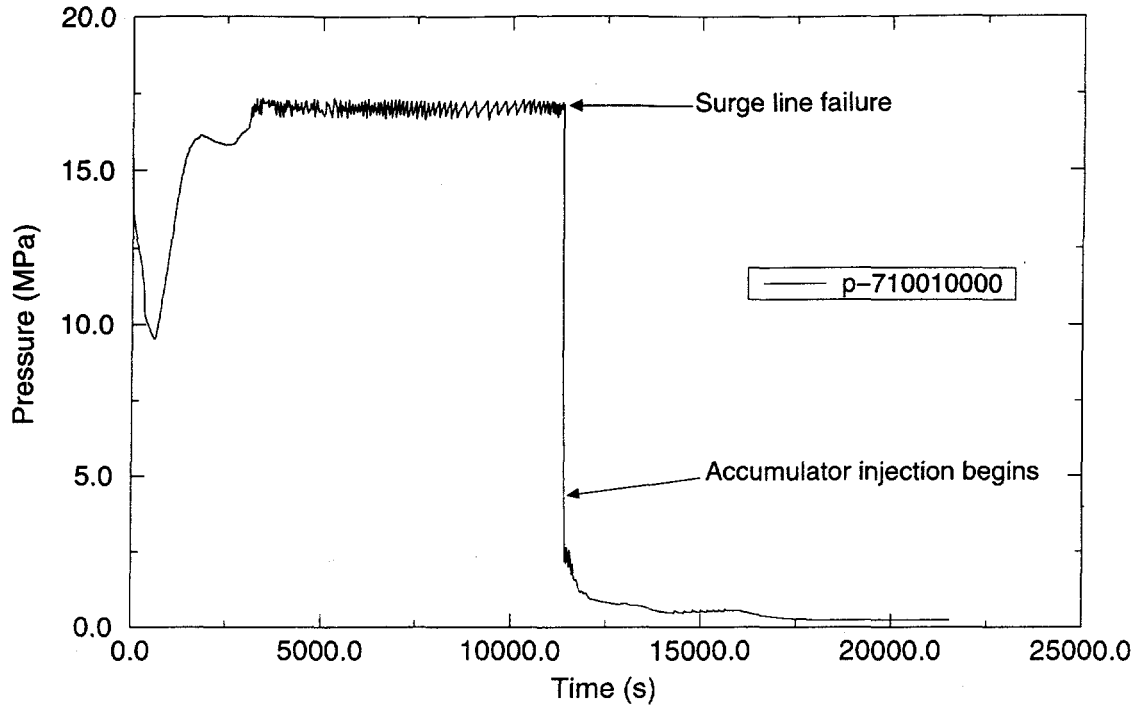

Figure 3.23. Pressure in the reactor vessel lower head: Case ANO2.

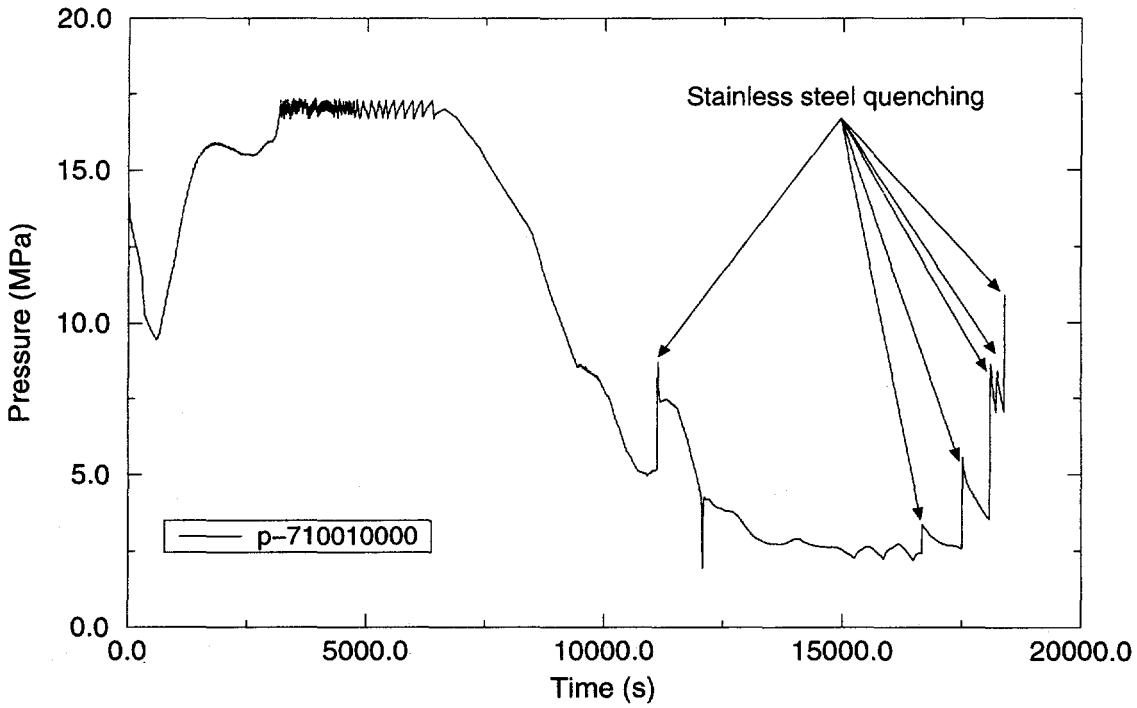

Figure 3.24. Pressure in the reactor vessel lower head: Case ANO3.

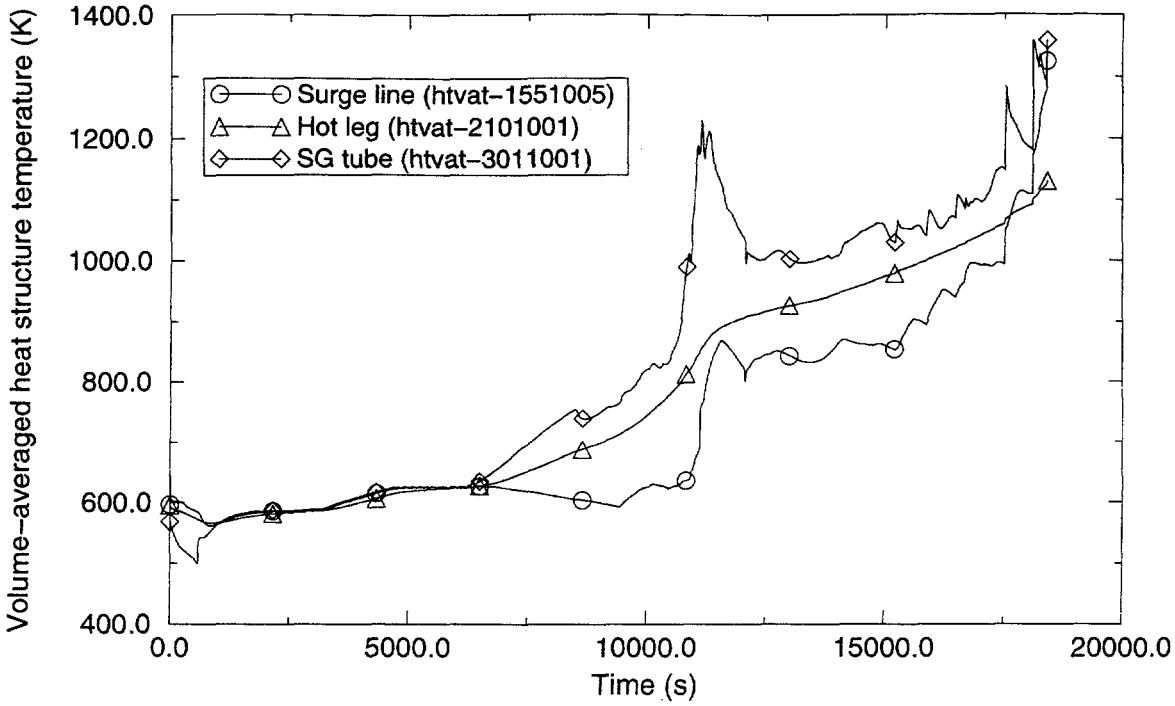

Figure 3.25. Structure temperatures in pressurizer loop: Case ANO3.

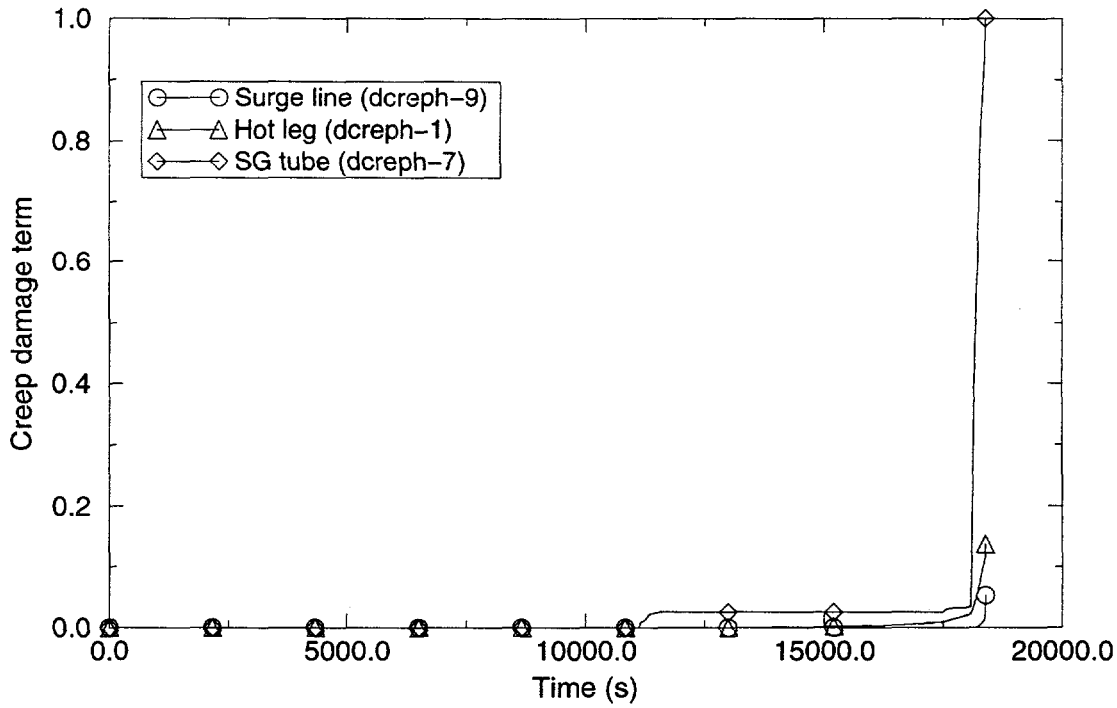

Figure 3.26. Pressurizer loop creep damage indices: Case ANO3.

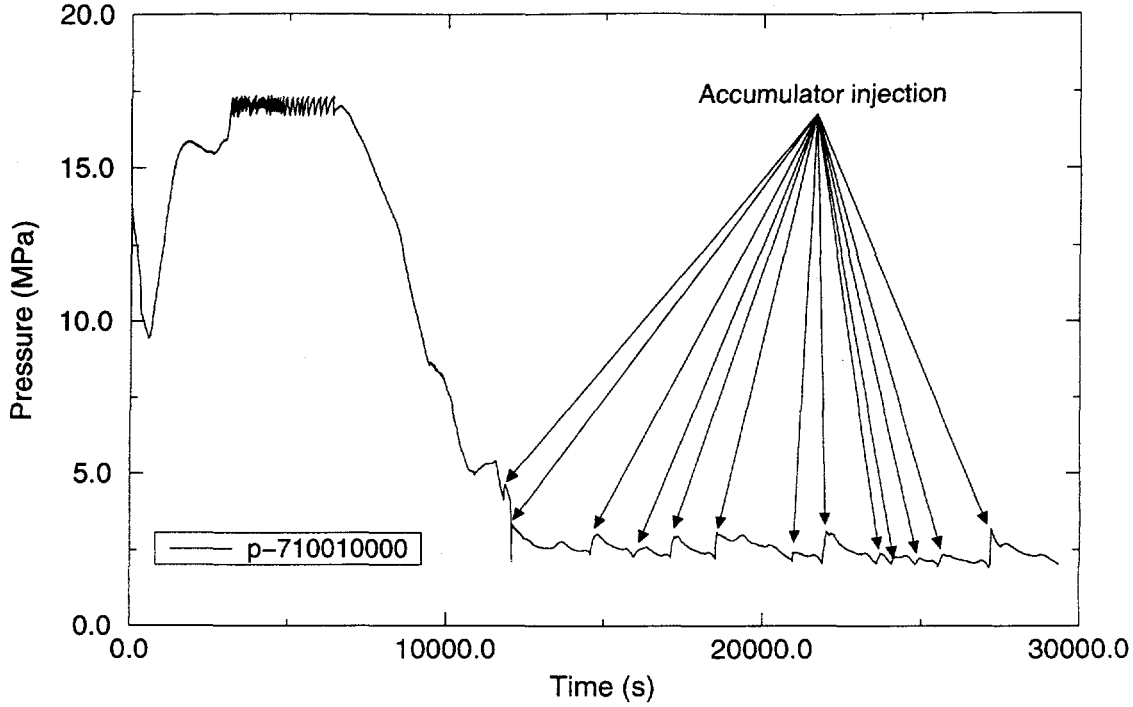

Figure 3.27. Pressure in the reactor vessel lower head: Case ANO4

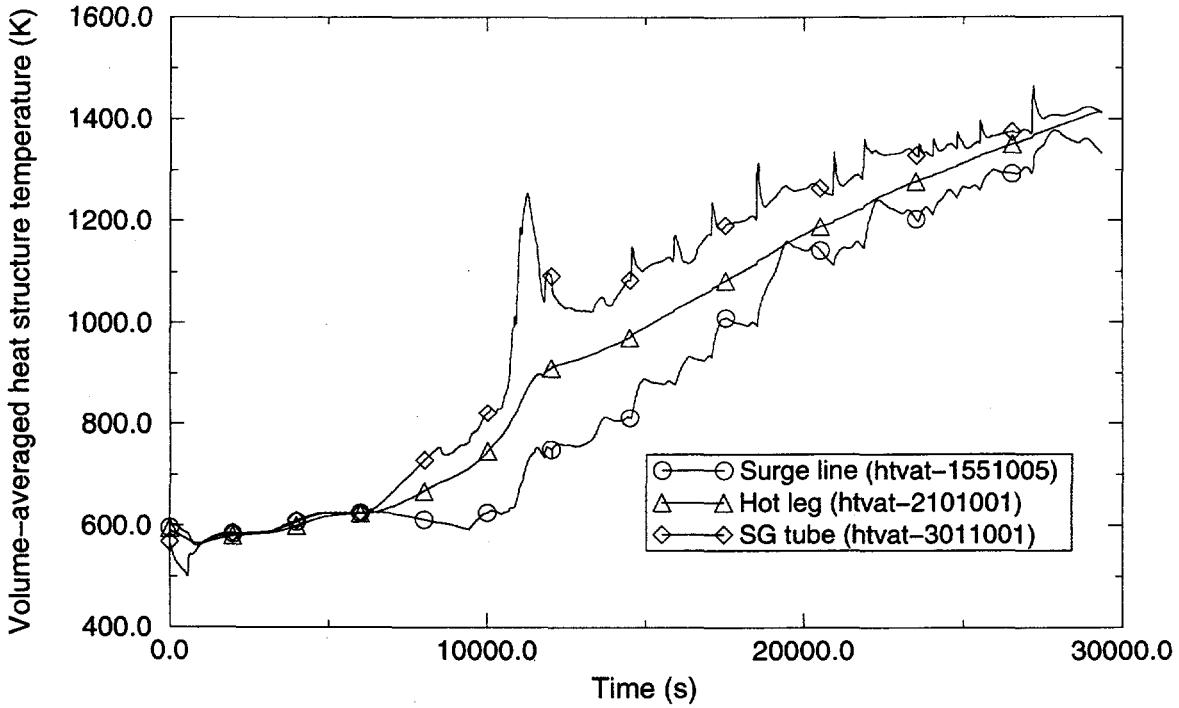

Figure 3.28. Structure temperatures in pressurizer loop: Case ANO4

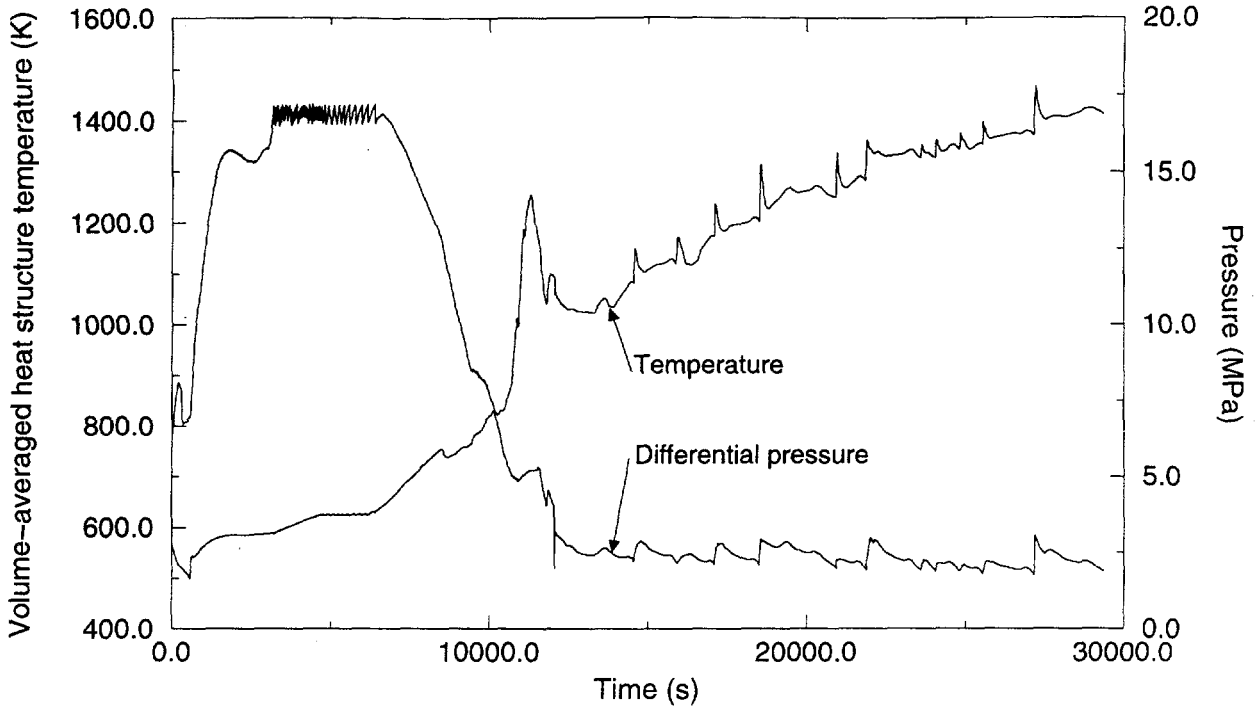

Figure 3.29. Pressurizer loop SG tube temperature and differential pressure: Case ANO4.

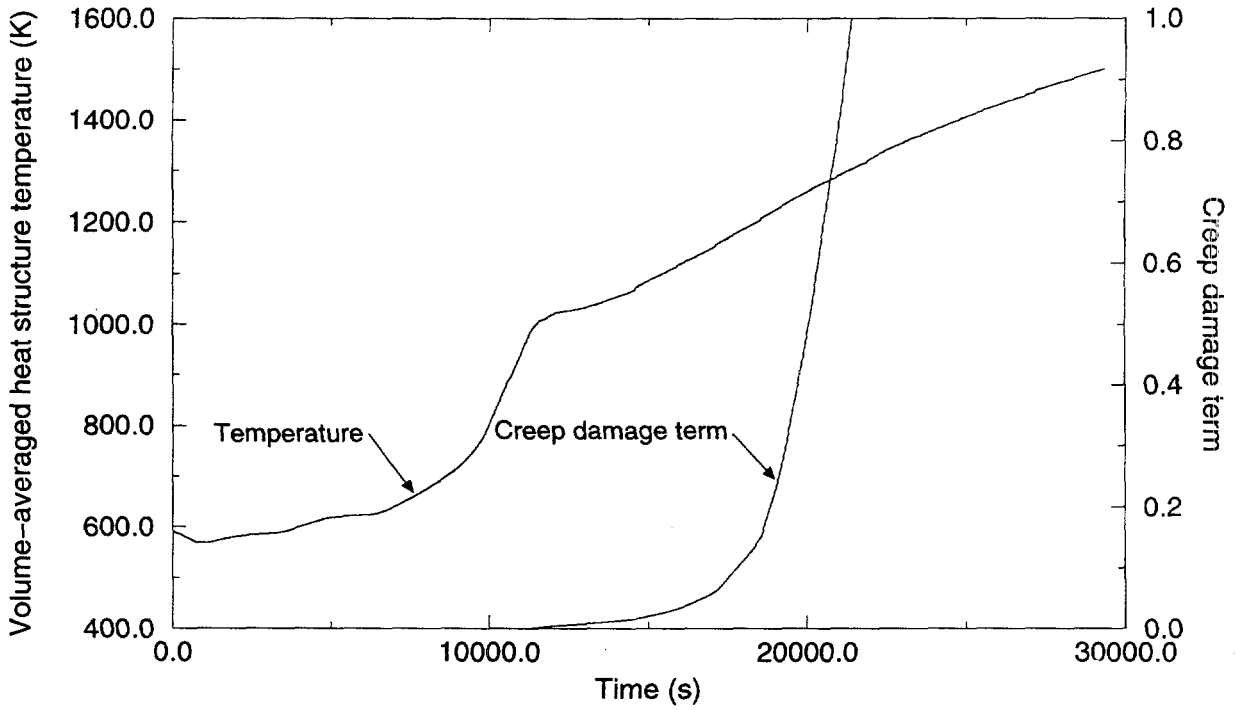

Figure 3.30. Non-pressurizer loop hot leg nozzle temperature and associated creep damage index: Case ANO4.

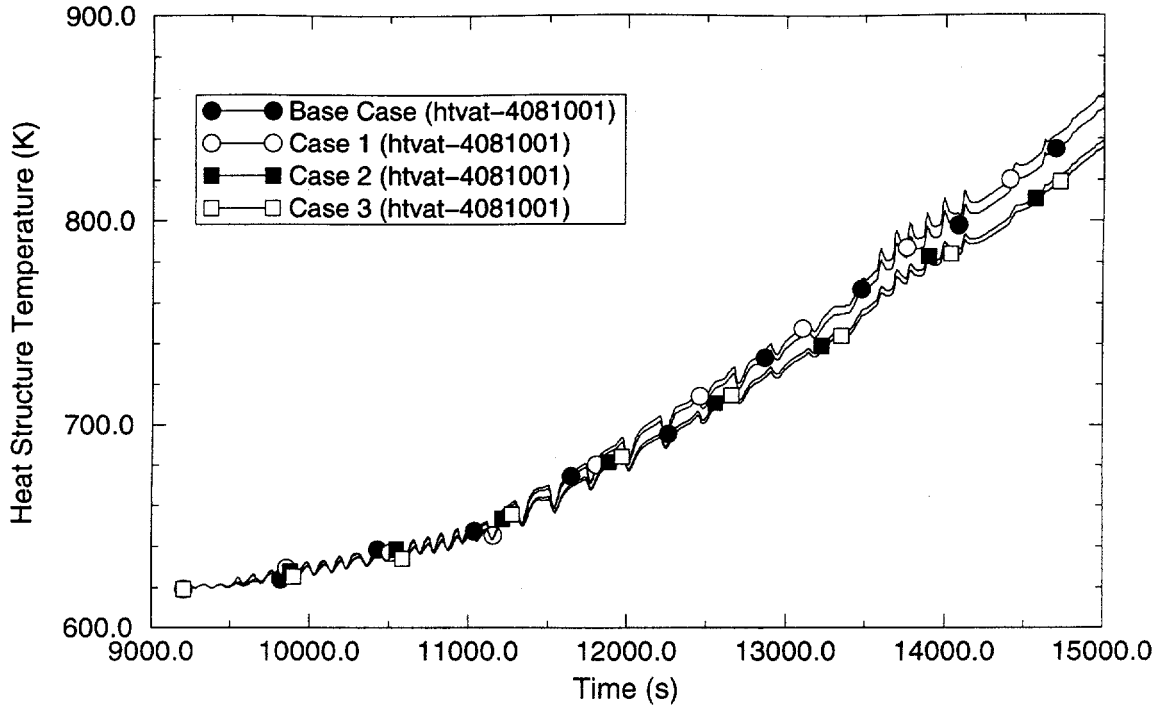

Figure 3.31. Volume-averaged SG tube temperatures above the tube sheet in the forward flow direction: Case 1N and Cases M1, M2, M3.

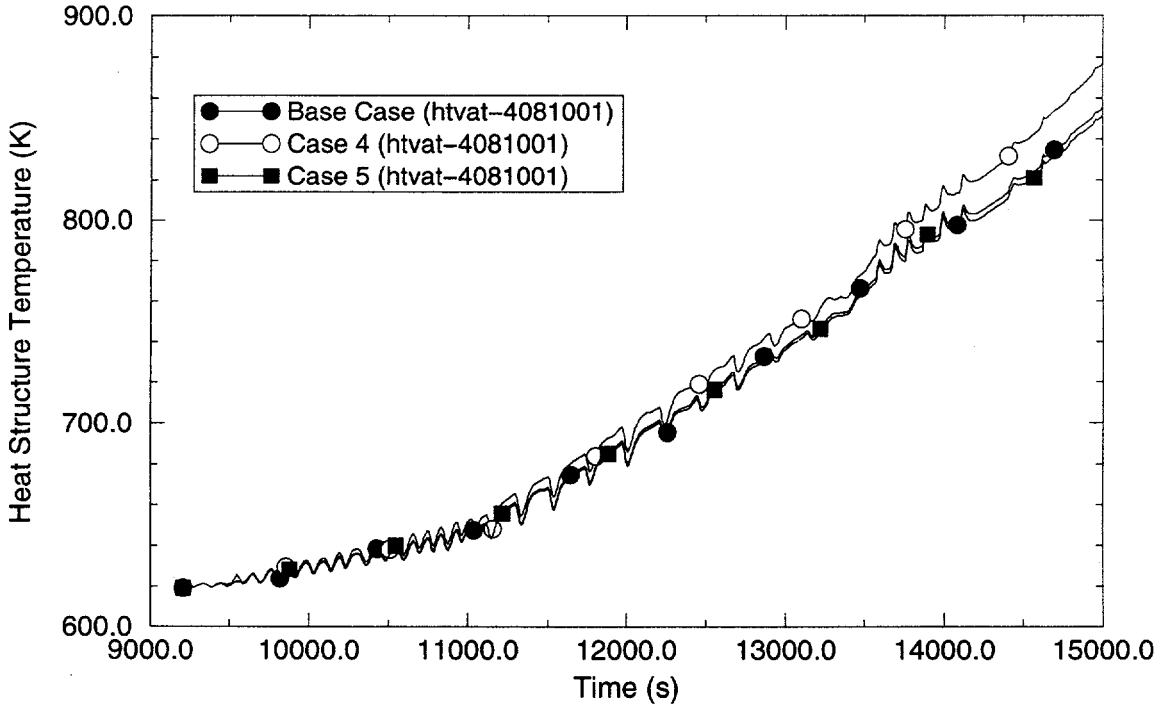

Figure 3.32. Volume-averaged SG tube temperatures above the tube sheet in the forward flow direction: Case 1N and Cases M4, M5.

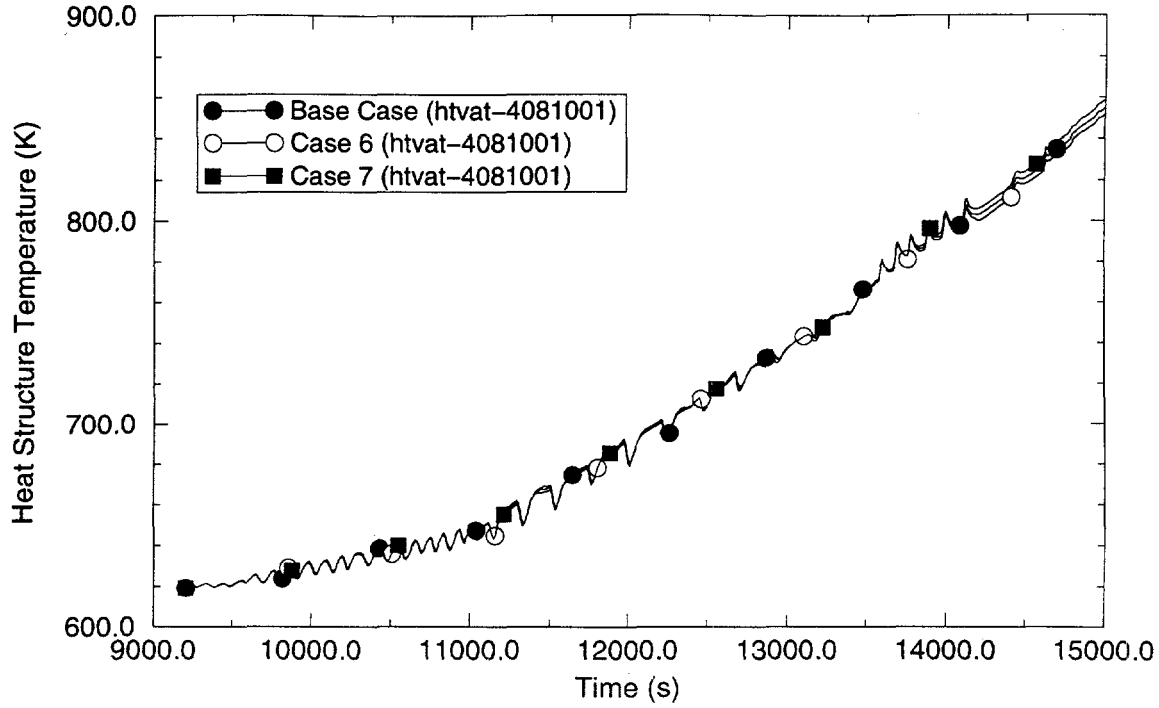

Figure 3.33. Volume-averaged SG tube temperatures above the tube sheet in the forward flow direction: Case 1N and Cases M6, M7.

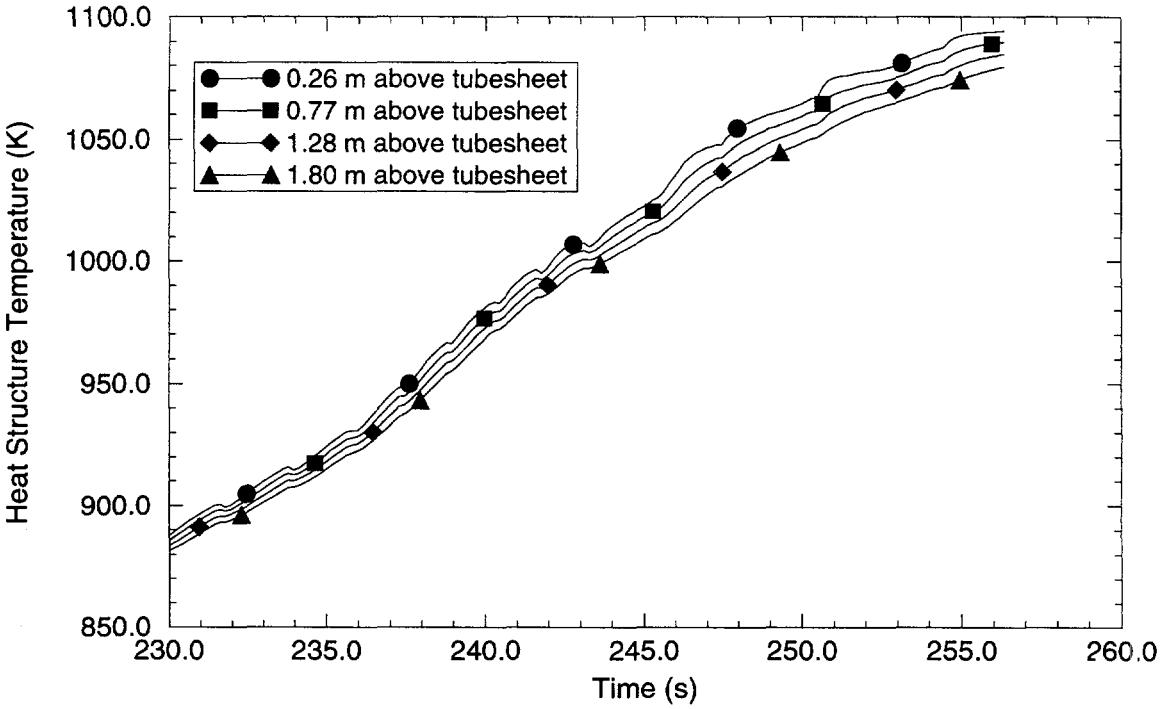

Figure 3.34. SG tube inlet temperatures for first four axial nodes above the tube sheet in the forward flow direction: Case 5N.

4 RCPB SEVERE ACCIDENT VULNERABILITIES

Section 4.1 considers the thermal challenge to components throughout the RCPB, while Section 4.2 discusses the flaw distributions considered in this analysis, and Section 4.3 explains the failure model for axially flawed tubes.

4.1 RCPB Component Performance Under Severe Accident Conditions

A fundamental step in the analysis to estimate severe accident containment bypass potential via SGTR is the calculation of tube failure probability relative to other RCPB components. Previous quantitative assessments typically considered the steam generator tubes, hot leg, pressurizer surge line, and reactor vessel. This study restricts a quantitative treatment to the tubes, surge line, and hot leg; however, other RCPB components will be threatened with failure under severe accident conditions, thereby affecting the potential for tube failures.

Besides the steam generator tubes, hot leg, and surge line, a variety of other locations in the reactor coolant system will be exposed to very high temperatures. The discussion in this section focuses on components deemed to have a potential to reach conditions leading to thermal failure. (These include flanged joints, tube repairs, and relief valves.) The information cited is specific to the Surry plant, and the thermal-hydraulic transient used was the INEL study conducted under contract to NRR (Ellison, 1996), designated 1N in Table 3.1. The study was performed for scoping purposes, to provide insights into the likelihood that components other than those quantitatively considered could impact the potential for tube failure. The results do not necessarily apply to other PWRs.

4.1.1 Degraded Steam Generator Tube Performance Under Severe Accident Conditions

In an attempt to understand tube response under severe accident conditions, the NRC sponsored a study (Ellison, 1996) conducted by INEL, which included engineering analyses to estimate the probability of severe accident tube failure. The failure mechanism selected for the study was axial outside diameter stress corrosion cracking (ODSCC), and tube failures were predicted using limit load analyses with flow stress values at elevated temperatures. Creep damage was not considered in the assessment, and the data for tube material characteristics at elevated temperatures was limited. INEL (also see Chavez, 1996) clearly pointed out that the study used simplifying assumptions regarding the degradation mechanism, the prior loading and temperature histories of the tubes, and material properties at high temperatures. The study provided bases for those assumptions; however, it demonstrated a need for experimental data to support the assessment of high-temperature tube behavior.

In order to better understand the behavior of steam generator tubes under severe accident conditions, the NRC conducted steam generator tube testing at Argonne National Laboratory (ANL). (This testing and its results are covered in greater detail in Section 4.3.) These tests provided sufficient information to show that the flow stress tube failure model was not sufficient, and that a creep basis should be used. The results were used in the development of a model, as described in Section 4.3, to predict degraded tube failures under a range of tube temperature and pressure histories. The accuracy of the predictions from this model depend upon the accuracy of the predicted tube temperature and pressure histories.

4.1.2 Relative Failure Times for RCS Components

Failure of non-flawed RCPB components is postulated to occur by creep, and is modeled using the Larson-Miller methodology (Larson, 1952). Normally, the Larson-Miller method yields a parameter that is used to assess reduction of a component's life as a result of creep in an elevated temperature range that is compatible with expected service conditions for the material (e.g., creep damage in a 2¼ Cr-1 Mo steel pipe in fossil plants).

Larson and Miller explain that the relationship they present is useful in assessing long-term creep behavior at lower temperatures on the basis of shorter-term higher-temperature rupture testing. This testing was performed at constant temperature with constant load. On the basis of the thermal-hydraulic information considered here, RCS components are subject to a reasonably steep ramp of increasing temperature, as well as to some minor changes in loading, since the pressure varies as a result of the PORV opening and closing. The steam generator tube testing results described in Section 4.3 have shown that a model either based on a creep or flow stress provides reasonable predictions for tube failure for the thermal-hydraulic transients considered. However, the creep model was shown to be more effective for predicting tube failure over a wider range of loading conditions.

In the case where the material weakens as it is heated and the temperature ramp is reasonably steep, the stress rupture solution essentially defaults to a limit load solution. The reader should note that long, slender steam generator tubes with more or less consistent grain size containing axial flaws are reasonably simple structures to analyze, since they are essentially constantly loaded and are damaged by short-term stress rupture resulting from excessively high temperatures.

It is more difficult to assess damage in a piping system than in a simple structure like a steam generator tube. The thermal-hydraulic analysis results indicate that very large top-to-bottom temperature gradients exist in the hot leg at the hot leg nozzle, as well as in the surge line. The bending loads from thermal gradients and their time-dependent nature, would be significant and could be expected to cause deformation in the piping.

Additionally, other concerns regarding the RCS piping integrity might arise at supports and terminal ends. For example, it appears that much more complex structural analyses of the piping would be required to account for system geometry, supports, and thermally induced deformation. In addition, weldments are present near the nozzles. J.A. Williams (1982) suggests that complex finite element models and verification experiments are needed to predict joint behavior in high-temperature materials operated in the range of 700 to 1100°C (1292 to 2012°F). In the case of a severe accident, this would be even more difficult since the RCS components would be operating well outside the temperature range ever considered in their design.

Analytic prediction of component failure would be difficult since factors such as microstructure, environment, impurities, notch sensitivity, weldments, and system configuration affect the time to failure. For example, the staff expended considerable resources in an attempt to assess the margins to failure for the Three Mile Island (TMI) reactor vessel lower head. This analysis also involved the cooling of core debris in the lower head and, therefore, was probably more complicated than tube heating. However, the precision in predicting failure times of thicker-walled components (such as the surge line and hot leg) using a simple Larson-Miller relationship may be questionable given uncertainties in predicted thermal-hydraulic conditions as well as other factors cited above. Given the close proximity of failure times predicted by the SCDAP/RELAP5 code for

the hot leg, surge line, and unflawed steam generator tubes, as well as the other factors discussed above, it is very difficult to determine what components would fail first.

4.1.3 Other RCS Weak Points

The staff has also identified and evaluated other RCS components that could fail and affect the likelihood for steam generator tube failure. The purpose of this evaluation is to determine if either flanged connections or valves in the RCS could fail under severe accident temperature conditions, and if so, to estimate when.

The staff used temperature/time profiles from the Case 1N SCDAP/RELAP5 analysis (see Table 3.1) to depict conditions at a number of locations in the RCS. The staff then used these analyses to provide temperature input for the calculations performed, and to estimate failure times for various components.

In the case of the flanged connections, the staff performed an evaluation to determine if there is (or probably would be) sufficient yielding of certain RCS flange bolting material to cause joint separation leading to significant leakage at the connection. Specifically, the flanged joints examined included the SG primary and pressurizer manways, and the bonnet flanges of the loop isolation valves. In addition, the staff evaluated the expected behavior of the pressurizer SVs and PORVs to ascertain if valve failure is credible and, if so, to estimate when.

The method used to determine the amount of bolt yielding, if any, expected for a preloaded flange connection involves the solution of simultaneous semi-elastic characteristic equations for the structurally coupled flange bolts and gasket in equilibrium with the system fluid pressure. In addition, the method includes thermal expansion of the individual flange components. The staff developed constitutive equations using a linear approximation of the material stress/strain relationships over a narrow range, and wrote a computer program to compute the results. The staff then verified some of the program results using representative hand calculations, and examined all of the results for reasonability. Additionally, the staff varied certain configuration parameters in an attempt to account for some uncertainties. However, the reader should note that the results are useful only for scoping analyses and need to be refined to determine the probability of component failure. For example, when the results predict a gap in a joint, it merely means that the joint gasket is calculated to unload. However, the gasketed joint will probably start leaking before the gap is predicted, since the analysis did not include the related hydrodynamic forces. The expected leakage may be significant, since erosion of the flange faces would be expected to cause increased leakage.

Two potentially important phenomena are involved in evaluating the behavior of a flanged connection under severe accident temperatures. Specifically, the bolts will creep and, as they get hotter, will eventually lose a substantial amount of their strength. Both phenomena elongate the bolts and unload the gasket, and either or both phenomena may control the response, depending on the temperature and time parameters. The Larson-Miller methodology is used to predict the material creep. Also, the staff drew upon various sources for high-temperature data, including the American Society of Mechanical Engineers (ASME) Boiler and Pressure Vessel Code and the Air Force Materials Handbook, to obtain necessary bolting mechanical properties.

4.1.3.1 46-cm (18-inch) Steam Generator Manway/Pressurizer Manway

The austenitic stainless steel clad carbon steel steam generator manway for Surry has sixteen 4.78-cm (1.88-inch) diameter SA 197-Gr B7(AISI 4140) bolts having room temperature yield and tensile strengths of 105 ksi and 125 ksi, respectively. The cover was estimated to be 16.5 cm (6.5 inches) thick, and the gasket was estimated to be .64 cm (0.25 inch) by 5.1 cm (2 inches) wide of the Inconel spiral wound type. The bolts are assumed to be preloaded to 3.4×10^5 N (77330 lbf) per bolt. The gasket is assumed to spring back about 25 percent when it is unloaded. The results from the analysis indicate that the joint separates at about 627°C (1160°F) under fluid pressure of about 16.5 MPa (2400 psi).

The model uses the Case 1N reactor coolant loop C (pressurizer loop) hot leg nozzle bottom temperature/time profile, predicting joint leakage (loss of the gasket) at about 270 minutes. The staff used this temperature since the thermal-hydraulic model noding of the steam generator inlet plenum does not support a direct estimate of manway temperature conditions. The staff considered the conditions at the bottom of the hot leg to be more representative of the fluid temperatures near the manway, since that fluid has just traveled from the walls of the inlet plenum and probably has not undergone the degree of mixing encountered by fluid entering the mixing volume.

As previously noted, these estimates did not consider hydrodynamic loads on the gasket, which shorten the time to failure. Leakage would therefore be expected to increase quickly with small increases in temperature, since the bolt material strength decreases sharply, resulting in a larger gap in the connection. In this calculation, the creep contribution is insignificant because of the rapid temperature ramp. Reduction of the bolt strength with increasing temperature and gasket spring-back are the controlling parameters in this case.

For this study, the staff did not conduct a rigorous analysis of the pressurizer manway bolting. Review of temperature profiles shows that the temperature in the pressurizer upper head is about 80K (144°F) less than that of the SG at 250 minutes. Furthermore, the temperature ramp is much more severe for the SG lower head than for the pressurizer upper head (the bolting material (SA 193 B7) is the same and the load is the same). Therefore, the gasketing on the SG manway would be likely to fail before the pressurizer manway joint.

4.1.3.2 76-cm (30-inch) Loop Isolation Valves

The valve bonnet flange consists of a cast austenitic stainless steel flange held to the valve body by twenty-six 7.6 cm (3-inch) "A-286" bolts with a 0.33-cm (0.13-inch) long by 3.81-cm (1.5-inch) wide 316 stainless steel flexitallic gasket. The bolts are made of a precipitation-hardened austenitic stainless steel alloy that provides good high-temperature strength and creep properties to more than 538°C (1000°F). Further, the thermal expansion properties of the bolts very closely match those of the flanges, such that no relaxation is expected as a result of expansion. Therefore, on the basis of a preliminary assessment, the staff believes that the joint would not separate until the temperature exceeds 538°C (1000°F). However, INEL temperature/time profiles show that the temperatures of the loop valves could reach 760°C (1400°F) in less than 250 minutes. In addition, the strength of the bolts would be reduced by about half at 760°C (1400°F). The staff has also completed calculations to verify that the bolted joint separates when the temperature reaches 766°C (1410°F). Therefore, the bolted joint would be expected to fail in less than 250 minutes.

4.1.3.3 Pressurizer Safety Valves/Power-Operated Relief Valves

The pressurizer safety valves (PSVs) have a bolted, flanged joint between the body and bonnet, which could experience substantial relaxation at high temperatures (similar to the manway discussed above). However, a more important phenomenon may involve the change in set point spring compression as the upper parts of the valve heat up during the accident.

The safety valves are designed so that thermal expansion of various parts is closely matched to avoid set point changes as the valve is heated through the normal design temperature range. The reader should note, however, that events have occurred in which set points have decreased somewhat with increasing temperature. However, if the valve spring is heated significantly, the value of Young's modulus (the rate of change of stress versus strain for a material, denoted E) will decrease significantly. For instance, the INEL temperature/time profiles for the pressurizer upper head indicate that the PSV body reaches 700 K (800°F) at 250 minutes. The reader should note, however, that the temperature/time profile shows that steam in the top head reaches 700 K (800°F) in about 225 minutes.

The inner part of the valve is in direct contact with the steam. In addition, the spring on a PSV is within a closed bonnet that impedes natural convection to the ambient air. As a result, the spring can be presumed to heat significantly. If the spring temperature is assumed to only reach 204°C (400°F) (half of the body temperature), E will drop from 2.07×10^6 to 1.89×10^6 MPa (30×10^6 to 27.4×10^6 psi), resulting in a decrease of approximately 9 percent in the spring constant and a similar drop in the set point. This indicates that, at this temperature, a PSV originally set at 17.1 MPa (2485 psig) will have a set point of about 15.7 MPa (2270 psig) (neglecting any additional decrease resulting from bonnet bolt relaxation or creep). If the safety valve opens, it is likely that the valve temperature would increase and, thereby, further reduce the set point. During this study, the staff completed additional computer analysis of the PSV heat transfer to obtain more precise information on potential changes to the PSV set point. This analysis verified that the decrease of 9 percent in the spring constant would likely bound the conditions from the temperature ramp used.

The reader should also note that the available thermal-hydraulic data indicate that the pressurizer PORVs are at a significantly higher temperature than the PSVs, since they pass primary fluid during the accident. The PORVs have an accumulator to supply air, and the solenoids are battery powered.

The PORVs would be expected to be operable with loss of offsite power (LOOP) to the station. From 150 to 250 minutes, the PORVs cycle about 50 times. In that time, the pressurizer upper head steam temperature increases from about 327°C (620°F) to 627°C (1160°F), but the maximum temperature established by the manufacturer for use of the valve is 360°C (680°F). Considering the materials comprising the valve stem (17-4 precipitation-hardened (PH) stainless steel) and bonnet guide (stainless steel), galling may well occur between these two components.

Moreover, the valve has very close tolerances, and galling has occurred at this location under design conditions. (See NRC Information Notice 94-55). In the case noted in IN 94-55, the misalignment resulted from an assembly problem; however, the PORV could stick given the large number of cycles under severe accident conditions, the stainless steel bonnet guide, the close valve tolerances and the fact that the 17-4 PH stem material changes dimensions when heated. Additional evaluation is therefore required to determine whether estimates of valve performance can be refined for postulated severe accident conditions.

4.1.4 Steam Generator Tube Plug and Sleeve Performance

Several competing factors occur when steam generator plugs and sleeves are subjected to severe accident conditions. Like the tube sheet, these plugs and sleeves expand as a result of the sharp increase in temperature. The tube sheet would have a temperature gradient from the hotter primary side to the cooler secondary side during an SBO, associated with secondary side depressurization. This would cause the tube sheet to bow toward the primary side (convex on the primary side), thereby expanding the holes on the primary face.

At a minimum, both mechanical and welded plugs and sleeves would also be deformed during installation to achieve intimate contact with the steam generator tube or tube sheet. Specifically, hard-rolled plugs or sleeves would be plastically deformed with a strain of about 1 to 3 percent to improve resistance to pull-out. Exposure to temperatures for the durations predicted by the thermal-hydraulic calculations would relieve the stress in the joints.

The third factor of concern would be the relative amount of thermal expansion of the plugs and sleeves relative to the tube sheet. Plugs and sleeves manufactured using Alloy 600 (also known as Inconel-600) would expand radially about 5 percent more than the holes in the carbon steel tube sheet would enlarge, and Alloy 690 (also known as Inconel-690) plugs and sleeves would expand about 10 percent more than the tube sheet if the temperatures of the components increased at the same rate. In addition, it is likely that a sleeve and, to a lesser extent, a plug in the tube sheet would heat up faster because the plug and sleeve temperatures would increase at about the ramp rate of steam at the tube sheet, whereas the tube sheet would experience a slower ramp rate because of its much greater mass. On the basis of the qualitative evaluation presented, mechanical plug/sleeve joints in the tube sheet would be expected to hold and not experience any significant increase in leakage. Welded plugs and sleeves in the tube sheet would also be expected to hold for the same reasons and because of the added assurance provided by the welded joint.

Two other issues are of interest:

- What would happen to a sleeve-to-tube mechanical joint under the conditions stated above?

- Would a good sleeve or plug fail before a good tube?

Sleeves are made from either Alloy 600 or Alloy 690 material and have similar thermal properties. If the tube were made from Alloy 600, the sleeve and tube would expand together at the joint, and any residual stresses would be relieved. Resistance to pull-out would originate from the deformed section at the top of the tube. Even if the top section of a tube that was cracked 360° through-wall began to pull out of the sleeve, any leakage would be limited by the annulus between the sleeve and tube since separation would be prevented by the "hop-off" length of the sleeve. Further, the tubes are most likely locked at the lower support plates, and would be at a much higher temperature than a depressurized steam generator shell. Thus, the thermal expansion of the locked tubes would induce compressive axial stresses. Therefore, separation of the joint is considered highly unlikely.

Most plugs and sleeves have slightly thinner walls than the steam generator tubes they are used to repair. Consequently, the part of a sleeve outside of the tube sheet would heat somewhat faster than the tube because of the air gap between the sleeve and tube. If the sleeve began to creep, this displacement would be limited by the tube (which would be at a

lower temperature). At that point, the effective wall thickness (in terms of structural integrity) would be that of the sleeve and the degraded tube. If a failure were to occur, it would most likely be in the unsleeved part of the tube. A plug would also be expected to fail by creep after a tube that would have steam flowing through it. Although the plug is exposed to steam in the lower plenum, the plug would be cooled by conduction where it is expanded to the tube/tube sheet. Given that the tube sheet heats at a slower rate because of its mass, a free portion of a tube conducting steam would heat faster and fail before the plug.

4.1.5 Effects of Leaking Tubes Under Accident Conditions

Traditionally, SG tube integrity has been evaluated relative to elevated differential pressure conditions resulting from design-basis accidents or transients. Events such as main steam line break or other secondary-side depressurizations with concurrent high primary system pressure have been considered. Under severe accident challenges, the tubes may experience elevated temperatures along with high differential pressures. The following sections discuss the effects of tube leakage under both sets of circumstances.

4.1.5.1 Design-Basis Accident Conditions

In the past, Westinghouse has evaluated the effects of steam generator tubes with large through-wall circumferential cracks in the free span. Recently, Westinghouse had the opportunity to evaluate these effects under steam line break conditions when the licensee for Point Beach proposed leaving sleeved steam generator tubes in service with circumferential cracks near the tops of the sleeves. As a result of this evaluation, Westinghouse concluded that the cracked tubes would not experience sufficient bending to contact or otherwise impact a neighboring tube.

In the case of the Mihama tube failure in February 1991, however, a tube in the U-bend region became severed during normal operation as the result of fatigue from flow-induced vibration because an anti-vibration bar was improperly installed by the steam generator manufacturer. The defect allowed the free end of the tube to oscillate, impacting neighboring tubes until the plant was shut down. Upon subsequent inspection by the Japanese Ministry of International Trade and Industry, the tubes were found to be somewhat damaged, but none other than the failed tube had experienced leakage.

In other instances, steam generator tubes have failed in service (usually an axial fish mouth rupture); however, the effects of jets from the ruptures have not damaged the neighboring tubes. In the case of a steam generator tube with a large leak or rupture under normal operating conditions, the jet velocity is not a significant concern because the temperatures are reasonably low (the reactor coolant system contains sub-cooled water), and water is present on the secondary side to quench the jet.

4.1.5.2 Severe Accident Conditions

Operating experience in non-nuclear boiler applications has been quite different from nuclear plant steam generators. For instance, pressure tubing in fossil fuel power plants is operated under higher temperatures and pressures than normal PWR primary system conditions. A staff member was involved in the failure analysis of 14 pressure tubes that were sequentially cut by jets of superheated steam in the course of an 8-hour period. The pressure tubes (1.12 cm (0.440 inch) wall thickness) were made using an austenitic stainless steel tube, welded with Inconel to a 2 ½ Cr-Mo steel tube. The tube was located in a

superheater in the unit and contained steam at 538°C (1000°F) and 24.1 MPa (3500 psi).

In order to evaluate the potential for cascading failures as a result of a jet from a severely leaking/burst steam generator tube, the staff performed a series of calculations. In addition, the staff obtained erosion/corrosion rates for Alloy 600 from testing performed to select candidate materials for coal gasification plant applications. The testing was performed at temperatures applicable to severe accident conditions for steam generator tubes; however, the velocity of the jet in the tests was 30.5 m/sec (100 ft/sec). During this study, the staff performed scoping calculations to determine the velocity of a jet expanded from sub-cooled water at 343°C (650°F), compared with the velocity of a jet from super-heated steam at 899°C (1650°F). These calculations suggest that the super-heated jet has 10 times the velocity of the jet from the sub-cooled water. Because the rate of erosion depends on the cube of the velocity, the effects of steam cutting from erosion of other tube failures, as experienced in non-nuclear applications (discussed below), appear reasonable.

The velocity of an escaping jet from a steam generator tube with a steam temperature of 899°C (1650°F) and a pressure of 17.2 MPa (2500 psig) was calculated to be 786 m/sec (2579 ft/sec), assuming choked flow conditions as shown in the analysis.

If a through-wall stress corrosion crack (SCC) existed in a steam generator tube, the velocity of the jet might initially be less than that calculated since the flow path could cause a pressure drop as the gas passed through the tight path. However, considering the thermal expansion of the steam generator tube resulting from the high temperatures, and the erosion effect on the crack faces, the staff believes that the choked flow conditions in the analysis would be reached very quickly for a through-wall SCC.

Further, since the gas used in the coal gasification test had about the same molecular weight as steam, the staff calculated the Alloy 600 erosion rate for a jet from a steam generator tube impinging on an adjacent tube (with and without particles in the stream). The calculations yielded a rate of 73.9 cm/hr (29.1 in/hr) for an erodent with particles, compared to a rate of 5.84 cm/hr (2.30 in/hr) for an erodent without particles. The calculations also indicated that the times to failure for a 0.102-cm (0.040-inch) thick steam generator tube wall are 4.9 and 62.6 seconds for erodent with and without particles, respectively. In addition, the staff's calculations included the rates of erosion and time to failure for the fossil plant failure discussed above. The results obtained from these calculations appear reasonably consistent with the chronology of the tube failures that occurred.

To address the question concerning the shortest length intergranular stress corrosion crack (IGSCC) that could produce a jet that would affect a neighboring tube, the staff considered the aspect ratio (length to depth) for the crack, as well as leakage data provided by the industry. Operating experience with IGSCC of steam generator tubes has shown that an aspect ratio of about 4 or 5 to 1 is about the smallest seen for this type of cracking. That is, if the aspect ratio of the crack was 5 and the steam generator tube wall was 0.127 cm (0.050 inch), the minimum crack length would be 0.64 cm (0.25 inch). Data from testing of ODSCC cracks at steam line break pressures with water at room temperature indicate that leakage would occur at a rate of about 10 liters per hour (2.6 gallons per hour).

At the elevated temperatures under consideration, the crack opening area would be considerably greater. Given the leakage behavior of a 0.64-cm (0.25-inch) crack under room temperature test conditions, leakage would be expected from this crack under severe accident conditions, with a jet sufficiently severe to damage an adjacent tube. Therefore the

selection of a minimum crack length of 0.64 cm (0.25 inch) appears reasonable.

The staff believes that the approach discussed above is more meaningful than trying to calculate a minimum crack opening area on the basis of mass transport. This is because the differences between the coal gasification testing and the steam generator case, as well as other complexities, could affect the evaluation with leaks from small, tight cracks.

The staff also addressed a question regarding possible degradation of steam generator tubes by a steam jet resulting from a widening crack in a neighboring tube. Staff calculations were refined to account for a pressure decrease in the crack, choked flow of the jet exiting the crack, supersonic flow as the jet expands, formation of a shock wave, subsonic flow impinging on the target tube, and the angle of impingement on the target. Calculations considered two cases, differing only in the assumed primary fluid temperature; 899°C (1650°F) and 704°C (1300°F). The other parameters used were: 64 cm (0.25 inch) crack length: 17.2 MPa (2500 psi) pressure drop: 12 crack widths from 0.0025 cm (0.001 inch) to 0.51 cm (0.200 inch): impact angles of 17°, 45°, and 90°: and jets with and without particles.

The results of these analyses show that a jet fed by a 899°C (1650°F) reservoir without particles from a very tight crack (0.0025 cm (0.001 inch)) would take about 45 to 268 hours to fail an adjacent tube, depending on the angle of incidence. A jet from a similar crack with a reservoir temperature of 704°C (1300°F) would take about the same time to fail an adjacent tube (43 to 256 hours), depending on the angle of incidence. Failure times range from 3.5 to 20.6 hours for a 0.025-cm (0.010-inch) open crack to 23 to 140 mins. for a 0.25-cm (0.100-inch) open crack. Therefore, it is apparent that crack opening size is the most significant parameter affecting time to failure of a neighboring tube from high-temperature jet impingement.

A particular focus for this analysis is whether or not a very tight axial through-wall crack, 0.64 cm (0.25 inch) long, would widen when exposed to predicted severe accident conditions. Several factors affect the crack opening width. For example, these may include bending from differential thermal expansion of the SG tube with respect to the SG shell (when the tube is locked at the tube support plates), deformation of the tube by creep or overstress of the tube as its temperature increases, as well as ablation of the crack from steam flow.

For a case where the primary side temperature rises to 899°C (1650°F) with a tight crack 0.635 cm (0.25 in.) long, tube failure is expected. ANL testing of SG tubes with 0.635-cm (0.25-in.) long cracks about 65 percent through-wall have shown that the tube would burst at about 799°C (1470°F) if the temperature were sharply ramped, and about 774°C (1425°F) if held at 704°C (1300°F) for 2 hours before increasing the temperature to failure.

Crack opening by creep damage as a function of time has been preliminarily assessed by ANL, and a relationship for crack opening rate in mils/min was developed. For a case with the primary side pressure at 16.2 MPa (2350 psi) and a temperature of 727°C (1340°F), a 0.635-cm (0.25-in.) long crack would open to 0.025 cm (0.010 in.) in 2 minutes. ANL developed a relationship of leakage flow through cracks which is considered an order of magnitude approximation. Using that relationship, a 0.635-cm (0.25-in.) long crack would be expected to leak at about 208 Lpm (55 gpm) in 10 minutes as a result of creep damage at 704°C (1300°F) and a pressure of 16.2 MPa (2350 psi).

The staff modified its model for impingment damage to an adjacent tube to account for crack

opening by ablation caused by jet flow through the crack. With the primary side temperature at 704°C (1300°F), the calculated velocity in a tight crack (.002 cm (0.001 in.) wide by 0.635 cm (0.25 in.) long) is about 396 m/sec (1300 ft/sec). Analysis shows that the crack would open rapidly, causing an adjacent tube to fail in about 15 to 60 minutes, depending on the adjacent tube and the assumed impingment angle within the crack. This estimate does not include crack opening by creep or deformation of the adjacent tube by bending.

The reader should be aware that the staff considers the analysis results presented to be at best scoping estimates for failure times of neighboring tubes. The staff believes that the analyses performed indicate that the jet from a tube with a through-wall crack 0.635 cm (0.25 in.) long, independent of the tightness of the crack before exposure to postulated severe accident conditions, would be expected to fail an adjacent tube in a relatively short time (between a few minutes and about an hour). Although the precision of the time to failure might be improved by experimental data, other uncertainties such as heating rate and maximum expected temperature, as well as additional factors mentioned above, might not allow much refinement in the failure time estimates for the adjacent tubes.

4.1.6 Conclusions/Recommendations

Reliable analytical prediction of the performance of nuclear power plant components under severe accident conditions is very difficult. In particular, most of the structural materials suffer a severe degradation of strength in the range of 538°C (1000°F) to 760°C (1400°F). In addition, uncertainty in the temperature/time histories from the thermal-hydraulic codes, as well as system geometries and material considerations, severely impact the precision of predicted times to failure. On the basis of the temperature/time profiles provided by INEL, the staff estimated that gasket failures of the steam generator manway and loop isolation valves will occur in about 250 minutes. In addition, the set points of the PSVs will drop below the PORV set point. If the PORV is cycled 50 times at these temperatures, the valve is likely to stick.

Additional evaluation of the PSVs and PORVs is warranted. To quantify the probability of failure for other components, PRA sequences and dominant failure modes should also be evaluated to include the engineering information contained in this evaluation.

From the results of the analysis and the comparison of the calculated erosion rates to the rates that were observed for failure of the fossil plant super- heater tubes, it appears that severe erosion of neighboring steam generator tubes would be likely to occur rapidly under severe accident conditions if a tube were to severely leak or burst. In addition, the staff believes that several steam generator tubes could fail by jet impingement before the primary system would depressurize. The basis for this opinion includes estimating the flow areas of a number of failed steam generator tubes compared with the flow area for a pressurizer safety valve. On the basis of the above evaluation, the staff determined that a through-wall crack, 0.64 cm (0.25 inch) long, would cause the failure of an adjacent tube under severe accident conditions. However, plugged and sleeved steam generator tubes would *not* be expected to lose their integrity before an unflawed tube.

Estimates of times to failure are imprecise but might be expected to be in the range from about a few minutes to less than hour. It is more likely that the failures would be earlier (on the order of minutes) because of other mechanisms (such as creep or deformation of the tubes by bending) that would accelerate crack opening.

4.2 Representative Flaw Distributions

Estimating the probability of tube failure for a steam generator requires an understanding of the population of flawed tubes. For this study, the staff attempted to produce "representative" frequency distributions of flaw sizes, since the progression of tube degradation is highly plant-specific.

The staff then considered two such representative distributions, including one developed by the NRR Division of Engineering, and another developed under contract to the RES Division of Engineering Technology. A key distinguishing characteristic between these distributions is that the one from NRR combines various types of flaws into a single distribution. The RES distribution is composed of distinct distributions for each of six types of degradation. Each is described in the following sections.

4.2.1 NRR Flaw Distribution

The representative flaw distribution described in this section was developed for plants with "low," "medium," and "high" susceptibility to flaws located in the first span of tubing on the hot leg side. The basis for these distributions is a mechanistic model employing a simplistic treatment of flaw initiation rates, flaw growth rates, and inservice inspection probability of detection (POD) performance. The staff benchmarked these distributions against actual operating experience concerning the frequency of SGTRs, forced outages resulting from tube leakage, and the tube plugging rates.

In addition, the staff conducted Monte Carlo simulations to assess the reasonableness of the distributions discussed herein. These simulations, which considered various flaw growth rate distributions and POD models as a function of flaw depth, revealed that the flaw distributions are highly sensitive to the assumed growth rate distributions and POD function. In turn, those growth rate distributions and POD functions vary widely from plant to plant. The results also indicate that the assumed distributions are reasonable; however, other functional forms for the distributions (significantly different from those herein) may also be reasonable.

Therefore, the flaw distributions considered here should not be interpreted as "bounding" for any category of plants (i.e., plants with high, medium, or low susceptibility to flaws). Instead, they should be interpreted simply as distributions that are consistent (but not uniquely consistent) with the available evidence. Actual distributions may vary widely from those presented here. However, these distributions provide a basis for evaluating the sensitivity of severe accident risk to different flaw distributions.

4.2.1.1 General Approach

Licensees periodically inspect steam generator tubing using the eddy current test method to characterize the condition of the tubing with regard to the tube plugging limit in the Technical Specifications (typically 40 percent of the initial tube wall thickness). However, the inspection results accumulated to date provide little direct basis for developing flaw distributions (as a function of flaw size) of the kind needed to realistically estimate conditional rupture frequencies.

The major difficulty stems from the limited capability of eddy current testing to accurately measure all of the attributes that affect a flaw's burst strength for a given pressure and temperature. This difficulty is most acute for stress corrosion cracking, which is by far

the dominant flaw mechanism affecting the tubing today. Eddy current measurements of crack depth are particularly unreliable, as are crack depth profiles along the length of the crack. In addition, stress corrosion cracks often occur as a network of crack segments interspersed with small ligaments of sound material. This network is generally not detectable by eddy current testing, but adds considerably to the burst strength of the affected tubing.

Thus, the staff set out to develop representative flaw distributions characterized by a simple model consistent with objectively observable operating experience. Flaws are assumed to initiate at a constant rate, to grow through the wall thickness at a constant rate, and to remain undetectable until crack depth reaches the "threshold of detection" (i.e., POD equals zero). At and beyond the detection threshold, the probability density function of flaws as a function of crack depth is assumed to be an inverse exponential, B*EXP(-Bx). The staff assumed the frequency distribution of flaws at or beyond the detection threshold, during a given reactor year, is the number of tubes plugged per reactor year multiplied by the probability density function. The frequency distribution between zero percent through-wall and the detection threshold depth is assumed to have a constant value equal to the calculated frequency at the detection threshold.

Operating experience indicates that flaw initiation rates for many corrosion mechanisms actually tend to increase with time at a given plant rather than remaining constant, as assumed here. Ultimately, however, higher flaw initiation rates lead to a higher incidence of tube plugging. The flaw distributions developed herein include separate distributions for plants experiencing plugging rates typical of the industry average, and those experiencing plugging rates that are 10 times the industry average. The distributions derived from the higher plugging rates should reflect increases in flaw initiation rates that could be expected to occur in all plants.

A variety of flaw types can potentially affect the steam generator tubing in the first span. These potential types include volumetric flaws such as wastage, pitting, intergranular attack (IGA), and fretting/wear associated with loose parts or foreign objects. The potential flaw types also include various types of stress corrosion cracking, which may have either an axial or circumferential orientation.

These different flaw types have been idealized as 1.27-cm (0.5-inch) or 2.54-cm (1-inch) long axial cracks with depths such that the tube burst pressure is equal to that for the actual flaw. This is done to be consistent with the conditional probability of rupture sensitivity calculations discussed later in this report. (Burst pressure as a function of idealized crack depth has been determined from equation 6-6 of the INEL report (Ellison, 1996) as shown in Figure 4.1). For 2.54-cm (1-inch) long cracks, the critical crack depth corresponding to burst under a postulated steam line break differential pressure of 17.7 MPa (2560 paid) is 76 percent through-wall for 2.2-cm (0.875-inch) diameter tubing. The critical crack depth corresponding to burst under a normal operating differential pressure of 9.7 MPa (1400 paid) is 89 percent through-wall.

The staff considered three categories of steam generators on the basis of whether the potential for degradation in the first span is low, medium, or high, as described below.

4.2.1.2 Case 1, Plants with Low Susceptibility to Degradation

The first category consists of replacement steam generators at 12 PWR facilities (not including Palisades) and 25 PWR facilities with Westinghouse Models Do steam generators that

employ improved tubing material (either Inconel-600TT or Inconel-690) and have not experienced any significant corrosion problems to date. The only potential problem currently affecting the first span in these steam generators is damage associated with loose parts. Arguably, the steam generators at Palisades (with replacement SGs) and certain relatively new units with their original generators and reporting no corrosion problems to date should also fall into this category; however, such plants are assumed to be in the second category, since corrosion-related problems can reasonably be expected to occur in the first 5 years of service.

Figure 4.2 depicts the assumed frequency distribution of flaws for plants in the first category. This distribution reflects the following characteristics:

(1) Degradation related to loose parts is volumetric and is assumed to have a detection threshold of 20 percent through-wall. These flaws have been idealized as 2.54-cm (1-inch) long axial cracks with depths such that the tube burst pressure is equal to that for the actual volumetric flaw, as previously discussed.

(2) The frequency distribution therefore, is a constant value between 0 and 20 percent through-wall, and is assumed to decrease (as a result of tube plugging or sleeving with detected indications) as follows:

$$F(x) = P \times B \exp(-Bx) \quad (1)$$

where

P = the average number of tubes plugged per year per steam generator due to loose parts/foreign objects
B = unknown constant
x = percent through-wall depth of flaw minus 20 percent

(3) Industry-wide, 235 tubes have been plugged (at Westinghouse and CE plants, over 1110 reactor years) as a result of damage related to loose parts. This amounts to 0.21 tubes/reactor year or 0.07 tubes/SG year (assuming three loops per plant). Tubes are plugged only after they are detected at ≥20 percent through-wall. Thus, 0.07 tubes represent the area under the flaw frequency distribution curve beyond 20 percent through-wall.

(4) Of the 235 plugged tubes, 2 were plugged after rupture. Rupture is assumed to have occurred when flaw depth was 89 percent through-wall with the pressure retaining capacity of the tubes reduced to 9.7 MPa (1400 psi). The corresponding frequency of rupture is 0.0006/SG year. In effect, this represents the area underneath the frequency distribution curve at or above 89 percent through-wall, which can be restated as the value of the cumulative frequency distribution at 89 percent through-wall.

(5) The cumulative frequency distribution is given by the following expression:

$$CF(x) = P \exp(-Bx) \quad (2)$$

This expression permits calculation of the unknown constant B, given that both P and F are known at 89 percent through-wall. Thus, the frequency distribution and

cumulative frequency distribution can be calculated as follows:

$$F(x) = 0.00482 \exp(-0.0689274x) \quad (3)$$

$$CF(x) = 0.07 \exp(-0.0689274x) \quad (4)$$

(6) An alternative approach is to determine the value of the coefficient B in Equation (2) on the basis of the conditional probability of rupture during a postulated MSLB (rather than the frequency of tube rupture). Considering operating experience with all degradation mechanisms, NUREG-0844 conservatively estimated the conditional probability of 0.05 for 1 or more tube ruptures in the faulted steam generator during an MSLB. At the time, the staff derived this estimate, NUREG-0844 reported the frequency of tube ruptures from all degradation mechanisms to be 1.5×10^{-2}/RY. As of 1996, the frequency of ruptures associated with loose parts and foreign objects has been shown to be 6×10^{-4}/RY. per SG, as discussed in item (4) above.

Assuming a direct relationship between rupture frequency and the conditional probability of rupture during an MSLB, the conditional probability of rupture associated with foreign objects or loose parts is estimated to be 0.006 (the value of the cumulative frequency distribution (Equation 2) at 76 percent through-wall). On this basis, the frequency distribution and cumulative frequency distribution are as follows:

$$F(x) = 0.0031 \exp(-0.0438109x) \quad (5)$$

$$CF(x) = 0.07 \exp(-0.0438109x) \quad (6)$$

(7) Figure 4.2 reflects the frequency derived from Equation (5), rather than Equation (3), since it is more conservative for the deeper flaws.

4.2.1.3 Case 2, Plants with Medium Susceptibility to Degradation

Plants in this category are treated as the "industry average." On the basis of data for Westinghouse plants, plants in this category plug an average of 130 tubes each calendar year. (This number is also assumed to apply reasonably well to CE plants.) Of these tubes, 20 to 25 percent (approximately 10 to 30 tubes per steam generator) are assumed to be plugged because of flaws located in the first span of the hot leg. (This assumption reflects industry experience and staff judgement.) These flaws may involve one or more of the following mechanisms:

- circumferential cracking at the top of the tube sheet
- circumferential cracking at the first support plate
- axial cracks between the top of the tube sheet and the first support plate
- general IGA, pitting, wastage, or damage related to loose parts or foreign objects between the tube sheet and first support plate

Figures 4.3 and 4.4 depict the assumed frequency distribution of flaws for plants in the second category. This distribution reflects the following:

- All flaws are idealized as 1.27-cm (0.5-inch) to 2.54-cm (1-inch) long axial cracks with depths such that burst pressures are equivalent to those for the actual flaw geometries. An equivalent axial crack for a circumferential crack can be assumed to be zero percent through-wall for circumferential cracks with average depths (over the entire circumference) of less than 50 percent through-wall. This is because the axial stress in a pristine tube is one-half the hoop stress, and eccentricity effects associated with non-axisymmetric crack geometries are negated by the lateral restraint to the tubes provided by the first support plate.

- The idealized axial cracks are assumed to become detectable when the equivalent crack depth reaches 40 percent. This is conservative for volumetric flaws, where the detection threshold is about 20 percent. Circumferential flaws become detectable when a significant portion of the crack reaches 40 percent through-wall. This can generally be expected to happen before the reduction in tube cross-sectional area reaches 50 percent. Therefore, an axial crack that is equivalent to a circumferential crack has a detection threshold of zero percent. Thus, the assumption of a 40-percent threshold of detection is conservative for the idealized axial cracks representing actual circumferential cracks.

- The 10 tubes plugged for each steam generator per year are assumed to consist of 1 tube with a 2.54-cm (1-inch) long crack and 9 tubes with 1.27-cm (0.5-inch) long cracks. This breakdown is consistent with the general observation (from industry experience) that stress corrosion cracks tend to have aspect ratios of less than 5:1. For 2.22-cm (0.875-inch) diameter tubing with a 0.127-cm (0.050-inch) thick wall, crack lengths would typically not be expected to exceed 0.64 cm (0.25 inch) when crack depth initially reaches 100 percent through-wall. The assumption that 90 percent of the population of idealized cracks are $\leq$1.27 cm ($\leq$0.5 inch) long is believed to be conservative. On the basis of the PNL burst pressure model illustrated in Figure 4.1, cracks in this category would not be expected to rupture during normal operation or under postulated steam line break conditions, even if entirely (100 percent) through-wall. Cracks greater than 1.27 cm (0.5 inch) long are represented as 2.54 cm (1 inch) long. The critical crack depths for these 2.54-cm (1-inch) long cracks are 89 percent through-wall for normal operating conditions and 76 percent for steam line break conditions.

- As in Case 1, the staff used Equations (1) and (2) to represent the frequency distribution and cumulative frequency distribution for the 1.27-cm (0.5-inch) and 2.54-cm (1-inch) long cracks beyond the assumed 40 percent detection threshold. The coefficient P is equal to 9 and 1, respectively, for the 1.27-cm (0.5-inch) and 2.54-cm (1-inch) long cracks.

- For the 1.27-cm (0.5-inch) long cracks, the staff determined coefficient B on the basis of the frequency of forced shutdowns caused by SG tube leakage. (1.27-cm (0.5-inch) long cracks would typically be expected to exhibit sufficient leakage to cause plant shutdown.) Industry-wide, the frequency of such forced shutdowns has been about 5 per year between 1989 and 1994. Assuming 3 steam generators per plant, this translates to a frequency of 0.024 forced outages per year per steam generator. Using that frequency, one can determine the value of B by setting the F in Equation (2) to 0.024 at x = 100 percent through-wall. Thus, the frequency

distribution and cumulative frequency distribution for 1.27-cm (0.5-inch) long cracks are as follows:

$$F(x) = 0.89283 \exp(-0.09920x) \quad (7)$$

$$CF(x) = 9 \exp(-0.09920x) \quad (8)$$

where: x = percent through-wall flaw depth minus 40 percent

Figure 4.3 illustrates the Case 2 frequency distribution for 1.27-cm (0.5-inch) long cracks.

- For the 2.54-cm (1-inch) long cracks, the staff determined the value of coefficient B on the basis of the conditional probability of rupture during a postulated MSLB. (This approach yields a more conservative distribution than determining the value of B on the basis of the tube rupture frequency.) As previously discussed, NUREG-0844 conservatively estimated the conditional probability for 1 or more tube rupture(s) in the faulted steam generator during an MSLB to be 0.05, considering operating experience for all degradation mechanisms. At the time the staff made this estimate, NUREG-0844 reported the frequency of tube ruptures from all degradation mechanisms to be 1.5×10^{-2}/RY. As of 1996, the frequency of ruptures attributable to corrosion-related mechanisms at Westinghouse and CE plants with Inconel 600 tubing has been shown to be 5.4×10^{-3}/RY. The frequency of ruptures associated with loose parts and foreign objects at Westinghouse and CE units is 1.8×10^{-3}/RY as of 1996 (this is consistent with the value given in Case 1, assuming a 3-loop plant). Thus, the frequency of rupture from all causes is 7.2×10^{-3}/RY.

  Assuming a direct relationship between rupture frequency and the conditional probability of rupture during an MSLB, the overall conditional probability of rupture is estimated to be 0.024. This estimate has been reduced by half (to 0.012) to reflect an assumption that only half of the tube ruptures would occur in the first span on the hot leg side. This assumption appears conservative, since only three of the seven tube ruptures to date have affected the first span on the hot leg side. This conditional probability is the value of the cumulative frequency distribution (Equation 2) at 76 percent through-wall. On this basis and with P = 1, the frequency distribution and cumulative frequency distribution are as follows:

$$F(x) = 0.12286 \exp(-0.12286x) \quad (9)$$

$$CF(x) = \exp(-0.12286x) \quad (10)$$

  Figure 4.4 illustrates this distribution.

4.2.1.4 Case 3, Plants with High Susceptibility to Degradation

The basis for the flaw distributions derived for plants in this category differs from that used in Case 2 in only one respect. Specifically, the plugging rate is assumed to be 10 times higher for Case 3 than for Case 2. Plants in Case 3 are assumed to have the same frequency of rupture, the same conditional probability of rupture under MSLB, and the same

frequency of forced outages resulting from leakage as assumed for Case 2. Experience suggests that tube ruptures during normal operation are no more likely to affect plants with high plugging rates than plants with moderate plugging rates. Ruptures have typically involved mechanisms that were previously unrecognized at the affected units. This experience is generally attributed to the fact that plants with higher susceptibility are subject to compensatory measures (such as more frequent inspections, larger inspection samples, improved inspection techniques, etc.).

Accordingly, the frequency distribution and cumulative frequency distribution for tubes with 2.54-cm (1-inch) long cracks are as follows:

$$F(X) = 1.84245 \exp(-0.184245X) \tag{11}$$

$$CF(X) = 10 \exp(-0.184245X) \tag{12}$$

For these equations, the coefficient B has been determined on the basis of the tube rupture frequency rather than the conditional rupture probability, since this yields a slightly more conservative distribution.

Similarly, the frequency distribution and cumulative frequency distribution for tubes with 1.27-cm (0.5-inch) long cracks are as follows:

$$F(X) = 12.3852 \exp(-0.13758X) \tag{13}$$

$$CF(X) = 90 \exp(-0.13758X) \tag{14}$$

Figures 4.5 and 4.6 depict the frequency distributions for the 1.27-cm (0.5-inch) and 2.54-cm (1-inch) long cracks, respectively.

4.2.2 RES Flaw Distribution

The flaw distribution described in this section was developed using a two-step process discussed in the Dominion Engineering, Inc. (DEI) report (Gorman, 1996). First, a Weibull analysis of historical data from tube inspections was used to estimate the number of cracks. Second, Monte Carlo evaluations were conducted to determine the numbers of tubes with flaws for the three cases of lightly affected, moderately affected, and severely affected plants, and adjustments were made for POD and other factors.

In particular, DEI considered seven types of degradation that would be experienced by a typical plant with Westinghouse Model 51 steam generators:

(1) circumferential cracks at the top of the tube sheet
(2) axial primary water stress corrosion cracking (PWSCC) at roll transitions
(3) freespan cracks
(4) axial ODSCC at tube support plates
(5) circumferential outer diameter cracks at tube support plate dents
(6) axial cracks associated with IGA/SCC in sludge piles

(7) flaws related to loose parts damage

DEI selected these types of degradation for study on the basis that, except for loose parts flaws, they represent most of the tube degradation currently detected in U.S. plants. Of these, the tube failure probability calculations described in Section 5.3 used only degradation represented by types (3) and (6). In addition, DEI generated hypothetical distributions to represent plants that were lightly affected, moderately affected, and severely affected by the selected types of degradation.

The method used (and described more fully in German's report) first estimates the number of cracks and determines the number of flawed tubes for each of the lightly affected, moderately affected, and severely affected plants. Next, the model adjusts the flaw distribution data derived through nondestructive examination (NDE) and data from pulled tubes to reflect measurement error and probability of detection. In addition, DEI developed analytical expressions to represent the distributions of flaws in terms of length and depth.

4.2.2.1 Freespan Cracking

Of the selected types of degradation observed at various plants, freespan cracking at Palo Verde 2 has been the best characterized, and was considered typical for the industry in cases where detailed inspections for freespan cracks have been performed. In such cases, crack length and depth distributions are taken to be independent. A gamma distribution of the crack length is used on the basis of data relating the length measured by rotating pancake coil (RPC) to structural length determined from destructive examination. Evaluation of these data yielded a mean error for length measurements of zero, and a standard deviation for length measurements of 1.27 cm (0.5 inch). The POD as a function of length was approximated as being zero at 0.25 cm (0.1 inch) long, and 0.95 at 0.76 cm (0.3 inch) long, with a linear variation between these two points. In addition, DEI adjusted the flaw size distribution to reflect measurement error and POD, to yield the distribution shown in Figure 4.7.

A distribution of estimated crack lengths for freespan cracks in Palo Verde 2 was used to generate the flaw depth distribution shown in Figure 4.8. Analysis of data presented in a Palo Verde submittal to NRC, yielded a mean error estimated at zero, and standard deviation at 14 percent of tube wall thickness. The POD as a function of flaw depth was set at 0.95 at 68 percent of wall thickness, and at approximately 0.1 at 20 percent of wall thickness. DEI adjusted the flaw size distribution to reflect measurement error and POD in the same manner as done for the length distribution.

DEI conducted a check of the probability of the length and depth distributions causing a tube burst. Monte Carlo analysis showed that there were no cases in 10,000 trials where a defect had a length over 4.57 cm (1.8 inches) and a depth more than 90 percent through-wall.

The flaw distribution discussed above is for a unit where a rupture had occurred, and very thorough, detailed inspections for freespan cracking had been performed. This is not the case for other plants where ruptures resulting from freespan plants have not occurred and relatively little freespan cracking has been detected. However, in such cases, routine inspection methods are typically used which could allow some short through-wall flaws to remain in service. This would lead to some (albeit small) chance of burst. To reflect this possibility, the depth distribution was adjusted to yield a 2 percent chance of a through-wall defect being present and a 0.1 percent chance of a defect causing a burst.

4.2.2.2 IGA/SCC in Sludge Piles

As the basis for this distribution, DEI used data from Westinghouse feedring steam generators. The distributions for IGA/SCC were then taken to be the same as for freespan SCC (discussed above). Figures 4.7 and 4.9 show the resulting flaw length and depth distributions.

4.3 Flawed Tube Failure Models

The following subsections describe the failure models considered for estimating tube failure probabilities in this study. Subsections 4.3.1 and 4.3.2 give the background and basis for structural analysis of cracked steam generator tubes, and Subsection 4.3.3 provides details of the flow stress and creep failure models. Subsections 4.3.4 and 4.3.5 discuss the experimental validation of the creep failure model using high-temperature burst test results from flawed tubes. Subsections 4.3.6 and 4.3.7 examine factors contributing to uncertainty in the model and its applicability.

The following nomenclature is used in the equations presented in these subsections:

Nomenclature

a	crack depth
c	crack half-length
dt	time increment
h	mean tube wall thickness
k	flow stress factor
m	bulging (magnification) factor for through-wall cracks
m_p	bulging (magnification) factor for part-through-wall cracks
P_{lm}	Larson-Miller parameter for creep rupture
p	pressure
p_b	failure pressure for an unflawed tube
p_{cr}	failure pressure for a tube with a through-wall crack
p_{sc}	ligament failure pressure for a tube with a part- through-wall crack
R_m	mean tube radius
s	standard deviation
t	time
t_f	time to tube failure
t_R	time to creep rupture of a uniaxial specimen at a given stress and temperature
T	temperature
T_f	failure temperature
$\alpha(a/h)$	parameter dependent on a/h used in ANL m_p correlation
Δp	error in the predicted failure pressure
Δa	error in the measured crack depth
λ	normalized crack length $[12(1-\nu^2)]^{\frac{1}{4}} \frac{c}{\sqrt{R_m h}} = \frac{1.82c}{\sqrt{R_m h}}$
ν	Poisson's ratio

σ	stress, hoop stress
σ_m	standard error of the mean estimate of the fitted variable flow stress
σ_y	yield strength
σ_u	ultimate tensile strength

4.3.1 Background

During design-basis accidents, the temperature of the steam generator tubing varies relatively little and remains less than 350°C. In this temperature range, creep effects are negligible in Alloy 600. However, in postulated severe accidents, much higher temperatures are possible. At these higher temperatures, plastic deformation is likely to be much more extensive than at normal reactor operating temperatures, and creep effects may no longer be negligible.

Substantial literature is available (Hahn, 1969; Erdogan, 1976; Eiber, 1971; Kiefner, 1973; Flesch, 1988; Kurtz, 1988 and 1990) concerning the development and validation of analytical models to describe the behavior of flawed tubes at normal reactor operating temperatures of 288 to 320°C (550 to 608°F). However, until recently, no validated model existed to predict the failure of flawed tubes at the temperatures associated with postulated severe accidents. Consequently, the NRC sponsored tests conducted at ANL to help develop such a model.

4.3.2 Analysis of Steam Generator Tubes with Cracks

The following sections outline the precedent for analyzing tubes with through-wall cracks using a bulging or magnification factor, m. The modifications made to the magnification factor to account for the effects of part-through-wall cracks are then presented (yielding m_p), as is an improved m_p correlation.

4.3.2.1 Through-Wall Cracks

The most widely used model for predicting the failure pressure of tubing with a through-wall axial crack was originally proposed by Hahn *et al.* and later modified by Erdogan. This model is based on the following calculation:

$$p_{cr} = \frac{\bar{\sigma} h}{m R_m} = \frac{p_b}{m} \qquad (15a)$$

where

$$\bar{\sigma} = k(\sigma_y + \sigma_u) \qquad k \approx 0.5 - 0.6 \qquad (15b)$$

$$m = 0.614 + 0.481\lambda + 0.386\exp(-1.25\lambda) \qquad (15c)$$

$$\lambda = [12(1-\nu^2)]^{\frac{1}{4}} \frac{c}{\sqrt{R_m h}} = \frac{1.82c}{\sqrt{R_m h}} \qquad (15d)$$

$$p_b = \frac{\bar{\sigma} h}{R_m} \qquad (15e)$$

The parameter $\bar{\sigma}$ with k= 0.5 is often referred to as the flow stress.

4.3.2.2 Part-Through-Wall Cracks

For part-through-wall axial cracks, the pressure required to fail the remaining ligament can be calculated using an empirical equation (as reported by Kiefner *et al.*):

$$p_{sc} = \frac{\bar{\sigma} h}{m_p R_m} = \frac{p_b}{m_p} \qquad (16a)$$

where

$$m_p = \frac{1 - \frac{a}{mh}}{1 - \frac{a}{h}} \qquad (16b)$$

It should be emphasized that Equation (16a) calculates only the pressure required to fail the remaining ligament. The stability of the resulting through-wall crack can be analyzed using Equation (15a). If $p_{cr} > p_{sc}$, the through-wall crack is stable. That is, although the crack will leak, it will not increase in length without a further increase in pressure. By contrast, if $p_{cr} < p_{sc}$, the resulting crack will be unstable and will rapidly increase in length without any additional increase in pressure.

In conjunction with an NRC-sponsored steam generator integrity program, Pacific Northwest National Laboratories (PNNL) conducted a series of tests (Kurtz, 1990) on tubes containing part-through-wall axial cracks. From these tests, PNNL developed an empirical formula for the failure pressure of a tube containing a part-through axial crack. This formula is of the same form as Equation (16a), but Equation (16b) is replaced by Equation (17a), as follows:

$$m_p = \left[1 - \frac{a}{h} + \frac{a}{h}\exp(-0.41\lambda)\right]^{-1} \qquad (17a)$$

More recently, Chavez *et al.* re-analyzed the PNNL tube test data and proposed that the value of k should be taken as 0.5973 and Equation (17a) should be modified as follows:

$$m_p = \left[1 - \frac{a}{h} + \frac{a}{h}\exp(-0.51\lambda)\right]^{-1} \qquad (17b)$$

On the basis of burst tests on tubes, Flesch and Cochet recommended the use of Equations (16a) and (16b) for flaw depths greater than 85 percent of the wall thickness. However, to reduce the degree of conservatism, they used σ_u instead of For predicting remaining

ligament failure by plastic instability of tubes with flaw depths between 20 percent and 85 percent of wall thickness, they recommended replacing Equation (16b) by the following empirical Equation (referred to as the EdF equation):

$$m_p = \left(\frac{1 - \frac{c}{h}\frac{a}{h}}{1 + \frac{c}{h}} \right)^{-1} \quad \text{for } 0.2 < a/h < 0.85, \tag{18a}$$

and

$$m_p = \frac{1 - \frac{a}{mh}}{1 - \frac{a}{h}} \frac{\bar{\sigma}}{\sigma_u} \quad \text{for } a/h > 0.85, \tag{18b}$$

4.3.2.3 Improved Correlation for m_p

As the crack depth approaches 100 percent of the tube wall thickness (i.e., a/h=1), Equations (16a), (16b), and (18b) predict that p_{sc} approaches zero, while Equations (17a) and (17b) predict a higher pressure for ligament failure associated with short, deep cracks. Eventually Equations (17a) and (17b) become unconservative for very deep cracks, since m_p is inversely proportional to crack depth in these equations. On the other hand, Equation (16b) tends to be too conservative for short and deep cracks. Therefore, ANL reanalyzed the PNNL tube test data (and re-measured the flaws using post-test fractography). As a result, ANL proposed that Equation (16b) should be modified as follows (referred to as the ANL equation):

$$m_p = \frac{1 - \alpha\left(\frac{a}{h}\right)\frac{a}{mh}}{1 - \frac{a}{h}} \tag{18c}$$

where

$$\alpha\left(\frac{a}{h}\right) = 1 + 0.9\left(\frac{a}{h}\right)^2\left(1 - \frac{1}{m}\right) \tag{18d}$$

Except for short, deep cracks, Equation (18d) predicts failure pressures similar to those obtained using Equation (16b).

Table 4.1 summarizes a comparison of the prediction errors of the PNNL burst test results (Kurtz, 1990) using the various models for m_p. These errors are expressed in terms of the root-mean-squared (RMS) errors for the entire test series and in terms of the RMS errors associated with a range of crack depths. Roughly equivalent numbers of tests were performed in each crack depth range. Table 4.1 also includes the EdF correlation for comparison; however, since that correlation involves a material characteristic (the ultimate tensile stress) and also geometric factors, it would be an unsatisfactory choice to use for high temperatures where creep damage is significant.

The models developed by PNNL and Battelle Columbus Laboratories (BCL) seem to yield significantly larger errors for deep cracks ($^{a}/_{h} > 0.75$) than shorter cracks. The INEL and ANL models have a more uniform distribution of errors with flaw depth. Although the errors associated with the predictions derived using Equation (18d) (with k=0.5) for the PNNL data set are slightly smaller than with the other correlations, the INEL correlation describes the PNNL tests almost as well.

Table 4.1 Relative Error Between Predicted and Observed Failure Pressures In PNNL Tests for Various M_p Models

	PNNL	INEL	EDF	BCL	ANL
Mean Error	-0.01	0.05	0.08	0.04	-0.02
RMS all	0.13	0.11	0.12	0.13	0.09
RMS $^{a}/_{h}=0$	0.03	0.03	0.03	0.03	0.03
RMS $0.25<^{a}/_{h}\leq 0.45$	0.09	0.09	0.09	0.09	0.09
RMS $0.45<^{a}/_{h}\leq 0.75$	0.14	0.14	0.14	0.11	0.12
RMS $0.75<^{a}/_{h}$	0.21	0.11	0.17	0.22	0.08

*Errors may differ from estimates in original reports because they are based on new measurements of a/h made at ANL. Three outlier tests (C-03-5, C-15-5, and C-44-3) were not included in the calculation of the errors.

Figures 4.10a and 4.10b compare the values of stress magnification factor m_p computed using the various equations. Although these values are within 20 to 30 percent of each other for shallow cracks (a/h = 0.5), they can differ by as much as a factor of 2 for short, deep cracks (≈ 6-mm (0.25-in.), a/h = 0.9).

Failure tests on tubes containing deep cracks (to be discussed later) have shown that the m_p values are more consistent with the ANL equation (Equation 18d) than the BCL equation (Equation 16b). To verify this analytically, ANL conducted detailed elastoplastic finite-element analyses for a 22-mm (0.875-in.) diameter tube with a 25-mm (1-in.) long and 50 percent deep axial crack and a 6-mm (0.25-in.) long and 90 percent deep axial crack subjected to rapidly increasing internal pressure at 300 and 750°C (572 and 1382°F). Figure 4.11a depicts the stress-strain curves at these temperatures.

The results (presented in Figure 4.11b) show that the maximum hoop stress magnification in the ligament for the shallower crack is independent of the stress-strain curve of the material. Further, the hoop stress magnification factor (defined as the ratio of the average hoop stress in the ligament and the average hoop stress in an unflawed tube) changes very little with internal pressure. Its variation with crack depth agrees more closely with the ANL equation than with the BCL equation.

4.3.3 Models for Predicting Failure Under Severe Accident Conditions

The behavior of flawed steam generator tubing during severe accidents has recently been considered in reports by INEL (Ellison, 1996) and EPRI (Fuller, January 1996). These reports describe the failure of unflawed tubing and other components (such as the surge line) in

terms of creep damage. Both analyses assume that failure of flawed steam generator tubing in severe accidents can be described by the models represented by Equations (15) through (17), taking the flow stress to be a function of temperature. With this assumption, the failure pressure of a flawed tube depends solely on the flaw geometry and temperature and is independent of the detailed time/temperature history.

Intuitively, failure would be expected to be controlled by flow stress if the temperature ramps are sufficiently rapid so that insufficient time is available for creep to influence the deformation or damage of the tube. At the other extreme, if the temperature ramps are sufficiently slow (in the limit, a constant temperature), failure should be controlled by creep processes. In loading histories at intermediate rates, however, the damage processes are more complex and are difficult to analyze.

Recent tests conducted at ANL have shown that pressure and temperature ramp rates have significant influences on failure pressure (Figure 4.12a) and temperature (Figure 4.12b), respectively. Therefore, ANL developed a creep rupture model for predicting failure of flawed and unflawed tubes. For the high-temperature tests conducted at ANL under a variety of loading histories, predictions on the basis of this model agree much more with the test results than predictions based on flow stress models. However, this report also discusses the flow stress models for completeness.

Consider a tube with a flaw subjected to a temperature history T(t) and nominal hoop stress history $\sigma(t)$. To analyze the behavior of a tube under such a general loading history, the following assumptions are usually made for both the flow stress and the creep rupture models:

- The failure time and temperature of a flawed tube are the same as those of an unflawed tube subjected to a nominal hoop stress history $m_p\sigma(t)$ and the same temperature history T(t).

- The values of the magnification factor m_p determined from burst tests of flawed tubes at low temperatures are also applicable at high temperatures.

These assumptions can be shown to be valid for certain classes of creep and plasticity problems (Finnie, 1959). They are not strictly valid for the problem considered here, but the test program at ANL has shown that they can provide a reasonable approximation.

4.3.3.1 Flow Stress Models

The flow stress models assume that, for any arbitrary history of hoop stress $\sigma(t)$ and temperature T(t), failure occurs at a temperature T and hoop stress σ whenever the following failure equation is satisfied, independent of stress-temperature history:

$$\sigma = \frac{\overline{\sigma(T)}}{m_p} \qquad (19)$$

Rigorous application of the flow stress models for predicting the failure temperatures of steam generator tubes requires the tensile properties of Alloy 600 tubes in the hoop direction as a function of temperature. Although fairly extensive tensile property data are available for tubing at room temperature (Kurtz, 1990), only limited data are currently available for higher temperatures. Rempe *et al.* (1993) reported tensile properties of Alloy 600 rods as a function of temperature. Chavez *et al.* (1996) expressed the sum of the yield

and ultimate tensile strengths of Alloy 600 bars (in MPa) as a function of temperature, as follows:

$$\sigma_y + \sigma_u = \begin{cases} 564.4 - 0.4546T + 1.5055\times10^{-3}T^2 - 1.9907\times10^{-6}T^3 \text{ for } 20°C \le T \le 727°C \\ 4308.9 - 11.381T + 1.030\times10^{-2}T^2 - 3.1734\times10^{-6}T^3 \text{ for } 727°C < T \le 1100°C \end{cases} \quad (20a)$$

To estimate the variation in the flow stress of Alloy 600 tubes with temperature, Chavez *et al.* multiplied Equation (20a) by a factor of 0.9. This is the same factor by which the sum of the yield and ultimate tensile strengths of Alloy 600 bars at room temperature (Rempe, 1993) has to be multiplied to obtain the sum of the yield and ultimate tensile strengths for Alloy 600 tubes at room temperature (Kurtz, 1990; Chavez, 1996).

Tensile data on hot rolled Alloy 600 bars as a function of temperature are also reported in the literature (International Nickel, 1964). Here, the sum of the yield and ultimate tensile strengths (in MPa) of hot rolled Alloy 600 bars was given as a function of temperature by the following equation:

$$\sigma_y + \sigma_u = 1780 - 9.84T + 0.0352T^2 - 5.08\times10^{-5}T^3 + 2.4\times10^{-8}T^4 \text{ for } 200°C \le T \le 870°C \quad (20b)$$

Figure 4.13 plots the flow stresses for Alloy 600 computed from the above data (with k=0.5) with others from various sources. (Most of these tests were conducted under stroke-control at a nominal strain rate of 34 percent/min.) Figure 4.13 also shows data from room-temperature tensile tests on the tubing being tested at ANL. As shown, the flow stress decreases markedly with temperature above 600°C (1112°F). Note (from Figure 4.13) that the flow stress may vary widely at low temperatures, but the heat-to-heat and product form variations in the flow stress diminish rapidly with increasing temperature. Therefore, the INEL flow stress curve, which covers the widest range of temperatures, is used for failure predictions.

Although the flow stress model is a straightforward extension of a model that has been well verified at normal operating temperatures, conceptual difficulties arise with the use of such a model at high temperatures. For example, the flow stress at elevated temperatures is a function of strain rate and temperature. In Figure 4.14, the results from isothermal pressure ramp tests at two ramp rates are used to define "effective" flow stresses, which are then compared with the flow stress curve derived from the INEL tensile tests. Note that, as expected, higher ramp rate leads to higher flow stress.

Conceptually, rate effects can be included within the framework of a flow stress model by developing a constitutive equation that expresses the flow stress as a function of both strain rate and temperature. Several such constitutive relations based on the so-called equation of state theory are available. However, besides being quite complex, they are not easily adapted to the problem of predicting the failure of steam generator tubes. This is particularly true for those relations that contain flaws and are subjected to typical temperature and pressure histories expected during severe accidents. In this report, the term "flow stress model" is used exclusively to denote simple rate-independent flow stress models that have been successfully used at low temperatures.

4.3.3.2 Creep Rupture Model

As reported in Finne (1959), a relatively straightforward analysis can be used to predict creep failure of an unflawed tube under varying stress and temperature histories using a linear time-fraction damage rule (as in Code Case N 47 of the ASME Code, Section III), as

follows:

$$\int_0^{t_f} \frac{dt}{t_R(T,\sigma)} = 1 \qquad (21a)$$

where t_R and T may both be functions of time.

A rigorous analysis of flawed tubes under a similar loading would be very complex. Therefore, ANL extended the creep failure model to flawed tubing using the assumptions referred to earlier. That is, ANL assumed that failure can be predicted by the following equation:

$$\int_0^{t_f} \frac{dt}{t_R(T,m_p\sigma)} = 1 \qquad (21b)$$

4.3.3.3 Creep Rupture Properties of Alloy 600

Creep rupture properties (particularly at short lives) of Alloy 600 tubes in the hoop direction are needed to apply the creep rupture model for predicting failure under severe accident conditions. As a result, ANL reviewed the available literature data on the creep rupture properties of Alloy 600. Figure 4.15 depicts a compilation of the available data in terms of the Larson-Miller parameter and the stress for both cold-worked and annealed materials. However, a preliminary examination of the data did not reveal any apparent bias associated with the different thermomechanical treatments, so information corresponding to both types of materials were included in the data fits. Figure 4.15 shows a least-squares bilinear best fit, along with estimated 95 percent confidence limits. The best-fit curves for the Larson-Miller parameter (P_{lm}) are:

$$\begin{aligned} \log_{10}\sigma &= 4.31 \pm 0.10 - 1.43\times10^{-4}P_{lm} \qquad \sigma \le 39.3\,Mpa \\ \log_{10}\sigma &= 5.03 \pm 0.13 - 1.81\times10^{-4}P_{lm} \qquad \sigma > 39.3\,Mpa \end{aligned} \qquad (22a)$$

where the time to rupture (t_R) is then

$$t_R = 10^{\frac{P_{lm}}{T}-15}, \quad t_R(h), T(k) \qquad (22b)$$

$$\begin{aligned} P_{lm} &= (24.3 \pm 0.7 - 3.0\ln\sigma)\times10^3 \qquad \sigma \le 5.7\,ksi \\ P_{lm} &= (23.2 \pm 0.7 - 2.4\ln\sigma)\times10^3 \qquad \sigma > 5.7\,ksi \end{aligned} \qquad (22c)$$

The variation in the Larson-Miller parameter reflected in Equations (22a) and (22c) is primarily attributable to differences in the heat-to-heat behavior of materials.

The "breakpoint" in the bilinear fit occurs at a stress that is relatively low compared with those of interest in steam generator tube failures. Even the nominal stress in a steam

generator tube with the secondary depressurized is greater than 130 MPa (19 ksi)–$\log_{10}\sigma \approx$ 2.1, and the stress is even higher in the crack ligament. Hence, for these applications, only Equation (22c) is actually used, and the variance is assumed to be the same for all stress levels, although this is unlikely to be true. Instead, the staff expects that the variance will be less at the higher stresses of actual interest. As noted, however, little data are available for higher stresses and quantifying this judgment is difficult. Nonetheless, the bounds predicted by Equation (22c) are expected to be conservative at the stress levels typical of flawed tubes.

Figure 4.16 depicts the Larson-Miller correlation currently used in SCDAP. This correlation shows a reasonable fit to the data, but there clearly is some change in slope that is not reflected in the correlation. In particular, it departs from the data at the high stress levels (low Larson-Miller parameter values) of interest in the present analyses.

To establish the applicability of Equations (22b) and (22c) to the tubing material, ANL conducted constant-pressure creep-rupture tests on unflawed 22-mm (0.875-in.) diameter tubes using both isothermal and constant temperature ramp loading. Figure 4.17 plots the experimental results against predicted times to rupture derived using Equations (22b) and (22c). In all cases, the predicted rupture lives are well within a factor of 2 of the experimental lives (which is typical of the scatter in the uniaxial creep rupture data). This indicates that the Larson-Miller representation of the data is adequate for the tube material.

4.3.4 Validation Tests for the Creep Rupture Model

To validate the creep rupture model, ANL conducted several types of tests on both flawed and unflawed steam generator tubes in a single-zone furnace using programmable temperature and high-pressure nitrogen gas to apply internal pressures. A temperature profile (measured transiently and also steady-state) showed a maximum of 5°C (9°F) axial variation within a central 50-mm (2-in.) section, with the center being the hottest. The maximum through-thickness temperature gradient was less than 1°C (2°F).

In addition, the tests were conducted on both unflawed and flawed tubing and tubing that was flawed using electro-discharge machining (EDM). Such notches are not as sharp as real cracks, but previous tests at lower temperatures have shown that crack tip geometry has very little effect on the failure loads (Kurtz, 1990). At higher temperatures, the effect of the crack tip geometry would be expected to be even less significant.

4.3.4.1 Isothermal Failure Tests

The ANL tests were conducted on flawed tubes by subjecting them to isothermal constant pressure loading. Table 4.2 summarizes those tests, with the failure times predicted by the creep rupture model. Figure 4.18a plots the failure times predicted using four different values of m_p against the experimental failure times for tubes containing a crack approximately 60 percent deep and 25 mm (1 in.) long. Besides the diagonal perfect prediction line, Figure 4.18a also shows differences of a factor of 2 between the predicted and observed times to failure by means of two additional lines that also represent typical scatter bands in creep rupture tests.

Except for a test at 667°C (1233°F), the failure lives predicted by the ANL m_p (Equation 18d) are within a factor of 2 of the experimental lives of the specimens. The predicted lives using m_p values as determined by the BCL Equation (16b) and the EdF Equation (18a) are also

reasonable, but those predicted by the INEL Equation (17b) are low by more than a factor of 2 in most cases. The reader should note that the flow stress model is incapable of predicting time to failure in tests of this type and, in fact, would predict that none of the tubes should have failed.

Table 4.2 Constant-Pressure Rupture Tests at Various Temperatures On Specimens with and Without Flaws

Test No.	Crack Geometry			Loading History		Failure Conditions			
	2c (in.)	a/h	m_p	T[a](°C)	p[b] (psi)	T_f(°C)	p_f (psi)	t_f(min)	Pred. t_f
T-37	1	0.59	1.96	667	2350	667	2350	336	128
T-56[c]	1	0.65	2.21	667	2350	667	2350	74	62
T-38	1	0.62	2.07	700	1915	700	1915	28	88
T-41	Unflawed	-	1	700	4500	700	4500[d]	38	42
T-61[e]	Unflawed	-	1	700	4450	700	4450	49	45
T-47	1	0.55	1.82	750	1400	750	1400	186	176
T-60	Unflawed	-	1	750	3290	750	3290	29	43
T-48	1	0.55	1.82	800	1400	800	1400	26	32
T-42	Unflawed	-	1	800	2350	800	2350	33	50

a. Ramp to temperature and hold
b. Constant pressure
c. Duplicate of test listed immediately above.
d. Pressure decreased gradually from 4750 psi to 4250 psi during hold.
e. Duplicate of test listed immediately above, but with pressure held constant at 4450 psi during hold.

4.3.4.2 Failure Tests of Specimens with Deep Cracks

As discussed earlier, there is some experimental evidence (Flesch, 1988) that the numerical values of m_p computed by the BCL equation for short and deep cracks are too high for tests conducted at low temperatures where a flow stress model is valid. Test results, summarized in Table 4.3 and shown in Figure 4.18b, confirm that this is also true at high temperatures. All of the test specimens referenced in this figure had cracks ≥90 percent deep. The BCL equation grossly overestimated the damaging influence (i.e., underestimated the time to rupture) of these cracks. The predictions derived using the INEL and ANL equations agree more closely with the results than those derived using the BCL model.

The predictions made using the EdF equation are not shown in Figure 4.18b because, at high temperatures, they are essentially the same as those based on the BCL equation. At low temperatures, the EdF model (Flesch, 1988) predicted a smaller m_p for cracks that are more than 85 percent deep because the flow stress in the BCL equation is replaced by the ultimate tensile strength in the EdF equation (see Equation 18b). However, little difference exists between the flow stress and the ultimate tensile strength at high temperatures because strain hardening is greatly reduced. Overall, as in the low temperature case, the ANL equation for

m_p gave the best predictions for failure lives of specimens with shallow and deep cracks, and was used for the analysis of the high-temperature tests.

Table 4.3 Constant-pressure Failure Tests with Deep Cracks

Test No.	Crack Geometry			Loading History		Failure Conditions			
	2c (in.)	a/h	m_p	T[a] (°C)	p[b] (psi)	T_f(°C)	p_f (psi)	t_f(min)	Pred. t_f
T-55	0.25	0.91	2.45	800[d]	750	800	750	420	180
T-78[c]	0.25	0.92	2.61	800	750	800	750	246	130
T-83	Unflawed	-	1	800	1800	800	1800	228	202
T-72	1	0.92	7.62	800	356	800	356	19	23
T-84	1	0.91	6.85	800	450	800	450	2	18
T-87	Unflawed	-	1	800	2910	800	2910	12	15
T-66	2	0.90	7.83	800	300	800	300	23	15
T-85	Unflawed	-	1	800	3000	800	3000	10	13

a. Ramp to temperature and hold
b. Constant pressure
c. Duplicate of test immediately above
d. Ramp in 1 hour to temperature, then pressurize and hold

4.3.4.3 Pressure and Temperature Ramp Tests

To evaluate the importance of loading rates on the failure conditions and compare the predictive capabilities of the creep rupture model and the flow stress model, ANL conducted two additional types of tests. In the first type, the specimens were heated to a given temperature and then pressurized isothermally at a constant pressure ramp until failure. In the second type, the specimens were first pressurized at low temperature and then, with the pressure held constant, they were subjected to a constant temperature ramp until failure.

Tables 4.4 and 4.5 summarize the results of all of the tests of these types conducted to date, together with the failure pressures and temperatures predicted by the creep rupture model. Results from both types of tests, plotted in Figures 4.12a and 4.12b, show that the loading rate (pressure or temperature), which is ignored in a simple flow stress model, has a significant influence for unflawed tubes. The reader should note that the experimental results are closer to predictions of the creep rupture model than those of the flow stress model in all cases.

At the higher pressure ramp rate, the creep rupture model overestimated the failure pressures by a maximum of 25 percent, whereas the flow stress model underestimated the failure pressures by as much as 50 percent. By contrast, the creep rupture model predicted the failure temperatures for the temperature ramp tests almost exactly, whereas the flow stress model either underestimated or overestimated the failure temperatures by 70°C (126°F). Figure 4.14 shows the results from pressure ramp tests on flawed and unflawed tubes, clearly

indicating that although the flow stress model would predict the failure pressures reasonably well for the lower ramp rate tests, it would underestimate the failure pressures at ≥800°C (1472°F) by a factor of 2 for the higher ramp rate tests if the INEL flow stress curve were used.

Table 4.4 Constant-Pressure Temperature Ramp Tests

Test No.	Crack Geometry			Loading History		Failure Conditions	
	2c (in.)	a/h	m_p	ΔT^a (°C/min)	p^b (psi)	T_f(°C)	Pred. T_f
T-62	Unflawed	-	1	Note c	2350	913	916
T-63	Unflawed	-	1	2	2350	843	838
T-71	Unflawed	-	1	0.2	2350	779	770
T-67	1	0.65	2.21	20	1065	892	916
T-68	1	0.65	2.21	0.2	1065	770	778
T-74	1	0.93	8.60	0.2	270	860	918
T-73	1	0.93	8.60	0.2	1065	612	604
T-76	0.25	0.89	2.22	20	1090	915	911
T-77	0.25	0.90	2.32	0.2	1040	778	766
T-59	2	0.79	3.93	2	750	810	801
T-79	2	0.92	9.68	0.2	245	815	914
T-80[d]	2	0.92	9.68	0.2	245	859	914
T-81	2	0.93	10.99	0.2	217	678	768

a. Ramp to temperature and hold
b. Constant pressure
c. Ramp to 600°C in 1 hour then 20°C/min
d. Duplicate of test immediately above

The failure pressures for both ramp rates are much closer to those predicted by the creep rupture model (see Figure 4.19a). For the temperature ramp tests on flawed specimens, ANL selected the pressures such that the product of m_p and the nominal hoop stresses were approximately equal for two-crack geometries. Thus, the predicted failure temperatures for both geometries fall approximately on a single line for either the creep rupture or flow stress models, as shown in Figure 4.19b. The experimental results agree much more closely with the predictions of the creep rupture model and confirm that the effect of flaws on failure can be characterized by the m_p approach. Therefore, the creep rupture model can be expected to reliably predict failure under varying temperature and pressure histories during severe accidents more accurately (relative to a simple rate-independent flow stress model).

Table 4.5 Isothermal Pressure Ramp Tests

Test No.	Crack Geometry			Loading History		Failure Conditions			
	2c (in.)	a/h	m_p	T[a](°C)	Δp (psi/min)	pf (psi)	t_f (min)	Pred. pf	Pred. t_f
T-35	Unflawed	-	1	840	2300[b]	3000	3.3	3000	5.8
T-36	Unflawed	-	1	840	2300[c]	4000	1.8	4000	2.8
T-46	Unflawed	-	1	840	2300	4190	1.8	4987	2.2
T-45	Unflawed	-	1	840	230	3090	13	3390	15
T-86	Unflawed	-	1	800	230	3730	16	4115	18
T-82	Unflawed	-	1	800	2300[d]	4800	2.2	4800	3.4
T-57	0.25	0.75	1.58	800	2300	3520	1.5	3520	1.8
T-58	1	0.79	3.32	800	2300	1590	0.7	2194	0.9
T-70	1	0.65	2.21	840	2300	2250	1.0	2570	1.1
T-69	1	0.65	2.21	800	2300	2740	1.2	3020	1.3
T-75	1	0.65	2.21	700	2300	3370	1.5	4860	2.1

a. Isothermal
b. Ramp to 3000 psi and hold
c. Ramp to 4000 psi and hold
d. Ramp to 4800 psi and hold

4.3.5 Failure Tests for Evaluating Postulated Severe Accident Time/Temperature Histories

ANL performed tests to determine the behavior of flawed tubes under time/temperature histories that could be used to evaluate the failure of steam generator tubes under postulated severe accident conditions. An additional purpose of the tests was to further validate a model for determining the time to failure of flawed tubes under time/temperature histories that could reach temperatures as high as 850°C (1562°F).

In all of the tests, ANL held the internal pressure constant at 16.2 MPa (2350 psi), conducting tests on both 19-mm (0.75-in.) and 22-mm (0.875-in.) outer diameter tubes with wall thicknesses of 1 mm (0.043 in.) and 1.3 mm (0.050 in.), respectively. In addition, ANL tested four different nominal flaw geometries with axial lengths of 6 mm (0.25 in.), 25 mm (1 in.), and 50 mm (2 in.) and depths varying from 20 percent to 65 percent of thickness. The actual flaw depths were determined by fractography following the tests. Commonly, they were also measured before the tests using a replica technique. The differences between the two measurements, when available, were not large. Duplicate tests were run for all of the 22-mm (0.875-in.) diameter tube tests to provide information on test consistency.

For the tests conducted to date, ANL considered two time/temperature histories. The first, referred to as the "INEL ramp," is based on Case 1N. (See Section 3 of this report for

thermal-hydraulic case designations.) In this analysis, the temperature rises fairly rapidly to ≈800°C (1472°F). Then, because the cladding is almost completely oxidized, the rate of temperature increase drops sharply. Shortly after this decrease in the heat up rate, the INEL analysis predicts failure of the surge line nozzle and depressurization of the system. Because the primary purpose of these tests was to help develop a failure model, the time/temperature history used for the tests have ignored the predicted depressurization. Thus, after rapidly heating from room temperature to 300°C (572°F) and equilibrating, the test specimens were subjected to a temperature ramp of 3.75°C/min. (6.75°F/min.) from 300 to 550°C (572 to 1022°F), followed by 7.5°C/min. (13.5°F/min.) up to 800°C (1472°F) and then 1.75°C/min. (3.2°F/min.) to failure.

The second time/temperature history, referred to as the "EPRI ramp," is based on a preliminary analysis reported by EPRI (Fuller, 1996). Here, the tubing temperature also rises rapidly, but the peak predicted temperature is only 667°C (1233°F).

Both the INEL (Ellison, 1996) and EPRI (Fuller, 1996) analyses predict a marked decrease in heat up of the tubes after oxidation of the cladding is completed. However, in the INEL results (Ellison, 1996) the temperature still increases at a significant rate, ≈2°C/min.(3.6°F/min.), whereas EPRI (Fuller, 1996) predicted that the temperature holds virtually constant at 667°C (1233°F) for about 5 minutes before the temperature decreases. EPRI (Fuller, 1996) also predicts depressurization of the primary system resulting from the failure of the surge line shortly after the tubing reaches 667°C (1233°F).

The time/temperature history used for the tests again ignores the predicted depressurization and reduction in temperature. After rapidly heating from room temperature to 300°C (572°F) and equilibrating, the temperature ramps from 300 to 564°C (572 to 1047°F) at 5.37°C/min. (9.67°F/min.), then to 582°C (1080°F) at 10.6°C/min. (19.1°F/min.), to 630°C (1166°F) at 28.24°C/min. (50.83°F/min.), and to 667°C (1233°F) at 14.80°C/min. (26.64°F/min.). To increase the contribution of creep damage, the EPRI ramp was somewhat arbitrarily modified from the history described in the analysis results (Fuller, 1996) to include a 2-hour hold time at 667°C (1233°F). If the specimen did not fail in 2 hours of constant temperature hold, it was subjected to a temperature ramp of 2°C/min. (3.6°F/min.) until failure.

The two time/temperature histories are shown in Figures 4.20a and 4.20b. Neither ramp chosen for the tests was intended to be an accurate representation of a particular sequence, but together they represent a range of histories for which a failure model would be needed. Thus, although the INEL and EPRI analyses predict that failure of the surge line nozzle and consequent depressurization of the system will occur before the failure of unflawed steam generator tubes, the tests at ANL were continued with full pressure until failure occurred.

ANL has performed 32 ramp tests using the INEL and EPRI time/temperature histories. Tables 4.6 and 4.7, along with Figures 4.21a and 4.21b, summarize the results from these tests. In addition to failure data, Tables 4.6 and 4.7 include crack depths measured by post-test fractography, and also the predicted failure temperatures derived using the creep rupture model. The predicted failure temperatures and times (above 300°C (572°F)) in Figures 4.21a and 4.21b were calculated using the creep rupture model and the ANL correlation for m_p (Equation 18d). Figures 4.22a and 4.22b report the test results to show the dependence of the time to failure on m_p. The abscissas of Figures 4.22a and 4.22b reflect the stress magnification factor (m_p), as calculated by Equation (18d); m_p may be considered a measure of crack severity that takes into account both the length and the depth of the crack.

Table 4.6 Flaw Sizes and Temperatures at Failure for INEL Ramp Tests

3/4 in. Diameter Tube					7/8 In. Diameter Tube			
2c (in.)	Test No.	a/h	T_f	Pred. T_f	Test No.	a/h	T_f	Pred. T_f
Unflawed	T-2	Unflawed	823°C	837°C	T-10	Unflawed	835°C	844°C
Unflawed	T-13	Unflawed	826°C	837°C	T-30	Unflawed	843°C	844°C
0.25	T-12	0.59	798°C	806°C	T-7	0.65	803°C	806°C
0.25	-	-	-	-	T-34	0.62	802°C	809°C
1	T-11	0.61	758°C	752°C	T-9	0.54	768°C	784°C
1	-	-	-	-	T-33	0.54	778°C	792°C
2	T-3	0.45	774°C	788°C	T-6	0.36	808°C	805°C
2	T-14	0.35	805°C	803°C	T-32	0.41	800°C	803°C
2	T-4	0.2	808°C	816°C	T-5	0.16	825°C	824°C
2	-	-	-	-	T-31	0.22	817°C	818°C

Compared with the failure temperature of an unflawed tube, as m_p increases, the reduction in temperature associated with flawed tube failure is magnified. The failure temperature depends on the time/temperature history. The EPRI ramp, which includes a 2-hour hold time, leads to lower failure temperatures than the INEL ramp, which does not include such a constant temperature hold. However, the deleterious effect of the 2-hour constant temperature hold of the EPRI ramp worsens with increasing severity of the crack. For the unflawed tubes, there is little difference between the failure temperatures for the two histories. For the most severe flaw geometries, however, there are significant reductions in the temperatures at which failure occurs for the EPRI ramp. This observation confirms that time/temperature history can have a significant influence on failure temperature.

Table 4.7 Flaw Sizes and Temperatures at Failure for EPRI Ramp Tests.

3/4 in. diameter tube					7/8 in. diameter tube			
2c (in.)	Test No.	a/h	T_f	Pred. T_f	Test No.	a/h	T_f	Pred. T_f
Unflawed	T-22	Unflawed	828°C	833°C	T-19	Unflawed	839°C	842°C
Unflawed	-	-	-	-	T-28	Unflawed	843°C	842°C
0.25	T-23	0.57	767°C	772°C	T-18	0.66	779°C	786°C
0.25		-	-	-	T-24	0.66	781°C	782°C
1	T-29	0.54	726°C	702°C	T-16	0.57	724°C	692°C
1	-	-	-	-	T-27	0.55	724°C	727°C
2	T-21	0.40	760°C	745°C	T-15	0.30	794°C	786°C
2	-	-	-	-	T-26	0.41	770°C	762°C
2	T-20	0.12	814°C	814°C	T-17	0.20	816°C	802°C
2	-	-	-	-	T-25	0.21	817°C	811°C

4.3.5.1 Evaluation of Stress Magnification Factor in Flawed Tubes for High-Temperature Tests

ANL also analyzed the INEL and EPRI ramp tests using other correlations for the stress magnification factor (m_p). Table 4.8 compares the test results with the predictions of the creep rupture model using the different m_p correlations, in terms of the errors in predicted temperatures at which failure occurred. Although the m_p models were based on the low-temperature tests, they appear capable of accurately predicting the effects of high temperature situations where creep damage is predominant (i.e., m_p seems to depend primarily on geometric factors not material characteristics).

Table 4.8 Comparison of Predicted Failure Temperatures

Errors (°C)	ANL	BCL	PNNL	INEL
Mean	2.5	7.5	11.6	14.5
RMS	9.7	14.2	18.9	18.8
Maximum	24.7	48.4	59.0	59.0

The ANL and BCL models give significantly better results than the PNNL and INEL models in these tests. Considering the relatively small differences in the predicted values of m_p for most crack depths and sizes, the differences are somewhat surprising. However, the matrix for these tests was heavily weighted toward cracks with $a/h \approx 0.6$, where the differences between the BCL models and the PNNL and INEL models are relatively large. The test results suggest that the ANL and BCL models are more accurate in this range.

Additional isothermal creep failure tests (discussed earlier in Section 4.3.4.1) performed with deep cracks ($a/h \approx 0.9$) showed that either the ANL or the INEL correlation for m_p was appropriate for this geometry. The results from these tests confirmed that the original BCL model overestimates m_p for such deep cracks, consistent with the behavior observed in the low-temperature tests at EdF and PNNL, and that the ANL and INEL models give much better predictions for such deep cracks. However, including both shallow and deep cracks, the ANL model gives the best overall predictions.

4.3.5.2 Predictions by Flow Stress Models

ANL used the flow stress models to predict the times and temperatures to failure (above 300°C (572°F)) into account for the INEL and EPRI ramp tests. Figures 4.23a and 4.23b compare the predictions of the flow stress models with the experimental results. The predicted values were calculated with the INEL flow stress curve (Figure 4.13, Equation 20a) and the ANL stress magnification factor (Equation 18d). While the predictions for the tests with the EPRI ramp are reasonably good, the failure temperatures and times for the tests using the INEL ramp were significantly under-predicted. The accurate prediction of the EPRI ramp tests is probably a fortuitous consequence of the average strain rates in the ligament being close to the strain rate used in the tensile tests from which the flow stress curve was derived. Overall, the results agree much more closely with the predictions of the creep rupture model.

4.3.6 Uncertainty in Predictions

As mentioned earlier, the uncertainty in the Larson-Miller parameter reflected in

Equation (22c) primarily results from differences in the heat-to-heat behavior of materials. For the tubes used in the validation tests at ANL, the best fit to the experimental data is obtained when the constant in Equation (22c) is taken as 23.1 (i.e., they seem to be fairly "average" heats of material). In "sampling" from the population represented by Equation (22c) when computing damage, a single member of the population represented by Equation (22c) is selected and used for the entire history; the sampling is done once for each history not for each time step.

The variability observed in replicate tests on the same heat of material could be taken into account by assuming that the accumulated damage at failure is distributed (i.e., at failure D = 1 + β where β is a random variable that could be estimated from the variability observed in replicate tests). However, this variability is small compared with that observed in heat-to-heat variations. For tubes with flaws, failure is assumed to be controlled by Equation (21b), where the effective stress is given by the nominal hoop stress multiplied by the magnification factor m_p (which is a function of crack geometry). For a given time/temperature history, the time to failure is a function only of m_p and the creep properties.

4.3.6.1 Uncertainty in the Stress Magnification Factor

For the low-temperature tests, the error in the predicted failure pressure (Δp) resulting from an error in crack depth measurement (Δa) is

$$\frac{\Delta p}{p} = m_p \frac{d\left(\frac{1}{m_p}\right)}{d\left(\frac{a}{h}\right)} \frac{\Delta a}{h} \qquad (23)$$

Assuming that the variance in crack depth (a) is independent of crack size, the total variance for the test series arising from errors in the measurement of (a) can be estimated from the following equation:

$$\sigma_p^2 = \left[\sum\left(m_p \frac{d\left(\frac{1}{m_p}\right)}{d\left(\frac{a}{h}\right)} \frac{1}{h}\right)^2\right] \sigma_a^2 \qquad (24a)$$

For estimates of σ_a derived using the uncertainty of the depth measurements originally reported by PNNL (±1.5 mils (3.8×10^{-5} m) or σ_a = 0.75 mils (1.9×10^{-5} m)), the estimate of σ_p obtained from Equation (24a) represents only a small portion of the observed error. However, in the 20 samples that have been re-examined by ANL to date, the standard deviation of the differences between the ANL measurement and the previous PNNL measurement is greater than 2.2 mils (5.6×10^{-5} m). This suggests that the uncertainty in the depth measurements is much larger than previously assumed, and most of the observed scatter in the values observed for m_p in the tests can be attributed to uncertainties in the crack size measurements.

Often, it is desirable to explicitly account for crack size uncertainties. Hence, it is of interest to try to estimate the "model error" (i.e., the error in the predicted m_p given that

the crack size is known exactly). The mean value of the observed m_p is a much better measure of the "true" m_p, and uncertainty estimates on the mean ought to provide a good estimate of the model error. Such estimates can be made by standard statistical techniques (see Draper, 1966). The standard error of the mean estimate of the fitted variable is given by the following equation:

$$\sigma_m = s\left\{\frac{1}{n} + \frac{(x-\bar{x})^2}{\sum_k (x_k-\bar{x})^2}\right\}^{1/2} \tag{24b}$$

where n is the total number of data points

$\bar{x}$ is the mean value of the x_k values at which observations are available

s is the estimated variance about the regression:

$$s^2 = \frac{\sum_k (y_k - \hat{y}_k)^2}{n-2} \tag{24c}$$

where y_k is the observed value of the variable

$\hat{y}_k$ is the value predicted by the regression equation

The standard error of the predicted values then is

$$\sigma_m = s\left\{1 + \frac{1}{n} + \frac{(x-\bar{x})^2}{\sum_k (x_k-\bar{x})^2}\right\}^{1/2} \tag{24d}$$

These limits are of course larger than those for the value of the mean value of y for a given x.

While the actual uncertainty estimates are nonlinear, the simple linear expression

$$m_p = \frac{1-\alpha\frac{a}{mh}}{1-\frac{a}{h}}\,(1\pm 0.06) \tag{25}$$

can be shown to bound the estimates of the 95-percent confidence interval on the mean.

4.3.7 Discussion of Models and Conclusions

The flow stress models can predict failure of flawed or unflawed steam generator tubes at low temperatures, <350°C (<662°F). However, it significantly overestimates the damaging influence of short, deep cracks (≥90 percent). The new correlation developed at ANL is more adept at handling cracks of all sizes. Also, finite element analyses have shown that the computed m_p factors agree more closely with those calculated by the ANL correlation than those calculated using the classical BCL correlation.

At high temperatures, >700°C (1292°F), the simple rate-independent flow stress model cannot account for the rate effects observed in isothermal pressure ramp tests or constant-pressure temperature ramp tests. Contrary to the test results, such a model predicts constant failure pressure and temperature, respectively, independent of the ramp rates, for these two types of tests. Further, the flow stress model incorrectly predicts no failure for the isothermal constant pressure failure tests, which actually experienced time-delayed failure.

Developing a flow stress model that can account for rate effects on failure of flawed steam generator tubes would require some major theoretical developments. The semi-empirical creep rupture model developed at ANL can account for the rate-effects reasonably well in all of the tests conducted to date by relatively simple calculations. It is also reasonably accurate in predicting the time to failure for the isothermal constant-pressure failure tests.

In general, the failure temperatures and times predicted by the flow stress models are closer to the experimentally measured values for the EPRI ramp than the INEL ramp. The flow stress models tend to underestimate the failure temperatures of the most severe cracks by ~60°C (108°F) for the INEL ramp tests. However, they appear to be more accurate in predicting the failure temperatures for the EPRI ramp tests, which include a 2-hour constant temperature hold.

Independent of any model, the EPRI ramp is observed to produce more damage than the INEL ramp (see Figure 4.22). For a given crack geometry, the flow stress prediction for the failure temperature is nominally independent of the temperature ramp history. In reality, the values obtained for the flow stress at high temperatures are quite sensitive to the strain rates at which the flow stress is measured. Also, the flow stress models would not be expected to give good results for histories that produced strain rates too different from those in the test used to determine the flow stress.

The flow stress models might therefore be expected to be more applicable to the loading history without a constant temperature hold. That the agreement is better for the EPRI ramp is probably fortuitous. Conservatism in the flow stress model that may be associated with the stress analysis or the strain rates used in the tensile tests to determine the flow stress are balanced by the additional damage associated with the 2-hour hold of the EPRI ramp. It is likely that predictions using the flow stress models would not be as favorable if the hold time for the EPRI ramp were at a lower temperature, ≤ 500°C (932°F) where creep is negligible, or if the hold time were at a higher temperature where creep damage would be more extensive.

The creep rupture model correctly predicts that the EPRI ramp is more damaging than the INEL ramp. Also, compared with the flow stress model, it more accurately predicts the failure times and temperatures for both ramps. In addition, the creep rupture model has been validated by tests with a variety of pressure and temperature histories for which the predictions by the flow stress model may be significantly incorrect. Therefore, the staff

chose to use the creep rupture model for evaluating failure of steam generator tubes during severe accidents. For convenience, this model is summarized as follows:

$$\int_0^{t_r} \frac{dt}{t_R(T, m_p, \sigma)} = 1 \qquad (21b)$$

where the mean value of m_p and its 95-percent confidence interval are given by

$$m_p = \frac{1-\alpha\frac{a}{mh}}{1-\frac{a}{h}}(1\pm 0.06) \qquad (25)$$

$$\alpha\left(\frac{a}{h}\right) = 1 + 0.9\left(\frac{a}{h}\right)^2\left(1-\frac{1}{m}\right) \qquad (18d)$$

$$m = 0.614 + 0.481\,\lambda + 0.386\exp(-1.25\,\lambda) \qquad (15c)$$

$$\lambda = [12(1-\nu^2)]^{\frac{1}{4}}\frac{c}{\sqrt{R_m h}} = \frac{1.82c}{\sqrt{R_m h}} \qquad (15d)$$

$$t_R = 10^{\frac{P_{lm}}{T}-15} \qquad (22b)$$

The mean Larson-Miller parameter with its 95-percent confidence interval is then given as:

$$\begin{aligned} P_{lm} &= (24.3\pm 0.7 - 3.0\ln\sigma)\times 10^3 \quad \sigma \le 5.7 ksi \\ P_{lm} &= (23.2\pm 0.7 - 2.4\ln\sigma)\times 10^3 \quad \sigma > 5.7 ksi \end{aligned} \qquad (22c)$$

Figure 4.1 Burst Pressure vs. Crack Depth (axial cracks, q = 0.9283)

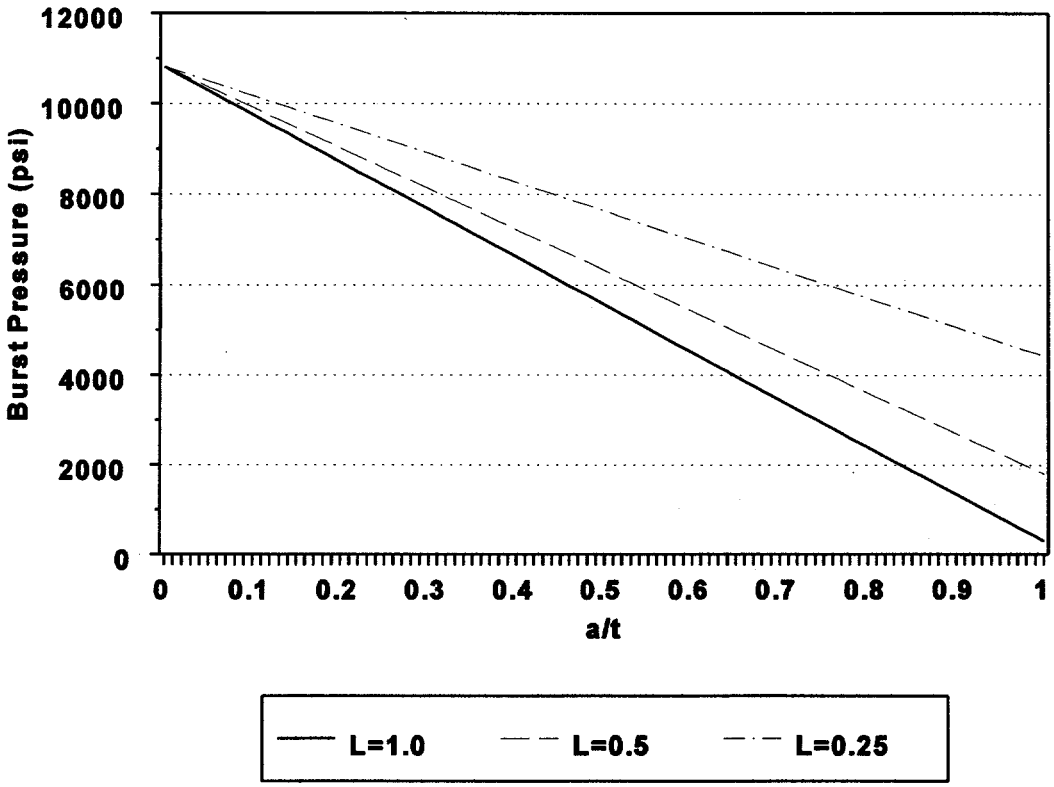

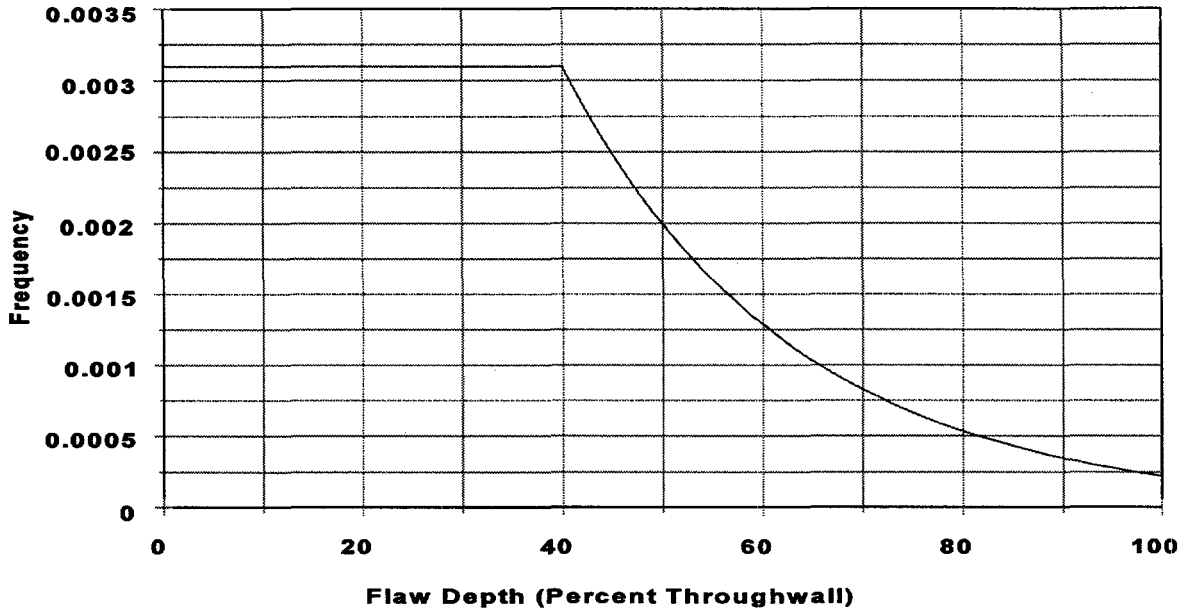

Figure 4.2 Frequency vs. Flaw Depth for Plants with Low Susceptibility (1-inch long flaws)

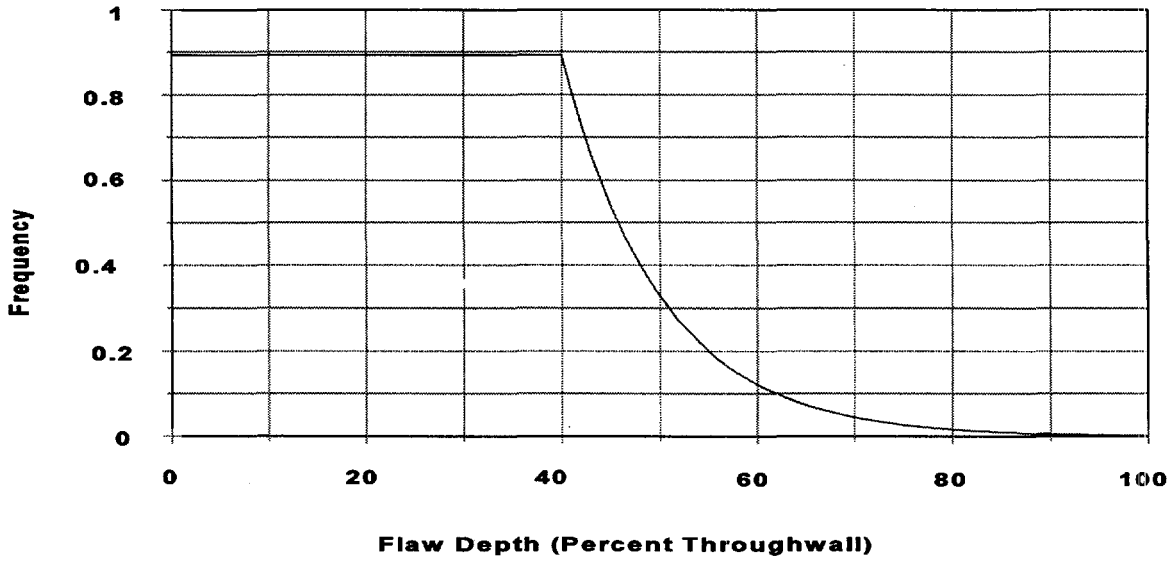

Figure 4.3 Frequency vs. Flaw Depth for Plants with Medium Susceptibility (0.5-inch long flaws)

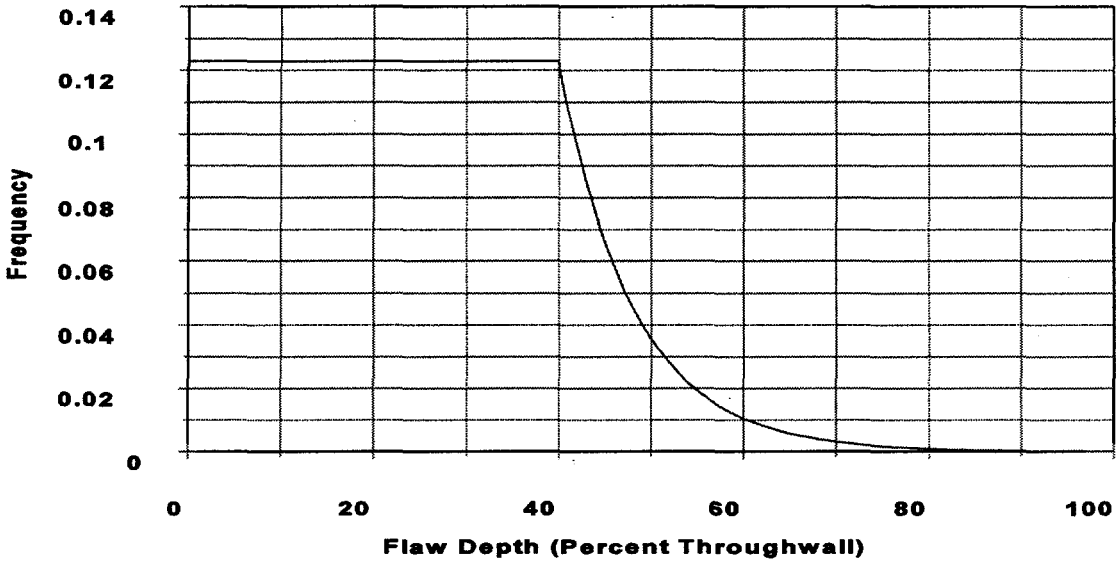

Figure 4.4 Frequency vs. Flaw Depth for Plants with Medium Susceptibility (1-inch long flaws)

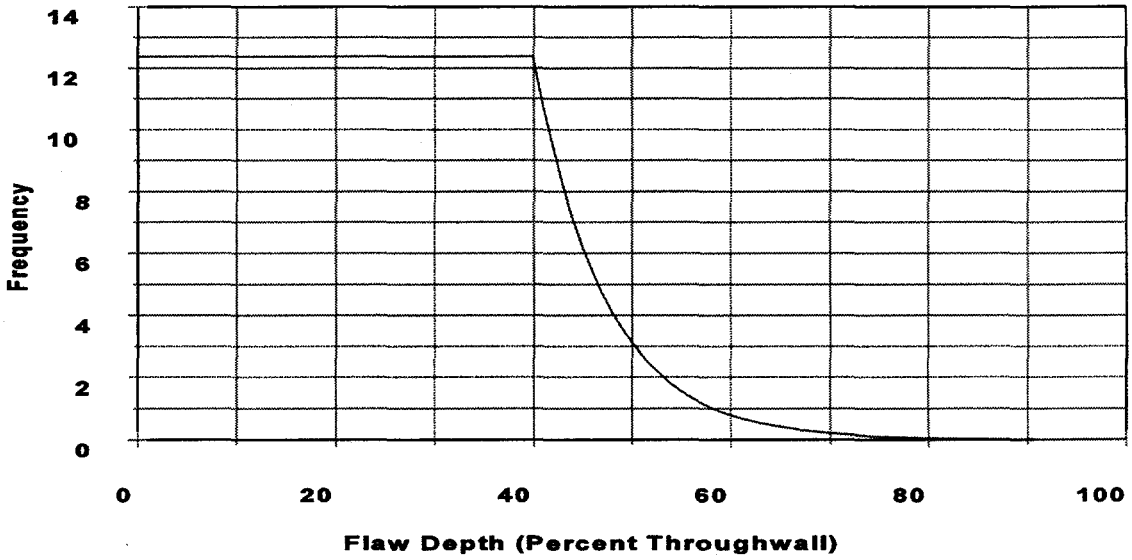

Figure 4.5 Frequency vs. Flaw Depth for Plants with High Susceptibility (0.5-inch long flaws)

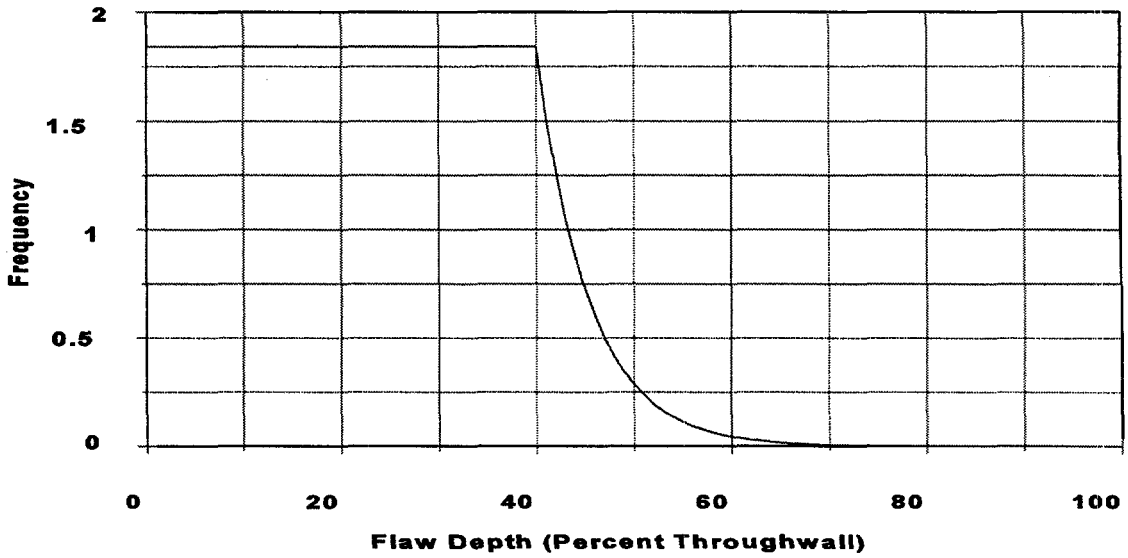

Figure 4.6 Frequency vs. Flaw Depth for Plants with High Susceptibility (1-inch long flaws)

Figure 4.7 Freespan Defect Length vs. Frequency

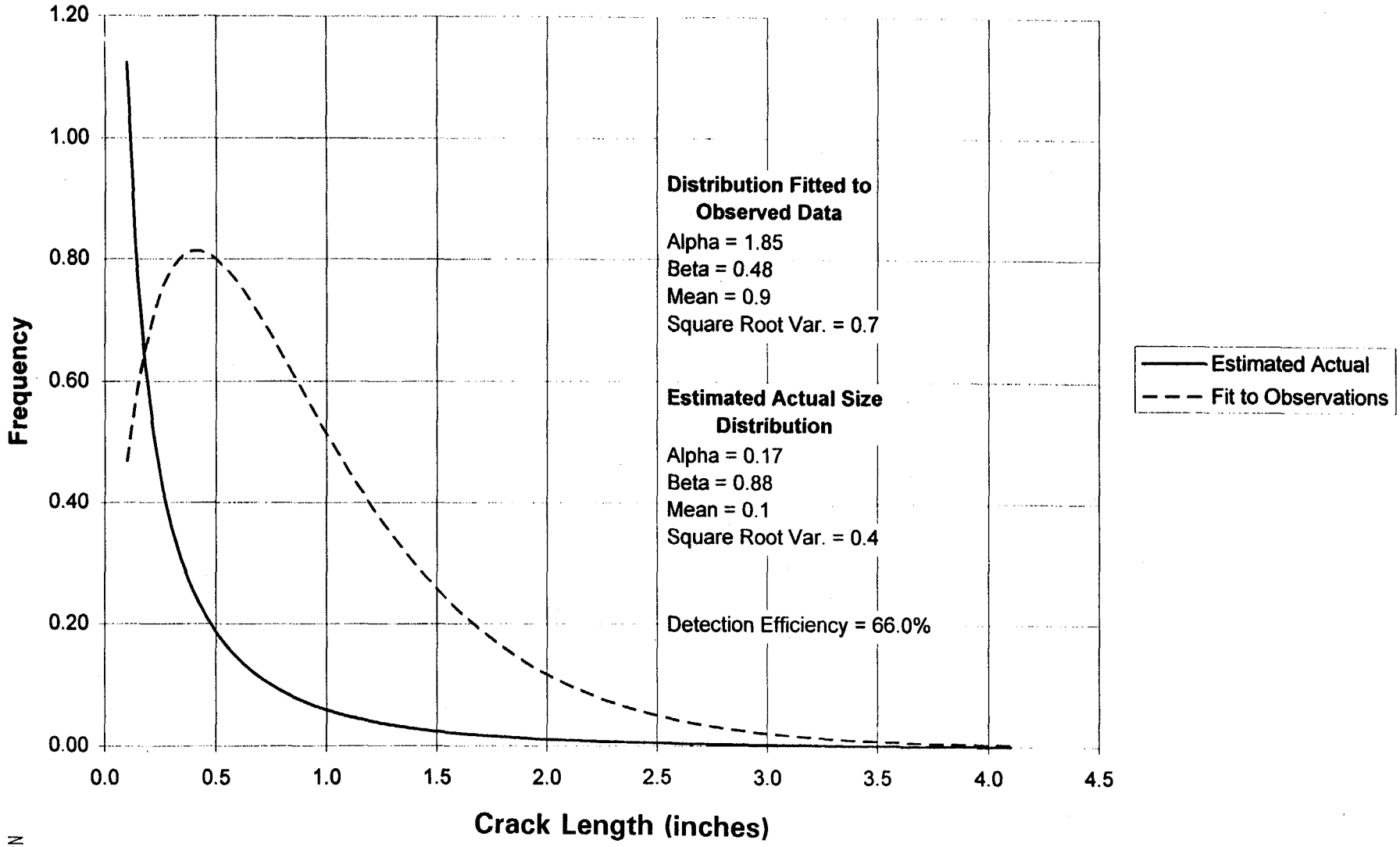

Figure 4.8 Freespan Defect Depth vs. Frequency

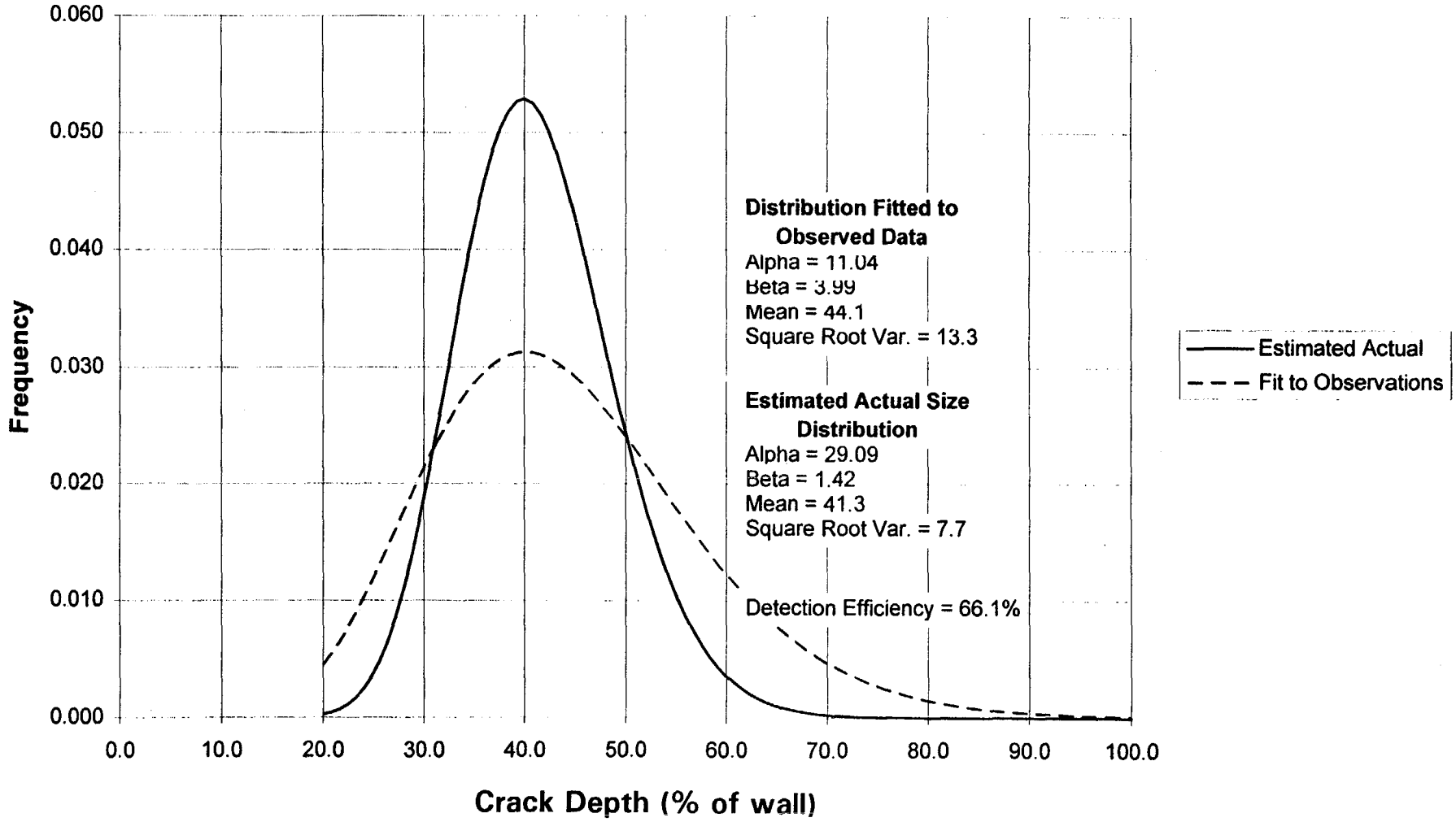

Figure 4.9 Cumulative Depth Distribution for Freespan Cracks

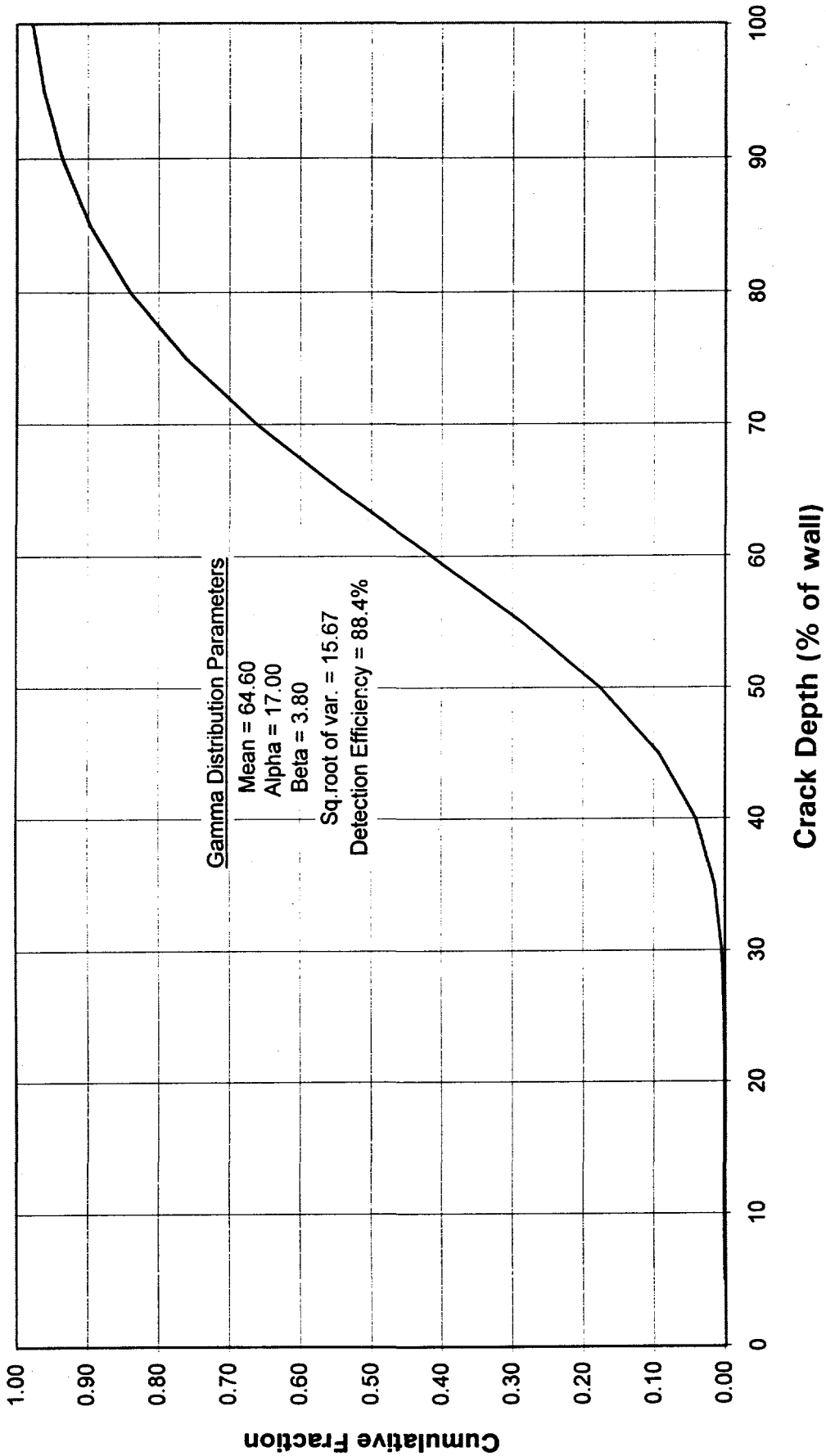

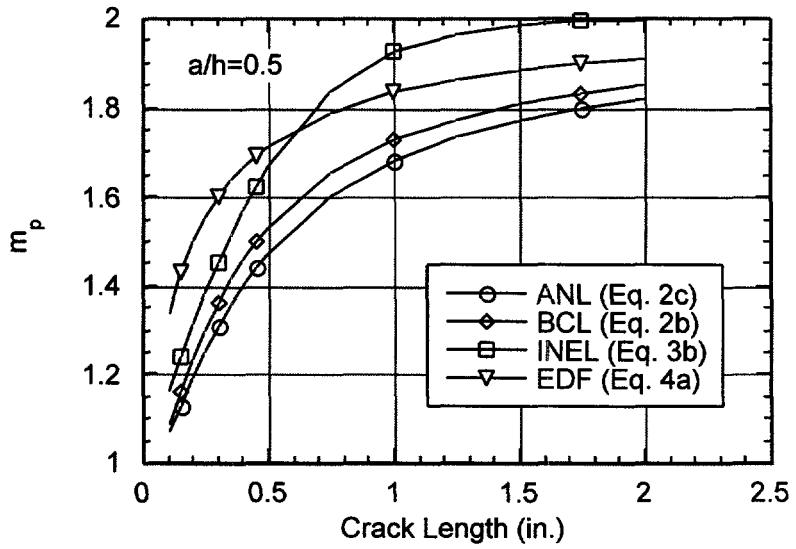

(a)

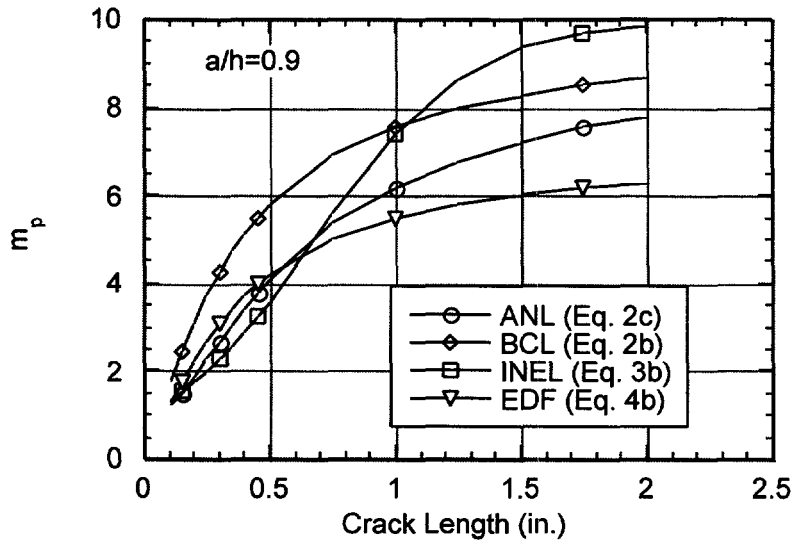

(b)

Figure 4.10 Magnification factor m_p as computed by BCL (Eq. 16b), ANL (Eq. 16c), INEL (Eq. 17b), and EDF Equations (Eqs. 18a-b) as a function of crack length for crack depth-to-thickness ratios (a) a/h=0.5 and (b) a/h=0.9.

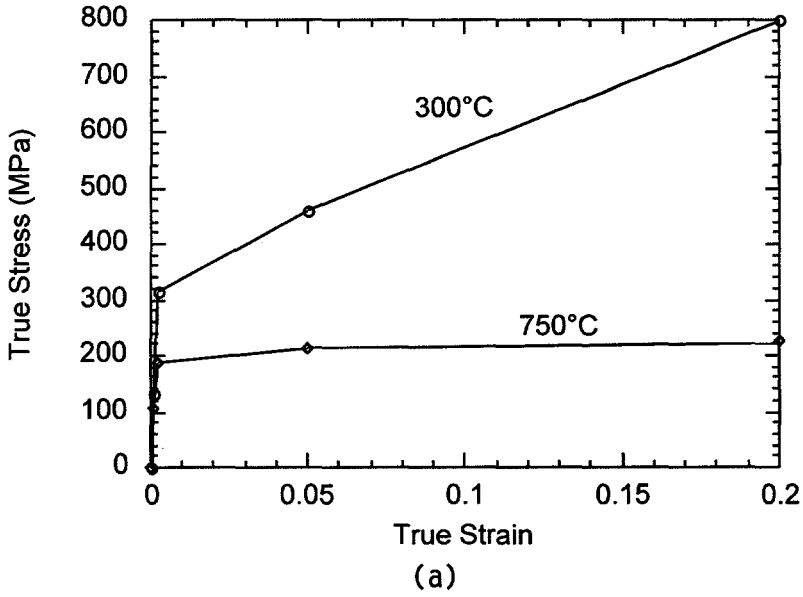

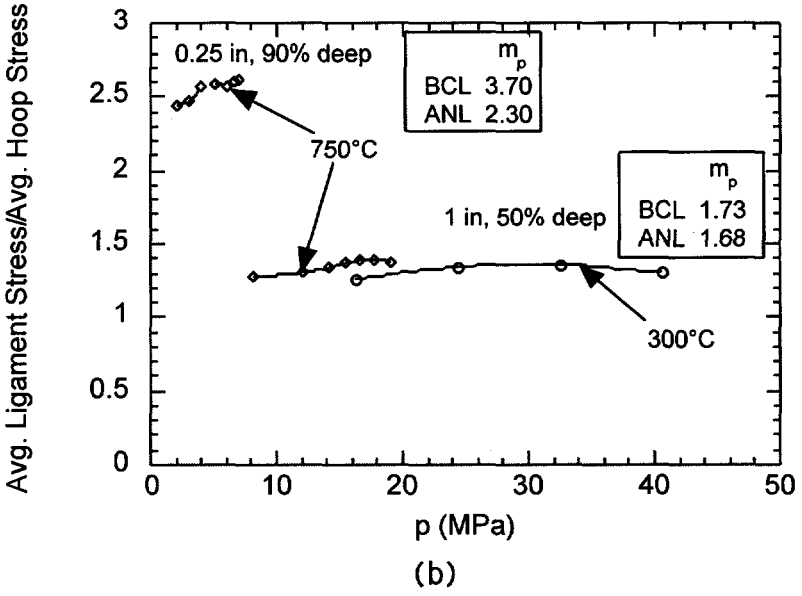

Figure 4.11 (a) True stress-strain curve used in finite-element analysis and (b) variation of calculated hoop stress enhancement factor in the ligament with pressure for a 22 mm (0.875 in.) dia. tube with two axial part-through crack geometries at 300 and 750°C.

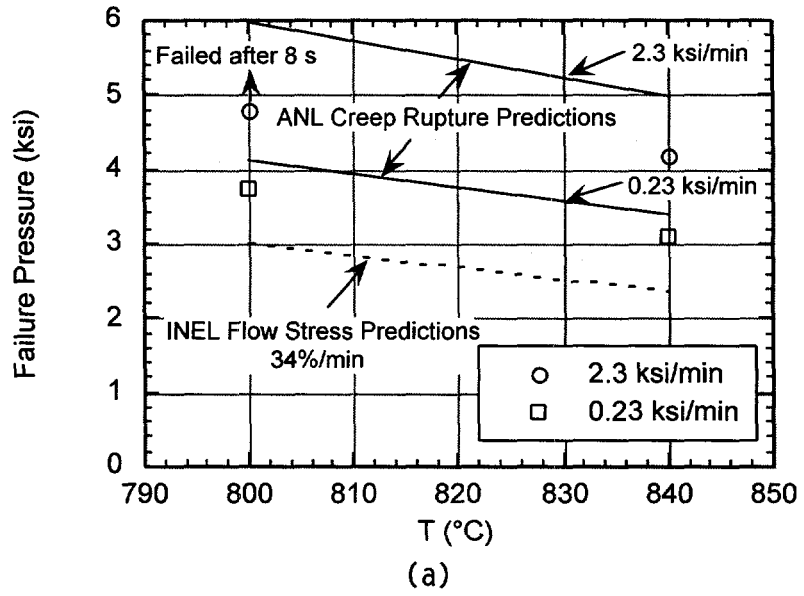

(a)

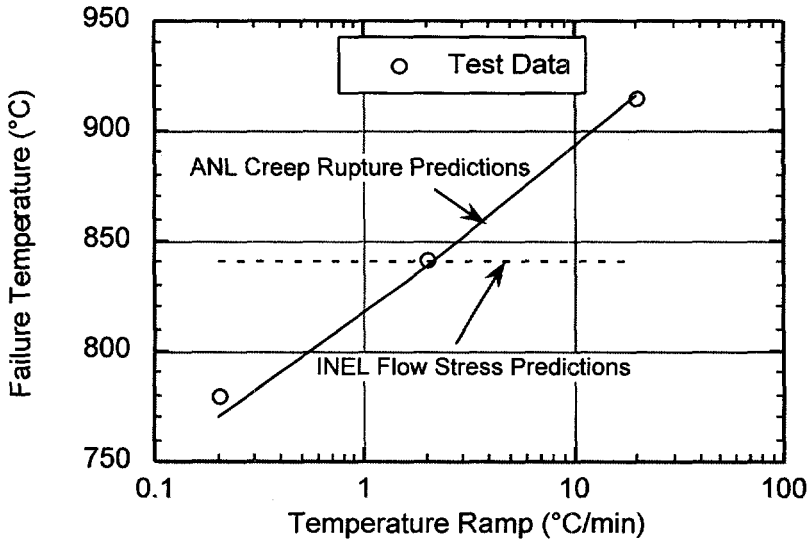

(b)

Figure 4.12 Effects of (a) loading rate on failure pressure in isothermal burst test and (b) temperature ramp on failure temperature in burst test at a constant pressure of 16 MPa (2.35 ksi) of unflawed 22 mm (0.875 in.) dia.Alloy 600 tube. Also shown are predicted failure pressures and temperatures by flow stress model (dashed lines) using INEL flow stress curve and by ANL creep rupture model (solid lines).

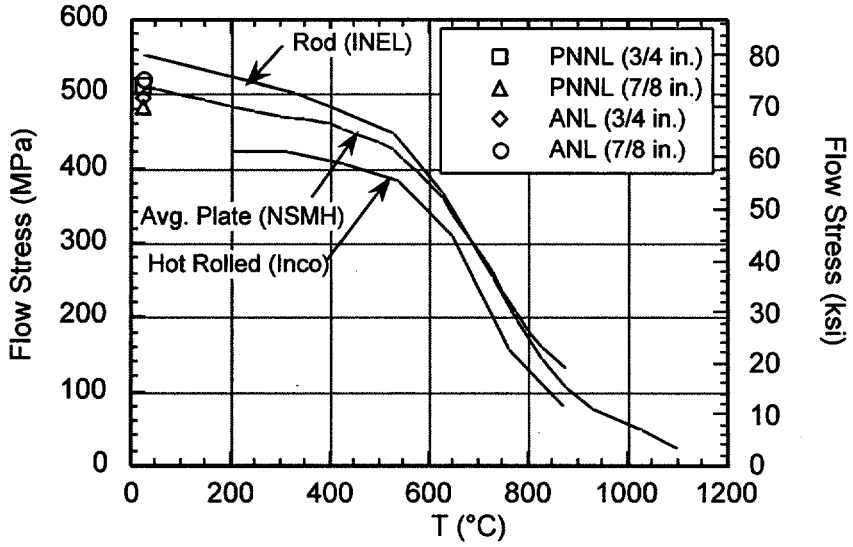

Figure 4.13 Flow stress curves (using k=0.5) for various product forms of Alloy 600

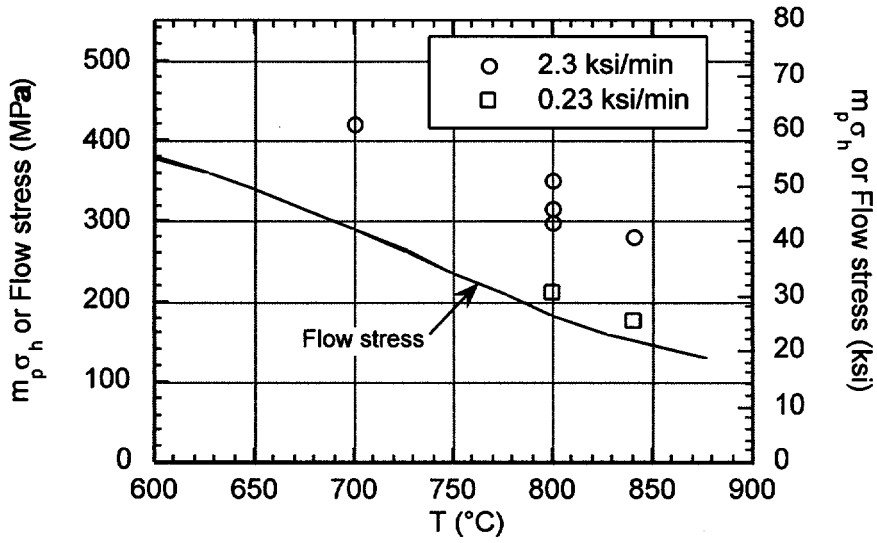

Figure 4.14 Comparison of flow stress curve with pressure ramp test results on flawed and unflawed tubes.

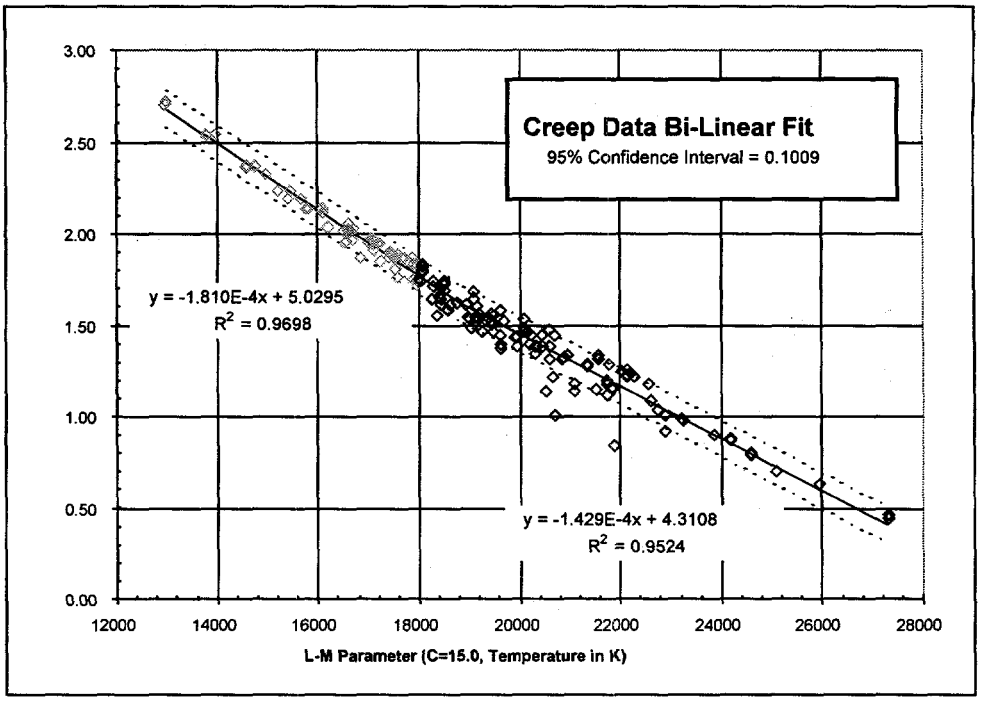

Figure 4.15 Bilinear Fit to Existing Creep Data for Alloy 600 (The three low outliers were not included in the analysis.)

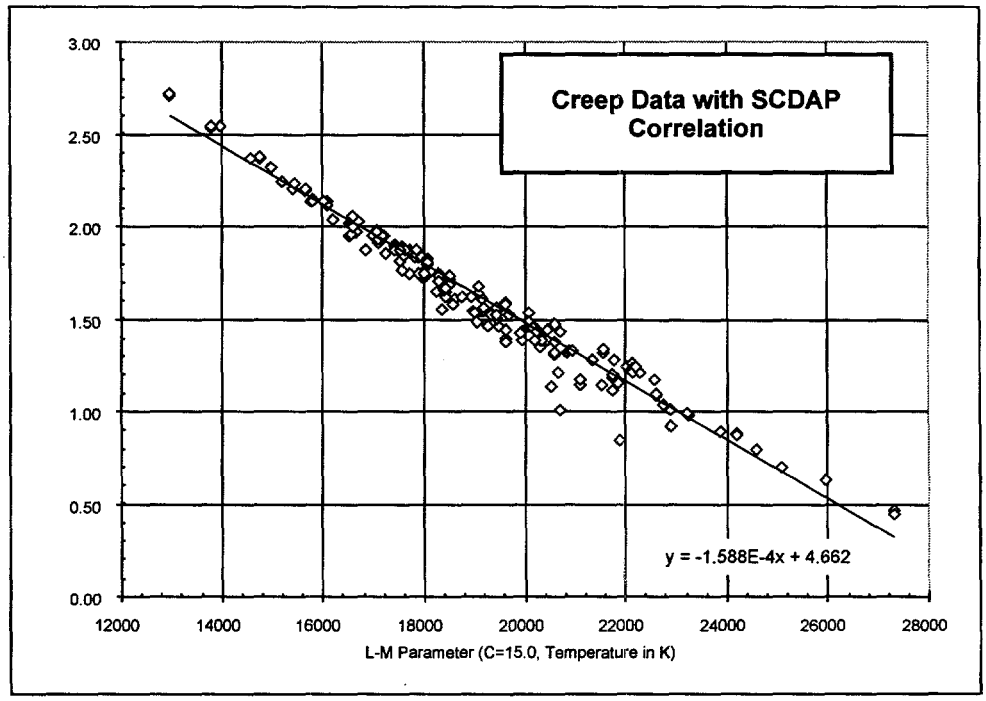

Figure 4.16 Comparison of the Current Correlation Used in SCDAP with existing data

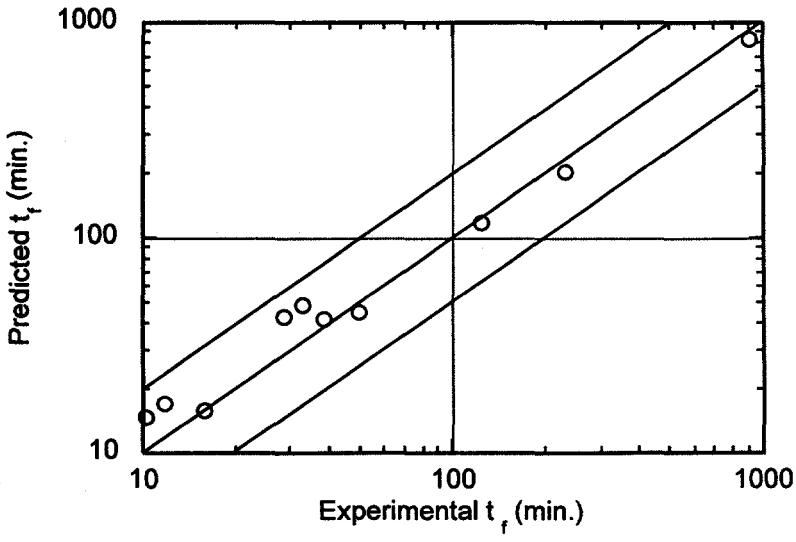

Figure 4.17 Comparison of experimental and predicted times to rupture of unflawed Alloy 600 tubing under constant internal pressure (Tests were conducted isothermally and under constant temperature ramps of 0.2°C/min., 2°C/min., and 20°C/min.)

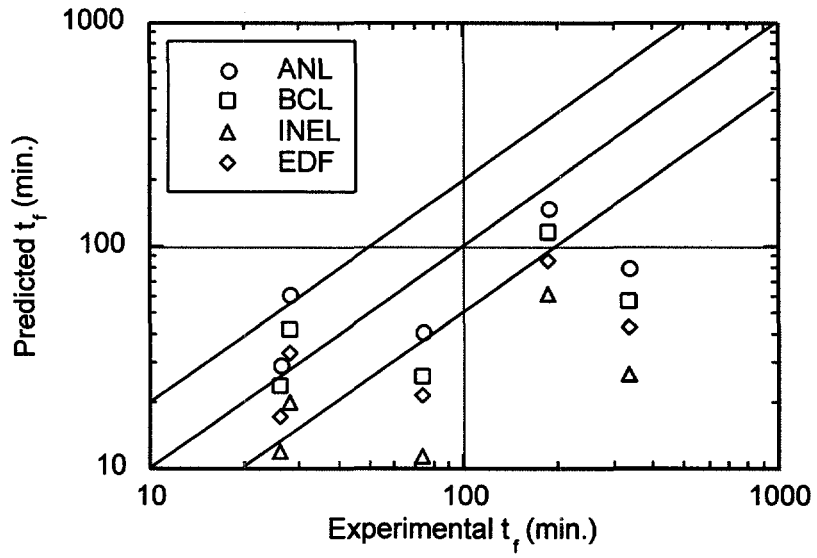

(a)

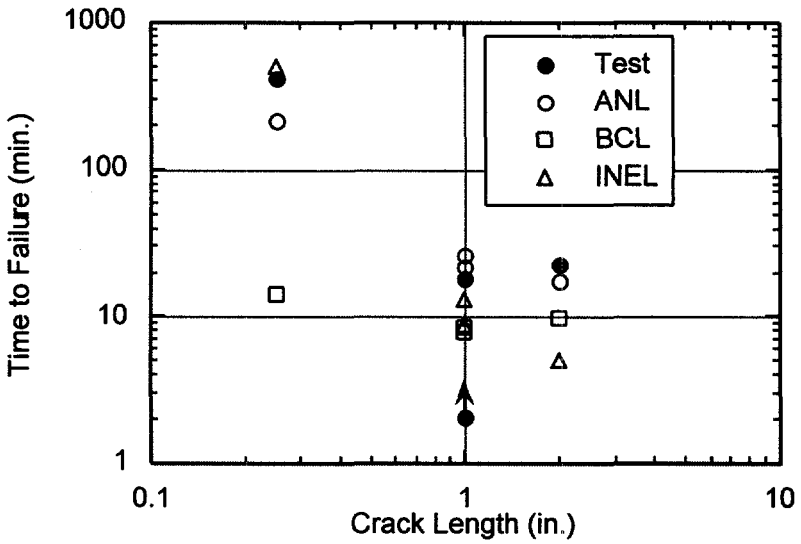

(b)

Figure 4.18 Comparison of experimental and predicted rupture times of flawed Alloy 600 tubing tested isothermally under constant internal pressure, for (a) shallow flaws 25 mm (1 in.) long and ranging from 56% to 65% deep, at temperatures between 667°C and 800°C and (b) deep flaws between 90% and 92% deep at a temperature of 800°C. Arrow indicates pin-hole failure in which pressure was undiminished after failure, during interrupted test.

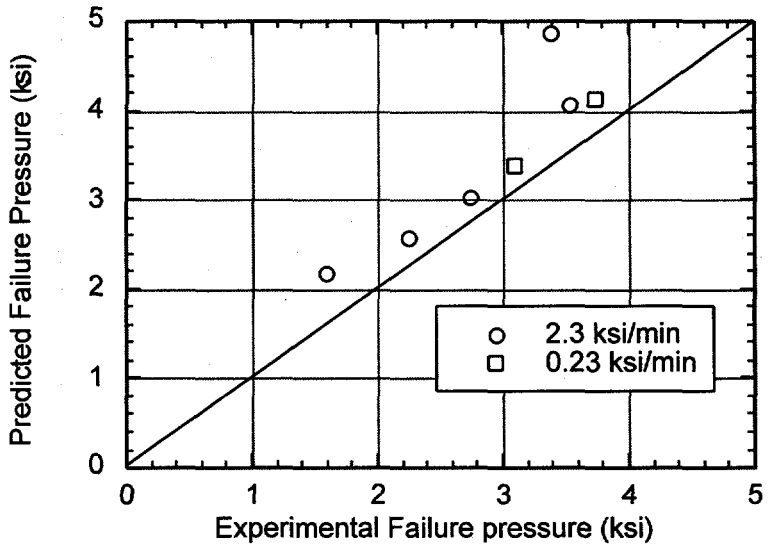

(a)

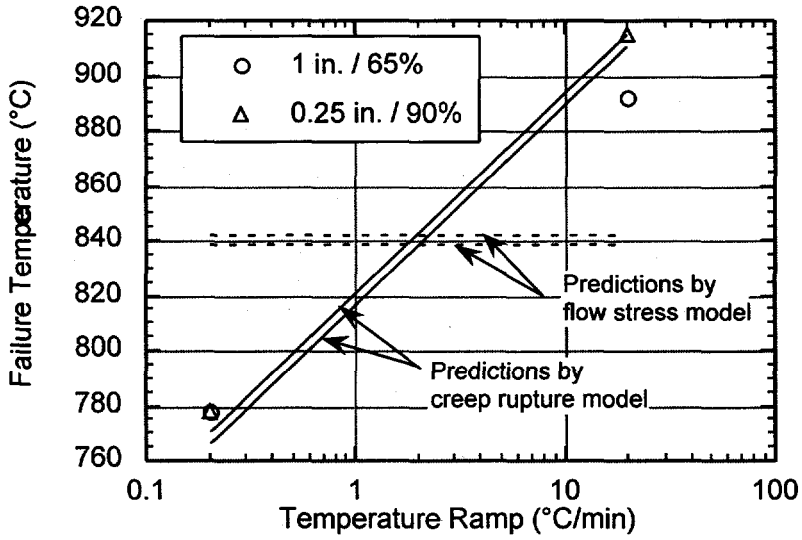

(b)

Figure 4.19 Comparison of experimental and predicted (a) failure pressures of flawed and unflawed tubes subjected to two pressure ramps isothermally at 700 - 840°C and (b) failure temperatures of flawed tubes subjected to two temperature ramps with constant internal pressures chosen such that the product of m_p and nominal hoop stress were kept approximately constant

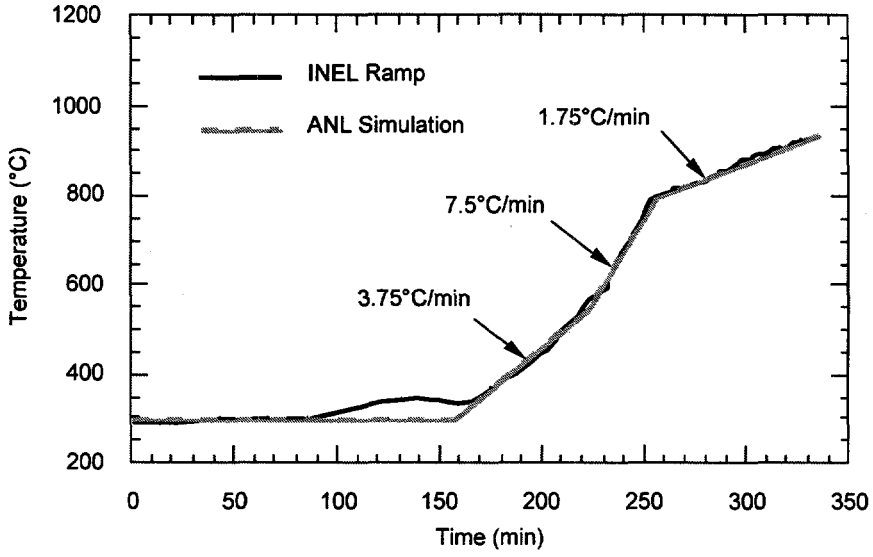

(a)

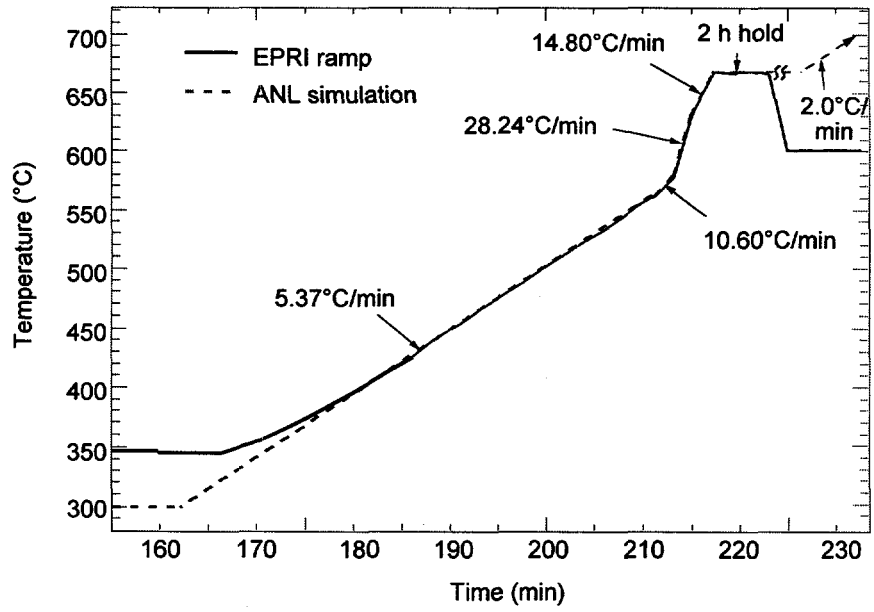

(b)

Figure 4.20 Calculated and ANL simulation of (a) INEL and (b) EPRI temperature ramps

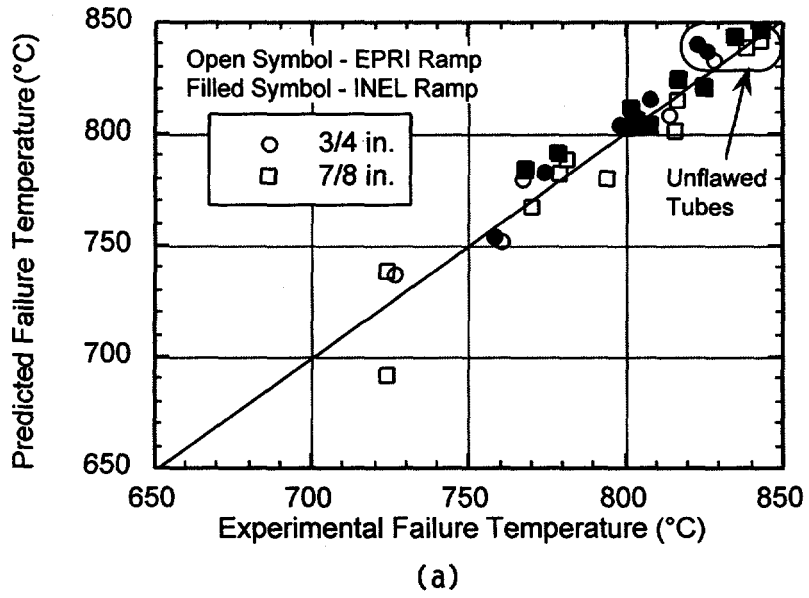

(a)

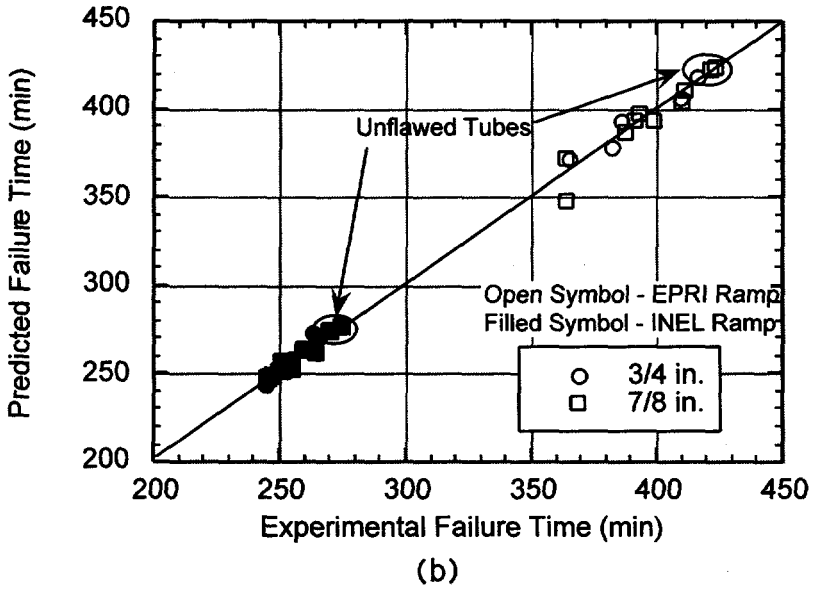

(b)

Figure 4.21 Comparison of predicted (by creep rupture model) and observed (a) failure temperatures and (b) times to failure for high-temperature rupture tests conducted with the INEL and EPRI temperature ramps.

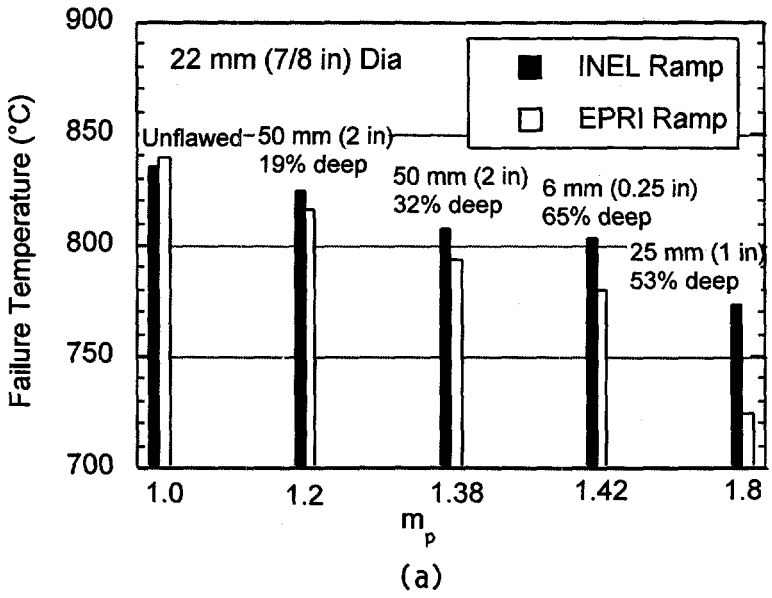

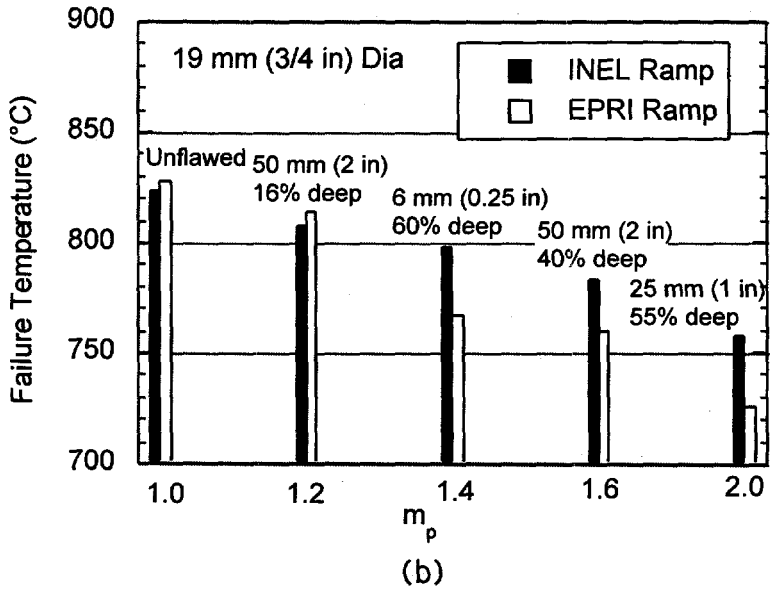

Figure 4.22 Summary of experimentally observed failure temperatures for the severe accident tests on the (a) 22 mm (0.875 in) tubes and (b) 19 mm (0.75 in) tubes (The abscissa shows average magnification factors (Eq. 17b) m_p for each crack configuration.)

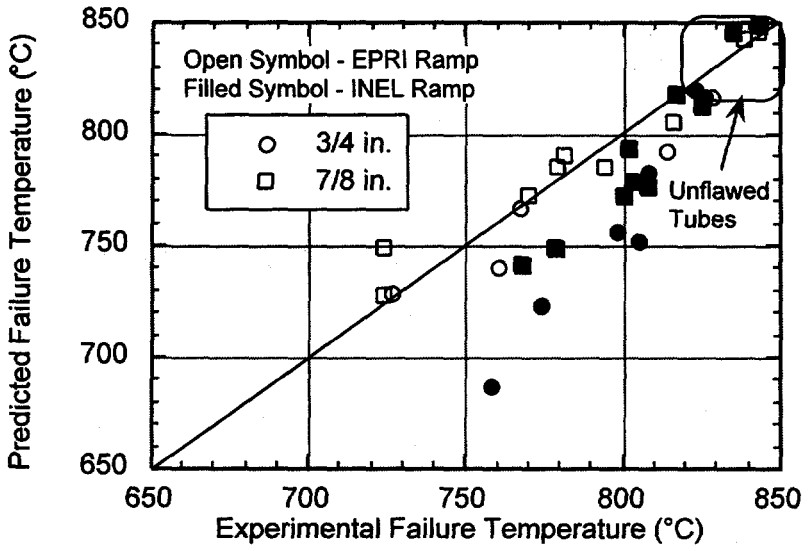

(a)

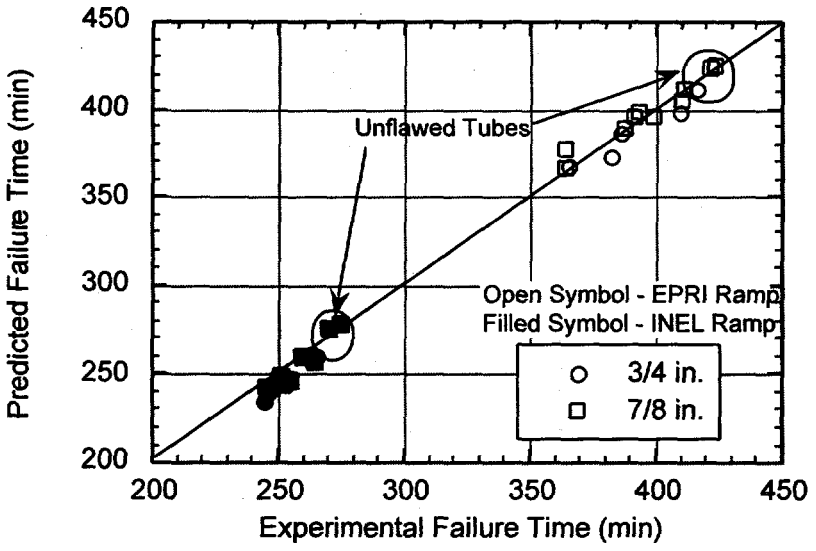

(b)

Figure 4.23 Comparison of predicted (by flow stress model) versus observed (a) failure temperatures and (b) times to failure for high-temperature rupture tests conducted with the INEL and EPRI temperature ramps.

5 RESULTS

This section draws upon material from the previous sections, using insights from thermal-hydraulic calculation results in Section 3 and modeling of tube high-temperature performance in Section 4 to complete quantification of the accident progression event tree assembled in Section 2. Section 5.1 discusses how the thermal-hydraulic results were applied to the APET. Section 5.2 provides the methods used to calculate estimated tube failure probabilities for the conditions assigned each APET endstate. Section 5.3 compiles the containment bypass frequency for the example, on the basis of the tube failure probability estimates associated with the endstates. Section 5.3 also details sensitivity studies performed using the APET and their impact on the containment bypass frequency estimate.

5.1 Final Event Tree Quantification

To arrive at an estimate of containment bypass probability, the staff found it necessary to quantify portions of the APET that were not previously addressed in this study using available component failure data or estimates. This final quantification process depended on assigning appropriate thermal-hydraulic cases to best represent the expected conditions for each endstate. Also, the staff needed to choose SG flaw distributions in order to generate the pressure-induced tube failure probability and then the temperature-induced failure probability. The following sections discuss this in greater detail.

5.1.1 Representative Sequences for APET Branches

For each branch of the APET, the staff selected a single accident sequence to represent the family of sequences defined by that branch. As part of the selection process, the staff considered the set of SCDAP/RELAP5 calculations completed for Surry, and identified those sequences that most closely matched the APET top event outcomes. For a limited number of branches where no suitable sequence analyses were initially available, the staff defined and evaluated additional sequences using SCDAP/RELAP5. The sequence that either directly reflects or conservatively represents the outcome of each top event on the branch was selected to represent each APET branch. The selected sequences are identified in the fourth column of Table 5.1a.

Several simplifying assumptions were made in assigning representative sequences in the analysis. In some cases further evaluations are still in progress or planned, as follows:

- Events with early and late failure of PORVs are represented by a single case with failure to reclose late in the event. As previously discussed, the timing of valve failure does not result in significantly different RCS pressure at the time of core damage. The staff based this finding on analyses performed for a short-term SBO sequence, but the finding would generally be applicable to long-term SBO sequences as well, since the conditions in the RCS at the onset of RCS boildown and PORV cycling (i.e., time of SG dryout) would be similar for short- and long-term SBO events.

- Cases with failure of one ADV (one SG depressurized and the remaining SGs intact) have been used to represent APET branches with different pressure conditions on the secondary side. For example, the thermal-hydraulic results for the intact loops in Case 6N are applied to the APET branch representing the situation with all SGs intact. Similarly, the thermal-hydraulic results for the depressurized loop in

Table 5.1a Probabilities of TI-SGTR for Relevant APET Branches

APET Sequence No.[1]	Primary Status	Secondary Status (No.of SGs Depressurized)	Basis for Probability [3]	Failure Probability[4]
1/**2**	Intact	None	3 x $1R_I$	0.0173
3/**4**, 22/**23**	"	1 SG	1 x $3R_D$	0.0791
6/**7**, 25/**26**	"	2 SG	$(1x3R_D+3x7R_D)/2$	0.0970
9/**10**, 28/**29**, 44/**45**	"	3 SG	3 x $7R_D$	0.1150
12	S/O PORV - Late	None	3 x $6N_I$	Note 5
13/**14**, 31/**32**	"	1 SG	1 x $6N_D$	0.0184
16/**17**, 34/**35/36**	"	2 SG	2 x $6N_D$	0.0365
19/**20**, 39/**40/41**, 47/**48**	"	3 SG	3 x $6N_D$	0.0542
83	S/O PORV - Early	None	3 x $6N_I$	Note 5
84/**85**, 93/**94**	"	1 SG	1 x $6N_D$	0.0184
87/**88**, 96/**97/98**	"	2 SG	2 x $6N_D$	0.0365
90/**91**, 101/**102/103**, 106/**107**	"	3 SG	3 x $6N_D$	0.0542
50	RCP Seal LOCA	None	2 x $9R_{I/I}$ + $9R_{I/C}$	Note 5 *0.137*
51/**52**, 62/**63**	"	1 SG	$9R_{D/I}$+$9R_{I/I}$+$9R_{I/C}$	0.392 *0.401*
55/**56**, 67/**68/69**	"	2 SG	2 x $9R_{D/I}$ + $9R_{I/C}$	0.582 *0.585*
59/**60**, 75/**76/77**, 80/**81** (See note 2)	"	3 SG	$9R_{D/C}$	1.0 *1.0*

1 - Sequences in bold result in bypass.
2 - The following sequences result in concurrent SG depressurization and loop seal clearing and were assigned a 1.0 failure probability: 53, 57, 60, 65, 71/72, 76/77, 81
3 - 1R, 3R, 7R, 6N, and 9R refer to thermal-hydraulic cases described in Section 3. Subscripts refer to specific SG loops as follows:
  I - loop with intact SG (and intact loop seal)
  D - loop with depressurized SG (and intact loop seal)
  I/I - loop with intact SG and intact loop seal
  I/C - loop with intact SG and cleared loop seal
  D/I - loop with depressurized SG and intact loop seal
  D/C - loop with depressurized SG and cleared loop seal
4 - Values in italics reflect recent corrections which are not reflected in the results in Section 5.3.
5 - Not Calculated. This failure was considered unlikely based on early work, and is not modelled in the APET.

Case 6N are applied to APET branches on which one SG is depressurized, as well as branches on which all SGs are depressurized. In the latter case, the probability of temperature-induced SG tube rupture (TI-SGTR) is adjusted to account for multiple SGs being depressurized.

This simplification is justified for Surry on the basis of a comparison of the probability of TI-SGTR between cases with no SGs, one SG, and all SGs depressurized, which shows the following probabilities:

(1) The probability of TI-SGTR in a depressurized loop in Case 7R (intact primary side, all SGs depressurized) is roughly equivalent to but conservatively bounded by the probability of TI-SGTR in the depressurized loop in Case 3R (intact primary side, one SG depressurized).

(2) The probability of TI-SGTR in an intact loop in Case 3R is roughly equivalent to

the probability of TI-SGTR in an intact loop in Case 1R (intact primary side, all SGs intact).

Table 5.1b Probabilities of PI-SGTR for Relevant APET Branches

APET Sequence #	# of SGs Depressurized	Failure Probability
5, 15, 24, 33, 54, 66, 86, 95	1	0.0549
8, 18, 27, 37/38, 58, 73/74, 89, 99/100	2	0.107
11, 21, 30, 42/43, 46, 49, 61, 78/79, 82, 92, 104/105, 108	3	0.156

- Cases representing a range of possible SG leakage rates are not included. Further calculations to explore the impact of SG tube leakage are planned. The results of such calculations should be reflected in the event tree if accident progression and SG tube challenge are substantially different for these events.

- Cases representing the range of likely RCP seal LOCA times and leak rates are not included. Different assumptions regarding LOCA sizes and timing could substantially alter the estimated likelihood of temperature-induced SGTR, particularly if loop seal clearing is not observed or is judged unlikely for other seal LOCA scenarios. Further calculations are planned to explore the impact of RCP seal LOCA assumptions. The results of such calculations should be reflected in the event tree if accident progression and SG tube challenge are substantially different for these events.

- Cases representing events with a concurrent RCP seal LOCA and open pressurizer PORV are not included. Although no events involving both a stuck open pressurizer valve and a RCP seal LOCA were modeled in NUREG-1150, these events are not mutually exclusive and can occur together, particularly if the PORVs are manually opened as an accident management measure. Further calculations are planned to explore the impact of an open PORV on the thermal-hydraulic response during an RCP seal LOCA event. The results of such calculations should be reflected in the event tree if accident progression and SG tube challenge are substantially different for these events.

The validity of these assumptions, as well as results from an expanded set of thermal-hydraulic analyses, would need to be further evaluated as part of a more complete analysis for other plants.

5.1.2 SG Flaw Distributions

The staff separately quantified the probability of flawed tube failure assuming different SG flaw distributions. The distributions were selected to encompass the range of SG degradation mechanisms and tube conditions relevant to operating PWRs, and can be broadly interpreted as representing plants with SGs that are in good, average, or poor condition. The region of interest in this analysis was limited to the freespan between the tube sheet and the second tube support plate, and within that region, to the tubes that carry outflow from the SG inlet plenum. The focus was limited to this region of the SG because tube temperatures are at maximum values there. As discussed in Section 3, peak tube temperatures drop off rapidly at higher elevations in the SG outflow tubes, and are lower in SG tubes that carry return flow. The number, depth, and length of flaws within this region are

accounted for in each distribution, on a per-SG basis. The specific distributions considered are presented and described in Section 4. The base-case APET quantification was established on the basis of the flaw distribution developed by RES for a plant with "moderate" SG tube degradation. In addition, the staff explored the impact of alternative flaw distributions on containment bypass frequency via a sensitivity study, as described in Section 5.4.

5.1.3 Probability of TI-SGTR for Representative Sequences

For each representative sequence, the staff generated separate pressure/temperature histories for piping/components in each RCS loop. These profiles were used in conjunction with the SG flaw distributions and the structural failure criteria (discussed in Section 4) to develop estimates of the time to failure for each RCS loop under its respective thermal-hydraulic conditions.

The staff then determined the probability that a flawed SG tube would fail before temperature-induced failures occur elsewhere in the RCS (i.e., in a hot leg or the surge line). The basis for this determination was an assessment of relative times to failure for the various components and SG tubes. The impact of uncertainties in SG tube material properties, dimensions, and differential pressure was explicitly incorporated into the analysis. By contrast, the impact of uncertainties in thermal-hydraulic analyses and flaw distribution estimates were addressed via sensitivity studies. The methodology for calculating the SG tube failure probability is described in Section 5.2. Supporting sensitivity analyses are described in Sections 3.3 and 5.3.

The probabilities of a thermally induced tube rupture in each SG loop are provided in Table 5.2 for each representative sequence, on the basis of the RES-developed flaw distribution for a plant with moderate SG tube degradation. These failure probabilities were assigned to the various branches of the APET, as described below.

5.1.4 Probability of TI-SGTR for APET Branches

To determine the probability of TI-SGTR for each APET branch, the staff considered the number of intact and depressurized SGs and appropriately combined the predicted probabilities of failure under each condition. For example, the APET branch leading to sequence 48 on Figure 2.3b was assigned a probability of 0.0542 ($P = 1-[1-0.0184]^3$), or essentially three times the estimated probability of TI-SGTR for a single depressurized SG in Case 6N, since this branch involves depressurization of all three SGs. The basis for the probability of TI-SGTR for each APET branch is summarized in the fourth column of Table 5.1a.

For APET branches involving depressurization of one or more SGs, the probability of TI-SGTR in the depressurized loop generally dominates the probability of TI-SGTR for that branch (resulting from the higher tube temperatures and differential pressures under depressurized conditions), with the intact loops having only a minimal probability of failure. An exception to this is the RCP seal LOCA sequence (Case 9R) in which loop seal clearing can occur. Accordingly, the probability of TI-SGTR in Case 9R is based on the combined probability of TI-SGTR in each of the loops. The assigned probabilities of TI-SGTR are summarized in the fifth column of Table 5.1a for relevant APET branches.

Table 5.2 Estimated Probabilities of TI-SGTR for Intact and Depressurized SG Loops (RES "Moderate" Flaw Distribution)[1]

Case	Probability of TI-SGTR (per SG)	
	Intact SG Loop	Depressurized SG Loop
1R	0.0058	Not Applicable
3R	- Note 2 -	0.0835
7R	Not Applicable	0.0399
6N	- Note 2 -	0.0184
9R	0.0 [0.115][3] *0.0088 [0.121]*[4]	0.313 [1.0][3] *0.313 [1.0]*[4]

1 - Except as noted for Case 9R, all sequences involve intact RCS loop seals.
2 - Not calculated; estimated to be similar to the value calculated for Case 1R
3 - Values in brackets represent probability of TI-SGTR given concurrent clearing of the RCS loop seals in the same SG.
4 - Values in italics reflect results of recent corrections. The results provided in Section 5.3 were not updated to reflect these changes.

The probability of pressure-induced tube rupture (PI-SGTR) is addressed for each APET branch in which the primary system is intact and one or more SGs are depressurized in the same time frame (early or late, as depicted in the icon on Figures 2.3a through 2.3d). The probability is also addressed for sequences involving an open pressurizer PORV or RCP seal LOCA (in conjunction with a depressurized steam generator) on the assumption that secondary side depressurization precedes the occurrence of these events and results in a pressure challenge to the SG tubes before the stuck-open relief valve (SORV) or seal LOCA can effectively reduce the primary system pressure. The probability is quantified on the basis of the probabilistic, limit-load calculation methodology and associated secondary system input parameters described in Section 5.2, in conjunction with the RES-developed flaw distribution for SGs with "moderate" degradation. The probability of a PI-SGTR is estimated to be 0.0549, 0.107, and 0.156 for events/APET branches involving depressurization of one, two, or three SGs, respectively. The assigned probabilities of PI-SGTR are summarized in Table 5.1b for relevant APET branches.

5.2 Estimation of Conditional Failure Probabilities for SG Tubes

The following sections describe the methods used to estimate the failure probability of flawed tubes. The calculational method uses the predicted thermal hydraulic conditions and the assumed tube degradation (depicted by the flaw population). The calculated tube failure probabilities are later used to estimate the containment bypass probability.

5.2.1 Methodology

For each sequence in the event tree, the staff performed a thermal-hydraulic calculation using the SCDAP/RELAP5 code to establish a record of temperature and differential pressure as functions of time for each component of interest. The SCDAP/RELAP5 code also produced a creep damage index as a function of time for these components, assuming specific dimensions, material properties, and the absence of flaws such as cracks. In previous studies, components were assumed to fail when their nominal creep damage indices reached a value of

1. However, the presence of preexisting flaws in the SG tubes would cause the tubes to fail at earlier times. In addition, the variability of the component dimensions and material properties will produce a probability distribution for the time of failure for each component. It is necessary to consider the probability distributions as a function of time for each component of interest, in order to estimate the probability that one or more SG tubes will be the first reactor coolant pressure boundary failure during a particular thermal-hydraulic sequence.

Stand-alone computer codes were developed to compute creep damage indices for certain components, on the basis of the time-dependent temperature and differential pressure files generated by SCDAP/RELAP5. The results of these codes were initially verified against the creep damage index results from SCDAP/RELAP5, using the same component dimensions and material properties used by SCDAP/RELAP5. The creep damage calculations in the stand-alone codes were then extended to cover a variety of component dimensions, material properties, and (for SG tubes) the existence of various flaw sizes.

The CRAB code generates the creep damage index for the surge line or hot leg, using a single value of the Larson-Miller parameter for creep damage and nominal component dimensions. The surge line and hot legs in the Surry plant are stainless steel. The CRAB code uses the thin-walled tube approximation of the creep failure prediction, as in SCDAP/RELAP5. For each thermal-hydraulic case (corresponding to an event tree sequence), the 5, 50, and 95 percentile values of the Larson-Miller parameter correlation were used to generate failure times of the surge line or the hot leg, if it was predicted to fail before the surge line. The resulting times are considered to be associated with probabilities of 95 percent, 50 percent, and 5 percent that the component has not yet failed at that time. A smooth function in time was established by fitting these three values with normal distributions.

Because the temperature of the components of concern is increasing rapidly at their respective times of failure, the later failure times can be closer to the 50 percent probability time than are the earlier times. This behavior was accommodated by fitting the times earlier than 50 percent with one normal distribution and the times later than 50 percent with a different normal distribution. Comparison of the results to a more detailed fit indicates they are accurate enough for the intended use. That use is to provide a probability value for surge line and/or hot leg failure before the time that a particular flawed tube is calculated to fail. Table 5.3 summarizes the times for 5 percent, 50 percent, and 95 percent probability of RCS pressure boundary failures (surge line or hot leg) for each thermal-hydraulic case.

The RCP seal LOCA sequence is an exception to this treatment. As a result of the pressure pulses and associated temperature excursions created by accumulator injection in this case (Case 9R), it was necessary to evaluate the probability of RCS pressure boundary failures as a more detailed function of time. The CRAB program was used to generate failure times for approximately 50 values of the Larson-Miller parameters for the surge line and each of the three hot legs. The resulting four probability distributions for time-to-failure of these components was combined into a single distribution for the probability of first failure of the RCS pressure boundary. This probability-time relationship is shown in Figure 5.1, and the RCS pressure as a function of time is shown in Figure 5.2.

It should be noted that the seal LOCA case (Case 9R) is the only one of the five thermal-hydraulic cases where the probability of a hot-leg failure dominates the probability of RCS pressure boundary failure (excluding tubes). In other cases, the surge line reaches a 95 percent failure probability before the hot legs reach 5 percent. However, thermal-

hydraulic calculations for other plant designs (e.g., Zion DCH study) indicate that the hot legs may fail before the surge line in different designs.

Table 5.3 Time of First RCS Pressure Boundary Failure (in minutes)

Thermal-Hydraulic Case	Probability of Failure		
	5 Percent	50 Percent	95 Percent
1R	234	235	236
3R	241	242	243
6N	231	234	237
7R	212	212	213
9R*	289	290	291

* Note that tube temperatures do not rise monotonically for this case.

The RCS pressure boundary failure information generated with the CRAB code is one input to the CRPROB code, which yields estimates of failure probability for specific SG tube flaws before the failure of the surge line or a hot leg. Probability estimates are produced for a specified set of flaws (length and depth) for each thermal-hydraulic case. The CRPROB code uses Monte Carlo methodology to combine the effects of tube diameter and thickness variability, Larson-Miller creep behavior variability, and the range of crack lengths and depths that are binned together in the flaw population size distribution for a representative plant.

The tube dimension variability is provided in the form of histograms developed from measurements of 9977 tubes made at Valinco NSSS Metal Products (Chavez, 1996). These histograms are independently sampled by selecting two random numbers. The variability of the Larson-Miller parameter for the tube material (Inconel 600) was determined by surveying nine data sources as the 95 percent and 5 percent bounds on the properties exhibited in a total of 233 monotonic failure tests. The CRPROB program uses a normally distributed random number to sample the distribution, with the values restricted to the range between 1 and 99 percent on the distribution tails.

Although temperature variations undoubtedly occur among tubes according to their respective position in the tube sheet, the temperature distribution is not established. As a result, the staff used the average temperature for the group of tubes that carry convective flow from the hot leg plenum to the cold leg plenum (35 percent of the tubes in each steam generator). Because creep damage is highly nonlinear with temperature, this simplification may not be conservative. SCDAP/RELAP5 does model the temperature variation along the length of the tubes. However, because most of the cracks are thought to be in the sludge pile area, and each segment of a tube would require individual Monte Carlo analysis of the creep damage failure time, all cracks were modeled as occurring in the tube segment directly above the tube sheet on the hot leg side. This is a conservative assumption because that is the hottest segment of the tube.

The crack dimensions are varied randomly within the length and depth dimensions associated

with the bins of the flaw distribution specification. Typically, cracks between 20 and 100 percent through-wall are separated into bins with 5 percent depth increments. Crack lengths are separated into the following two bins:

- those that are long enough to fail as ruptures at the pressure differentials associated with depressurization of the secondary side of a SG at normal operating temperatures

- those that would not fail as ruptures under the preceding conditions, but would rupture when the temperatures were elevated by core oxidation during severe accident sequences

The lengths of cracks within those bins were sampled according to the function specified for the length distribution. For each crack dimension bin in the flaw population distribution, probability values were calculated for 1000 or 3000 randomly selected combinations of tube diameter, thickness, Larson-Miller correlation, and crack length and depth. The CRPROB output is the average of the probabilities for each flaw size bin.

Tables 5.4a and 5.4b show these probabilities for each thermal-hydraulic case considered. The probability values in these tables are associated with loops where SGs have depressurized and loop seals have not cleared. (Columns labeled 9Rs represent exceptions, as discussed below.)

For Case 9R, the thermal-hydraulic calculations resulted in clearing one loop seal. That case also had one depressurized SG, but it was not on the loop where the loop seal was cleared. Thus, there are four possible combinations of loop seal and SG secondary integrity to consider. In addition, the columns labeled 9Rs in Tables 5.4a and 5.4b are the results for the loop with a pressurized SG and a cleared loop seal. The case of cleared loop seal with depressurized SG secondary was assumed to fail even unflawed tubes before any other part of the RCS pressure boundary, on the basis of SCDAP/RELAP5 analyses conducted at INEL (Ellison, 1996).

The values in Tables 5.4a-b for Case 9R are also more complicated than for the other cases because two sets of tubes were considered for the loop with the depressurized SG and intact loop seal. As in the other four thermal-hydraulic cases, the staff divided the SG tubes into those that carry hot gas from the hot-leg plenum to the cold-leg plenum (35 percent) and those that carry gas back from the cold-leg plenum to the hot-leg plenum (65 percent). However, the pressure pulses in Case 9R cause both sets of tubes to temporarily flow from the hot-leg plenum to the cold-leg plenum. This allows 100 percent of the tubes to experience hot gases from the hot-leg plenum, but with different time/temperature histories. Figure 5.3 illustrates the temperature histories of both sets of tubes. The values in Tables 5.4a-b are for the hotleg end of each group of tubes.

To calculate the conditional probability of tube rupture during a specific thermal-hydraulic sequence, the staff combined a flaw population size distribution with the rupture probability information for the given sequence. Because the flaw size distributions vary greatly among plants and because different size cracks are poorly distinguished by currently available eddy current inspection techniques, two different methods were used to estimate three different flaw size distributions associated with different degrees of SG tube degradation. The development of the distributions is described in Section 4 of this report, and the numbers of flaws in each size bin of each distribution is provided in Table 5.5.

Table 5.4a Creep Failure Probabilities for Steam Generator Tube Flaws During Specific Thermal-Hydraulic Sequences (On the Basis of NRR Flaw Distribution)

Crack Length (inches)	Crack Depth (percent through wall)	Probability of Failure						
		1R	3R	6N	7R	9Ro	9Rr	9Rs
1.00	0.75 to 0.80	0.000	0.566	0.000	0.132	0.881	0.000	0.078
1.00	0.70 to 0.75	0.000	0.238	0.000	0.012	0.717	0.000	0.026
1.00	0.65 to 0.70	0.000	0.070	0.000	0.000	0.548	0.000	0.000
1.00	0.60 to 0.65	0.000	0.013	0.000	0.000	0.396	0.000	0.000
1.00	0.55 to 0.60	0.000	0.001	0.000	0.000	0.277	0.000	0.000
1.00	0.50 to 0.55	0.000	0.000	0.000	0.000	0.158	0.000	0.000
1.00	0.45 to 0.50	0.000	0.000	0.000	0.000	0.047	0.000	0.000
1.00	0.40 to 0.45	0.000	0.000	0.000	0.000	0.019	0.000	0.000
1.00	0.35 to 0.40	0.000	0.000	0.000	0.000	0.000	0.000	0.000
1.00	0.30 to 0.35	0.000	0.000	0.000	0.000	0.000	0.000	0.000
1.00	0.25 to 0.30	0.000	0.000	0.000	0.000	0.000	0.000	0.000
1.00	0.20 to 0.25	0.000	0.000	0.000	0.000	0.000	0.000	0.000
0.50	0.95 to 1.00	0.588	1.000	0.873	1.000	1.000	0.764	0.937
0.50	0.90 to 0.95	0.000	0.996	0.093	0.902	1.000	0.059	0.505
0.50	0.85 to 0.90	0.000	0.782	0.000	0.339	0.960	0.000	0.167
0.50	0.80 to 0.85	0.000	0.333	0.000	0.034	0.767	0.000	0.036
0.50	0.75 to 0.80	0.000	0.085	0.000	0.001	0.565	0.000	0.000
0.50	0.70 to 0.75	0.000	0.014	0.000	0.000	0.399	0.000	0.000
0.50	0.65 to 0.70	0.000	0.001	0.000	0.000	0.270	0.000	0.000
0.50	0.60 to 0.65	0.000	0.000	0.000	0.000	0.149	0.000	0.000
0.50	0.55 to 0.60	0.000	0.000	0.000	0.000	0.049	0.000	0.000
0.50	0.50 to 0.55	0.000	0.000	0.000	0.000	0.025	0.000	0.000
0.50	0.45 to 0.50	0.000	0.000	0.000	0.000	0.000	0.000	0.000
0.50	0.40 to 0.45	0.000	0.000	0.000	0.000	0.000	0.000	0.000
0.50	0.35 to 0.40	0.000	0.000	0.000	0.000	0.000	0.000	0.000
0.50	0.30 to 0.35	0.000	0.000	0.000	0.000	0.000	0.000	0.000
0.50	0.25 to 0.30	0.000	0.000	0.000	0.000	0.000	0.000	0.000
0.50	0.20 to 0.25	0.000	0.000	0.000	0.000	0.000	0.000	0.000

*Case 9R is divided into three sets of tubes: 9Ro gives the probabilities for "out-flow" tubes that normally flow by convection from the hot-leg plenum to the cold-leg plenum; 9Rr gives the probabilities for the "return" tubes that normally flow convectively from the cold-leg plenum to the hot-leg plenum. 9Rs gives the probabilities for all tubes in a SG that has full-loop natural circulation attributable to loop seal clearing, but with the secondary side pressurized. Table entries for all other cases are for tubes that flow convectively from the hot-leg plenum to the cold-leg plenum. The probability of thermally induced flaw failure is negligible in the "return" tubes for those cases, because of their lower temperatures.

Table 5.4b Creep Failure Probabilities for Steam Generator Tube Flaws During Specific Thermal-Hydraulic Sequences (on the basis of RES Flaw Distribution)

Crack Length (inches)	Crack Depth (percent through-wall)	Probability of Failure						
		1R	3R	6N	7R	9Ro	9Rr	9Rs
≥ 1.00	0.75 to 0.80	0.000	0.745	0.000	0.317	0.961	0.000	0.191
≥ 1.00	0.70 to 0.75	0.000	0.423	0.000	0.085	0.836	0.000	0.095
≥ 1.00	0.65 to 0.70	0.000	0.176	0.000	0.012	0.680	0.000	0.036
≥ 1.00	0.60 to 0.65	0.000	0.053	0.000	0.001	0.556	0.000	0.000
≥ 1.00	0.55 to 0.60	0.000	0.010	0.000	0.000	0.416	0.000	0.000
≥ 1.00	0.50 to 0.55	0.000	0.000	0.000	0.000	0.319	0.000	0.000
≥ 1.00	0.45 to 0.50	0.000	0.000	0.000	0.000	0.215	0.000	0.000
≥ 1.00	0.40 to 0.45	0.000	0.000	0.000	0.000	0.127	0.000	0.000
≥ 1.00	0.35 to 0.40	0.000	0.000	0.000	0.000	0.035	0.000	0.000
≥ 1.00	0.30 to 0.35	0.000	0.000	0.000	0.000	0.000	0.000	0.000
≥ 1.00	0.25 to 0.30	0.000	0.000	0.000	0.000	0.000	0.000	0.000
≥ 1.00	0.20 to 0.25	0.000	0.000	0.000	0.000	0.000	0.000	0.000
0.25 to 1.00	0.95 to 1.00	0.525	0.997	0.899	0.975	1.000	0.933	0.881
0.25 to 1.00	0.90 to 0.95	0.000	0.848	0.492	0.663	0.965	0.647	0.572
0.25 to 1.00	0.85 to 0.90	0.000	0.555	0.000	0.323	0.861	0.295	0.321
0.25 to 1.00	0.80 to 0.85	0.000	0.309	0.000	0.099	0.773	0.000	0.198
0.25 to 1.00	0.75 to 0.80	0.000	0.129	0.000	0.017	0.656	0.000	0.088
0.25 to 1.00	0.70 to 0.75	0.000	0.043	0.000	0.001	0.517	0.000	0.000
0.25 to 1.00	0.65 to 0.70	0.000	0.009	0.000	0.000	0.417	0.000	0.000
0.25 to 1.00	0.60 to 0.65	0.000	0.001	0.000	0.000	0.327	0.000	0.000
0.25 to 1.00	0.55 to 0.60	0.000	0.000	0.000	0.000	0.246	0.000	0.000
0.25 to 1.00	0.50 to 0.55	0.000	0.000	0.000	0.000	0.150	0.000	0.000
0.25 to 1.00	0.45 to 0.50	0.000	0.000	0.000	0.000	0.089	0.000	0.000
0.25 to 1.00	0.40 to 0.45	0.000	0.000	0.000	0.000	0.018	0.000	0.000
0.25 to 1.00	0.35 to 0.40	0.000	0.000	0.000	0.000	0.000	0.000	0.000
0.25 to 1.00	0.30 to 0.35	0.000	0.000	0.000	0.000	0.000	0.000	0.000
0.25 to 1.00	0.25 to 0.30	0.000	0.000	0.000	0.000	0.000	0.000	0.000
0.25 to 1.00	0.20 to 0.25	0.000	0.000	0.000	0.000	0.000	0.000	0.000

*Case 9R is divided into three sets of tubes: 9Ro gives the probabilities for "out-flow" tubes that normally flow by convection from the hot-leg plenum to the cold-leg plenum; 9Rr gives the probabilities for the "return" tubes that normally flow convectively from the cold-leg plenum to the hot-leg plenum. 9Rs gives the probabilities for all tubes in a SG that has full-loop natural circulation attributable to loop seal clearing, but with the secondary side pressurized. Table entries for all other cases are for tubes that flow convectively from the hot-leg plenum to the cold-leg plenum. The probability of thermally induced flaw failure is negligible in the "return" tubes for those cases, because of their lower temperatures.

Table 5.5 Flaw Population Size Distributions
(Number of flaws per plant, distributed by length and depth bins)

Crack Depth (percent through-wall)	NRR Distributions			RES Distributions				
	Length	"Good"	"Average"	"Severe"	Length	"Light"	"Moderate"	"Severe"
0.95 to 1.00	1.00	-	0.00160	0.000717	≥ 1.00	0.00995	0.0216	0.0581
0.90 to 0.95	1.00	-	0.00296	0.00183	≥ 1.00	0.0159	0.0347	0.0932
0.85 to 0.90	1.00	-	0.00447	0.00453	≥ 1.00	0.0242	0.0527	0.142
0.80 to 0.85	1.00	-	0.0101	0.0114	≥ 1.00	0.0355	0.0772	0.207
0.75 to 0.80	1.00	-	0.0187	0.0286	≥ 1.00	0.0484	0.105	0.283
0.70 to 0.75	1.00	-	0.0345	0.0718	≥ 1.00	0.0619	0.135	0.362
0.65 to 0.70	1.00	-	0.0638	0.180	≥ 1.00	0.0735	0.160	0.429
0.60 to 0.65	1.00	-	0.118	0.453	≥ 1.00	0.0799	0.174	0.467
0.55 to 0.60	1.00	-	0.218	1.139	≥ 1.00	0.0784	0.170	0.458
0.50 to 0.55	1.00	-	0.403	2.861	≥ 1.00	0.0682	0.148	0.398
0.45 to 0.50	1.00	-	0.745	7.188	≥ 1.00	0.0517	0.112	0.302
0.40 to 0.45	1.00	-	1.377	8.06	≥ 1.00	0.0325	0.071	0.190
0.35 to 0.40	1.00	-	1.734	5.24	≥ 1.00	0.0165	0.0360	0.0967
0.30 to 0.35	1.00	-	1.734	25.24	≥ 1.00	0.00639	0.0139	0.0373
0.25 to 0.30	1.00	-	1.734	25.24	≥ 1.00	0.00172	0.00373	0.0100
0.20 to 0.25	1.00	-	1.734	25.24	≥ 1.00	0.00028	0.00061	0.00164
0.95 to 1.00	0.50	-	0.0451	0.0695	0.25 to 1.00	0.0431	0.0937	0.252
0.90 to 0.95	0.50	-	0.0740	0.138	0.25 to 1.00	0.0691	0.150	0.404
0.85 to 0.90	0.50	-	0.122	0.275	0.25 to 1.00	0.105	0.228	0.614
0.80 to 0.85	0.50	-	0.200	0.547	0.25 to 1.00	0.154	0.335	0.899
0.75 to 0.80	0.50	-	0.328	1.088	0.25 to 1.00	0.210	0.456	1.226
0.70 to 0.75	0.50	-	0.538	2.165	0.25 to 1.00	0.268	0.584	1.569
0.65 to 0.70	0.50	-	0.884	4.308	0.25 to 1.00	0.318	0.692	1.861
0.60 to 0.65	0.50	-	1.452	8.571	0.25 to 1.00	0.346	0.753	2.022
0.55 to 0.60	0.50	-	2.384	17.05	0.25 to 1.00	0.340	0.738	1.985
0.50 to 0.55	0.50	-	3.915	33.93	0.25 to 1.00	0.295	0.642	1.727
0.45 to 0.50	0.50	-	6.430	67.5	0.25 to 1.00	0.224	0.487	1.310
0.40 to 0.45	0.50	-	10.56	134.3	0.25 to 1.00	0.141	0.306	0.823
0.35 to 0.40	0.50	-	12.75	173.5	0.25 to 1.00	0.0717	0.156	0.419
0.30 to 0.35	0.50	-	12.75	173.5	0.25 to 1.00	0.0277	0.0602	0.162
0.25 to 0.30	0.50	-	12.75	173.5	0.25 to 1.00	0.00743	0.0162	0.0435
0.20 to 0.25	0.50	-	12.75	173.5	0.25 to 1.00	0.00122	0.00264	0.00710

For a specific distribution and thermal-hydraulic case, the flaws in each bin were first considered to be subject to normal operational temperatures and pressure differentials. Those that would have ruptured or leaked in service were removed from consideration during

accident sequences, since they could be assumed to have been repaired. The response of the remaining flaws was then considered when they were exposed to an increased pressure difference (still at normal operating temperatures) that is appropriate to the thermal-hydraulic sequence, and the probability of rupture is estimated on the basis of limit-load analysis.

Next, the staff combined the results for each flaw bin to produce the probability that one or more flaws will rupture as a result of the increased differential pressure that occurs early in the sequence. This result is used in the event tree evaluation. Flaws that would rupture under these conditions were removed from the distribution, and the remaining flaws were considered to be exposed to the higher-temperature conditions at the appropriate differential pressure for the thermal-hydraulic sequence. Again, the staff combined the results from each bin to produce the probability that one or more flaws will rupture during the core oxidation phase of the sequence. This result was also used in the event tree evaluation.

The limit-load analyses for the two normal-temperature conditions depend upon the same parameters (materials, tube dimensions, and flaw dimensions) selected for each Monte Carlo trial of the creep rupture calculations. Thus, it would be most appropriate for the Monte Carlo analysis to include calculations for which tubes would fail in normal operation or upon initial increase of the pressure differential. However, to expedite the analysis, the staff estimated the normal-temperature rupture probabilities on an average basis before performing the Monte Carlo analyses for creep rupture probability.

For the flaw bins with lengths of 2.54 cm (1 inch) and longer, flaws more than 89 percent through-wall were assumed to fail in normal service and, therefore, were not present during an accident sequence initiated by some other event. Flaws in those same length bins that were between 76 and 89 percent through-wall were assumed to rupture when subjected to elevated pressure differentials at normal operating temperatures.

Flaws in the bins with lengths shorter than 2.54 cm (1 inch) were considered to leak in normal service and were removed if they were 100 percent through-wall. This may not be conservative, because some of those flaws may not leak sufficiently to require shutdown and plugging. However, partially offsetting this effect is the assumption that the shorter flaws that were nearly 100 percent through- wall would not propagate through-wall and leak significantly during normal service. Although these flaws might propagate through-wall at the beginning of the thermal-hydraulic sequences associated with accidents, the two length bins were intended to represent flaws that would and would not rupture (i.e., exceed critical length) at normal temperatures. Therefore, flaws in the short bin were not considered to rupture until exposed to elevated temperatures.

The two approaches to estimating flaw size distributions provided two different representations of flaw length. The NRR distribution used two distinct crack lengths, 2.54 cm (1 inch) and 1.27 cm (0.5 inch), while the RES distribution provided a continuous gamma distribution of length.

Limit-load analysis indicated that the critical length at normal operational temperatures could range from about 2.03 cm (0.8 inch) to more than 3.05 cm (1.2 inches), depending on variations in tube dimensions and material properties (i.e., flow stress). The dividing line between the two length bins for the RES flaw distribution was chosen as 2.54 cm (1 inch), because that is near the middle of the range and must be consistent with the analyses conducted for the NRR flaw distributions. The cutoff for the lower end of the

short flaw length bin for the RES distribution was set at 0.64 cm (0.25 inch). Critical lengths for flaws at the elevated temperatures are very sensitive to the temperatures and pressures of the individual sequences. Estimates range from about 1.02 cm (0.4 inch) to 1.52 cm (0.6 inch) for most of the thermal-hydraulic cases considered. However, flaws that exceeded 0.64 cm (0.25 inch) and propagated through-wall at high temperature may be subject to rapid enlargement by erosion, and could represent a threat to adjacent tubes as a result of impingement by very hot, high-velocity gas jets. Therefore, failure of flaws measuring 0.64 cm (0.25 inch) or longer at high temperatures was treated as being equivalent to burst.

The results of the calculations for the probability of SG tube failures were examined for indications that the simplifying assumptions described above were important to the outcome of the analyses. The results do not appear to be very sensitive to any of the simplifications except for the selection of the lower boundary of the short length bin for the RES distribution. It is important to note that use of 0.64 cm (0.25 inch) as the lower boundary of the shorter flaw length bin excludes from the analysis *84 percent of the flaws in the RES distributions*. If the boundary were placed at 1.02 cm (0.4 inch), the population in the short bin would be reduced to 60 percent of the value used in this analysis. If the boundary were placed at 0.25 cm (0.1 inch), the population in the bin would be increased by 80 percent compared to the value used.

The complete evaluation of the accident progression event tree for a single flaw distribution requires the analysis described above to be conducted for each thermal-hydraulic sequence that is associated with a path through the event tree. The event tree is separately evaluated for several flaw population size distributions as a sensitivity study on that input.

Implicit in these analyses are assumptions about the progression of the thermal-hydraulic sequence once the RCPB has been breached. If the first breach of the RCPB is a rupture of the surge line or hot leg, it is assumed that the RCS is depressurized rapidly enough to preclude subsequent rupture of SG tubes. The results of thermal-hydraulic analyses, including the effects of RCS depressurization (e.g., Cases 2R and 4R), showed this. If the first failure of the RCPB is a SG tube, this is assumed to result in a containment bypass-type release.

It was not considered feasible to extend the thermal-hydraulic analysis to determine whether enough tubes would rupture to sufficiently depressurize the RCS precluding a subsequent failure of the surge line or hot leg. If the surge line or hot leg did fail after only one or two SG tubes failed, it would greatly diminish the force driving the emission of radioactive materials into the atmosphere outside the containment, substantially reducing the threat to the public. However, the ability to model the effects of a single tube rupture on the adjacent tubes was not considered sufficiently accurate to predict the number of tubes that would ultimately rupture in a sequence. Therefore, all tube ruptures were considered to result in substantial bypass of the containment. This assumption creates an unknown degree of conservatism in the estimates for the frequency of bypass-type releases.

5.2.2 Results of TI-SGTR Probability Analysis

As described in Section 4.2, the staff used two methods were used to estimate the number and size distribution of flaws in the SGs. Each method produced three estimates corresponding to plants that were lightly, moderately, or severely affected by tube degradation processes. The analyses described in this section focused primarily on the flaw distributions provided by RES, with the distribution provided by NRR serving to illustrate the sensitivity of the

results to the accuracy of the flaw size distribution. It is important to note that this analysis considered only axial cracks that are not confined by tube sheets or tube support plates. An appropriate failure model for circumferential cracks at elevated temperatures was not available, so they were not addressed by this analysis.

Table 5.6 shows the results for each of the five thermal-hydraulic cases used for the event tree analyses for the estimated RES and NRR flaw distributions. Table 5.2 provides the outputs from the CRPROB code that support these results for the RES average flaw distribution.

The CRPROB code uses two parameters that are uncertain. Specifically, these parameters are the tube temperature and the magnification factor used to represent the effect of a crack on the stress used in the Larson-Miller creep damage model. Because confidence intervals were not established for the uncertainty in the tube temperatures, it was not possible to perform a parametric uncertainty analysis with these two parameters. Therefore, the staff performed sensitivity studies on each.

Figure 5.4 illustrates the sensitivity of selected thermal-hydraulic case results to variations in tube temperature. The RES flaw distribution for a moderately affected plant was the basis for three of the curves shown. Tube temperatures in each case were increased in a manner intended to represent the uncertainty in the relationship of the tube temperatures to the temperature of the component (surge line or hot leg) that might fail before the tubes. In each case, tube temperatures were assumed to be accurately known at 560K (548 °F) but to deviate as a linear function of temperature above that value. The linear temperature deviation, as a function of tube temperature, was separately established for each case by setting it to the specified offset value at the temperature that the tubes achieved in the SCDAP/RELAP5 calculations at the time that those calculations predicted the first RCS pressure boundary failure.

Also shown for comparison in Figure 5.4 are the results for a similar calculation with the NRR flaw distribution. The sensitivity curves cross at a temperature offset of approximately 70K (126 °F) because the RES flaw distribution is higher than the NRR distribution for deep cracks, but lower for the shallow cracks that fail only at the higher temperatures.

The staff also evaluated the event tree for the tube failure probability results using a temperature offset of +70K (126 °F) on all five thermal-hydraulic cases. The offset value, chosen to ensure conservatism before the completion of thermal-hydraulic sensitivity studies, envelops the stated tube temperature variability of ±20K (36 °F), and all of the variabilities seen in the sensitivity studies (Section 3.3). The analysis using the temperature offset was intended to provide a measure of the sensitivity of the bypass frequency to the uncertainty in tube temperature calculations. Table 5.6 gives the tube failure probabilities for each thermal-hydraulic sequence used for that sensitivity calculation.

Figure 5.5 illustrates the sensitivity of the RES flaw distribution and RES thermal-hydraulic Case 3R to the uncertainty in the flaw stress factor (m_p). The value of m_p was estimated from the results of 93 burst tests of tubes with EDM notches. The results were assumed to have a normal distribution, and the uncertainty of the mean was used for the uncertainty in the value of m_p. Comparison of the figures reveals that the 95 percent confidence value of m_p is equivalent to a temperature offset of approximately 10K (18 °F) for both flaw distributions.

Table 5.6 Probabilities for PI- and TI-SGTR During Severe Accident Sequences

T-H Sequence	Pressure-Induced			Temperature-Induced			Sequence Description
	NRR Dist.	RES Dist.	RES w/ 70K Temp Offset	NRR Dist.	RES Dist.	RES w/ 70K Temp Offset	
Average Plant	Values in parentheses are per SG						
1R	0.0	0.0	0.0	0.0092 (0.0031)	0.0174 (0.0058)	0.0243 (0.0081)	No SG's depressurized
9R	0.0059	0.0549	0.0549	0.2009	0.3125	0.5433	Seal LOCAs/depress. SG
	0.0059	0.0549	0.0549	[1.0]	[1.0]	[1.0]	- depress. SG; cleared loop seal
	0.0	0.0	0.0	0.0080	0.0088	0.0088	- intact SG; loop seal intact
	0.0	0.0	0.0	0.0360	0.1212	0.4013	- intact SG; cleared loop seal
3R	0.0059	0.0549	0.0549	0.0390	0.0791	0.2441	1 SG depressurized
6N	0.0059	0.0549	0.0549	0.0054	0.0184	0.0358	1 SG depressurized; Pzr PORV open
7R	0.0175	0.1646	0.1646	0.0547 (0.0186)	0.1149 (0.0399)	0.3419 (0.1302)	All SGs depressurized
Severe Plant	Values in parentheses are per SG						
1R	0.0	0.0	0.0	0.0142 (0.0048)	0.0471 (0.0157)	-	No SG's depressurized
9R	0.0064	0.1474	0.1474	0.6450	0.6421	-	Seal LOCAs/depress. SG
	0.0064	0.1474	0.1474	[1.0]	[1.0]	-	- depress. SG; cleared loop seal
	0.0	0.0	0.0	0.0189	0.0236	-	- intact SG; loop seal intact
	0.0	0.0	0.0	0.0664	0.2983	-	- intact SG; cleared loop seal
3R	0.0064	0.1474	0.1474	0.0839	0.2003	-	1 SG depressurized
6N	0.0064	0.1474	0.1474	0.0086	0.0490	-	1 SG depressurized; Pzr PORV open
7R	0.0190	0.4423	0.4423	0.1025 (0.0354)	0.2814 (0.1043)	-	All SGs depressurized

Flaws in the 1" length bin were assumed to be removed from the distribution by spontaneous rupture at depths ≥ 89 percent through-wall.
Flaws in the 1" length bin were assumed to rupture when a steam generator was depressurized at depths ≥ 79 percent through-wall, provided that the primary-side pressure remained at the pressurizer PORV or SV setpoint.
Flaws in the ½" bin ≥ 100 percent through-wall were assumed to be removed from the distribution by forced shutdown due to leakage.

The staff also checked the pressure sensitivity of the calculations. All of the thermal-hydraulic calculations performed with SCDAP/RELAP5 assumed that the pressurizer PORVs were functioning. If they were not available (as would be the case for SBO sequences that lasted through station battery depletion) the pressurizer safety valves would control RCS pressure during the core damage phase of the sequence. Because the SV set point is 0.7 MPa (100 psi) greater than the PORV set point, RCS pressures could be higher by that amount during core oxidation for Cases 1R, 3R, and 7R. Case 3R was evaluated with a 0.7-MPa (100-psi) increase in differential pressure across the SG tubes, but the effect on the surge line failure time was not considered. The result was an increase in tube failure probability from 0.0791 to 0.0892. That effect is equivalent to the effect from an increase in tube temperature of about 15K (27 °F).

The staff then evaluated the sensitivity to uncertainty in the failure time of the surge line and hot legs. This evaluation was similar to the sensitivity evaluation performed for the tube temperatures, because relative temperature differences lead to differences in relative failure times. However, the modeling of the surge line and hot leg creep damage was relatively crude (i.e., a thin-walled, long, straight-tube approximation) which may lead to error in the applied failure time probability density function. As a sensitivity study, the surge line failure time probability density function for thermal-hydraulic Case 3R was shifted in time by as much as 10 minutes. Figure 5.6 shows the results for both the RES and NRR flaw distributions.

For this thermal-hydraulic case, it can be seen that the earlier failure times have a minor effect on the probability of TI-SGTR. However, delaying the surge line failure time by more than 3 minutes substantially increases the probability of TI-SGTR. This effect is most conspicuous for the NRR flaw distribution. The RES flaw distribution is not considered realistic in the later time shifts because it has an unrealistically low population of flaws with shallow cracks. Caution should be used in extending this result to other thermal-hydraulic sequences. In particular, Case 9R has a much more rapid increase in the probability of reactor coolant pressure boundary failure than the other cases, because of rapid temperature and pressure increases caused by accumulator injection. Therefore, that case may exhibit much greater sensitivity to arbitrary shifts in the pressure boundary failure time. However, the failure time in that case may be less uncertain because of the same phenomena.

The staff also conducted a limited evaluation of thermal-hydraulic Case 6R, in order to consider the sensitivity of TI-SGTR results to the number of tubes assumed to carry flow out of the SG inlet plenum. This is similar to Case 3R, but it assumes that 53 percent of the tubes carry flow out of the inlet plenum, compared to 35 percent for Case 3R. The resulting TI-SGTR probability for the depressurized SG is 0.0659 for Case 6R, compared to 0.0835 for Case 3R, using the RES flaw distribution for an average plant. This is not a substantial difference.

Finally, the staff evaluated the TI-SGTR probability associated with thermal-hydraulic Case ANO1, which is similar to Surry thermal-hydraulic Case 3R, to investigate the effect of design-specific variations in plant thermal-hydraulic response to severe accidents. The average plant RES flaw distribution that was used for the Surry plant was applied to ANO-2 for comparison purposes. The resulting TI-SGTR probability for ANO-2 was 0.4017, compared to 0.0835 for Surry.

Because ANO-2 has two SGs instead of three, the flaw distribution used for the Surry plant would produce a PI-SGTR probability *per SG* that is 50 percent greater than the value that same distribution creates for Surry. In order to make the assumed ANO-2 PI-SGTR probability match the value used for Surry (i.e., approximately 0.05), it was necessary to decrease the overall flaw population for ANO-2 by one-third. This reduction decreased the TI-SGTR value for ANO-2 to about 0.27, still more than three times the value calculated for the Surry plant. Consequently, the staff does not believe that it is prudent to consider the Surry results representative of all other plants.

5.2.3 Conclusions Regarding Probability of Tube Failure

The staff has developed a suitable method to treat SG tube failure probabilistically. This methodology accounts for the presence of a population of flaws in the SG tubes.

The results of this method are shown to be most sensitive to the following uncertainties:

- the size distribution of the flaws
- the relationship between the temperatures of the SG tubes and the other parts of the RCS pressure boundary that might fail first

Sensitivity of the results to uncertainties in the flaw burst correlation and the RCS pressure are much less significant.

Because there is insufficient information available to specify probability density functions for the two most sensitive parameters in these calculations, it was not possible to provide a meaningful parametric uncertainty study of the results. However, a series of sensitivity studies was provided that illustrated the sensitivity of this calculation and allowed the sensitivity to be propagated through the bypass frequency calculations. In addition, the TI-SGTR results were found to be very sensitive to plant design-specific variations in thermal-hydraulic response to severe accidents. Therefore, these results for the Surry plant should not be considered directly applicable to plants with other designs.

5.3 Estimate of Containment Bypass Frequency

The following sections address the estimated frequency of containment bypass resulting from pressure- and temperature-induced SGTR. The frequency of containment bypass under base case assumptions is presented in Section 5.3.1. The potential impact of plant-specific features or operator actions that could influence primary and secondary system integrity/depressurization is addressed in Section 5.3.2 through parametric variation (sensitivity analyses) of split fractions for relevant APET top events. The sensitivity of base case results to variations in SG flaw distributions is addressed in Section 5.3.3.

5.3.1 Base Case

The APET for the base case is illustrated in Figures 2.3 through 2.3d and described in Section 2.3. The initiating event frequency and the APET split fractions for all but two top events (dealing with the conditional probability of a pressure- or temperature-induced SGTR) were derived from the results of the NUREG-1150 analysis for Surry, as described in Section 2.3. Base case values are summarized as follows:

- initiating event frequency of 1.6×10^{-5}/RY (top event A)

- 14 and 18 percent probabilities that the event involves a stuck-open PORV/SV or RCP seal LOCA, respectively (top events B and C)
- 36 and 38 percent probabilities that the event involves depressurization of all SGs or one SG, respectively (top events D and E)
- a 50 percent probability that the RCS pressure is maintained to time of maximum tube temperature, given that it is intact at the time of core uncovery (top event F)
- a 50 percent probability that the secondary side pressure is maintained to time of maximum tube temperature, given that it is intact at the time of SG dryout, with the balance of the probability partitioned among events with leakdown of one, two, or three SGs (top events G, H, and I)

Collectively, within the framework of the APET, these values establish the frequency of pressure and temperature challenges to the SG tubes.

Split fractions for top events dealing with the probability of a pressure- or temperature-induced SGTR (top events J, K, and L) are quantified on the basis of thermal-hydraulic analyses, creep-rupture experiments and models, and expert judgements regarding flaw distributions that were developed as part of the present study (as discussed previously). The resulting probability values are summarized in Section 5.1.

Table 5.7 APET Sensitivity Cases

Sensitivity Case No.	Description	Situation Represented by Sensitivity Case
1	No late SG depressurization as a result of MSIV leakage	Impact if high confidence in secondary side integrity can be demonstrated (e.g., through MSIV leak testing and assessment of relevant operating event data)
2	Lower early SG depressurization probability (0.05 based on Sequoyah, NUREG 1150)	Plants with highly reliable ADV/MSSVs, and no tendency toward manually depressurized SGs in severe accidents
3	Cases 1 and 2 combined	Optimal secondary side performance
4	Probability of late primary depressurization = 1.0	Impact of providing AC-independent depressurization capability. High probability of pressurizer valve failure resulting from liquid cycles (as claimed by EPRI) or severe accident temperature
5	Probability of late primary depressurization = 0	Plants with highly reliable PORV/SVs, and no tendency/capability to manually depressurize RCS using PORVs
6	No RCP seal LOCAs	Reduced contribution of RCP seal LOCAs at plants with AC-independent RCP seal cooling systems. Lower probability of RCP seal LOCA at plants with Byron Jackson pumps
7	Increase temperature histories by 70K (RES "moderate" flaw distribution)	Impact if SG temperatures are substantially under-estimated in SCDAP/RELAP5 calculations
8	Pristine SG tubes	Impact if all SG flaws are eliminated or all SGs are replaced
9	No loop seal clearing in RCP seal LOCA sequences	Impact if further technical assessment or plant-specific analyses show loop seal clearing will not occur

Table 5.8 Containment Bypass Frequencies per Reactor Year for APET Base Case and Sensitivity Cases

Contribution	Case Number									
	Base	1	2	3	4	5	6	7	8	9
TI-SGTR	2.4×10^{-6}	2.1×10^{-6}	1.3×10^{-6}	2.3×10^{-7}	2.2×10^{-6}	2.7×10^{-6}	8.0×10^{-7}	*3.4×10^{-6}*	1.7×10^{-6}	1.8×10^{-6}
From Seal LOCA	1.8×10^{-6}	1.5×10^{-6}	9.5×10^{-7}	1.0×10^{-7}	1.8×10^{-6}	1.8×10^{-6}	0	*1.6×10^{-6}*	1.7×10^{-6}	1.1×10^{-6}
PI-SGTR	1.5×10^{-6}	1.1×10^{-6}	5.4×10^{-7}	7.0×10^{-8}	1.4×10^{-6}	1.4×10^{-6}	1.4×10^{-6}	*1.1×10^{-6}*	0	1.5×10^{-6}
Total Bypass Freq	3.9×10^{-6}	3.2×10^{-6}	1.9×10^{-6}	3.0×10^{-7}	3.6×10^{-6}	4.1×10^{-6}	2.2×10^{-6}	*4.5×10^{-6}*	1.7×10^{-6}	3.3×10^{-6}
Cond Cont Bypass Prob	.25	.20	.12	.019	.22	.26	.14	*.28*	.11	.20

Base - RES Flaw Distribution for "Moderate" plant, $P_{TI\text{-}SGTR}$ on the basis of RES Cases 1, 3, 7, 9, and NRR Case 6
1 - No late SG depressurization resulting from MSIV leakage
2 - Lower early SG depressurization probability (0.05 on the basis of Sequoyah NUREG-1150)
3 - Cases 1 and 2 combined
4 - Probability of late primary system depressurization = 1.0
5 - Probability of late primary system depressurization = 0
6 - No RCP seal LOCAs
7 - Increase temperature histories by 70K
8 - Pristine SG tubes (no flaws)
9 - No loop seal clearing in RCP seal LOCA sequences

The results for the base case quantification are summarized in the second column of Table 5.8. The frequency of containment bypass is approximately 3.9×10^{-6}/RY. Thus, about 25 percent of the initiating events (events involving core damage at high RCS pressure with a dry secondary side) result in containment bypass. About 60 percent of the bypass frequency is attributable to TI-SGTR (2.4×10^{-6}/RY), with PI-SGTR accounting for the balance (1.5×10^{-6}/RY).

The major contribution to TI-SGTR (75 percent) is from RCP seal LOCA sequences. Although RCP seal LOCA sequences represent only about 18 percent of the initiating event frequency, they account for nearly half of the containment bypass frequency because of the high probability of TI-SGTR for these sequences. These higher probabilities stem from severe SG tube temperature excursions associated with accumulator injections that occur during rapid cladding oxidation and enhance transport of hot gases within the RCS. The temperature challenge is further aggravated by clearing an SG loop seal (as predicted in SCDAP/RELAP5 calculations for Surry).

It is interesting to note that the temperature excursion in a loop with coincident SG depressurization and loop seal clearing is expected to fail even unflawed tubes. A smaller contribution to bypass frequency comes from the failure of flawed tubes in loops with loop seal maintained but with depressurized SGs, and from the failure of flawed tubes in loops with loop seals cleared but where the SGs remain pressurized. The contribution to containment bypass frequency from flawed and unflawed tubes is provided in Table 5.9. The impact of eliminating loop seal clearing on the respective contribution is also shown and is further discussed in Section 5.3.2.9 as Sensitivity Case 9.

5.3.2 APET Sensitivity Analyses

The potential impact of plant features or operator actions that influence the likelihood of primary and secondary system integrity/depressurization or the thermal-hydraulic challenge to SG tubes is illustrated through a series of sensitivity analyses. In these analyses, the impact of various plant-specific features or operator actions on containment bypass frequency was assessed by changing the split fractions for relevant APET top events and determining the change in bypass frequency (i.e., the frequency of APET endstates assigned to release categories RC-1 or RC-2). Two additional sensitivity analyses were performed to address the sensitivity of results to an arbitrary offset in the SG temperature profile and the complete elimination of all SG flaws.

A total of nine sensitivity cases were considered. These cases and their corresponding results are summarized in Tables 5.7 and 5.8 and are briefly discussed below.

5.3.2.1 Eliminate Potential for Late SG Depressurization

The first case illustrates the impact on results if the potential for late SG depressurization is eliminated. In this case, the probability of late SG depressurization resulting from MSIV leakage (top event G) was set to zero. Such a result might be applicable if a licensee could demonstrate, through periodic type C leak testing of MSIVs and an assessment of relevant operating event data regarding MSSV leakage following repeated cycling, that there is a high probability that the secondary side will remain substantially pressurized within the time period between SG dryout and first RCS structural failure.

Eliminating the potential for late SG depressurization reduces the bypass frequency by about 20 percent (to 3.2×10^{-6}/RY). Thus, 20 percent of the initiating events result in containment

bypass in this case. The impact of late SG depressurization is small because, in the majority of events (74 percent of the initiating event frequency), one or more SGs are already depressurized at the time the late depressurization question is asked. The relative contribution to bypass frequency from temperature- and pressure-induced SGTR, and RCP seal LOCA sequences is not substantially different from the base case.

5.3.2.2 Reduced Probability of Early SG Depressurization

The second case illustrates the impact on results if the probability of early SG depressurization is substantially lower than determined from the NUREG-1150 analysis for Surry. In this case, the split fractions for top events D and E were set to values determined from the NUREG-1150 analysis for Sequoyah, which exhibited a high probability of secondary side integrity, i.e. (about a 95 percent probability that all SGs are pressurized at the time of core uncovery, and 3 and 2 percent probabilities that one or all SGs are depressurized, respectively. Such a result might be applicable if a licensee can demonstrate that ADV/MSSV integrity will be maintained after repeated cycling, and that operator actions to depressurize SGs early in an event will not result in the SGs being dry and depressurized at the time of core damage.

The reduction in the probability of early SG depressurization (to 5 percent) results in a 50 percent reduction in bypass frequency (to 1.9×10^{-6}/RY), and a reduction in the conditional containment bypass frequency (to about 12 percent). The significant impact on results largely results from the magnitude of the change from the base case (i.e., 74 percent of the events depressurized early in the base case, compared to 5 percent in the sensitivity case). Even though the potential for late depressurization is subsequently considered for those events that are not depressurized early, the net frequency of maintaining secondary side pressure is much higher. By maintaining secondary side pressure in these events, the likelihood of PI-SGTR is substantially reduced, and the likelihood of TI-SGTR is evaluated for intermediate rather than full differential pressures and is significantly reduced. About 70 percent of the bypass frequency is a result of TI-SGTR (1.3×10^{-6}/RY), with PI-SGTR accounting for the balance (5.4×10^{-7}/RY). The much smaller contribution from PI-SGTR is commensurate with the reduction in the frequency of early SG depressurization. As in the base case, RCP seal LOCA sequences represent the major contributor to TI-SGTR, and account for about half of the containment bypass frequency.

5.3.2.3 Reduced Probability of Early and Late SG Depressurization

The third sensitivity case shows the combined effect if the probability of early SG depressurization is substantially lower than in the base case, *and* the potential for late SG depressurization is eliminated. In this sensitivity case, the probability of early SG depressurization (top events D and E) was set to values determined for Sequoyah as in Sensitivity Case 2, and the probability of late SG depressurization resulting from MSIV leakage (top event G) was set to zero as in Sensitivity Case 1.

Reducing the probability of early SG depressurization to 5 percent and eliminating the potential for late SG depressurization reduces the bypass frequency by about a factor of 10 (to 3.0×10^{-7}/RY), and reduces the conditional containment bypass frequency to about 2 percent. Although this case represents a combination of sensitivity Cases 1 and 2, the reduction in bypass frequency achieved is far greater than the sum or product of the reduction achieved for either case individually. This is because the SG tubes are exposed to full differential pressure in only 5 percent of events, considering both early and late secondary side depressurization combined. About 76 percent of the bypass frequency is

attributable to TI-SGTR (2.3×10^{-7}/RY), with PI-SGTR accounting for the balance (7.0×10^{-8}/RY). The much smaller contribution from PI-SGTR is commensurate with the reduction in the frequency of early and late SG depressurization. RCP seal LOCA sequences account for about 40 percent of the frequency of TI-SGTR, and about 30 percent of the containment bypass frequency.

5.3.2.4 Assure Late Primary System Depressurization

The fourth sensitivity case shows the potential impact if the pressurizer SV/PORV fails open or is manually opened late in all sequences. In this sensitivity case, the probability of late primary system depressurization (top event F) is set to 1.0. This case would reflect the following probabilities:

- a much higher probability of valve failure resulting from hydrodynamic effects early in the event
- a much higher probability of valve failure resulting from thermal loads on the valve late in the event
- the potential benefits of providing AC-independent primary system depressurization capability (i.e., a "perfect" depressurization system)

This case is consistent with claims by EPRI that the probability of pressurizer safety valve failure is extremely high (0.98 for a pressurizer safety valve with a 5 percent dead band) because of the large number of valve cycles in which liquid is discharged (Fuller, July 1996). Because no thermal-hydraulic case was available to illustrate the effect of opening a pressurizer PORV after a seal LOCA has occurred, this action was assumed to have no effect on the seal LOCA sequences for this sensitivity case.

As modeled, late primary system depressurization reduces the bypass frequency by only about 10 percent (to 3.6×10^{-6}/RY). Thus, 22 percent of the initiating events result in containment bypass in this case. The impact of late primary system depressurization is small because of the following factors:

- Late depressurization is assumed not to affect the dominant contributors to bypass frequency (i.e.,PI-SGTR and TI-SGTR in RCP seal LOCA sequences).
- Where it is effective, late depressurization reduces (but does not completely eliminate) the probability of TI-SGTR.

The relative contribution to bypass frequency from RCP seal LOCA sequences and temperature- and pressure-induced SGTR, is not substantially different from the base case. When a thermal-hydraulic analysis becomes available for late opening of a pressurizer PORV concurrent with a seal LOCA, this sensitivity case will be re-evaluated.

5.3.2.5 Preclude Late Primary System Depressurization

The fifth sensitivity case is the opposite of Sensitivity Case 4, and shows the impact if the pressurizer SV/PORVs always reclose and actions are not taken to manually depressurize the RCS. In this sensitivity case, the probability of late primary system depressurization (top event F) is set to zero. This case is optimistic from the point of view of valve performance, and would reflect essentially flawless valve performance under all accident loads, including repeated valve cycling with liquid discharge, and continued operation at elevated temperatures associated with the core damage portion of the event.

Precluding late primary system depressurization increases the bypass frequency by only about 5 percent (to 4.1×10^{-6}/RY). Thus, in this case, 26 percent of the initiating events result in containment bypass. The impact of late primary system depressurization is small for the same reasons cited for Sensitivity Case 4. That is, late depressurization does not affect the dominant contributors to bypass frequency (i.e., PI-SGTR and TI-SGTR in RCP seal LOCA sequences) and, where modeled within the APET, precluding late depressurization does not substantially increase the probability of TI-SGTR. The relative contribution to bypass frequency from RCP seal LOCA sequences and temperature- and pressure-induced SGTR, is not substantially different from the base case.

5.3.2.6 Eliminate RCP Seal LOCA Sequences

The sixth case illustrates the effect if RCP seal LOCA events are completely eliminated from the risk profile. In this sensitivity case, the fraction of high/dry events that involve RCP seal LOCA (top event C) is set to 0. This case represents the risk reduction achievable if RCP seal LOCA sequences are eliminated through some type of system modification, for example, the addition of AC-independent seal cooling systems. It is also consistent with industry claims that RCP seal LOCA sequences have a negligible contribution to CDF in CE plants because the Byron-Jackson RCPs used at CE plants may not be as susceptible to seal LOCAs.

Eliminating RCP seal LOCA sequences results in a 40 percent reduction in bypass frequency (to 2.2×10^{-6}/RY), and reduces the conditional containment bypass frequency to about 14 percent. Bypass frequency is substantially reduced since RCP seal LOCA sequences account for approximately half of the bypass frequency in the base case. The frequency contributions from TI-SGTR in non-seal LOCA cases and from PI-SGTR is essentially unchanged from the base case and accounts for about 40 and 60 percent of the bypass frequency, respectively.

5.3.2.7 Increase SG Temperature Histories

The seventh case shows the impact if the temperature histories of the SG tubes are systematically increased by 70K (126 °F). In this sensitivity case, the split fractions associated with the probability of TI-SGTR (top event I) are replaced with values on the basis of probabilistic creep-rupture calculations in which the SG tube temperature histories from SCDAP/RELAP5 were offset by 70K (126 °F). These calculations and resulting probabilities are described in Section 5.2.2 and Table 5.6. This sensitivity case conservatively bounds the uncertainties in temperature predictions, on the basis of the range of thermal-hydraulic analysis results discussed in Section 3. An under-prediction of this degree is extremely unlikely, on the basis of the results of the sensitivity analyses discussed in Section 3 and the results of corresponding severe accident analyses using the MAAP 4.0 code (Fuller, January 1996), which suggest that SG temperature histories may be somewhat over-predicted in the underlying SCDAP/RELAP5 analyses on which the base case is predicated.

Increasing the SG temperature histories increases the bypass frequency by nearly 40 percent (to 4.5×10^{-6}/RY). Thus, in this case, 28 percent of the initiating events result in containment bypass. Essentially all of this change results from the increased frequency of TI-SGTR in non-seal LOCA sequences. Seal LOCA sequences are not impacted since the likelihood of TI-SGTR is already very high in these sequences because of SG temperature excursions in conjunction with RCS loop seal clearing. The contribution of PI-SGTR is not affected by SG temperature increases (since the likelihood of PI-SGTR is evaluated before SG

heatup) and is also unchanged from the base case. About 76 percent of the bypass frequency results from TI-SGTR (3.4×10^{-6}/RY), with PI-SGTR accounting for the balance (1.1×10^{-6}/RY). RCP seal LOCA sequences account for nearly half of the TI-SGTR frequency.

5.3.2.8 Eliminate All Flaws in SG Tubing

The eighth sensitivity case illustrates the impact if the SG tubes contain no flaws. Probabilistic creep-rupture calculations indicate that the probability of temperature-induced creep failure of pristine SG tubes before creep failure elsewhere in the RCS (e.g., in the hot leg or surge line) is essentially zero for all evaluated severe accident sequences, with the exception of RCP seal LOCA sequences. The probability of TI-SGTR remains significant in seal LOCA sequences because of the high probability of tube failure (essentially 1.0) in those instances where the loop seal clearing and secondary side depressurization occur within the same SG loop, even for pristine SG tubes. In this sensitivity case, the probability of PI-SGTR (top event J) was set to zero for all APET branches, and the probability of TI-SGTR (top event L) was set to zero for all APET branches except those involving concurrent loop seal clearing and secondary side depressurization. (See note 2 on Table 5.1a for a description of which branches involve this condition.)

Eliminating all flaws in the SG tubes results in a 55 percent reduction in bypass frequency (to 1.7×10^{-6}/RY), and reduces the conditional containment bypass frequency to 11 percent. The impact on the results is attributable to the complete elimination of PI-SGTR in all sequences, and elimination of TI-SGTR in all non-seal LOCA sequences and many seal LOCA sequences. TI-SGTRs continue to occur in those RCP seal LOCA sequences with concurrent loop seal clearing and secondary side depressurization, since the pressure/temperature challenge in these sequences is large enough to threaten unflawed tubes and account for all remaining bypass frequency.

5.3.2.9 No Loop Seal Clearing in RCP Seal LOCA Sequences

The probability of TI-SGTR is significant in RCP seal LOCA sequences, in part because of the high probability of tube failure (essentially 1.0) in those instances where the loop seal clearing and secondary side depressurization occur within the same SG loop. The ninth sensitivity case illustrates the impact if clearing of the SG loop seal is precluded in RCP seal LOCA sequences. In this sensitivity case, the probability of loop seal clearing (top event K) was set to zero for all APET branches, and the probability of TI-SGTR (top event L) was determined from values calculated for SG loops in which the loop seal is maintained (i.e., the unbracketed values shown in the second and third columns of Table 5.2 for Case 9R). Accordingly, failure probabilities of 0.313, 0.528, and 0.676 were assigned to APET branches involving one, two, or three depressurized SGs, respectively.

Eliminating loop seal clearing yields only a 15 percent reduction in bypass frequency (to 3.3×10^{-6}/RY), and reduces the conditional containment bypass frequency to 20 percent. The impact on results is not significant because the probability of TI-SGTR remains relatively high because of the high failure probability per depressurized SG and the preponderance of events (slightly more than 50 percent) involving depressurization of more than one SG. In addition, the significance is small because the probability of PI-SGTR is unaffected by changes in the loop seal clearing probability.

It is interesting to note that the contribution from TI-SGTR in this case is entirely attributable to flawed tubes and, as shown in Table 5.9, is about twice the contribution from unflawed tubes in the base case, and roughly equivalent to the contribution from PI-

SGTR. The contribution from flawed tubes increases because event frequency, which was previously associated with guaranteed TI-SGTR (as a result of coincident loop seal clearing and SG depressurization), is redirected to the TI branch (top event L) where a large fraction of the events result in TI-SGTR for the reasons discussed above.

Table 5.9 Contribution to Containment Bypass Frequency from Flawed and Unflawed SG Tubes

Contributor	Containment Bypass Frequency (/RY)	
	Base Case	No Loop Seal Clearing[1]
PI Failure (of Flawed Tubes)	1.5×10^{-6}	1.5×10^{-6}
TI Failure (of Unflawed Tubes)	1.5×10^{-6}	0
TI Failure (of Flawed Tubes)	9.0×10^{-7}	1.8×10^{-6}
Total	3.9×10^{-6}	3.3×10^{-6}
1 - See Sensitivity Case 9		

5.3.3 Impact of Different Flaw Distributions

As discussed in Section 4, the staff considered two generalized flaw distributions during this study. In addition to the sensitivity studies previously described, the staff estimated containment bypass frequency for the base case using the NRR flaw distribution rather than the RES distribution. This does not necessarily represent a limiting case (which could exist at a facility). Instead, the difference in the tube failure frequencies between the cases using different flaw distributions, as evidenced in Table 5.6, shows that the containment bypass potential would be reduced using the NRR distribution.

Applying the temperature- and pressure-induced tube failure probabilities associated with the NRR flaw distribution from Table 5.6 for the "average plant," yields a containment bypass frequency of 1.95×10^{-6}/RY. This represents a 39 percent reduction over the base case containment bypass value. This large reduction is not unexpected, since the pressure-induced tube failure probabilities using the NRR distribution are an order of magnitude lower than those on the basis of the RES distribution. The temperature-induced failure probabilities are also significantly reduced, although not as much as the pressure-induced values.

A notable impact on the results is that the portion of containment bypass frequency attributable to RCP seal LOCA sequences is greater using the NRR distribution. Not unlike the results for Sensitivity Case 8, reducing the failure frequency for flawed tubes does not significantly affect the potential for tube failure in the RCP seal LOCA situations. Using the NRR distribution, the RCP seal LOCA sequences account for approximately 75 percent of the containment bypass frequency of 1.95×10^{-6}/RY. In this case, the alternative flaw distribution yielded a result close to the assumption of unflawed tubes (Sensitivity Case 8). Thus, using a flaw distribution on the basis of different assumptions and inputs can significantly impact the estimated containment bypass frequency.

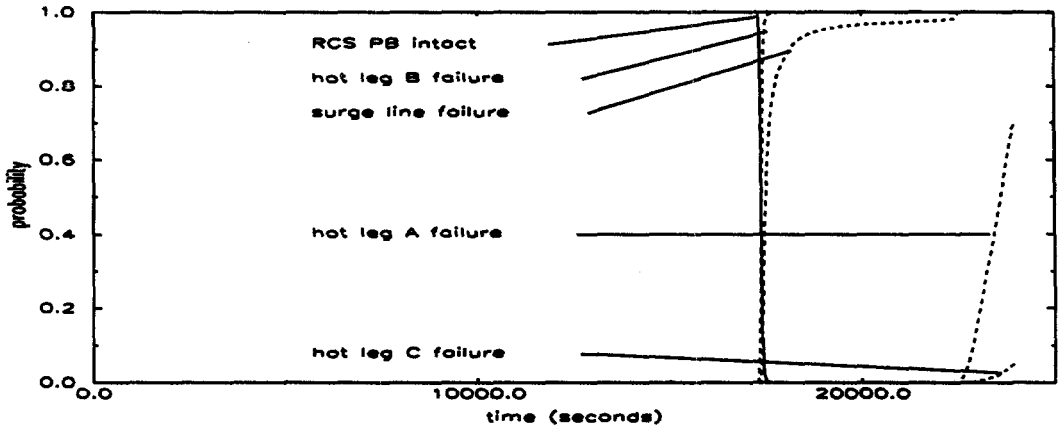

Figure 5.1 Case 9R RCS Pressure Boundary Failure Probabilities as a Function of Time

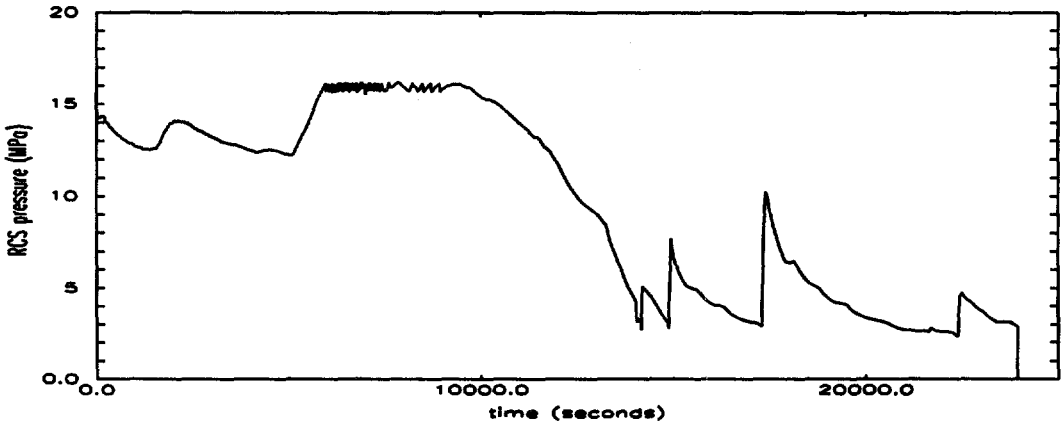

Figure 5.2 Case 9R RCS Pressure as a Function of Time

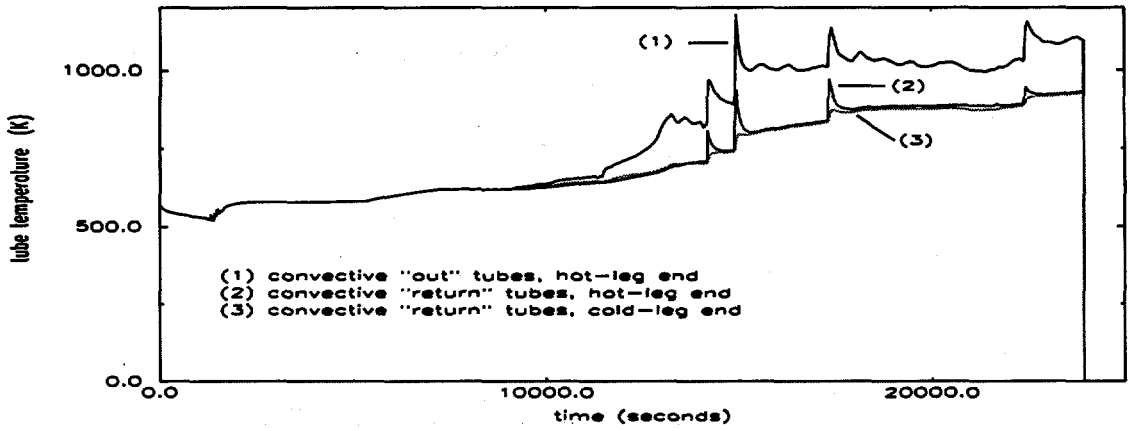

Figure 5.3 Case 9R Steam Generator "C" Tube Temperatures as a Function of Time

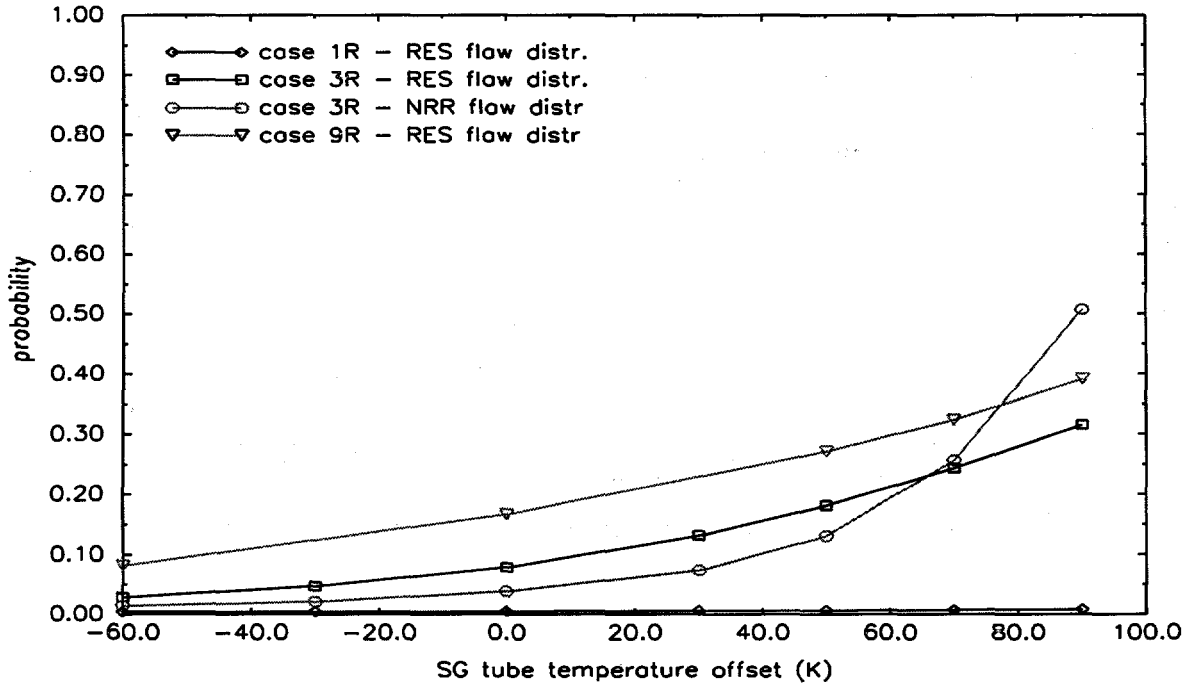

Figure 5.4 Sensitivity of SG Tube Flaw Failure Probability to Error in Tube Temperature Prediction for Selected Thermal-Hydraulic Cases (Depressurized SGs, only)

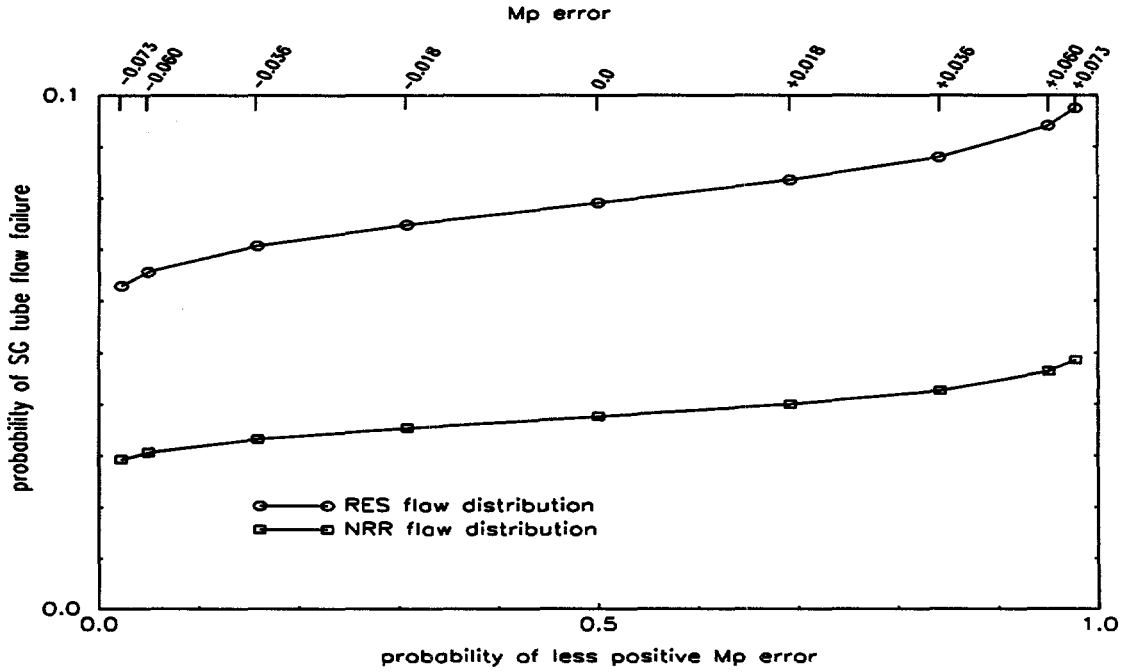

Figure 5.5 Sensitivity of Case 3R to Error in Estimation of the Flaw Stress Concentration Factor (Mp)

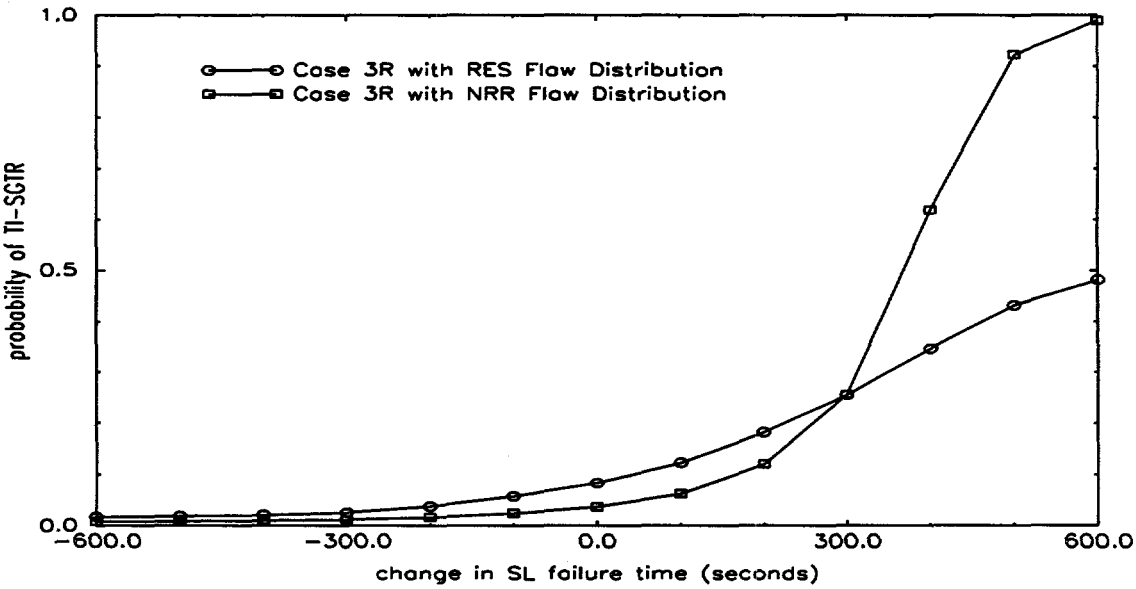

Figure 5.6 Sensitivity of Case 3R to Error in Prediction of Surge Line Failure Time

6 CONCLUSIONS

The staff has conducted a representative analysis to gain insight into the potential for containment bypass resulting from TI-SGTR during core damage sequences. The analysis used Surry as the example plant and was based on information and estimated SG tube conditions considered representative for similar facilities.

This section summarizes the results from the staff's representative analysis, and highlights the plant- and design-specific considerations that appear to influence the results of the assessment. This section concludes by discussing the general findings that arose from this study.

6.1 Surry Results

The staff's representative analysis yielded a containment bypass frequency (associated with severe accident-induced tube failure) of approximately 3.9×10^{-6}/RY for Surry, indicating a reduction of approximately 1-in-4 from the initiating frequency for core damage associated with high RCS pressure/dry secondary. Considering the possible range for initiating frequencies among PWRs (see Figure 2.4), plant-specific results could range from 10^{-7} to near 10^{-5} per reactor-year.

An important characteristic of the results for Surry is that 60 percent of the bypass frequency (2.4×10^{-6}/RY) is attributable to TI-SGTR, with PI-SGTR accounting for the balance (1.5×10^{-6}/RY). Also, the major contribution to TI-SGTR (75 percent) is from RCP seal LOCA sequences. Although such sequences represent only about 18 percent of the initiating event frequency, they account for nearly half of the containment bypass frequency because of the higher probability of TI-SGTR for these sequences. These higher probabilities stem from severe SG tube temperature excursions associated with the clearing of an RCS loop seal in the sequence analyzed, combined with accumulator injection effects that could be associated with these events.

The staff also drew significant conclusions from the results of sensitivity studies conducted on the basis of the representative analysis (see Section 5.3.2). First, the impact of RCP seal LOCA on tube failure was evident in the results of Sensitivity Case 6. Despite the RCS depressurization benefit that could be assumed from an RCP seal leak, the Surry analysis showed that the associated potential to clear an RCS loop seal greatly contributed to the tube failure potential for the sequences studied. Further examination of the conditions, probability, and factors contributing to RCP seal failure and loop seal clearing during severe accident sequences may improve the staff's confidence in the estimate of induced tube failure probability.

Next, the significance of secondary system pressure integrity appears to be at least as important to tube survivability as is the ability to depressurize the reactor coolant system. This is apparent from comparison of the results of Sensitivity Cases 3 and 4 listed in Table 5.8. Although plant-specific differences could yield somewhat different values for these estimates at other facilities, the large impact of secondary system pressure integrity would probably be evident in the other plant-specific analyses. The sensitivity cases also demonstrated that the assumed flaw distribution can have a major impact on the results.

An insight underlying the representative analysis is that the range of uncertainties encountered, along with their plant- and design-specific nature, limits the generic

applicability of the results. While the staff could not demonstrate the associated risk at all facilities through a generic analysis, plant-specific analysis could demonstrate the containment bypass vulnerability at a particular plant. In estimating containment bypass probability, uncertainties should be addressed in such areas as those listed below. The effects of a range of plant-specific factors should also be considered. Plant configurations could affect thermal-hydraulic conditions and event progressions, and tube degradation states could vary among facilities, but these could be specified for plant-specific analyses.

6.2 Plant- and Design-Specific Factors

A more detailed analysis should address uncertainties and variabilities in the following areas:

- Event Tree Quantification: Additional operational or component failure data could be developed as a basis for failure frequencies associated with important pressure-relief components in the RCS and secondary systems. Also, the failure frequency of reactor coolant pump seals and the magnitude of the resulting leak might be design-specific, and the differences should be considered. Plant-specific configurations and procedures should explicitly be accounted for to determine the extent to which they would affect the structure and split fractions composing the event tree.

- Thermal-Hydraulic Modeling: Plant- and design-specific factors that could influence thermal-hydraulic performance should explicitly be accounted for in plant-specific analyses.

- Tube Performance Model: The analysis described here is founded on the effects of axial cracks on high-temperature tube performance. A similar characterization should account for the particular degradation experienced at a facility. Other failure modes should also be considered, such as the potential for propagation to gross tube failure associated with tube leakage under high-pressure core damage conditions.

- Reactor Coolant Pressure Boundary Weak Points: The analysis estimated times to thermal failure for the surge line and hot leg relative to the SG tubes. Other locations in the RCS may also be threatened with thermal failure, thus altering the potential for thermal failure of the tubes.

- Flaw Distribution: The estimated SG flaw distribution used in estimating tube failure frequency can vary significantly depending on plant tube degradation experience. A plant-specific, flaw-size-based distribution should be obtained, but there are recognized difficulties given the current state-of-the-art in tube inspection capability. This is a significant drawback in the practical application of the methods described in this report.

- Crack Opening Area: A key area currently receiving staff attention centers on uncertainties existing in the prediction of a crack opening area, and the overall nature of tube leaks under severe accident conditions. The estimates made in EPRI report TR-106194 (Fuller, January 1996) appear reasonable, although the leakage rates may be somewhat underestimated. The staff will revisit the representative analysis presented in this report to ensure that it appropriately considers all findings concerning severe accident tube leakage.

The staff is pursuing analyses to address these areas and other details of the analyses presented in this study.

6.3 General Findings

The staff reached some key conclusions in this study through analysis of the Surry plant. Consideration of the results in terms of containment bypass frequency indicates that some PWRs may be subject to a containment bypass risk attributable to tube failure during severe accidents. However, the staff found that if tube conditions do not degrade beyond those associated with current tube repair criteria defined in plant technical specifications, undue public risk from such occurrences should be avoided.

The staff also found that reactor coolant pump seal leakage model assumptions are important factors requiring further consideration. RCP seal LOCAs were found to be a key factor in exposing tubes to more severe thermal challenges by contributing to conditions resulting in full loop circulation. The more severe thermal conditions may challenge unflawed tube integrity.

To assess the impact of plant features or operator actions, as well as analytical assumptions on the containment bypass frequency estimate, the staff conducted several sensitivity analyses, as discussed in Section 5. The results show that although some risk reduction benefits can be gained by focused changes in factors (such as the ability to depressurize the RCS during an SBO), only modest gains could be realized. Examination of Table 5.8 shows that secondary system pressure integrity appears to be as important to tube survivability as is the ability to depressurize the reactor coolant system. The risk benefits that could be gained from ensuring MSIV integrity (late secondary system depressurization) are not as significant as those achieved by preventing early secondary system depressurization (e.g., from failed ADVs). However, it is clear that for the representative plant analyzed, either of these changes provides a greater benefit than improving the ability to depressurize the RCS during core damage events.

7 REFERENCES

Avallone, E.A., Baumeister, T., ed., *Mark's Standard Handbook for Mechanical Engineers*, Ninth Edition, McGraw-Hill, New York, 1987.

Bahr, J., *et al.*, "Valve Inlet Fluid Conditions for Pressurizer Safety and Relief Valves in Combustion Engineering-Designed Plants," EPRI Report NP-2318, December 1982.

Bayless, P.D., *et al.*, "Severe Accident Natural Circulation Studies at the INEL," NUREG/CR-6285, Idaho National Engineering Laboratory, February 1995.

Bixler, N.E., "VICTORIA Studies of Induced Steam Generator Tube Rupture During the Early Stages of a TMLB' Sequence," Letter Report, Sandia National Laboratories, October 20, 1996.

Chavez, S.A., *et al.*, "Estimating Structural Failure Frequency of Degraded Steam Generator Tubes," *ICONE 4: Proceedings Vol. 5, ASME/JSME International Conference on Nuclear Engineering: New Orleans, LA*, American Society of Mechanical Engineers, 1996.

Clark, R.L., "Effects of Aging and Service Wear on Main Steam Isolation Valves and Valve Operators," NUREG/CR-6246, Oak Ridge National Laboratory, March 1996.

Coryell, E.W., *et al.*, "SCDAP/RELAP/MOD 3.1 Code Manual," NUREG/CR-6150, June 1995.

Draper, N.R., and Smith, H., *Applied Regression Analysis*, Wiley, New York, 1966.

Eiber, R.J., *et al.*, "Investigation of the Initiation and Extent of Ductile Pipe Rupture," BMI-1908, Battelle Memorial Institute, June 1971.

Ellison, P.G., *et al.*, "Steam Generator Tube Rupture Induced from Operational Transients, Design-Basis Accidents, and Severe Accidents," INEL-95/0641, Idaho National Engineering Laboratory, August 1996.

EPRI Committee for Alternate Repair Limits for EZ PWSCC, "PWR Steam Generator Tube Repair Limits: Technical Support Document for Expansion Zone PWSCC in Roll Transitions – Rev. 2," EPRI Draft Report NP-6864-L, Revision 2, August 1993 (proprietary information; not publicly available).

EPRI SGDSM/PSA Working Group, "Probabilistic Safety Analysis Support for Steam Generator Degradation Specific Management," Revision 1, Draft EPRI report TR-106388, March 1996 (proprietary information; not publicly available).

EPRI Valve Test Program Staff, "EPRI PWR Safety and Relief Valve Test Program: Safety and Relief Valve Test Report," EPRI Report NP-2628-SR, December 1982 (proprietary information; not publicly available).

Erdogan, F., "Ductile Failure Theories for Pressurized Pipes and Containers," *International Journal of Pressure Vessels and Piping*, Vol. 4, 1976.

Finnie, I., and Heller, W.R., *Creep of Engineering Materials*, McGraw-Hill, New York, 1959.

Flesch, B., and Cochet, B., "Crack Stability Criteria in Steam Generator Tubes," International Congress on Pressure Vessel Technology, Beijing, September 1988.

Fuller, E.L., *et al.*, "Risks From Severe Accidents Involving Steam Generator Tube Leaks or Ruptures," EPRI Draft Report TR-106194, January 1996.

Fuller, E.L., *et al.*, "Safety Valve Performance Considerations During High-Pressure Station Blackout Severe Accidents," EPRI Draft Report TR-106194-V2, July 1996.

Gorman, J.A., Turner, A.P.L., "Estimating Probable Flaw Distributions in PWR Steam Generator Tubes," Dominion Engineering, presented at the 24th Water Reactor Safety Information Meeting, October 1996.

Hahn, G.T., Sarrate, M., and Rosenfeld, A.R., "Criteria for Crack Extension in Cylindrical Pressure Vessels," *International Journal of Fracture Mechanics*, Vol. 5, No. 3, 1969.

Hanson, D.J., *et al.*, "Depressurization as an Accident Management Strategy to Minimize the Consequences of Direct Containment Heating," NUREG/CR-5447, October, 1990.

International Nickel Company, "Engineering Properties of Inconel Alloy 600," Technical Bulletin T-7, 1964.

Kiefner, J.F., *et al.*, "Failure Stress Levels of Flaws in Pressurized Cylinders," in *Progress in Flaw Growth and Fracture Toughness Testing*, (Kaufman, J.G., ed.), National Symposium on Fracture Mechanics (6th: 1972: Philadelphia), American Society for Testing and Materials, Committee E-24 on Fracture Testing of Metals, ASTM Special Technical Publication 536, Philadelphia, 1973.

Knudsen, D.L., and Dobbe, C.A., "Assessment of the Potential for High-Pressure Melt Ejection Resulting from a Surry Station Blackout Transient," NUREG/CR-5949, Idaho National Engineering Laboratory, November 1993.

Knudsen, D.L. (INEL), letter to Lee, R. (NRC), "Revision 1 of Steam Generator Tube Rupture Analyses Under JCN W6242-DLK-4-96," June 6, 1996.

Knudsen, D.L. (INEL), letter to Lee, R. (NRC), "Revision 1 of Additional Surry SGTR Analyses Under JCN W6242-DLK-9-96," December 17, 1996.

Knudsen, D.L. (INEL) letter to Lee, R. (NRC), "Revision 1 of Surry SGTR Analyses with RCP Seal Leaks Under JCN W6242-DLK-1-97," February 4, 1997.

Kurtz, R.J., *et al.*, "Steam Generator Tube Integrity Program: Phase II Final Report," NUREG/CR-2336, PNL, Richland, Washington, August 1988.

Kurtz, R.J., *et al.*, "Steam Generator Tube Integrity Program/Steam Generator Group Project, Final Project Summary Report," NUREG/CR-5117, PNL, Richland, Washington, May 1990.

Larson, F.R., and Miller, J., "A Time-Temperature Relationship for Rupture and Creep Stresses," *Transactions of the ASME*, July 1952.

REFERENCES (continued)

Meliksetian, A., and Sklencar, A.M., "Valve Inlet Fluid Conditions for Pressurizer Safety and Relief Valves in Westinghouse-Designed Plants," EPRI Report NP-2296, December 1982.

Rempe, J.L., *et al.*, "Light-Water Reactor Lower Head Failure Analysis," NUREG/CR-5642, October 1993.

Ruger, C. (BNL) letter to Shaukat, S.K. (NRC), October 5, 1995.

Singh, A. (ed), "Safety and Relief Valves in Light-Water Reactors," EPRI Report NP-4306-SR, December 1985.

Smith, T.W. (INEL) Email to Long, S.M. (NRC), "93-95 Scram Rates," March 28, 1996.

Stewart, W.A., *et al.*, "Experiments on Natural Circulation in a Vertical Hot Leg," EPRI Project Number RP2177-5, Interim Report, May 24, 1989 (proprietary information; not publicly available).

Stewart, W.A., Pieczynski, A.T., and Srinivas, V., "Natural Circulation Experiments for PWR High-Pressure Accidents," EPRI Report TR-102815, August 1993 (proprietary information; not publicly available).

U.S. Nuclear Regulatory Commission, "Severe Accident Risks: An Assessment for Five U.S. Nuclear Power Plants," NUREG-1150, December 1990.

U.S. Nuclear Regulatory Commission, "Individual Plant Examination Program: Perspectives on Reactor Safety and Plant Performance," NUREG-1560, October 1996.

U.S. Nuclear Regulatory Commission, NUREG-0844, "NRC Integrated Program for the Resolution of Unresolved Safety Issues A-3, A-4, and A-5 Regarding Steam Generator Tube Integrity," September 1988

U.S. Nuclear Regulatory Commission, NUREG/CR-4551, Part 1, "Evaluation of Severe Accident Risks: Quantification of Major Input Parameters," Vol. 2, Rev. 1, December 1990,

U.S. Nuclear Regulatory Commission, Draft NUREG-1477, "Voltage-Based Interim Plugging Criteria for Steam Generator Tubes," June 1993

U.S. Nuclear Regulatory Commission, Information Notice 94-55, "Problems With Copes-Vulcan Pressurizer Power-Operated Relief Valves."

Wheeler, T.A., *et al.*, "Analysis of Core Damage Frequency from Internal Events: Expert Judgement Elicitation," NUREG/CR-4550, Sandia National Laboratories, SAND86-2084, Vol. 2, April 1989.

Williams, J.A., "Methodology for High-Temperature Failure Analysis," in *Behaviour of Joints in High-Temperature Materials*, T.G. Gooch, *et al.* eds., Elsevier Science Publishing Co., Inc., New York, 1982.

Wong, S.K., "Heatup of Steam Generator Tubes During Severe Accidents," Draft EPRI report TR-103672, June 1993 (proprietary information; not publicly available).

APPENDIX A

FREQUENCY OF HIGH PRIMARY/DRY SECONDARY CHALLENGE FROM NUREG-1150

The staff evaluated the frequency of core damage sequences that result in high pressure in the RCS and empty SGs at time of core damage. As the basis for this evaluation, the staff relied on point estimate values for sequences and plant damage states tabulated in NUREG/CR-4550, Vol. 3, Rev. 1, Part 1, "Analysis of Core Damage Frequency: Surry Unit 1 Internal Events" (Wheeler, 1989).

The point estimate of the total core damage frequency is 3.3×10^{-5}/RY. Of this total, 2.2×10^{-5}/RY (68 percent) begins the core damage phase with the RCS at relatively high pressure and the steam generators dry. Of these high RCS pressure/dry steam generator sequences, 2.2×10^{-6}/RY (6.6 percent of the total CDF) have pressurizer PORVs or SVs stuck open at the onset of core damage. Also, steam generators have depressurized through stuck-open valves in sequences having a frequency of at least 1.8×10^{-5}/RY (82 percent of the high RCS pressure/dry steam generator sequences). The joint frequency of stuck relief valves on the primary and secondary sides is 5.1×10^{-7}/RY (about 2.3 percent of the high RCS pressure/dry steam generator sequences).

This report uses 1.6×10^{-6}/RY as the high-dry frequency. This value results from certain corrections in the NUREG-1150 RCP seal LOCA cases, as described in Section 2.3.1 of this report.

The initiating events for the high RCS pressure/dry steam generator sequences are mostly single- and double-unit losses of offsite power (92 percent), with the rest being transients involving a loss of main feedwater (6.7 percent), loss of a DC bus (1.3 percent), and spontaneous SGTR (0.4 percent):

- Of the sequences initiated by loss of offsite power, all exhibit failure of emergency AC power (i.e., station blackout), with core damage occurring as a result of battery depletion (7.7×10^{-6}/RY), RCP seal LOCA (6.4×10^{-6}/RY), stuck-open PORV (2.2×10^{-6} /RY), or failure of turbine-driven AFW (4.2×10^{-6}/RY).

- Of the sequences initiated by loss of main feedwater or loss of a DC bus, core damage occurs as a result of the loss of AFW and failure of feed-and-bleed attributable to pressurizer PORV failures (1.1×10^{-5}/RY) or high-pressure injection (HPI) failures (7.2×10^{-7}/RY).

The high RCS pressure/dry steam generator sequence initiated by spontaneous SGTR leads to core damage associated with the failure of AFW (1.0×10^{-7}/RY).

APPENDIX B

OTHER SGTR CONTRIBUTIONS TO CORE DAMAGE FREQUENCY AND CONTAINMENT BYPASS FREQUENCY

The body of this report addressed containment bypass frequency attributable to core damage sequences that create a potential for thermally induced rupture of degraded steam generator tubes. (Pressure-induced tube ruptures during the portions of those sequences that occur at near-normal operating temperatures were also included.)

In order to comprehensively address the risk associated with degradation of steam generator tubes, it is necessary to consider two additional classes of SGTR sequences that result in core damage with containment bypass. One class comprises the sequences beginning with spontaneous rupture of a steam generator tube during normal operation. The other class comprises the sequences beginning with transients during normal operation that create abnormally high pressure differences across the steam generator tubes, leading to pressure-induced tube ruptures under normal temperature conditions. This second class of events can be further divided into sequences with abnormally high primary system pressure (created by ATWS), and sequences with abnormally low secondary system pressures (created by stuck-open steam relief valves or ruptured steam system piping).

The purpose of this appendix is to summarize the results of studies concerning normal temperature SGTR sequences as a context for the results from this study of thermally induced rupture, as described in the body of this report.

B.1 Spontaneous Tube Rupture Sequences

Most PRAs include core damage sequences beginning with spontaneous rupture of a steam generator tube during normal operation. In such instances, the frequency of spontaneous tube rupture is taken from operational data, and it averages about 7×10^{-3}/RY. The failure to mitigate this initiating event is usually dominated by operator errors, with failures of the HPI system sometimes contributing significantly, as well. The resulting core damage frequency in NRC-sponsored PRAs is typically in the low-10^{-6}/RY range. Core damage frequencies attributable to spontaneous tube ruptures reported in licensees' IPEs vary from the high-10^{-6} range to the low-10^{-8}/RY range. This large variability apparently results, in part, from differences in modeling assumptions and techniques, as well as plant-specific differences in design and operation.

The NRC-sponsored PRA performed for the Surry plant and reported in NUREG-1150 estimated a core damage frequency of 1.8×10^{-6}/RY, based on an initiating event frequency of 1×10^{-2}/RY. All sequences result in containment bypass-type releases with the magnitude depending on the RCS pressure and secondary safety valve condition during the accident progression.

One approach would be to project the spontaneous tube rupture probability to the end of each fuel cycle, with a limiting value of 5×10^{-3}/RY. Substituting this initiating event frequency in the NUREG-1150 model for the Surry plant, the estimated core damage frequency with containment bypass attributable to spontaneous tube rupture becomes 6×10^{-7}/RY.

B.2 Pressure-Induced Tube Rupture Sequences

Section 2.1.3 of this report discusses the sequences involving ATWS events that could

rupture tubes by substantially increasing the RCS pressure. In addition, sequences that involve depressurization of the secondary side of the steam generators can induce steam generator tube ruptures by increasing the pressure difference across the tubes. These sequences are not addressed by most current PRAs. However, they were addressed by NUREG-0844 and NUREG-1477, and most recently in draft INEL report 95/0641 (Ellison, 1996). All of these documents concluded that depressurization events associated with steam line safety valve malfunction were more important initiators than pipe break events. In addition, all of those documents concluded that human error dominated the probability of failure to mitigate the events.

One difference between NUREG-0844 and more recent work is the interpretation of the frequency of and risk associated with events involving ruptures of multiple tubes. This is now considered to be less likely for ruptures caused by depressurization of the secondary side of the steam generators. The logical basis for that change arises from critical appraisal of the mechanisms that could lead to multiple ruptures.

First, there is the pressure difference across the tubes. During secondary depressurization sequences, the differential pressure substantially increases only after the secondary-side water inventory has boiled away and the primary system pressure begins increasing as a result of water injection by ECCS systems. The cooling effect of the boil-off depressurizes the RCS, and automatically actuates the ECCS system. As ECCS injection to the RCS increases pressure back toward normal operational levels, the differential pressure across the tubes rises because the steam side is now depressurized. However, if a tube ruptures, reactor coolant begins to escape the RCS, and the net flow into the RCS is reduced, thereby causing the pressure to rise more slowly. Only a few tubes could rupture before the resulting loss of reactor coolant would balance the inflow from the ECCS system, terminating the pressure increase and preventing the rupture of more tubes. The number of tubes that can be ruptured by this effect is therefore limited by the capacity of the ECCS pumps. Review of a sample of ECCS designs indicates that they could cause double-ended ruptures of about three tubes, or a larger number of axial ruptures with an equivalent flow rate.

The staff also considered other mechanisms that could create multiple tube ruptures that would not be self-limiting. For example, the blowdown forces associated with large pipe breaks in the steam system would put the steam generator tubes into tension along their axes. If the tensile force is large enough, it could lead to tube ruptures along circumferential flaws in the tubes. However, evaluation of the forces on the tubes that are associated with extreme blowdown events indicates that they are relatively small, compared to the axial forces created by the internal pressure. In addition, the frequency of extreme blowdown events is estimated to be very low. Therefore, this type of event is not expected to contribute significantly to the total risk.

Another mechanism that has been suggested as a possible path to multiple tube ruptures is the effect of a ruptured tube on adjacent tubes. Tubes that have ruptured at circumferential cracks have exhibited a whipping motion of their unconstrained ends which has caused them to hit and damage the surface of adjacent tubes. However, in the few such events that have occurred, no adjacent tubes were ruptured. Review of the degree of damage caused by this effect indicates that rupture of adjacent tubes is unlikely.

Therefore, steam-side depressurization sequences are not expected to involve rupture of more than three steam generator tubes, with smaller numbers being more probable. INEL-95/0641 provides a method for estimating the core damage frequency attributable to PI-SGTRs resulting from steam-side depressurization. For sequences involving no more than three

tubes, operator action is required to depressurize the RCS, initiate residual heat removal (RHR), and cool the RCS to less than 100°C (212°F) before the RWST inventory is depleted. The human error probability for these actions is estimated as 10^{-2} for the sequence, which dominates the probability of failure to mitigate the event. The RHR hardware failure probability is multiplied by a nonrecovery probability derived from actual data, which makes it much less important than the human error.

Other factors in the dominant sequence include the initiating steam line depressurization at 7.6×10^{-3}/RY and the probability of inducing one or more tube ruptures. Thus, the frequency of core damage attributable to PI-SGTRs caused by steam-side depressurization is estimated at 3.8×10^{-6}/RY. All of these events are expected to lead to substantial bypass of the containment because the secondary side of the steam generator is open to the environment through the same breach that caused the depressurization event.

APPENDIX C

COMPARISONS TO OTHER NPP DESIGNS USING THE IPE DATABASE

During the course of this study, the staff the IPE database (as of May 1996) to determine whether the information from the Surry NUREG-1150 analysis regarding the frequency of challenge was reasonably consistent with available information from the IPEs. In addition, the staff interviewed several IPE reviewers to glean their qualitative insights. This appendix summarizes the results of this assessment.

C.1 IPE Database Search

In searching the IPE Database, the staff focused on core damage events with the primary system at high pressure and the secondary system dry. The IPE Database can automatically query for high-pressure core damage events, but secondary system water level is not an explicit field in the database records. Thus, a direct automated search for the sequences of interest is not possible. Instead, the staff searched the database for sequences of high primary pressure and loss of all feedwater.

The search yielded a set of 1351 sequences from 41 PWR IPEs. (Some of these IPEs represent two plants. For example, North Anna, Surry, and Zion each have one IPE that applies to both units at the given facility.) To make analysis of the large number of sequences more tractable, the staff formatted the results of the database search in a manner compatible with a spreadsheet program, and conducted the remainder of the analysis with the aid of that spreadsheet.

All 41 IPEs had some sequences that were "hits" in the database search. The sum of CDFs for each plant ranged from a low of 4.9×10^{-7}/RY (McGuire 1&2) to a high of 7.9×10^{-5}/RY (Indian Point 2). A plot of these CDFs appears as Figure 2-4. Most plants fell in the range of 2×10^{-6}/RY to 4×10^{-5}/RY.

To identify initiating events and design biases, the staff used two approaches. First, the staff examined the sequences from the three IPEs with the greatest "hi&dry" CDFs. Second, the staff examined the top five sequences in all of the IPEs. This was a qualitative analysis, but it was directed by the CDFs and should have found most (if not all) of the sequences that have not previously been considered in induced SGTR analyses.

The three highest CDFs belonged to Indian Point 2, North Anna 1&2, and Surry 1&2. (Since the existing work revolved around Surry, this analysis was stopped at the Surry IPE. All other IPEs had "high & dry" CDFs lower than Surry). Station blackout and battery depletion frequently appeared in these sequences, as expected. The specific initiators included loss of offsite power, reactor scram, turbine trip, loss of main feedwater, loss of DC power, loss of emergency service water, and ATWS. These are to be expected, since they can all lead to secondary dryout, although not all involve station blackout.

In addition, some principal contributor sequences were initiated by loss of HVAC or internal flooding. Neither of these were explicitly considered before this study. Internal flooding is quite plant-specific, and is not surprising in retrospect. By contrast, loss of HVAC is not intuitively obvious. The loss of HVAC (at Indian Point 2) can cause loss of required ventilation cooling to the AFW pumps and the emergency generators, as well as some other equipment. If the operators fail to open some roll-up doors to provide passive ventilation,

an accident may result. (The utility is considering some plant modifications to address this vulnerability.)

Finally, it is possible to get into a high primary pressure, dry secondary situation by initiating the sequence with an SGTR. This sequence is moot for the purposes of the current study, however, since bypass would occur regardless of whether the core melt causes tube failure.

The staff also examined the top five sequences of all PWR IPEs. Essentially all of the above sequences appear in these plants as well (including the HVAC initiator). In addition, loss of component cooling water, loss of instrument air, loss of onsite AC power (some plants have onsite sources in addition to the diesels), steam line break inside containment, and loss of ultimate heat sink appear in the list, some with frequencies as high as 10^{-6}/RY.

C.2 Qualitative Insights

In addition to the IPE Database search, the staff interviewed several IPE reviewers to gather their qualitative insights. Several items of interest arose in these discussions concerning induced SGTR:

- Some CE plants have no PORVs on the pressurizer. One would assume that this would imply a greater probability that a core damage accident would occur at high primary pressure. However, these plants have generally put procedures in place to depressurize the primary by means of valves installed for low-temperature overpressure protection.

- Some Westinghouse plants have procedures that direct the operator to turn the reactor coolant pumps back on during the scenario of interest. There would be little water to pump in this scenario, of course, but turning on the pumps would likely clear the loop seal in the cold leg piping. In addition, the pumps would probably last long enough to act as blowers to circulate hot gases around the primary system.

C.3 Conclusion

On the basis of the IPE Database search and qualitative insights from the IPE reviewers, the staff reached the following conclusion:

> It is clear that there are other sequences of interest in addition to station blackout. However, choosing the definition of the initiating event for the tree as all sequences with a high primary pressure and a dry secondary should cover all of these sequences. Moreover, there is nothing in these sequences that would alter the remainder of the event tree.

APPENDIX D

EFFECT OF FISSION PRODUCT TRANSPORT AND DEPOSITION ON STEAM GENERATOR TUBE INTEGRITY

During the course of this study, the staff performed SCDAP/RELAP5 analyses to determine the thermal-hydraulic boundary conditions for estimating the probability of a steam generator tube failure. While SCDAP/RELAP5 models the decrease in decay heat generation resulting from the release of fission products from the fuel, SCDAP/RELAP5 does not model transport and deposition of fission products and other core materials within the reactor coolant system (RCS). Therefore, the staff also used VICTORIA (Bixler, 1996) to evaluate the release, transport, and deposition of these materials in an effort to determine whether the thermal-hydraulic boundary conditions may be affected by consideration of these phenomena.

VICTORIA is a mechanistic computer code for analyzing fission-product behavior within the RCS during a severe accident. The code provides detailed predictions of the release of fission products and other materials from the core and the transport of these materials in the RCS during core degradation. The major models in VICTORIA are vaporization of core materials; aerosol formation, growth, and deposition; and chemical reactions and phase changes. On the basis of a review of SCDAP/RELAP5 thermal-hydraulic results, the staff developed a VICTORIA nodalization scheme and determined representative temperatures, pressures, and steam flow rates for input to VICTORIA. A schematic of the VICTORIA nodalization is shown in Figure D.1. Building on the similarity of conditions between loops, the staff used one loop with the total flow and surface areas of all three loops. The nodalization of the core is more coarse than that of SCDAP/RELAP5, because the thermal-hydraulic conditions in many of the SCDAP/RELAP5 nodes are essentially the same (as far as release of core materials is concerned). The nodalization of the steam generator tubes is the same as in SCDAP/RELAP5 to provide a detailed estimate of the deposition pattern in the tubes and to allow direct comparison of tube heating rates resulting from convected steam and from deposited and suspended fission products in the tubes.

D.1 VICTORIA Results

The results of Case 3 in the SCDAP/RELAP5 analysis were used as boundary conditions for the VICTORIA analysis. The significant features of Case 3 are that the primary system is at high pressure with no pump seal leakage, 35 percent of the tubes have forward flow and 65 percent have reverse flow, and the secondary side is at low pressure because of a stuck-open ADV.

At the time of tube failure predicted by SCDAP/RELAP5 (15,560 sec), VICTORIA predicted a fission product release of primarily noble gases, iodine, and cesium, containing about 5 percent of the core decay heat. Thus, 95 percent of the decay heat remained in the core at this time.

Table D.1 summarizes the VICTORIA results for decay power in the upper plenum and the loop with the pressurizer. The decay power is from both suspended and deposited fission products. Most of the decay power is from the iodine, and most of the iodine is deposited in the steam generator tubes because of the large surface area. In the tube segments where there are upward facing surfaces (i.e., the top of the tube bundle), the dominant deposition mechanism is gravitational settling. In the remainder of the tube segments, the dominant deposition mechanism is turbulent deposition, with Reynolds numbers on the order of 10,000.

Table D.1 Decay Power from Deposited and Suspended Fission Products

Reactor Outlet to SG

Node No.[1]	6	7	8	9	10	11	12	13	14	15	16	17
Decay Power (kw)	19	3	5	15	13	12	28	19	5	5	5	11

SG to Reactor Inlet

Node No.[1]	23	24	25	26	27	28	29	30	31	32	33	34
Decay Power (kw)	7	3	2	2	2	2	9	20	3	3	3	3

Note 1: Node numbers refer to those depicted in Figure D.1

As Table D.1 illustrates, the decay heating is spread throughout the tubes, with the top of the tubes receiving additional heat because of settling onto the upward facing surfaces in that area.

The first segment of tubes in the forward direction is predicted by SCDAP/RELAP5 to have the highest temperature and therefore to be the most likely location of temperature-induced tube failure. Figure D.2 compares the heating rate of this segment of tubes by steam with the heating rate from decay heat of deposited and suspended fission products. As shown in Figure D.2, the magnitude of the decay heat in the tubes is insufficient to noticeably affect the tube temperature. Also, the total decay heat in the tubes is about 0.15 MW/steam generator, which is minimal when compared with the total decay heat in the core of (about 20 MW) and the additional heat generated in the core from oxidation of zircaloy cladding.

The staff also used VICTORIA results to address the issue of whether fission product deposition in the steam generator tubes was significant enough to affect the flow or heat-transfer conditions in the steam generator tubes. VICTORIA predicted a core release of about 350 kg (772 lbs) of condensible material. At the time of predicted tube failure, the maximum deposited thickness of condensible material in the steam generator tubes is about 10 microns (about 4×10^{-4} in.), which is small when compared with the tube thickness of 1270 microns (0.05 in.) and the tube diameter of 20,000 microns (0.8 in.). An additional 10 microns (4×10^{-4} in.) of deposited material in the steam generator tubes is not expected to have a significant effect on the thermal-hydraulic conditions in the reactor coolant system.

Finally, the staff performed additional calculations with VICTORIA to investigate the sensitivity of the results to the following conditions:

- Upper plenum surface area – To account for uncertainties in the retention of fission products in the upper plenum, the surface area in the upper plenum was reduced by one third.

- Upper plenum temperatures – Because higher temperatures of upper plenum gas and structures will result in less fission product retention in the upper plenum, gas and structure temperatures in the upper plenum were increased.

- Entrances of the tubes – Since tube entrance effects may cause additional deposition, a vena-contracta model was used for the entrances of the tubes.

- Deposition pattern in the tube bundle – To account for uncertainties in the amount of material that will be preferentially deposited by settling in the top segments instead of by turbulent flow in the first segment, no floor area was used in the top segments of the steam generator tube bundle.

Overall, the sensitivities studied did not yield results that were significantly different from the base case and, therefore, did not affect the conclusions of this analysis. (The difference in decay power in the first segment of tubes was on the order of a few kW.)

D.2 Conclusions

Fission product transport and deposition in the reactor coolant system have a negligible effect on the thermal-hydraulic conditions used to evaluate steam generator tube integrity. This is because the fission product release is relatively small and occurs late in the transient. The heating rate from decay heat of deposited and suspended fission products in the hottest segment of tubes is a small fraction of the heating rate by steam. Also, the thickness of deposits in the tube is a small fraction of the thickness of the tube wall and an even smaller fraction of the tube cross-sectional flow area. Thus, the staff concluded that flow characteristics would not be materially altered.

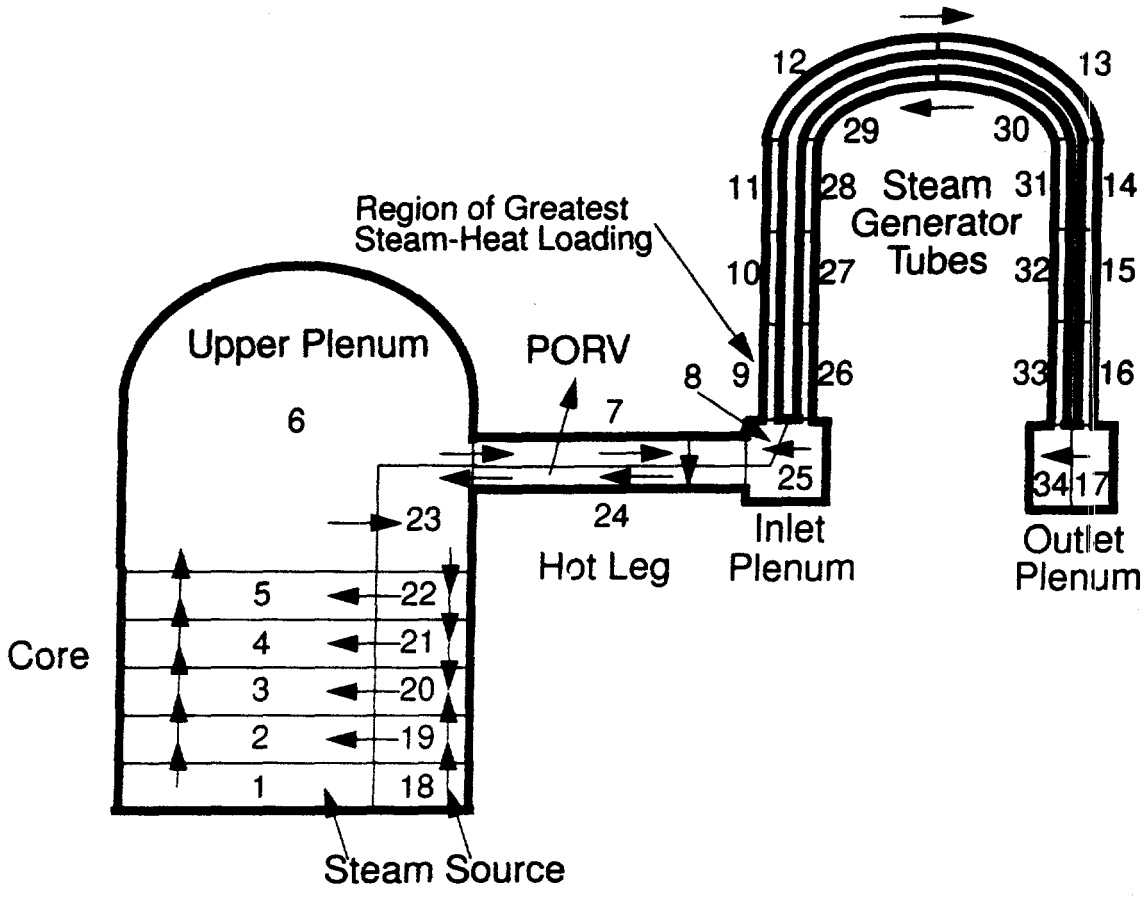

Figure D.1 Schematic of the VICTORIA nodalization of the core, upper plenum, and three primary circuits.

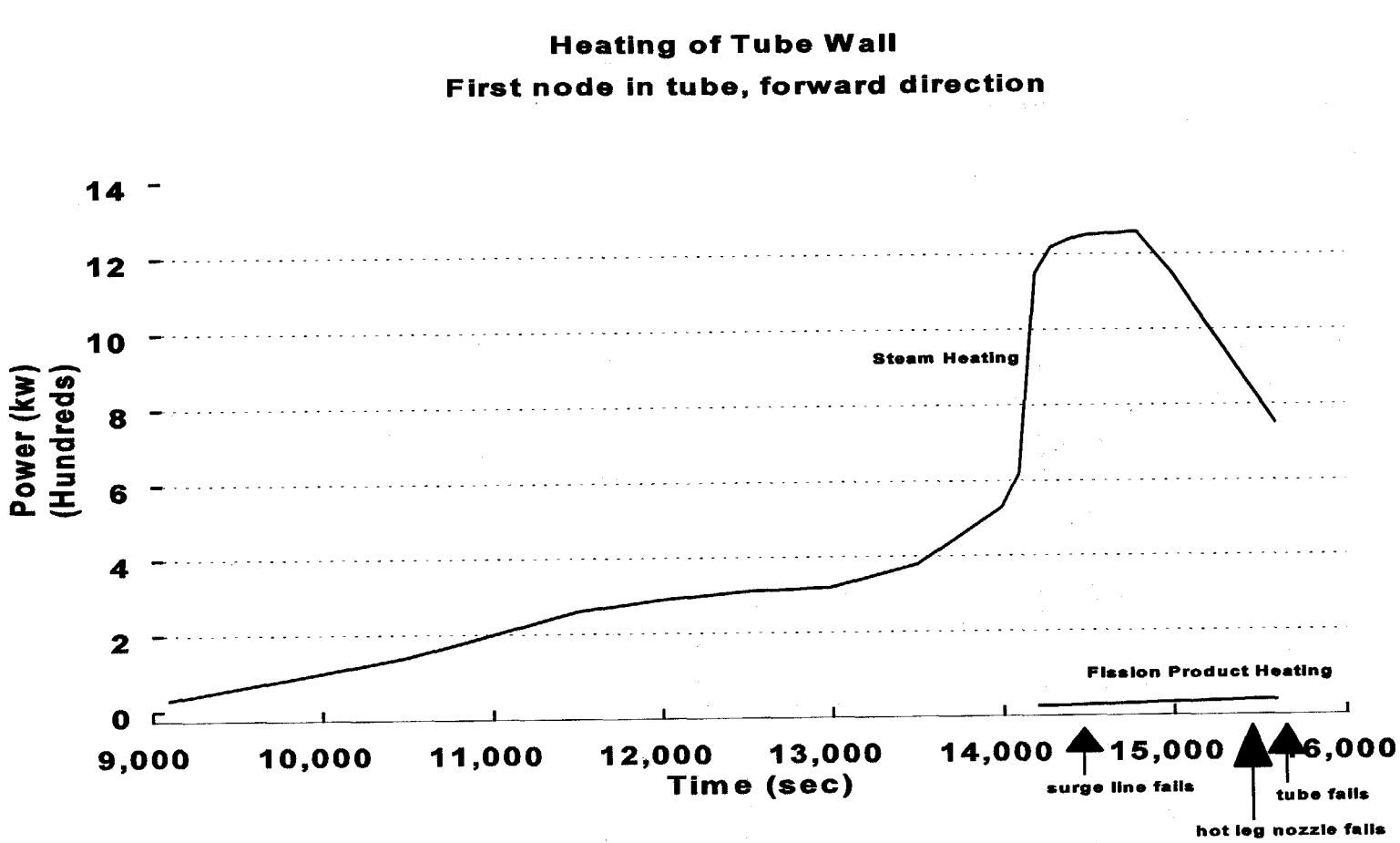

Figure D.2 Comparison of Steam Heating and Fission Product Heating

NRC FORM 335 (2-89) NRCM 1102, 3201, 3202

U.S. NUCLEAR REGULATORY COMMISSION

BIBLIOGRAPHIC DATA SHEET

(See instructions on the reverse)

1. REPORT NUMBER (Assigned by NRC, Add Vol., Supp., Rev., and Addendum Numbers, if any.)

NUREG-1570

2. TITLE AND SUBTITLE

Risk Assessment of Severe Accident-Induced Steam Generator Tube Rupture

3. DATE REPORT PUBLISHED

MONTH	YEAR
March	1998

4. FIN OR GRANT NUMBER

5. AUTHOR(S)

SGTR Severe Accident Working Group

6. TYPE OF REPORT

Technical

7. PERIOD COVERED *(Inclusive Dates)*

June 1997

8. PERFORMING ORGANIZATION - NAME AND ADDRESS *(If NRC, provide Division, Office or Region, U.S. Nuclear Regulatory Commission, and mailing address; if contractor, provide name and mailing address.)*

Division of Systems Safety and Analysis
Office of Nuclear Reactor Regulation
U.S. Nuclear Regulatory Commission
Washington, DC 20555-0001

9. SPONSORING ORGANIZATION - NAME AND ADDRESS *(If NRC, type "Same as above"; if contractor, provide NRC Division, Office or Region, U.S. Nuclear Regulatory Commission, and mailing address.)*

Same as above

10. SUPPLEMENTARY NOTES

11. ABSTRACT *(200 words or less)*

This report describes the basis, results, and related risk implications of an analysis performed by an ad hoc working group to assess the containment bypass potential attributable to steam generator tube rupture (SGTR) induced by severe accident conditions. The SGTR Severe Accident Working Group, comprised of staff members from the NRC's Offices of Nuclear Reactor Regulation (NRR) and Nuclear Regulatory Research (RES), undertook the analysis beginning in December 1995 to support a proposed steam generator integrity rule. The work drew upon previous risk and thermal-hydraulic analyses of core damage sequences, with a focus on the Surry plant as a representative example. This analysis yielded new results, however, derived by predicting thermal-hydraulic conditions of selected severe accident scenarios using the SCDAP/RELAP5 computer code, flawed tube failure modeling, and tube failure probability estimates. These results, in terms of containment bypass probability, form the basis for the findings presented in this report.

12. KEY WORDS/DESCRIPTORS *(List words or phrases that will assist researchers in locating the report.)*

pressurized-water reactor, steam generator, steam generator tubes, severe accidents, risk assessment,

13. AVAILABILITY STATEMENT

unlimited

14. SECURITY CLASSIFICATION

(This Page)

unclassified

(This Report)

unclassified

15. NUMBER OF PAGES

16. PRICE